25 April 2008 | $10

Science

Plant Genomes

AAAS

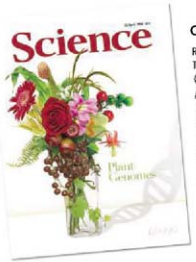

COVER

Representatives of diverse species from the plant kingdom. The genomes of thale cress (*Arabidopsis thaliana*), grape (*Vitis vinifera*), rice (*Oryza sativa*), and the moss *Physcomitrella patens* have been sequenced, and there is ongoing genetic research on apple (*Malus domestica*), rose (*Rosa* spp.), tomato (*Solanum lycopersicum*), Gerbera daisy (*Gerbera hybrida*), monkey flower (*Mimulus lewisii*), columbine (*Aquilegia formosa*), maize (*Zea mays*), wheat (*Triticum aestivum*), tulip poplar (*Liriodendron tulipifera*), and the fern *Ceratopteris richardii*. The special section beginning on page 465 includes News stories and Perspectives exploring plant biology, ecology, economic applications, and the future of plant genomics research.

Photo illustration: Kelly Krause/Science (images: Jupiter Images, Getty Images, USDA, Oregon State University)

DEPARTMENTS

419 *Science* Online
421 This Week in *Science*
426 Editors' Choice
428 Contact *Science*
429 Random Samples
431 Newsmakers
463 AAAS News & Notes
551 New Products
552 *Science* Careers

EDITORIAL

425 Seeds of a Perfect Storm
by Nina Fedoroff
>> *Plant Genomes section p. 465*

SPECIAL SECTION

Plant Genomes

INTRODUCTION

Green Genes 465

NEWS

GM Crops: A World View 466
Tough Lessons From Golden Rice 468
GM Papaya Takes on Ringspot Virus and Wins 472
Is the Drought Over for Pharming? 473
Uncorking the Grape Genome 475
A Life With Grapes
Sowing the Seeds for High-Energy Plants 478

PERSPECTIVES

Genome-Enabled Approaches Shed New Light on Plant Metabolism 479
D. DellaPenna and R. L. Last
Genomic Plasticity and the Diversity of Polyploid Plants 481
A. R. Leitch and I. J. Leitch
Selection on Major Components of Angiosperm Genomes 484
B. S. Gaut and J. Ross-Ibarra
Synteny and Collinearity in Plant Genomes 486
H. Tang et al.
The Epigenetic Landscape of Plants 489
X. Zhang
Extending Genomics to Natural Communities and Ecosystems 492
T. G. Whitham et al.
From Genotype to Phenotype: Systems Biology Meets Natural Variation 495
P. N. Benfey and T. Mitchell-Olds

>> *Editorial p. 425;* Science *Express Reports by K. Baerenfaller* et al. *and J. R. Dinneny* et al.*;* Science *Careers article by S. Williams; for online content see p. 419 or go to www.sciencemag.org/plantgenomes/*

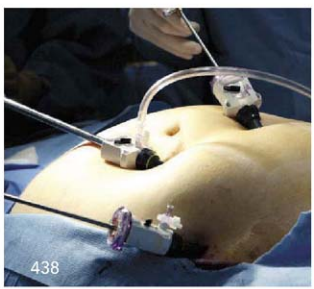

NEWS OF THE WEEK

New Superconductors Propel Chinese Physicists to Forefront 432
When Hobbits (Slowly) Walked the Earth 433
Two Geologic Clocks Finally Keeping the Same Time 434
>> *Research Article p. 500*
SCIENCESCOPE 435
Europe Takes Guesswork Out of Site Selection 436
Rebuilding the Injured Warrior 437

NEWS FOCUS

Bypassing Medicine to Treat Diabetes 438
Japanese Experts Steal a Glance at Once-Taboo Royal Tomb 441
Pardis Sabeti: Picking Up Evolution's Beat 442
A Renowned Field Station Rises From the Ashes 444

CONTENTS continued >>

Science

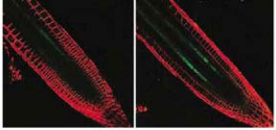

SCIENCE EXPRESS

www.sciencexpress.org

CLIMATE CHANGE

The Sensitivity of Polar Ozone Depletion to Proposed Geoengineering Schemes

S. Tilmes, R. Müller, R. Salawitch

Calculations imply that injection of sulfur into the atmosphere to counteract global warming would threaten the ozone layer, as occurred after the Mount Pinatubo eruption.

10.1126/science.1153966

IMMUNOLOGY

Coordination of Early Protective Immunity to Viral Infection by Regulatory T Cells

J. M. Lund, L. Hsing, T. T. Pham, A. Y. Rudensky

In mice infected with herpes virus, an usually immunosuppressive T cell is necessary for rapid arrival of immune cells and elevated cytokine levels at the site of infection.

10.1126/science.1155209

PLANT SCIENCE

Cell Identity Mediates the Response of *Arabidopsis* Roots to Abiotic Stress

J. R. Dinneny et al.

In *Arabidopsis* root tips exposed to high salinity or iron deficiency, clusters of genes are induced that are unique to one or both of these stress responses.

>> Plant Genomes section p. 465

10.1126/science.1153795

PLANT SCIENCE

Genome-Scale Proteomics Reveals *Arabidopsis thaliana* Gene Models and Proteome Dynamics

K. Baerenfaller et al.

The *Arabidopsis* proteome shifts as the plant develops, and proteins not predicted from genome analysis, some derived from introns and pseudogenes, are expressed.

>> Plant Genomes section p. 465

10.1126/science.1157956

LETTERS

Parsing the Evolution of Language 446
B. D. Joseph and S. S. Mufwene
Response *Q. D. Atkinson* et al.
Inspecting Urban Health *E. Thomas* Response *C. Dye*
The Quest for Stronger, Tougher Materials *R. O. Ritchie*
Response *Y. Dzenis*

TECHNICAL COMMENT ABSTRACTS

OCEAN SCIENCE

Comment on "Eddy/Wind Interactions Stimulate Extraordinary Mid-Ocean Plankton Blooms" 448
A. Mahadevan, L. N. Thomas, A. Tandon
full text at www.sciencemag.org/cgi/content/full/320/5875/448b

Response to Comment on "Eddy/Wind Interactions Stimulate Extraordinary Mid-Ocean Plankton Blooms"
D. J. McGillicuddy Jr., J. R. Ledwell, L. A. Anderson
full text at www.sciencemag.org/cgi/content/full/320/5875/448c

BOOKS *ET AL.*

Fruits and Plains The Horticultural Transformation of America *P. J. Pauly, reviewed by S. Kingsland* 449

Most Dangerous Catch *D. Elisco, Director;* 450
FLOW: For Love of Water *I. Salina, Director;*
Building the Future—Energy *N. Brown, Director;*
Gimme Green *I. Brown and E. Flagg, Directors;*
Scarred Lands and Wounded Lives: The Environmental Footprint of War *A. Day and L. Day, Directors*

POLICY FORUM

Harvesting Data from Genetically Engineered Crops 452
M. Marvier et al.

EDUCATION FORUM

The Advantage of Abstract Examples in Learning Math 454
J. A. Kaminski, V. M. Sloutsky, A. F. Heckler

PERSPECTIVES

Enigmas of Blood Clot Elasticity 456
J. W. Weisel

Identifying Ancient Asteroids 457
T. H. Burbine >> Report p. 514

A One-Sided Signal 458
G. D. Fain and S. Grinstein >> Reports pp. 528 and 531

Carbon Crucible 460
M. Marquis and P. Tans

RNA Metabolism and Oncogenesis 461
D. L. Johnson and S. A. S. Johnson

BREVIA

PALEONTOLOGY

Molecular Phylogenetics of Mastodon and *Tyrannosaurus rex* 499
C. L. Organ et al.
Phylogenetic analyses of collagen protein fragments from fossils and 21 extant organisms group mastodons with elephants and *Tyrannosaurus rex* with birds.

RESEARCH ARTICLE

GEOCHEMISTRY

Synchronizing Rock Clocks of Earth History 500
K. F. Kuiper et al.
Tying an argon-argon dating standard to a section dated with Earth's orbital variations yields older ages for the standard and for other events, including the K-T boundary. >> News story p. 434

REPORTS

MATERIALS SCIENCE

Sign Change of Poisson's Ratio for Carbon Nanotube Sheets 504
L. J. Hall et al.
When stretched, a sheet made of carbon nanotubes contracts or expands in the opposite direction, depending on how many multiwalled tubes form zig-zag networks.

CONTENTS continued >>

REPORTS *CONTINUED...*

MATERIALS SCIENCE

Stretchable and Foldable Silicon Integrated Circuits 507
D.-H. Kim et al.
High-performance, bendable, and stretchable electronic devices are fabricated on an elastic plastic substrate by placing the critical electronic components in the neutral bending plane.

APPLIED PHYSICS

Near-Field Plates: Subdiffraction Focusing with Patterned Surfaces 511
A. Grbic, L. Jiang, R. Merlin
A grating near the focal plane can focus microwave radiation to a spot size well below the diffraction limit.

PLANETARY SCIENCE

Ancient Asteroids Enriched in Refractory Inclusions 514
J. M. Sunshine et al.
Spectral data imply that some asteroids contain higher concentrations of early solar system grains and materials than are found in any sampled meteorite. >> *Perspective p. 457*

CLIMATE CHANGE

Human-Induced Arctic Moistening 518
S.-K. Min, X. Zhang, F. Zwiers
Comparison of 22 climate models to observations show that human activity has increased precipitation in the Arctic over the past 50 years, altering its timing and distribution.

BIOCHEMISTRY

Efficient Inhibition of the Alzheimer's Disease β-Secretase by Membrane Targeting 520
L. Rajendran et al.
Tethering an inhibitor to a membrane anchor renders it effective against a membrane enzyme that creates the amyloid fragments deposited in Alzheimer's disease, even in vivo.

MEDICINE

Plastin 3 Is a Protective Modifier of Autosomal Recessive Spinal Muscular Atrophy 524
G. E. Oprea et al.
Expression of a protein that promotes axonal growth can compensate for the gene deletion in spinal muscular atrophy, indicating that axonal growth deficiencies cause the disease.

CELL BIOLOGY

Role of *C. elegans* TAT-1 Protein in Maintaining Plasma Membrane Phosphatidylserine Asymmetry 528
M. Darland-Ransom et al.
A phospholipid translocase enzyme keeps a critical membrane lipid localized to the inner leaflet of the cell membrane so it does not trigger engulfment by immune cells.
>> *Perspective p. 458; Report p. 531*

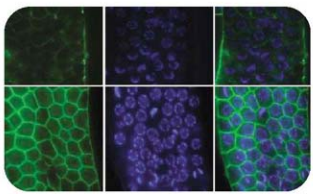

458, 528, & 531

VIROLOGY

Vaccinia Virus Uses Macropinocytosis and Apoptotic Mimicry to Enter Host Cells 531
J. Mercer and A. Helenius
To infect host cells, vaccinia virus exposes phosphatidylserine on its surfaces, which signals host cells to recognize the virus as cellular debris and take it up for clearance.
>> *Perspective p. 458; Report p. 528*

CELL BIOLOGY

Encoding Gender and Individual Information in the Mouse Vomeronasal Organ 535
J. He, L. Ma, S. Kim, J. Nakai, C. R. Yu
Mice can recognize the pheromones from individual mice through unique patterns of receptor activation in the vomeronasal organ.

GENETICS

Rare Structural Variants Disrupt Multiple Genes in Neurodevelopmental Pathways in Schizophrenia 539
T. Walsh et al.
Patients with schizophrenia carry multiple small deletions and duplications in their DNA that are associated nonrandomly with neuronal signaling and brain development pathways.

EVOLUTION

Metabolic Diversification—Independent Assembly of Operon-Like Gene Clusters in Different Plants 543
B. Field and A. E. Osbourn
Through strong selection, similar clusters of genes for triterpene biosynthesis have arisen independently through gene duplication and neofunctionalization in several plant lines.

GENETICS

Mechanism of Self-Sterility in a Hermaphroditic Chordate 548
Y. Harada et al.
The sea squirt prevents self-fertilization with two genetic loci, each of which encodes a tightly linked sperm-egg receptor-ligand pair, a system similar to that of flowering plants.

AAAS
ADVANCING SCIENCE, SERVING SOCIETY

SCIENCE (ISSN 0036-8075) **is published weekly on Friday, except the last week in December, by the American Association for the Advancement of Science, 1200 New York Avenue, NW, Washington, DC 20005.** Periodicals Mail postage (publication No. 484460) paid at Washington, DC, and additional mailing offices. Copyright © 2008 by the American Association for the Advancement of Science. The title SCIENCE is a registered trademark of the AAAS. Domestic individual membership and subscription (51 issues): $144 ($74 allocated to subscription). Domestic institutional subscription (51 issues): $772; Foreign postage extra: Mexico, Caribbean (surface mail) $55; other countries (air assist delivery) $85. First class, airmail, student, and emeritus rates on request. Canadian rates with GST available upon request, GST #125439822. Publications Mail Agreement Number 1069624. **Printed in the U.S.A.**

Change of address: Allow 4 weeks, giving old and new addresses and 8-digit account number. **Postmaster:** Send change of address to AAAS, P.O. Box 96178, Washington, DC 20090-6178. **Single-copy sales:** $10.00 current issue, $15.00 back issue prepaid includes surface postage; bulk rates on request. **Authorization to photocopy** material for internal or personal use under circumstances not falling within the fair use provisions of the Copyright Act is granted by AAAS to libraries and other users registered with the Copyright Clearance Center (CCC) Transactional Reporting Service, provided that $20.00 per article is paid directly to CCC, 222 Rosewood Drive, Danvers, MA 01923. The identification code for Science is 0036-8075. Science is indexed in the *Reader's Guide to Periodical Literature* and in several specialized indexes.

CONTENTS continued >>

SPECIAL SECTION

Plant Genomes

ONLINE FEATURE: Plant Genomes >>
An interactive presentation featuring informational graphics, video commentary, and an animation.
www.sciencemag.org/plantgenomes/feature.html

SCIENCE CAREERS

www.sciencecareers.org/career_development CAREER RESOURCES FOR SCIENTISTS

Plumbing the Green Genome
S. Williams
Plant genomics addresses several of the world's most pressing problems.

SCIENCENOW

www.sciencenow.org DAILY NEWS COVERAGE

Mutation Makes Good Medicine
Gene variant works like heart-sparing drugs in many African Americans.

Sleep Deprivation for Germs
Study suggests new way to target persistent bacteria.

Gene Studies Tell Placenta's Tale
Mother-fetus lifeline evolved from a combination of ancient and new genes.

Research career on the fast track.

SCIENCE CAREERS

www.sciencecareers.org/career_development
CAREER RESOURCES FOR SCIENTISTS

Young Swedish Scientist Reveals Fast-Track Career Secrets
L. Laursen
By age 35, Thomas Helleday was heading labs in two countries and winning several awards.

Educated Woman, Postdoc Edition, Chapter 15: This Strange, Funny Feeling
M. P. DeWhyse
Could Micella's new feeling be joy?

10 Years Ago This Week: Dysfunctional Advisee-Adviser Relationships
P. Fiske
Students know the nature of an adviser's esteem and the risks of too much candor.

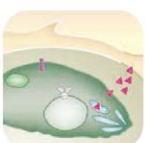

T. gondii escaping from host cells.

SCIENCE SIGNALING

www.sciencesignaling.org
THE SIGNAL TRANSDUCTION KNOWLEDGE ENVIRONMENT

PERSPECTIVE: Notch Signaling in Osteoblasts
E. Canalis
Notch signaling plays a role in bone remodeling by inhibiting the differentiation of osteoblasts and osteoclasts.

PERSPECTIVE: Back from the Dormant Stage—Second Messenger Cyclic ADP-Ribose Essential for *Toxoplasma gondii* Pathogenicity
A. H. Guse
The protozoan parasite *T. gondii* uses a plant-like signaling pathway to exit host cells.

CREDITS: (SCIENCE CAREERS) S. SEEGER; (SCIENCE SIGNALING) P. MUDY

SCIENCEPODCAST

Download the 25 April *Science* Podcast to hear about how mice process pheromones, future directions for plant genomics, a radical treatment for diabetes, and more.

www.sciencemag.org/about/podcast.dtl

Separate individual or institutional subscriptions to these products may be required for full-text access.

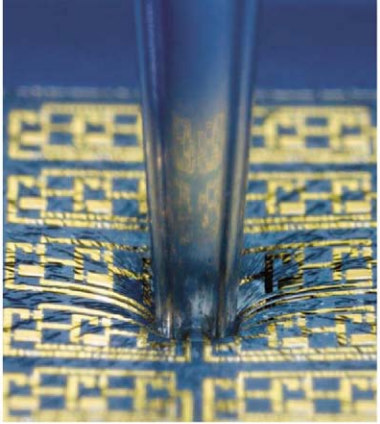

<< Bend Me, Stretch Me

Flexible electronics have been developed using conducting organic materials, but their performance is much poorer than that of inorganic materials. **Kim *et al.*** (p. 507, published online 27 March) have developed a way to combine nanoribbons of silicon with thin plastic or rubbery substrates to create robust, flexible, and bendable electronics without sacrificing electronic performance. A key feature of their design is that the electronics layer lies in the neutral bending plane which experiences almost no strain, even when the overall device is very bent.

Dating Fish Canyon Tuff

A major uncertainty in accurate dating using the common Ar-Ar method is that it requires a standard, and current uncertainties in the standards themselves are about 1% (or 1 million years in a 100-million-year-old age). One way to improve the calibration is calibration against an astronomically dated rock section in which many orbital cycles are preserved in a cyclically layered sediment sequence. **Kuiper *et al.*** (p. 500; see the news story by **Kerr**) do this comparison for the Fish Canyon Tuff in Colorado, one of the main geochronologic standards, reducing its age uncertainty to about 0.1%, which reveals an older primary age for the standard. This finding changes the age estimates of several meteorites and the K-T boundary.

Arctic Rain

Global warming is expected to affect the amount and pattern of precipitation all over the world, but such changes are difficult to detect, and to attribute to human influence. One area in which precipitation is anticipated to change most dramatically is in the Arctic. The Arctic is also of particular interest because of its contribution to the Meridional Overturning Circulation of the North Atlantic Ocean, which itself exerts a fundamental control on climate. **Min *et al.*** (p. 518) compare observations of precipitation with simulations from 22 coupled-climate models and conclude that the amount of rainfall in the northern high latitudes (above 55°N) has increased considerably over the last 50 years. The anthropogenic influence is consistent with earlier reported increases in Arctic river discharge and sea-surface water freshening, and confirms one more way that human activity has modified the environment.

CREDITS: (TOP TO BOTTOM) BECKMAN INST./UIUC; BURBINE ET AL.

Exploring Space Dust

Grains rich in calcium and aluminum oxides (CAIs) are thought to be some of the first materials to have condensed in our solar nebula. The oldest meteorites contain about 10% of these grains. **Sunshine *et al.*** (p. 514, published online 20 March; see the Perspective by **Burbine**) compare laboratory spectra of these grains with spectra obtained from several asteroids and show that these asteroids may contain 30% CAIs. The high abundance of CAIs might indicate that these bodies formed extremely early in our solar system and, if so, may be worth examining further for other material reflecting this time period.

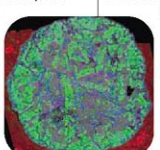

Beyond Carbon Paper

As a cork is stretched or compressed, there are only minimal changes in shape in the radial direction, which is due to cork's near-zero Poisson's ratio. Most materials have a positive Poisson's ratio, while a few, like some polymer foams have a negative ratio, so that they actually expand in the lateral direction as they are stretched. **Hall *et al.*** (p. 504) now describe the creation of a paper-like material from mixtures of single and multiwalled carbon nanotubes. By varying the fraction of multiwalled tubes, they could change the in-plane Poisson's ratio from positive to negative values. This tunability was due to changes in the bending and stretching of the papers with composition, which could be described by a simple model.

Location, Location

Rational drug design often involves the production of small molecule inhibitors of specific steps in a pathological pathway. **Rajendran *et al.*** (p. 520) describe the design of inhibitors of a key event in Alzheimer's disease pathology, an event that occurs at a particular intracellular membrane: the β-secretase–mediated cleavage of the amyloid precursor protein (APP) in endosomes. A transition-state inhibitor that inhibits purified β-secretase failed to inhibit β-secretase in the cellular context. However, anchoring the very same inhibitor to the membrane, which promoted its delivery to the endosomes, enabled it to inhibit β-secretase effectively both in cultured cells and in two animal model systems, mouse and *Drosophila*.

Plastin Protection in SMA

Spinal muscular atrophy (SMA) is a neuromuscular disorder that leads to death early in childhood in more than half of the patients. It is caused by the homozygous deletion of the survival motor neuron gene 1 (*SMN1*), but the severity of the disease is influenced by the copy

Continued on page 423

Continued from page 421

number of the highly homologous *SMN2* gene. However, in rare instances, siblings with identical *SMN1* mutations, identical *SMN2* copy numbers, and identical haplotypes have completely different phenotypes: Some are affected while others are fully asymptomatic. This discrepancy suggests the influence of independent modifying factors capable of protecting against SMA. By differential expression analysis using RNA from six SMA discordant families, **Oprea *et al.*** (p. 524) identified plastin 3 as a candidate protective modifier against SMA. The influence of plastin 3 upon the SMA phenotype was mainly due to expression variability, which is often triggered by transacting factors.

Distinctive Individual Smells

Pheromones are critical for social communication in many animals. A lot of information about an animal's status is represented in the complex pheromone components in urine. In mice, detection of such complex chemical signals by the vomeronasal organ (VNO) plays an important role in triggering endocrine changes and eliciting stereotyped innate behaviors. **He *et al.*** (p. 535) developed a system to probe neuronal receptor dynamics using genetically encoded fluorescent sensors. They observed distinct populations of VNO neurons that responded specifically to male and to female urine signals. Mouse strain and individual recognition were determined by combinatorial activation across a population of neurons. Such combinatorial activation was unique, allowing each individual animal to be discriminated and recognized.

Exploiting Surface Phosphatidylserine

Many animals use the presence of the phospholipid, phosphatidylserine (PS), on the outer leaflet of the plasma membrane as a way to recognize and destroy apoptotic cells by phagocytic engulfment. In this issue, two papers illustrate the differential roles played by PS in normal cells and during virus infection (see the Perspective by **Fairn and Grinstein**). **Darland-Ransom *et al.*** (p. 528) identified an enzyme in *Caenorhabditis elegans*, aminophospholipid translocase 1 (TAT-1), which appears normally to restrict PS to the inner side of the plasma membrane. Animals lacking TAT-1 had increased PS on the cell surface and random cells were lost from the animals in a process that depended on PSR-1, a PS receptor involved in the clearance of apoptotic cells. **Mercer and Helenius** (p. 531) used live cell imaging to follow vaccinia virus entry into tissue culture cells. Viruses first bound to actin-rich cell-surface protrusions, filopodia, along which the viruses surfed to the cell body. At the cell body the incoming virus stimulated its own uptake, due to the presence of PS on the viral membrane, mimicking the uptake of apoptotic cell corpses.

Genetics of Schizophrenia

Although complex disorders such as schizophrenia have a heritable component, identifying the genetic components associated has been very difficult. **Walsh *et al.*** (p. 539, published online 27 March) found that multiple, individually rare, structural mutations (genomic microdeletions and microduplications) occurred more frequently in 150 individuals with schizophrenia than in controls. The enrichment was more than threefold among schizophrenia cases generally and more than fourfold among schizophrenia cases with onset by age 18. The genes disrupted by the genomic breakpoints of mutations in the schizophrenia patients were not random, but were disproportionately members of pathways controlling neuronal signaling and brain development.

Animal Self-Sterility Genes

Self-sterility is widely observed among hermaphroditic plants and animals. Although insights have been made for self-incompatibility systems of plants, relatively little is known about animal mechanisms. **Harada *et al.*** (p. 548, published online 20 March) now show that self-sterility in the hermaphroditic chordate *Ciona intestinalis* is controlled by two genetic loci. The self/nonself-discriminating gamete interaction takes place on the basis of allele-specific molecular interactions between fibrogen-like ligands on the egg coat and sperm-borne polycystin 1–like receptors, which are homologs of the causative gene of a hereditary human disease. Genes for the receptors and ligands are linked and are polymorphic, similar to self-sterility genes in plants.

CREDIT: J. MERCER, ETH, ZURICH

Nina Fedoroff is the Science and Technology Adviser to the U.S. Secretary of State and the administrator of the U.S. Agency for International Development.

Seeds of a Perfect Storm

DEMAND FOR PLANT PRODUCTS HAS NEVER BEEN GREATER. MORE PEOPLE, RISING AFFLUENCE, and expanding biofuels programs are rapidly pushing up the prices of grain and edible oil. Boosting supply isn't easy: All the best farm land is already in use. There's an acute need for another jump in global agricultural productivity—a second Green Revolution. Can it happen? Will it happen?

My career has spanned astounding leaps in our ability to decipher and use genetic information to understand and improve crop plants. DNA sequencing methodology was just breaking open when I was a postdoctoral fellow in the mid-1970s. I was able to sequence a complete gene, a goal that had seemed unattainable just a few years earlier, though today it is a routine part of a biologist's toolkit. A chance encounter with the legendary plant geneticist Barbara McClintock drew me into the wonderful phenomenology of maize transposons. I decided to study the molecular behavior of these jumping genes, although there were doubts that plant DNA could even be cloned.

The doubts are gone. We've accumulated vast amounts of plant sequence data, ranging from the complete genomes of rice and the model plant *Arabidopsis thaliana* to extensive collections of gene and genome sequence data from many agricultural plants, including maize, wheat, and soybeans, as well as plants across the plant kingdom, from mosses to trees. Sequence information has profoundly transformed plant genetics and increased its power. Rapid advances in the ability to add genes to plants have made it possible to improve and protect plants in very specific ways. Our growing understanding of how plants handle such stresses as insufficient water and too much heat, salt, or toxic metals permits directed genetic modifications that enhance plants' ability to remain productive under adverse environmental conditions.

So the techniques and knowledge for a new Green Revolution are in hand. The Green Revolution of the 20th century was driven by genetics (mutations that changed plant architecture) and chemistry (fertilizers that increased plants' ability to make sugar out of air and water). It was accomplished by just a handful of plant breeders working on the world's few major grain crops: corn, wheat, and rice. Perhaps the agricultural successes, even excesses, of the past century gave us a false sense of food security.

Last December, the *New York Times* quoted a top United Nations food and agriculture official as saying that "in an unforeseen and unprecedented shift, the world food supply is dwindling rapidly and food prices are soaring to historic levels." Josette Sheeran, executive director of the World Food Program, was quoted as saying: "We're concerned that we are facing the perfect storm for the world's hungry." She said that poor people were being "priced out of the food market." In the months since, there have been food riots in Africa, Asia, the Middle East, the former Soviet Union, and Central and South America.

How did this happen? Genetically modified (GM) cotton and corn with built-in protection from boring insects, and herbicide-resistant soybeans, have been adopted very rapidly in some countries, particularly the United States and Canada, increasing yields and decreasing the use of pesticides and herbicides. But despite a quarter-century's experience and a billion acres of GM crops grown worldwide, there are many nations that remain adamantly opposed to food from plants modified by molecular techniques. Others hesitate to adopt them for fear of losing markets in nations that reject GM technology.

Big grains are only part of the story. There are many food, beverage, and fiber crops, each with its characteristic pests and diseases. Moreover, there are more than 400 million small farms, primarily in the developing world, growing a large variety of crop plants on a small scale, often without the benefit of either genetically improved seeds or fertilizer. A new Green Revolution demands a global commitment to creating a modern agricultural infrastructure everywhere, adequate investment in training and modern laboratory facilities, and progress toward simplified regulatory approaches that are responsive to accumulating evidence of safety. Do we have the will and the wisdom to make it happen? **– Nina Fedoroff**

10.1126/science.1158889

CREDITS: (TOP TO BOTTOM) PENNSYLVANIA STATE UNIVERSITY; PAULA BRONSTEIN/GETTY IMAGES

GEOLOGY

Taper or Channel?

Near the base of the Himalayas, a major fault system (the Main Central Thrust and related faults) is exposed that accommodated the collision and subduction of India into and beneath Asia around 50 million years ago. The metamorphic minerals there record the pressure and temperature conditions before and during the displacement along the thrust; dating of minerals and recognition of zoning or overgrowths provide a time sequence that in turn can be used to infer how the collision and thrusting occurred. Two major models have been proposed, one involving formation and maintenance of a taper extending back from the thrust fault, and the other extrusion through a lubricating channel formed from hot weak crust along the fault. Kohn has synthesized the metamorphic data in rocks near the Main Central Thrust to test these models. Just below the fault, rocks were heated to about 550°C at depths of about 25 km, whereas above it the rocks were heated to about 725°C at depths of ~35 km. The data support the first model over the second, suggesting that the active fault progressively deepened as erosion stripped material from the top of the Himalayan taper. — BH

Geol. Soc. Am. Bull. **120**, 259 (2008).

BIOMEDICINE

Depressing Ceramide

Cystic fibrosis, a genetic disease associated with frequent lung infections and a shortened life span, is caused by a defect in the *CFTR* gene, which encodes a membrane transporter. Although it is not clear exactly how defective *CFTR* links to the symptoms, the mutant protein is known to increase the pH in intracellular organelles. On the basis of results obtained from patients' cells and from mice carrying mutated *Cftr* (which produces a cystic fibrosis–like disease), Teichgräber *et al.* suggest that this rise in pH increases susceptibility to lung infection by altering levels of ceramide, a membrane constituent that can also trigger cell death. The higher pH inhibits the enzyme that breaks down ceramide, and the resulting excess of ceramide increases vulnerability to lung infection. Blocking the biosynthesis of ceramide via acid sphingomyelinase normalizes ceramide levels and, most tellingly, renders the *Cftr*-deficient mice resistant to lung infections. This block can be achieved with amitriptyline (Elavil), a drug approved for treatment of depression. Normalization of ceramide levels in the lungs of patients with cystic fibrosis may be a promising therapeutic approach. — KK

Nat. Med. **14**, 382 (2008).

CHEMISTRY

Gazing Down a Funnel

Because electrons generally move about much more rapidly than nuclei, most chemical reactions are modeled using a framework of potential energy surfaces in which effectively instantaneous electronic transitions between surfaces precede vibrational rearrangements confined to a single surface. However, this framework can break down in certain polyatomic reactions that couple vibrational and electronic motion through a feature linking two surfaces in a cone-shaped, or conical, intersection. Farrow *et al.* use ultrafast spectroscopy to extract the precise timing and details of vibrational coupling as electrons rush down through such a funnel in the energetic landscape after excitation of a square planar naphthalocyanine molecule coordinated to a central silicon moiety. Specifically, they monitor the polarization anisotropy decay of the electronic absorption signal, upon which periodic intensity fluctuations are superimposed that correspond to coherent vibrational motion. Modeling of the data supports a transition time of <200 fs for the relatively modest relaxation energy pertaining in this molecule; the electrons still outpace the nuclear vibrations, though only by a small margin. The data suggest that in chemical reactions with much higher driving forces, transitions through conical intersections could occur within several femtoseconds. — JSY

J. Chem. Phys. **128**, 144510 (2008).

EVOLUTION

Pine Cones, Squirrels, and Crossbills

Selection for coevolutionary adaptations is buffeted by geographical variation in community composition and species interactions. To explore how geographic selection mosaics are influenced by resource variability, feeding specialization, and vagility of interacting taxa, Parchman and Benkman examine interactions in the western United States among ponderosa pine (*Pinus ponderosa*), two allopatric species of tree squirrel (*Sciurus*), and one type of red crossbill (*Loxia curvirostra*). Feeding by western gray squirrels (*S. griseus*) selects for cone traits (such as size) that greatly reduce crossbill use of pine seeds, and crossbill specialization on ponderosa is limited to areas outside the gray squirrel's range. Preferentially foraging on inner bark, Abert's

CREDITS: (TOP TO BOTTOM) PETER BARRETT/ALAMY; ELIZABETH RAHEL

squirrels (*S. aberti*) cut twigs with developing cones, thereby depressing seed supply and lowering the selective impact of crossbills on the pine. Thus, crossbill-ponderosa coevolution is strongest in the absence of both squirrels. But high interannual variation in cone crop encourages the birds to be nomadic and move regularly among areas with and without Abert's squirrels. Such movements prevent strong selection mosaics and the local differentiation of crossbill populations found where they feed on more consistent seed supplies. — ShJS

Evolution **62**, 348 (2008).

IMMUNOLOGY

Skin-Deep Selection

T cells come in two flavors—gamma delta (γδ) and alpha beta (αβ)—that are distinct in function and dispersed differently through the body, with γδ cells defined by a regional distribution of subsets at sites such as mucosa and skin. Boyden *et al.* have identified a gene cluster in mice that influences the development, and likely the function, of γδ T cells in the skin. They linked deficiency of a specific subset of epidermal γδ T cells in a mouse strain to a mutation in a gene named *Skint1* (selection and upkeep of intraepithelial T cells) on chromosome 4. *Skint1* was characterized as a cell surface member of the immunoglobulin supergene family, with two extracellular domains, three transmembrane domains, and a short cytoplasmic tail. The presence of other members of the *Skint* family and the variation in expression between haplotypes point to the rapid evolution of the *Skint* family in mice, although functional orthologs appear to have been lost, possibly more than once, during mammalian evolution. Further work will be needed to establish the contribution of *Skint1* and other members of this family to the immune function of γδ T cells. — SJS

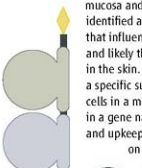

Predicted structure of Skint1.

CREDITS: BOYDEN *ET AL.*, *NAT. GENET.* 40, 10.1038/NG.108 (2008)

Nat. Genet. **40**, 10.1038/ng.108 (2008).

MEDICINE

The ABC's of Herceptin

The breast cancer drug trastuzumab (Herceptin) has been heralded as a breakthrough in translational oncology because its development was based on the detailed characterization of a signaling pathway that promotes tumor cell growth. Trastuzumab is a humanized monoclonal antibody whose antigen-binding domain Fab recognizes a tyrosine kinase receptor (HER2/erbB2) that is overexpressed in some breast cancers, and its anticancer activity is thought to involve disruption of cell proliferation signaling through this receptor. Although some patients with HER2/erbB2-positive breast tumors improve when treated with trastuzumab, about 70% do not respond, and the reasons for this have been unclear.

Musolino *et al.* provide clinical evidence that trastuzumab's anticancer activity may be due, at least in part, to a completely distinct mode of action—antibody-dependent cell-mediated cytotoxicity (ADCC), a process by which immune effector cells such as natural killer cells lyse a target cell bound to an antibody. Studying 54 patients with HER2/erbB2-positive metastatic breast cancer, the authors discovered a correlation between the patients' response to trastuzumab and certain germline sequence variants in genes encoding Fcγ receptors, a class of proteins critically involved in ADCC. These results not only suggest how to predict which breast cancer patients would be most likely to respond to trastuzumab, but also raise the possibility that manipulations aimed at enhancing the drug's capacity to induce ADCC might improve or broaden its clinical efficacy. — PAK

J. Clin. Oncol. **26**, 1789 (2008).

OCEAN SCIENCE

North Versus South

The Atlantic meridional overturning circulation (AMOC) transports shallow, warm water to the north and deeper, cold water to the south. The strength of this circulation, and in particular the amount of heat it transports northward, is thought to have a major influence on climate. Presently, much of the northward surface flow of the AMOC originates as nutrient-rich water from intermediate depths in the South Atlantic, and it has been suggested that those southern waters penetrated less into the north during past cold intervals when the AMOC was weaker. Came *et al.* present a record of the nutrient content of the northward flow of the AMOC over the past 23,000 years, preserved by benthic foraminifera in a sediment core recovered from near Florida, in order to determine how the contribution of southern water varied since the beginning of the last deglaciation. Their data allow them to document in more detail the changes in ocean circulation during the transition from glacial to interglacial conditions, and to illustrate how North Atlantic deep water formation, Antarctic intermediate water production, and North Atlantic climate were linked over that time period. — HJS

Paleoceanography **23**, PA1217 (2008).

www.sciencemag.org

Science

1200 New York Avenue, NW
Washington, DC 20005
Editorial: 202-326-6550, FAX 202-289-7562
News: 202-326-6581, FAX 202-371-9227
Bateman House, 82-88 Hills Road
Cambridge, UK CB2 1LQ
+44 (0) 1223 326500, FAX +44 (0) 1223 326501

Subscription Services For change of address, missing issues, new orders and renewals, and payment questions: 866-434-AAAS (2227) or 202-326-6417, FAX 202-842-1065. Mailing addresses: AAAS, P.O. Box 96178, Washington, DC 20090-6178 or AAAS Member Services, 1200 New York Avenue, NW, Washington, DC 20005

Institutional Site Licenses please call 202-326-6755 for any questions or information

Reprints: Author Inquiries 800-635-7181
Commercial Inquiries 803-359-4578

Permissions 202-326-7074, FAX 202-682-0816

Member Benefits AAAS/Barnes&Noble.com bookstore www.aaas.org/bn; AAAS Online Store http://www.apisource.com/aaas/ code MKB6; AAAS Travels: Betchart Expeditions 800-252-4910; Apple Store www.apple/eppstore/aaas; Bank of America MasterCard 1-800-833-6262 priority code FAA3YU; Cold Spring Harbor Laboratory Press Publications www.cshlpress.com/affiliates/aaas.htm; GEICO Auto Insurance www.geico.com/landingpage/go51.htm?logo=17624; Hertz 800-654-2200 CDP#343457; Office Depot https://bsd.officedepot.com/portalLogin.do; Seabury & Smith Life Insurance 800-424-9883; Subaru VIP Program 202-326-6417; VIP Moving Services http://www.vipmayflower.com/domestic/index.html; Other Benefits: AAAS Member Services 202-326-6417 or www.aaasmember.org.

science_editors@aaas.org (for general editorial queries)
science_letters@aaas.org (for queries about letters)
science_reviews@aaas.org (for returning manuscript reviews)
science_bookrevs@aaas.org (for book review queries)

Published by the American Association for the Advancement of Science (AAAS), *Science* serves its readers as a forum for the presentation and discussion of important issues related to the advancement of science, including the presentation of minority or conflicting points of view, rather than by publishing only material on which a consensus has been reached. Accordingly, all articles published in *Science*—including editorials, news and comment, and book reviews—are signed and reflect the individual views of the authors and not official points of view adopted by AAAS or the institutions with which the authors are affiliated.

AAAS was founded in 1848 and incorporated in 1874. Its mission is to advance science and innovation throughout the world for the benefit of all people. The goals of the association are to: foster communication among scientists, engineers and the public; enhance international cooperation in science and its applications; promote the responsible conduct and use of science and technology; foster education in science and technology for everyone; enhance the science and technology workforce and infrastructure; increase public understanding and appreciation of science and technology; and strengthen support for the science and technology enterprise.

Information for Authors

See pages 634 and 635 of the 1 February 2008 issue or access www.sciencemag.org/about/authors

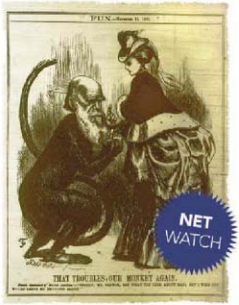

Delving Into Darwin

With everything from his field notebooks to his college admission notice already on the Web, you might think there aren't many Darwin-related documents left to post. But last week, another 20,000 items—previously available only to scholars—were poured onto the Internet by The Complete Work of Charles Darwin Online, hosted by the University of Cambridge in the U.K.

Included in the new stash are background information for his writings, book drafts, and a collection of contemporary caricatures (above). There's also a manuscript of the 1842 essay that first lays out Darwin's evolutionary theory, allowing readers to compare the never-published original with the posthumously released version transcribed and edited by his son Francis. Another item undercuts the standard image of a fearful Darwin concealing his heretical thinking. He originally floated the possibility that species change not in some secret notebook but in a synopsis of his bird collections, "a document intended for somebody else" to read, says the site's curator, Cambridge science historian John van Wyhe.

The additions aren't all hard-core science. Visitors can check out the cream-heavy dishes in his wife's recipe book and browse her diary.

>> www.darwin-online.org.uk

Pets as Toxin-Catchers

Spot and Puff not only lighten our lives, they may also act as canaries in the domestic coal mine, giving early warnings of toxicity from household chemicals, an environmental group reports.

The Washington, D.C.–based Environmental Working Group (EWG) took blood and urine samples from 20 dogs and 37 cats in nearby Virginia and analyzed them for 70 industrial chemicals and pollutants—including heavy metals, fire retardants, stain removers, and plastic softeners—implicated in cancers, thyroid problems, and neurological and other disorders. Among their findings: 35 chemicals in cats, including mercury levels five times as high as in humans, and fire-retardant levels 23 times as high. More than a dozen endocrine toxins may help explain the thyroid disease frequently seen in cats, said EWG scientist Olga Naidenko.

"Pets may well be serving as sentinels for the health of our own children," EWG's vice president for research, Jane Houlihan, said at a press conference. She argued that rising rates of diagnosis of problems such as attention deficit disorder are mirroring "increasing rates of behavioral problems in pets, so much so that there's now Prozac for dogs." The group is pushing for legislation to tighten safety testing for new products.

More Work for The Tooth Fairy

Norwegian scientists are taking environmental toxicology to a new level. They aim to collect milk teeth from 100,000 children in the hopes of detecting links between prenatal and childhood chemical exposure and diseases later in life.

Helene Meyer Tvinnereim, a dental biomaterials researcher at the University of Bergen in Norway, is getting infant choppers from the long-term Norwegian Mother and Child Cohort Study, which collects blood, urine, and detailed medical data from its subjects. "Nobody ever had so much information to connect to teeth," Tvinnereim says. Parents have so far donated dozens of teeth for the study, which she says could become the world's largest tooth bank.

To analyze the teeth, researchers embed them in epoxy and slice them into thin sections. With a laser they remove and vaporize samples from specific layers for chemical analysis. The elements in the enamel form a record of chemical exposure in early life that the study will link to the children's health as adults. The teeth could reveal environmental precursors to diverse disorders including asthma and schizophrenia, says Tvinnereim.

Ellen Silbergeld, an environmental health scientist at Johns Hopkins University in Baltimore, Maryland, says the study—which is facilitated by a streamlined national health-care and record-keeping system—makes American researchers "green with envy."

Compressed Dress

This spray-on dress—which comes completely out of a can labeled Fabrican—is one of the outfits featured at TechnoThreads, "a glimpse into the future of fashion," opening this week at Trinity College's Science Gallery in Dublin. Other fashions on display include "victimless leather" (cells cultured to form a layer of leatherlike tissue on a polymer matrix); a garment fermented from the "skin" generated by adding sugar to Guinness stout; and "Hug Shirts" embedded with sensors that pick up warmth and pressure from the body and transmit them to other hug shirt wearers.

CREDITS: (TOP TO BOTTOM) UNIVERSITY OF CAMBRIDGE; PETER DAZELEY/GETTY; GENE KRIEGEL/© WWW.GENEKRIEGEL.COM

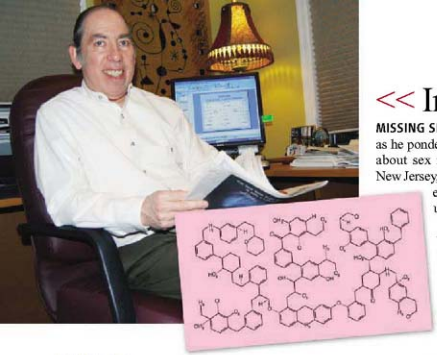

CREDITS: (TOP TO BOTTOM) COURTESY OF ALAN ROSAN; JOON MO KANG; BRUCE DALE/GETTY IMAGES; MIT

<< In Print

MISSING SEX? Carbon atoms can't have five bonds, chemist Alan Rosan thought as he pondered an illustration accompanying a *New York Times* review of a book about sex research. So Rosan, a professor at Drew University in Madison, New Jersey, e-mailed a dart to the paper wondering if the error represented the molecule's wanton desire "to form new, revealing bonding relationships" unheard of "in our more staid and prudish chemistry."

But the joke was on him. The illustration actually spelled the word "sex," pointed out an editor's note accompanying Rosan's letter and a similar complaint from a chemistry graduate student.

Rosan confesses to his mistake. "I tell my students all the time about the difference between looking and seeing. … In this case, I was guilty of not seeing," says Rosan. However, he still thinks that the illustrator could have made the point without breaking the rules of chemistry.

AWARDS

LET'S TRY IT. Alexander Varshavsky has thought of a new way to kill cancer cells, winning $1 million from a new prize that encourages people to share untested ideas in cancer research.

Tumor cells often lose sections of DNA and pass the deletion to their daughter cells. Healthy tissues, however, still have the DNA. Varshavsky, a molecular biologist at the California Institute of Technology in Pasadena, wants to introduce a vector—a small piece of engineered DNA—throughout a patient's body. The vector would code for a toxin to kill cancer cells and for proteins that detect whether a cell contains the deletions. The vector would self-destruct in healthy cells without the deletions.

"I would be very surprised if this strategy ever works all the way to the bedside … in the shape that I suggested," Varshavsky says, noting that the technical details are likely to evolve during actual implementation. Although the award—created by Joel Greenblatt and Robert Goldstein of Gotham Capital—is for personal use, Varshavsky says it will bolster his research, too.

Varshavsky's idea was chosen from more than 500 submitted. A six-member scientific panel also awarded neurosurgeon and entrepreneur Mark Carol the $250,000 Ira Sohn Conference Foundation Prize in Pediatric Oncology for insights into radiation therapy.

MOVERS

BIOWARRIOR. A microbiologist with vaccine industry experience will head a new Department of Health and Human Services (HHS) agency aimed at helping companies combat bioterrorism. Robin Robinson, 52, will be the first director of the 1-year-old Biomedical Advanced Research and Development Authority (BARDA).

BARDA was created by Congress after companies complained about the hurdles to preparing drugs and vaccines for eligibility in BioShield, the federal biodefense procurement program (*Science*, 7 July 2006, p. 28). Robinson joined HHS in 2004 and has been "very successful" at leading the development and stockpiling of the first human vaccine against H5N1 influenza, says Brad Smith of the University of Pittsburgh Center for Biosecurity in Baltimore, Maryland. But BARDA's so far $100-million-a-year budget is a tiny fraction of the $3.4 billion a year that Smith estimates is needed.

DEATHS

EYE FOR DETAIL. The father of modern chaos theory, meteorologist Edward Lorenz, died 16 April in his home in Cambridge, Massachusetts, at age 90. Lorenz had "plain old intelligence [and] was also an extremely persistent scientist. He would not settle for anything less than perfection in his work," says meteorologist Kerry Emanuel of the Massachusetts Institute of Technology, where Lorenz spent his 60-year career.

That trait served Lorenz well in the early 1960s, when he got quite different results from two computer simulations of the weather because of an inadvertent, tiny difference in the simulated atmosphere's starting condition. A decade later, at the annual meeting of the American Association for the Advancement of Science (the publisher of *Science*), he gave a talk with a title that quickly entered popular culture: "Predictability: Does the Flap of a Butterfly's Wings in Brazil Set Off a Tornado in Texas?" Chaos and the atmosphere's exquisite sensitivity to initial conditions permeate meteorology today, from setting the limits of prediction to making the most of the computer's predictive powers.

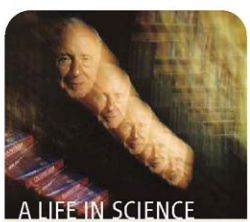

A LIFE IN SCIENCE

UNABASHED. Theoretical physicist John Wheeler, who died on 13 April at age 96, was insatiably curious and not afraid to look foolish, says William Unruh, a theorist at the University of British Columbia in Vancouver, Canada. Unruh recalls how Wheeler spent a year in unsuccessful pursuit of the idea that the uncertainties of quantum mechanics might be related to Gödel's incompleteness theorem, which says that, given a set of mathematically consistent axioms, there are true statements that can never be proved so. "He was like a little boy. He would jump into the stream and turn over the rocks, even if he got his pants wet," says Unruh. That unselfconsciousness extended to Wheeler's personal life, Unruh adds. Wheeler loved the water but never learned to swim. So he would simply array himself in floats and go for a daily dip.

In a career spanning 7 decades, Wheeler helped explain nuclear fission, established general relativity as an essential part of astrophysics and cosmology, and pioneered the study of quantum gravity. A list of students reads like a who's who in gravitational theory.

Got a tip for this page? E-mail people@aaas.org

Resetting the rock clock 434

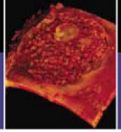

Military regeneration 437

CONDENSED MATTER PHYSICS

New Superconductors Propel Chinese Physicists to Forefront

Hai-Hu Wen went to work as soon as he heard the news. In late February, the 44-year-old physicist at the Institute of Physics (IOP) at the Chinese Academy of Sciences in Beijing learned from a colleague that researchers in Japan had discovered a new superconductor that carried electricity without resistance at a relatively balmy temperature of 26 kelvin. He immediately looked up the paper—via Google—and set his group to work. "We ordered the materials the same day," Wen says. "Within 3 or 4 days, we had the first samples."

Wen's group is one of several in China that, building on the discovery by materials scientist Hideo Hosono of the Tokyo Institute of Technology, has cranked out a new family of high-temperature superconductors, materials that conduct electricity without any resistance at inexplicably high temperatures. Physicists around the world are hailing the discovery of the new iron-and-arsenic compounds as a major advance; the only other known high-temperature superconductors are the copper-and-oxygen compounds, or cuprates, discovered in 1986. Those older materials netted a Nobel Prize and ignited a firestorm of research, but physicists still don't agree about how they work. High-temperature superconductivity remains the biggest mystery in condensed matter physics, and some researchers hope the new materials will help solve it.

"It's possible that these materials will provide a cleaner system to work with, and suddenly [the physics of] the cuprates will become clearer," Wen says. But Philip Anderson, a theorist at Princeton University, says the new superconductors would be more important if they *don't* work like the old one: "If it's really a new mechanism, God knows where it will go."

The torrent of results from China also signals the country's emergence as a power in condensed matter physics, many say. "What surprises me—probably it shouldn't—is the number of good papers coming out of Beijing," says Peter Hirschfeld, a theorist at the University of Florida, Gainesville. "They've really jumped on this."

Structure. Planes of iron (red) and arsenic (gold) interleave with those of oxygen (white) and lanthanum or other elements (blue).

Superconductivity is nature's best parlor trick. Electrons flowing in an ordinary metal lose energy as they ricochet off defects in crystalline material. In superconductors, the electrons experience no such drag. Below a certain temperature, they form pairs, and deflecting an electron then requires breaking a pair. At low temperatures, there isn't enough energy around to do that, so the duos waltz along unimpeded.

What holds the negatively charged electrons together? In an ordinary superconductor, such as niobium chilled below 9.3 kelvin, the "glue" is supplied by vibrations rippling through the material. When one electron moves, it sets off a vibration that drags the second electron in its wake. Most physicists, however, think this cannot explain the cuprates, which work at temperatures as high as 138 kelvin. Each cuprate compound contains planes of oxygen and copper ions. Electrons hop from copper ion to copper ion and somehow pair, although physicists do not agree on how that happens.

Like the cuprates, the new materials are layered, containing planes of iron and arsenic along which the electrons presumably glide (see figure, below). Between the planes lie elements such as lanthanum, cerium, or samarium mixed with oxygen and fluorine. On 23 February, Hosono and colleagues reported in the *Journal of the American Chemical Society* that lanthanum oxygen fluorine iron arsenide ($LaO_{1-x}F_xFeAs$) becomes a superconductor at 26 kelvin. That was a surprise, Hosono says, because iron is magnetic, and magnetism and superconductivity generally don't mix.

Then Chinese researchers jumped in. On 25 March, Xianhui Chen of the University of Science and Technology of China in Hefei reported on the arXiv preprint server (www.arxiv.org) that samarium oxygen fluorine iron arsenide ($SmO_{1-x}F_xFeAs$) superconducts at 43 kelvin. Four days later, Zhong-Xian Zhao of IOP reported on the server that praseodymium oxygen fluorine iron arsenide ($PrO_{1-x}F_xFeAs$) has a "critical temperature" of 52 kelvin. On 13 April, Zhao's team showed that the samarium compound becomes a superconductor at 55 kelvin if it is grown under pressure. Calculations suggest that vibrations provide too little pull to produce such high critical temperatures.

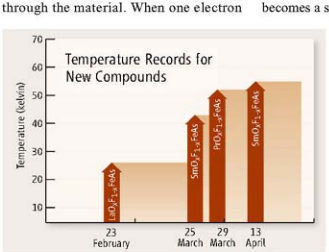

Warming trend. Physicists have quickly bumped up the compounds' highest critical temperature. Some say things may get hotter still if researchers can find crystal structures that pack more iron-and-arsenic planes into a given volume.

At least four different Chinese groups, including three working independently at IOP, have synthesized new compounds and posted results on the arXiv. IOP's Nan Lin Wang says his team was already working on lanthanum oxygen iron arsenide when word came that adding fluorine was key. "We had the materials, the glove boxes, everything was ready," he says. China also has a bumper

CREDIT: (TOP) Y. KAMIHARA ET AL., J. AM. CHEM. SOC. 130 (2008)

Radical cure?
438

Geek cool
442

crop of young researchers and is investing heavily in basic research, he says. IOP has 288 staff members in 50 research groups and a $25 million budget, says Director Yupeng Wang: "We get about 10 new members each year and will keep that pace in the near future." However, he adds, "funding for fundamental research is still quite low compared to Western countries."

The tsunami of results from China has heightened American researchers' worries about the health of condensed matter physics in their country. "What is striking is not only that it's coming out of China but that it's not coming out of the United States," says Steven Kivelson, a theorist at Stanford University in Palo Alto, California. He notes that a U.S. National Research Council report released in June warned that the country is in danger of losing its edge in condensed matter physics as funding stagnates.

All agree it's too early to tell exactly how the new materials work. "The community has to accumulate more data on high-quality samples," Nan Lin Wang says. Don't be surprised if the samples and data come from China first. **–ADRIAN CHO**

PALEOANTHROPOLOGY

When Hobbits (Slowly) Walked the Earth

COLUMBUS, OHIO—Fans of J.R.R. Tolkien know that hobbits walked shoeless on large, hairy feet. Now anthropologists have gotten an eagerly awaited glimpse of the feet of their own hobbit, a meter-tall skeleton from the island of Flores on Indonesia, and the results are almost Middle-earthly. When the discovery was announced in 2004, the world was riveted by the hobbit's astonishingly small brain: 400 cubic centimeters, about the size of a chimp's. At the American Association of Physical Anthropology meetings here (9–12 April), anatomist William Jungers of Stony Brook University in New York revealed that the most controversial member of the human family was strange right down to its soles.

The partial skeleton of the hobbit, a specimen known as LB1 from Liang Bua Cave on Flores, had large, flat feet and a high-stepping gait unlike that of living people; it would have been a poor runner, Jungers said. He argued that the anatomy links the 18,000-year-old hobbit with 2-million- to 3-million-year-old human ancestors from Africa and may offer "a window into a primitive bipedal foot."

The data-rich presentation is part of "a continued drip of [hobbit] analyses done responsibly and carefully" that are illuminating the mystery of what the discovery team considers to be a new species, *Homo floresiensis*, said paleoanthropologist Bernard Wood of George Washington University (GWU) in Washington, D.C. But several hypotheses about the origin of the hobbit are still in play. Some researchers argue that the creature emerged by evolutionary dwarfing from a more recent ancestor. Others note that although discoverers say they have remains of about 12 individuals, so far most of the distinctive anatomy has been described only in LB1, leaving open the possibility that the specimen is a diseased *H. sapiens*. Whatever LB1 is, the new analyses are bringing its anatomy into sharper focus. "We've moved beyond the brain," says Leslie Aiello, director of the Wenner-Gren Foundation for Anthropological Research in New York City.

In Columbus, Jungers showed photos and measurements of the nearly complete left and partial right foot bones of LB1 to a ballroom overflowing with what Aiello calls "hobbit groupies," who flocked to every talk on the subject. Jungers reported that LB1's foot was a whopping 70% as long as its very short femur; living people's feet are only about 55% of femoral length. The "big" toe was "incredibly short," whereas the other toes were quite long, and the shape of the bones suggests that the foot was not arched.

CREDIT: W. JUNGERS/STONY BROOK UNIVERSITY

Not built for speed. Foot bones of the hobbit skeleton suggest that it walked differently from the way we do and was a poor runner.

LB1 would have been a poor runner with a high-stepping gait, according to Jungers, rather like a living person wearing oversized shoes. "Don't bet on *Homo floresiensis* to win a marathon," he said. But the big toe was also stiff, as it is in humans, and was aligned so that the hobbit could "toe-off" as we do when taking a step.

Jungers and his co-authors also compared the shape of the hobbit foot bones with a large database on the foot of people and apes. LB1 sorted not with our species but with African hominins—ancient members of the human lineage—such as *H. habilis* and even the primitive *Australopithecus afarensis*, which is known from about 2 million to 3 million years ago. LB1's femur also resembles the femurs of early hominids when analyzed according to eight standard measurements, Brian Richmond of GWU reported in a separate talk. "It shows just how very primitive the morphology of *H. floresiensis* is," he said.

All this fits with previous data on other parts of the skeleton, Aiello says. Analyses of the jaw, shoulder, wrist (*Science*, 21 September 2007, p. 1743), and most recently, the cranium (*Science*NOW, 17 March: sciencenow.sciencemag.org/cgi/content/full/2008/317/3) put LB1 with *H. erectus* or even earlier African hominins. "It's 18,000 years ▶

old, but it seems to correspond to a grade of hominin that ceased to walk on the Earth a few million years ago," says Wood. "How it got there and managed to persist—that's clearly a challenge to explain."

One explanation is that the hobbit stems from a very ancient migration of a primitive hominin out of Africa. *H. habilis*, for example, had a short stature and a smaller brain than later hominins did, so it's easier to derive something hobbitlike from such an ancestor, Jungers said.

But there's no other evidence anywhere in the world of such an early exodus out of Africa. Such a hypothesis requires "special pleading," says paleoanthropologist Russell Ciochon of the University of Iowa, Iowa City. Australopithecine expert William Kimbel of the Institute of Human Origins at Arizona State University in Tucson agrees. "I'm not ready to go back to the Early Pleistocene of Africa for an ancestor," he says. "That spans a lot of time and space, and I'm not comfortable with those gaps." Ciochon thinks the evidence suggests that a more recent ancestor, perhaps *H. erectus* itself, shrank to hobbit size in an evolutionary dwarfing process.

Brainteaser. Researchers continue to puzzle over why the hobbit's cranium is so tiny.

For other researchers, the whole debate is moot because they view LB1 as simply an aberrant *H. sapiens*. The foot "is such a mixture of characters, requiring very convoluted evolutionary and biomechanical explanations, that a developmental anomaly in a pathological human seems much more parsimonious," says paleopathologist Maciej Henneberg of the University of Adelaide in Australia, a longtime hobbit critic.

A few recent papers have expressed such skepticism. The authors of a controversial report on small-bodied *H. sapiens* skeletons on the island of Palau argue that LB1 could have been a small-bodied *H. sapiens*, too (*Science*NOW, 11 March: sciencenow.sciencemag.org/cgi/content/full/2008/311/1). And several papers have attributed LB1's peculiarities to microcephaly, Laron syndrome, and most recently, cretinism, in a procession Dean Falk of Florida State University in Tallahassee calls

GEOCHEMISTRY

Two Geologic Clocks Finally Keeping the Same Time

First the bedroom clock reassures you that you're right on schedule. Moments later, the kitchen clock tells you that you're running minutes behind. If you find that annoying, pity the geochronologists. For decades, two of their workhorse timepieces—isotopic clocks ticking to the steady decay of two different radioactive elements—have been disagreeing by millions of years.

Now geochronologists have recalibrated one of the clocks, bringing it into agreement with the other. They've tried it before, but this time it looks like the fix will stick. "This is a huge step forward," says geochronologist Mike Villeneuve of the Geological Survey of Canada in Ottawa. "You'd like to see it reproduced, but it looks very solid to me." The synchronization of clocks lends more support to a link between huge volcanic eruptions and mass extinctions.

The clocks in question are argon-argon radiometric dating, based on the decay of potassium-40 to argon-40, and uranium-lead dating, based on the decay of uranium-238 to lead-206. Both techniques have been yielding increasingly precise ages, but argon-argon dating was giving slightly younger ages for the same rocks than the uranium-lead technique. Researchers suspected that they had gotten the decay rate of potassium-40 wrong, but they couldn't really say.

So isotope geochronologists looked around for an absolute measure of passing time to which they could tie their argon-argon ages. They settled on orbital variations, the regular nodding and wobbling of Earth's rotation axis and the changing elongation of its orbit. On page 500, Klaudia Kuiper, now at Vrije Universiteit Amsterdam, and colleagues from Utrecht University, the Netherlands, and the Berkeley Geochronology Center in California report on the latest linking of astronomical variations and argon-argon dating.

They found their chronological connection in 6-million- to 7-million-year-old layered rocks exposed in northern Morocco. Back then, the Melilla Basin was undersea. Orbitally induced climate variations translated Earth's rhythmic orbital variations into marine sediment layers of alternating mineral composition. Astrodynamicists had calculated the subtleties of orbital-variation timing over the ages. That made the Melilla layering a time scale readable with an accuracy of 10,000 years.

At random intervals over the same time period, nearby volcanoes were peppering the sea with ash containing large grains of the mineral sanidine, ideal for high-precision argon-argon dating. The group dated the sanidine grains in a particular layer of ash by noting the layer's position relative to astronomically dated sediment layers. And they measured how far potassium-40 decay had gone in the layer's sanidine grains. Then they compared their measurements with analyses of sanidine in a rock known as the Fish Canyon Tuff, which has long been used as the standard for argon-argon dating

In effect, Kuiper and her colleagues linked the poorly dated Fish Canyon standard to the metronomic astronomical time scale via the volcanic ash of the Melilla Basin. By this astronomical recalibration, the Fish Canyon standard is 0.65% older than had been thought. Recalculate previous argon-argon ages using the standard's new age, and everything ever dated using the technique becomes 0.65% older.

The new calibration "gives us a much better hook to hang our ages on," says Villeneuve. "It's a very nice piece of work," agrees geochronologist Samuel Bowring of the Massachusetts Institute of Technology in Cambridge. "It brings us closer to agreement between argon-argon and uranium-lead, [although] we need to see a lot more of these" studies.

Using their new calibration, Kuiper and her colleagues recalculate some key dates in geologic history. Going back in time, they move the great impact 65.5 million years ago and the accompanying extinction of the dinosaurs to 66.0 million years

CREDIT: DEBBIE ARGUE

"disease of the week." In her talk, she added more data to her rebuttal of Laron syndrome (*Science*, 10 August 2007, p. 740); a cretinism rebuttal is in the works.

At the Columbus meeting, the pathology scenario took a blow from an unexpected source, in a talk by mammalian tooth-development expert Jukka Jernvall of the University of Helsinki in Finland. Jernvall has been working for years on a model of how teeth grow and develop, finding that the first molar sets the template for the size of the second and third. This is true in living people and also for ancient hominins, although the precise relationship among the molars varies somewhat among species.

If development is disrupted, as by an illness, the molar relationship falls apart, says Jernvall. For example, in pituitary dwarfs—one of the syndromes suggested for LB1—the second molar is small as predicted, but the third molar usually doesn't appear at all.

And LB1? Although small overall, it retains the tooth proportions typical of larger bodied hominins, as does a second hobbit jaw, LB6, Jernvall says. "If you look at it from a tooth-development point of view, the drop in size looks like an evolutionary process, not a medical condition," he says.

Critics were unswayed, saying that even if one kind of pathology has been refuted, hundreds of others remain possible. And several experts would prefer not to discuss the whole issue, saying that they're still taking a wait-and-see approach. Given the wildly diverging opinions on the hobbit, "*Somebody's* going to take a big fall here," says paleoanthropologist C. Owen Lovejoy of Kent State University in Ohio. He's waiting for DNA from LB1 or for a second skull. On that, at least, groupies and skeptics agree: All are hoping for another skull when the discovery team returns to dig at Liang Bua this summer.

–ELIZABETH CULOTTA

Tick, tick, tick. The rhythmic layering of sediments in this seaside cliff at Zumaia, Spain, reflects precisely timed variations in Earth's orbit used to calibrate an isotopic time scale.

ago. That shift matters particularly to astronomical daters because they use the impact as a benchmark when working farther back in time. The argon-argon age of the mother of all mass extinctions—the Permian-Triassic—moves from 251.0 million years ago to 252.5 million years ago. The new date puts it precisely at the group's preferred uranium-lead age for the Siberian Traps eruptions, the mother of all volcanic outpourings. That supports the claim that the eruptions could have triggered the extinction (*Science*, 17 September 2004, p. 1705).

Older argon-argon ages would likewise make another of the big-three mass extinctions—the Triassic-Jurassic—coincide precisely with the great volcanic outpourings of the central Atlantic magmatic province. That's according to a new uranium-lead age that places the extinction at 201.6 million years ago, as published by geochronologist Urs Schaltegger of the University of Geneva, Switzerland, and colleagues in the 1 March issue of *Earth and Planetary Letters*. So a fraction of a percent multiplied by geologic time can make a difference.

–RICHARD A. KERR

CREDIT: K. F. KUIPER ET AL., SCIENCE

ID at the Box Office

A new film that links Darwinism and Nazism and accuses the scientific community of bullying proponents of intelligent design (ID) grossed $2.9 million at U.S. theaters over the weekend, ranking fourth among newly released movies. But Glenn Branch of the National Center for Science Education (NCSE) in Oakland, California, predicts that Ben Stein's *Expelled: No Intelligence Allowed* won't affect public attitudes toward evolution. NCSE debunks many of the movie's claims at www.expelledexposed.com.

David Beckwith, an aerospace engineer in suburban Maryland who took his family straight from an evangelical church service to see the show, says he buys the film's claim that persecuting those who question Darwinism is an attack on academic freedom. "I am more convinced than ever that there are a lot of scientists who think intelligent design should get a fair hearing," he says. But a recent college graduate who says she's politically conservative but not religious says she was disappointed that the movie did not "present any arguments in support of intelligent design."

–YUDHIJIT BHATTACHARJEE

Small Business Looms Large

A planned 20% increase in a $2-billion-a-year program to promote research by small companies through a tax on current budgets is moving rapidly through Congress, even as scientists complain that federal basic research is strapped for cash.

This week, the House of Representatives was expected to approve a bill that would boost the share set aside for the Small Business Innovation Research (SBIR) program from 2.5% to 3% of an agency's budget. Some 11 federal agencies operate the program, begun in 1982 to help commercialize basic research discoveries. Although academics with start-up companies are part of the intended audience—companies with fewer than 10 employees receive 30% of the competitive awards from the National Science Foundation, for example—most science lobbying groups have long viewed it with suspicion. The Bush Administration also opposes any increase in the set-aside, which was last raised in 1995. "This is the wrong time to do it," Representative Vern Ehlers (R–MI) argued unsuccessfully last week as a House science subcommittee marked up its bill, which the next day was folded into a nearly identical version approved by the small business committee. In the Senate, a companion bill that would boost SBIR's share to 5% is temporarily stalled.

–JEFFREY MERVIS

FACILITIES

Europe Takes Guesswork Out of Site Selection

Picking a home for a large international research facility is usually fraught with tension. Political alliances hold sway over technical considerations, and deals are often struck during whispered conversations in the corridors of government (*Science*, 19 October 2007, p. 380). But hoping to teach politicians how to make a decision that is best for the science, the three cities vying to host a €1 billion neutron beam research center called the European Spallation Source (ESS) will this week submit bids to a specially created, independent panel of "wise people." "Rational criteria are better than the handshake of two powerful people," says Colin Carlile of Lund University in Sweden, director of the ESS-Scandinavia consortium.

The assessment panel won't choose a winner or rank the candidate sites, but it does represent the start of an effort for European science to avoid the horse-trading that takes place now whenever a proposed facility needs a home. "Europe as a whole should have a mechanism to choose sites," says Peter Allenspach of Switzerland's Paul Scherrer Institute, chair of the European Neutron Scattering Association.

Fifteen years ago, Europe was preeminent in the science of neutron scattering with the world's top two neutron sources sited in France and the United Kingdom. Neutrons are subtle probes that penetrate to the heart of materials and reveal where atoms are and what they do. Neutron beams are used by, among others, physicists, materials scientists, crystallographers, and biologists. Throwing them requires either a nuclear reactor or a particle accelerator to fire a beam of protons at a fixed target, knocking out neutrons—a process known as spallation.

European neutron researchers had a plan to keep their lead: They would build a next-generation spallation source so big it would need to be an international facility. The design and cost estimate were finished by 2002, but European politicians never became convinced a new facility was needed. The project foundered and its central project office closed in 2003. Meanwhile, the United States built the Spallation Neutron Source in Tennessee, and Japan built a source as part of its nearly complete J-PARC facility at Tokai.

ESS was given new impetus, however, by the European Strategy Forum on Research Infrastructures (ESFRI), a body tasked by the European Union with drawing up a list of planned large facilities that E.U. nations should work together on. ESS was one of 35 projects in the first ESFRI road map released in 2006 (*Science*, 27 October 2006, p. 580). Three cities were soon vying to host ESS—Lund in Sweden, Bilbao in Spain, and Debrecen in Hungary—and seeking allies. The Lund team is building an alliance of five Scandinavian nations, the three Baltic states, and Poland. Debrecen is working on its central European neighbors (including Poland) as well as Russia. And the Debrecen and Bilbao teams pledged to support each other should one of them have a face-off with Lund.

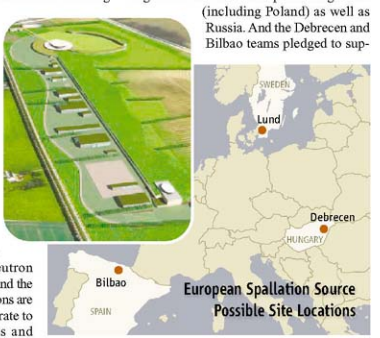

Face-off. After 15 years of planning, researchers are ready to build the European Spallation Source. The three candidate sites must gather support from other nonbidding governments to spread the cost of construction and operation.

ESFRI, which was last year developing a general strategy for deciding on the sites of international facilities, saw a chance to help. The candidates were not from one of Europe's science powerhouses, and none was gathering support from other countries fast enough. "It was a race, but no one had defined the distance or how long it should run. The winner would emerge when the other two were exhausted," Carlile says.

In February, ESFRI sent a 50-page questionnaire to the candidates, asking about issues such as nearby research centers, local infrastructure, economics of the bid, and political support within the host country and its neighbors. The bidders were due to submit their answers on 25 April. An ESFRI working group also drew up criteria for judging the sites and a long list of potential assessors—authoritative neutral figures with science policy backgrounds or experience constructing or building large user facilities. All three cities were asked to approve the criteria and assessors. Now that the questionnaires are in, the ESFRI group will select three to five of the evaluators to analyze the answers and visit the sites. "The wise people will express their opinions on how well the criteria are met," says Carlo Rizzuto, president of Italy's Trieste Synchrotron and ESFRI chair.

What happens after ESFRI receives those opinions in September is far from clear. The horse-trading between potential partner states, now armed with more detailed briefs, will likely begin again. "The report will give the criteria, but politicians will put their own weighting on those criteria," says John Wood of Imperial College London, former ESFRI chair. Many involved hope the ESFRI assessment will nonetheless speed the process, allowing a site decision by an E.U. meeting on research infrastructures at the end of this year.

Although ESS may be entering its endgame, other European facilities, including a high-powered laser called the Extreme Light Infrastructure, are just starting to look for a home. Will the ESS strategy help those contests? Most scientists agree that the ESFRI process will be beneficial but say that it would be better if governments cede some authority to a pan-European body that plans out, and even funds, the region's research facilities. A few fields already have such a body, such as ESA for space science, says Rizzuto, but in others "there is not yet an institution capable of strategic planning." Some hope that the newly formed European Research Council could take on that role.

Neutron researchers are just looking forward to a new place to call home. Says Carlile: "This has been on the go for 15 years now. I want to refocus our energy onto the project itself." —DANIEL CLERY

CREDIT (INSET): ESS SCANDINAVIA

REGENERATIVE MEDICINE

Rebuilding the Injured Warrior

In an initiative to speed treatments for wounded soldiers, the U.S. Department of Defense (DOD) is entering the fast-growing field of regenerative medicine. Over the next 5 years, at least $250 million will be funneled into two university-led consortia that compose the new Armed Forces Institute of Regenerative Medicine (AFIRM), DOD announced last week.

AFIRM will focus on regrowing severed fingers, recreating shattered bones, reconstructing mutilated faces, and covering burn victims with genetically matched skin. "We hope to get products into patients within 5 years," says tissue engineer Anthony Atala of Wake Forest University Baptist Medical Center in Winston-Salem, North Carolina, co-director of one consortium led by Wake Forest and the University of Pittsburgh in Pennsylvania.

Last year, Atala reported isolating from amniotic fluid highly versatile stem cells (*Science*, 12 January 2007, p. 170), which are likely to figure prominently in the new technologies. Embryonic stem cells or their equivalents aren't in the mix here. Rather, says Atala, the focus is on getting rapidly to the clinic, using cells that can get quick Food and Drug Administration approval.

DOD decided 2 years ago that it was time to make a major commitment to regenerative medicine treatments, largely at the instigation of dental researcher Robert Vandre, director of combat casualty care research at the U.S. Army Medical Research and Materiel Command at Fort Detrick, Maryland. Vandre says he originally managed to round up a commitment for $8.5 million a year, including $500,000 a year from the U.S. National Institutes of Health (NIH). Then after receiving competitive proposals for a single consortium, he got a call "out of the blue" from the White House, which ended up telling DOD to double the funding from $42.5 million to $85 million over 5 years. That made it possible to fund two consortia that had come in neck-and-neck in the competition. Vandre, who is AFIRM's DOD manager, says the 5-year total should top $265 million, including $80 million in public and private funds to match DOD's input and some $100 million in NIH grants already held by researchers in the consortia's 28 research groups.

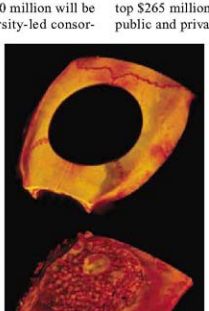

Bridging the gap. Defective rat skull (*top*) shows bone formation 12 weeks after implant of scaffold with bone growth factors (*bottom*).

CREDIT: COURTESY OF J. S. PATEL, S. YOUNG, AND A. G. MIKOS/RICE UNIVERSITY

A top priority will be engineered skin that can be quickly grown to treat burn victims. Atala points out that at present there is "no real skin replacement" because skin grafts from cadavers are prone to rejection; supply is also short. One of the earliest fruits of the venture may be a method to grow a patient's own skin rapidly enough to use as a graft for life-threatening burns. Ultimately, says chemist Joachim Kohn of Rutgers University in New Brunswick, New Jersey, co-head of the other consortium, led by Rutgers and the Cleveland Clinic in Ohio, "you could take a skin sample from every soldier in danger zones and store it" so that the moment a soldier is injured, people back at the Army medical center in San Antonio, Texas, could start growing a graft.

Another major focus is on "compartment syndrome": internal muscle trauma from blast or other injuries that results in rapid swelling of arm or leg tissues so they compress nerves and blood vessels. If not treated swiftly, muscles die, and amputation is often necessary, says Kohn, who adds that so far the Iraq war has resulted in about 800 amputations. Other high priorities are wound healing, cranial-facial reconstruction, and regrowing severed fingers and toes.

"I'm fighting the perception that we will regrow limbs and heads and arms," says Kohn. Rather, "what we want to do is take our ability to grow 2 inches of bone and extend it into 6 inches of bone. … We are pushing the border of where limbs can be salvaged further and further out."

–CONSTANCE HOLDEN

Grass-Roots Malaria Funding

Even small donors can now support malaria research using a new Web site that connects them with African scientists. The site, MalariaEngage.org, provides descriptions of research projects. Donors can contribute as little as $10 to a specific project and follow its progress online.

Peter Singer and Abdallah Daar of the McLaughlin-Rotman Centre for Global Health in Toronto, Canada, teamed up with Tom Hadfield, a successful entrepreneur and Harvard University undergraduate, to create the site with $200,000 from Genome Canada and the Bill and Melinda Gates Foundation. Scientists at the National Institute for Medical Research in Dar es Salaam, Tanzania, selected the first seven featured projects and will oversee the donations. Singer says the goal is to ensure that good ideas "aren't flushed down the drain for lack of capital." –ELSA YOUNGSTEADT

A Step Too Far Ahead?

Japan is planning to vaccinate 6000 health care and quarantine workers against the deadly H5N1 virus. The workers will get one of two killed, adjuvanted vaccines derived from different strains in a pilot project that, if successful, could lead to the vaccine being given to 10 million people considered at risk of exposure to a pandemic virus.

The scientific community is split on the idea of vaccinating before a strain emerges. Peter Palese, a virologist at Mount Sinai School of Medicine in New York City, supports more research but adds that "vaccinating humans with a vaccine against a disease which might never materialize in humans is probably not appropriate." –DENNIS NORMILE

A NIFty Idea

A coalition of science policy wonks has proposed a federally funded National Innovation Foundation (NIF) to bring order and leadership to current efforts. "There's nobody in the government who wakes up every morning and says, 'My job is to drive innovation in the U.S. economy,' " says Robert Atkinson of the Information Technology & Innovation Foundation in Washington, D.C., who co-authored a paper with the Brookings Institution's Howard Wial that is offered as advice to the next Administration.

The $1-billion-a-year entity, modeled perhaps on the National Science Foundation, could also provide one-stop shopping for states, says Ray Scheppach, executive director of the National Governors Association in Washington, D.C. –JEFFREY MERVIS

Bypassing Medicine to Treat Diabetes

By altering the gut's production of hormones, gastric bypass surgery may be able to eliminate type 2 diabetes. But scientists worry that this radical operation can also cause dangerously low blood sugar

IN 1980, BARIATRIC SURGEON WALTER Pories of East Carolina University School of Medicine in Greenville, North Carolina, performed his first gastric bypass surgery on an obese patient with type 2 diabetes, then a second, then a third. He noticed right away that the patients no longer needed insulin. Family doctors confirmed that what Pories had considered a transient phenomenon seemed like something more: Each person's diabetes had disappeared, even before they'd lost much weight. Pories was convinced that the doctors had erred. "I said, 'You guys don't know how to work up diabetes. Diabetes is an incurable disease.' " After the fourth patient, Pories and an endocrinologist took matters into their own hands. "We marched right down to the lab, very self-righteous," and accused the lab employees of incorrectly measuring blood sugar levels. ("If you're a doctor, you like to blame other people," Pories explains.)

As the number of patients with vanishing diabetes mounted, Pories recognized that the effect was real. Still, the concept that diabetes could be reversed surgically was so outlandish, he says, that "we didn't dare publish" the results. Instead, Pories began tracking his patients. In 1995, he reported in the *Annals of Surgery* that among 146 people with diabetes who had had the surgery in the past 14 years, 121, or 83%, had quickly become diabetes-free. The result was far superior to that achieved by any other treatment at the time—or now.

"The surgical world noted that paper," says endocrinologist David Cummings of the University of Washington, Seattle. But it took "another 10 years for the rest of us" to catch up, he says. Now, endocrinologists are beginning to pay close attention to the effects of gastric bypass surgery, which had long been a backwater of medicine, in part because obesity was not considered a genuine disease.

As America and other countries confront surging rates of obesity, with few treatments that shrink the widest waistlines, the surgery's popularity is soaring. The most common form in the United States, Roux-en-Y gastric bypass, was performed on more than 120,000 people in 2007, according to estimates. That's almost double the number 5 years ago. Doctors often learn from their patients, and the hundreds of thousands of people who have had gastric bypass surgery are now prompting an overhaul in our understanding of metabolism and diabetes. Scientists are also going back to animals to figure out the impacts of the procedure. They are finding that the surgery's rerouting of the intestines and closing off of much of the stomach appears to have drastic effects on gut hormones and disease, independent of the weight loss that accompanies it.

These effects can also have dire consequences. Beginning in 2000, F. John Service, an endocrinologist at the Mayo Clinic in Rochester, Minnesota, began seeing patients with some alarming symptoms: confusion, abnormal behavior, seizures, and unconsciousness. In each case, the culprit was a low level of blood sugar that struck after eating, which is when it rises in healthy people. Every patient, it turned out, had undergone gastric bypass surgery months or years earlier. The Mayo Clinic now sees at least two new patients a month with this unusual hypoglycemia disorder, which was the topic of a meeting at the Joslin Diabetes Center in Boston earlier this month.* As a last resort, surgeons have removed part or even all of the pancreas, which churns out insulin, from many of these patients.

How to decipher and harness the surgery's metabolic effects is prompting much debate. On the one hand, some surgeons are already operating on less obese people with diabetes as a treatment for that disease. But others would prefer to wait until the science catches up, especially because the surgery isn't harmless, with a death rate ranging from 0.1% to 2%, depending on where it's performed. "Surgeons have for too long acted in a vacuum. ... Most of them aren't thinking about the mechanisms of what they're doing," says John Dixon, an obesity researcher at Monash University in Melbourne, Australia. "But we need to dissect out" what's happening in these patients.

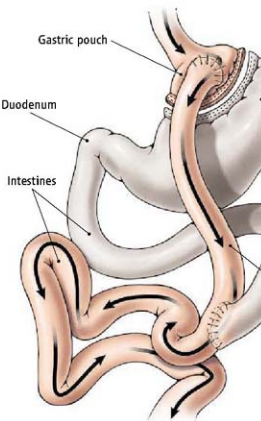

Unintended effects. Roux-en-Y gastric bypass surgery reduces the stomach to a fraction of its original size and skips past part of the small intestine, which causes profound metabolic changes in the gut.

CREDIT: C. BICKEL/SCIENCE, ADAPTED FROM DEMARIA, *NEW ENGLAND JOURNAL OF MEDICINE* 356, 21 (2007)

Early clues

Gastric bypass was inspired by similar intestinal operations employed for ulcers and gastric cancer that induced dramatic and enduring weight loss and were reported to reverse diabetes as far back as the 1950s. "As soon as we started doing the operation, we were aware of the fact that before the patients got out of the hospital, they no longer needed insulin," says Edward Mason, a retired surgeon from the University of Iowa in Iowa City who developed the procedure for weight loss. Most current forms of gastric bypass,

*"Hyperinsulinemic Hypoglycemia Following Gastric Bypass: Pathogenesis and Treatment Symposium, Boston, Massachusetts, 7 April.

Beyond fat. From the early days, doctors recognized that for many patients, diabetes vanished after gastric bypass.

CREDIT: NDLAS UNLIMITED/CORBIS

and Mason's original operation, have one element in common: A newly created exit from the stomach is reconnected to a piece of small intestine a few feet lower down, "bypassing" the upper portion of the small intestine. In addition, the stomach is drastically restricted, by about 95%. (Another weight-loss surgery, gastric banding, seals off most of the stomach but leaves the intestines intact and is not considered gastric bypass.) Today, most gastric-bypass patients shed 30% of their body weight and keep it off.

Mason, now 87 years old, recalls that he and others explained away the reversals of type 2 diabetes because their patients weren't eating right after surgery, which would lower blood glucose levels and, in turn, their need for insulin. (The surgery does not have the same effect on type 1 diabetes, in which afflicted individuals cannot produce insulin.) But Pories's study years later slowly began to convince people that something more fundamental was occurring.

Almost a decade later, a second report strengthened the case. In 2003, Philip Schauer, a bariatric surgeon now at the Cleveland Clinic in Ohio, published follow-up data from 1160 obese people who in the preceding 5 years had undergone Roux-en-Y gastric bypass, which gets its name from a French surgeon who developed the technique. Of the 191 people with diabetes or impaired glucose metabolism who could be tracked down, 83%, precisely the figure reported by Pories, no longer had the problem.

Although impressive, it's not yet clear if these success rates will hold up in clinical trials. These are "typically the observations of a single surgeon or group of surgeons" and "very anecdotal," says David D'Alessio, an endocrinologist at the University of Cincinnati in Ohio.

Getting at biology

After years of absence, science is slowly making inroads into gastric bypass surgery. "The development of the field was not based on real research," says Francesco Rubino, a bariatric surgeon at Weill Cornell Medical College in New York City. "That has tarnished the field somewhat."

"Surgeons have for too long acted in a vacuum. ... Most of them aren't thinking about the mechanisms of what they're doing."
—JOHN DIXON, MONASH UNIVERSITY

Recently, however, a growing number of studies are suggesting that the surgery has a profound effect on gut hormones, which could explain its impact on appetite, diabetes, and the low blood sugar that's turning up. One of the first clues emerged in 2002, when Cummings looked into a well-recognized oddity. Gastric bypass restricts the stomach, forcing people to eat smaller meals. One might then expect "that people would be compelled to sip milkshakes all day long," says Cummings. That's not what happens. Many move away from calorie-dense foods altogether.

Curious, Cummings began examining levels of ghrelin, a hormone produced mainly by the stomach that stimulates appetite. Most people have peaks and valleys in ghrelin levels throughout the day as they consume meals and then become hungry again. In those who've had gastric bypass, Cummings found, ghrelin levels in blood were low and changed little all day, suggesting that something about the surgery dampens ghrelin production and hence appetite.

The role this plays in diabetes resolution has not been firmed up, and researchers are now more closely examining how gastric bypass affects other hormones. Rubino's work, for example, has focused on the intestines, which produce a different suite of chemicals and hormones from those the stomach churns out. In 1999, Rubino turned to rats to examine whether the surgery's effects on diabetes were due to calorie restriction and weight loss alone. He tried to tease apart distinct features of his "patients"—the rats, in this case—and different features of surgery. When performed on lean animals with type 2 diabetes, gastric bypass had the same positive effects on the diabetes as in obese ones, suggesting that weight loss was largely irrelevant. Furthermore, Rubino performed the

intestinal bypass portion of the operation, skipping past the duodenum and the jejunum that link up to the stomach, but leaving the stomach intact. There was a "direct antidiabetic effect," he says.

Rubino's rat work dovetails with a popular theory: that a hormone produced by the intestines called glucagon-like peptide 1 (GLP-1) lies behind the vanishing diabetes in many gastric bypass patients—and may be linked to the hypoglycemia that later strikes others, most of whom did not have diabetes before the surgery. The GLP-1 theory is that the small intestine goes into overdrive making hormones in gastric bypass patients. Because of the surgical rerouting, food "empties directly into this part of the intestine that it normally wouldn't see at that stage" of digestion, says Mary-Elizabeth Patti, an endocrinologist at the Joslin Diabetes Center.

In healthy people, GLP-1 has a variety of effects, including increasing insulin secretion, and a diabetes drug on the market, called Byetta, mimics the effects of GLP-1. Physiologist April Strader of Southern Illinois University in Carbondale is now performing an intestinal surgery in rats that leaves the stomach intact and prompts the animals to secrete more GLP-1. Strader is examining whether that in turn causes proliferation of insulin-producing cells in the pancreas.

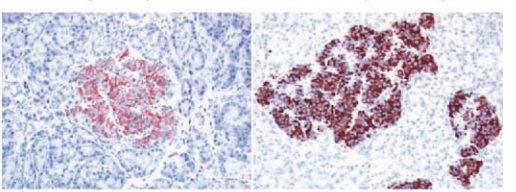

Insulin overload? An islet in the pancreas (*left*, red) appears larger in a gastric bypass patient (*right*) who suffers from dangerously low blood sugar, but scientists dispute whether the surgery changes that organ.

Linking the good and bad

GLP-1's impact on the pancreas may also explain the hypoglycemia originally seen by the Mayo Clinic. One sharp contrast between the disappearance of diabetes and the hypoglycemia stemming from the surgery is that the former occurs immediately or within weeks, whereas the latter takes several years to show up. At the Boston meeting, the 40 or so surgeons, endocrinologists, pathologists, and others gathered there admitted that they couldn't explain this but wondered whether changes to the pancreas over time generated the low-blood-sugar problems, whereas diabetes improvement might be due to other nonpancreatic effects.

When Service and his Mayo colleagues examined the pancreatic tissue removed to help their hypoglycemic patients, they noted islets that appeared larger than normal. Joslin researchers have also reported an excess of insulin-producing cells in three hypoglycemic patients, two women and a man, who had a portion of their pancreases removed. The hypoglycemia is "diabetes reversal in people who don't have diabetes," says Patti.

D'Alessio is now trying to study GLP-1 in people who have had gastric bypass surgery and are suffering from hypoglycemia to determine whether the hormone might induce such pancreatic changes. But not everyone agrees that gastric bypass surgery alters the pancreas. Peter Butler, an endocrinologist at the University of California, Los Angeles, examined the pancreases from Mayo at Service's request and found that they looked like pancreases from obese individuals. He attributes this difference of opinion to his more extensive analysis, which did not identify an upsurge in insulin-producing cells.

Butler did make one intriguing find, however. Obese people tend to produce more insulin over time to accommodate the growing amount of tissue that requires the hormone. Based on the appearance of the islet cells, Butler deduced that the gastric bypass pancreases hadn't made the adjustment to their host's new weight: They were still producing just as much insulin as before the surgery, effectively increasing the insulin available. That this occurs after meals would make sense, because this is when the pancreas normally releases extra insulin. In these patients, the insulin they secrete would far exceed what's needed.

Stephen Bloom, an obesity researcher at Imperial College London, notes that it's far from clear whether GLP-1 has the same effect on human pancreases as it does on those of rodents. Furthermore, the small intestine secretes dozens of hormones, many of them poorly understood. "It's still too soon to rule out everything else," says Strader. Rubino agrees that researchers need to think expansively. Instead of largely undigested food stimulating hormone secretion from the intestines it's dumped into, it's possible that when food does not touch the walls of the duodenum, as happens in gastric bypass, that has hormonal effects of its own. Rubino says his recent findings in animals suggest such antidiabetic effects.

Surging popularity

As research picks up pace, gastric bypass surgeries continue unabated, and some surgeons, particularly outside the United States and Europe, are beginning to operate on less obese patients with diabetes. Bariatric surgery is "kind of the Wild West," says D'Alessio. There's "huge demand, no regulation, everybody's got their own operation, [and] patients are willing to do whatever it takes to get it."

Currently, U.S. National Institutes of Health guidelines recommend that gastric bypass surgery be considered only for people who have a body mass index (BMI) of at least 35. (A BMI of 18.5 to 25 is considered normal.) At a meeting in Rome last year, 78% of attendees supported lowering the limit to a BMI of 30 for those with diabetes. Should the number be even less? "We need more data to know if a lower bar is okay or if there should be any bar at all" when the goal is diabetes treatment, says Cummings.

But many still view gastric bypass as extreme therapy for diabetes. Some who undergo the operation have serious problems, such as infections, gallstones, and hernias, that can require additional surgery. And given the time lag between gastric bypass and the severe hypoglycemia that Service, Patti, and others are just now documenting, no one knows how prevalent the side effect will be nor how much such patients will affect the cost-benefit analysis. The death rate from gastric bypass surgery also scares many diabetes researchers. "We had a death in a 28-year-old recently; she had a complication but didn't want to come to the hospital," says Bloom. "When you see that and have to go to the funeral, you don't think it's such a harmless procedure."

Yet type 2 diabetes isn't harmless, either, contributing to more than1 million deaths worldwide each year. "There is a barrier we need to get over" in considering gastric bypass as a diabetes treatment, says Rubino. He points to a paper published last summer, concluding that the surgery reduces diabetes deaths by 92%. "It's the most profound effect in terms of mortality from diabetes ever reported," Rubino says. "What is the price of that?"

–JENNIFER COUZIN

CREDITS: SERVICE *ET AL.*, *NEW ENGLAND JOURNAL OF MEDICINE*, **313**, 3 (2005)

ARCHAEOLOGY

Japanese Experts Steal a Glance At Once-Taboo Royal Tomb

Japan's key-shaped burial mounds offer tantalizing glimpses into prehistory. Researchers have been given access for the first time to those built for the imperial family

NARA, JAPAN—From a nearby street, the wooded hill beyond the pond looks ordinary. But looks are deceiving at Gosashi Kofun. Centuries ago, earth was deliberately mounded into tiers, in a keyhole pattern, and surrounded by a moat to serve as the final resting place of a powerful person, perhaps the legendary 3rd century Japanese empress Jingu. But just who was buried there, and when, are among a host of questions that archaeologists and historians hope to resolve. Other unknowns include how the kofun (mounds) were constructed and what clues they give about society and religion in an era just before written records appeared in Japan.

Kofun raiding. Koji Takahashi and colleagues got a first glimpse at a 2000-year-old imperial burial mound, Gosashi Kofun (obscured by trees).

Gosashi Kofun and some 900 other sites presumably holding the remains of imperial family members promise a tantalizing peek into a formative period in Japan's early days as a nation. "The imperial tombs are a very important resource for understanding Japanese history," says Koji Takahashi, an archaeologist at Toyama University. But for more than a century, the imperial mounds—the cream of Japan's 30,000 known kofun—have been off-limits to prying eyes. Last February, 16 researchers were for the first time permitted a direct look at Gosashi Kofun. At a symposium here earlier this month, they shared their impressions and recounted the outstanding questions.

Burial mounds, or tumuli, are found throughout the world. Only in Japan do they come in a distinctive keyhole shape. A typical keyhole-shaped kofun has a high, circular, rounded mound at one end containing the burial site, a stone chamber entered through a passageway cut into the mound. Early sites contain a simple pit. The other end of the keyhole usually has a lower platform that may have been used for funerary rites. The largest kofun cover more area than Egypt's largest pyramids, though they are not as high. Often the mounds are studded with arrangements of terra cotta sculptures, or haniwa, that range from simple cylinders to figures including armored warriors, animals, boats, and household implements. The purpose of the haniwa is not fully understood. But their embedded cylindrical bases may have helped stabilize mound slopes.

The appearance of kofun marked the emergence of an aristocratic state with considerable wealth and military power. Mounds were de rigueur for rulers and clan chieftains during the 300-plus years of Japan's Kofun Period, beginning in the middle of the 3rd century. In the absence of written histories, burial goods and haniwa are indispensable sources of information about societal structure, as well as contemporary weapons, tools, and clothing. The presence of exotic items such as bronze mirrors, armaments, and pottery from mainland Asia attest to brisk commercial, cultural, and even military ties between Japan's chiefdoms and kingdoms on the Korean peninsula and China.

Although archaeologists have explored many kofun, the largest and most elaborate are the 900 associated with the imperial family. Since the 1970s, researchers have petitioned the Imperial Household Agency for access. But, aside from allowing a few researchers to occasionally accompany maintenance crews, the agency rejected the requests on the grounds of preserving the "peace and dignity" of the graves.

Then something surprising happened: The imperial agency relented. Early last year, in response to a petition from 16 academic societies, the agency agreed to allow entry onto an unspecified number of mounds. After a year of negotiations, the first visit took place on 22 February, when one representative from each of the 16 societies was permitted to examine the lower part of Gosashi Kofun. The researchers were not allowed to ascend to the burial site or upper levels, do any digging, or collect artifacts. They were permitted to make drawings and take notes and photos, though they were asked not to make the photos available to the press.

Most of the discussion at the symposium centered on where Gosashi fits into kofun evolution based upon minutiae such as the number of tiers and the precise shape of the corners of the lower platform. Fumiaki Imao, an archaeologist at the Nara Prefectural Archaeological Institute in Kashihara, says that better dating of kofun and the order in which they were built may yield clues as to the location of the seat of power at a given time, the dates when rulers reigned, and who is interred in which tomb. The unprecedented inspection of Gosashi added to the list of questions. The researchers stumbled upon the partially embedded remains of a line of cylindrical haniwa along the moat. "This is such an unusual location, I wonder why it was placed there," says Imao. Haniwa have typically been found on top of mounds.

Whether these haniwa are peculiar to Gosashi or a regular feature of imperial mounds of this period might be answered if researchers win more access to the kofun. Takahashi says the Imperial Household Agency has agreed in principle to allow more visits. The next could take place toward the end of this year. Which tomb, how many researchers, and the ground rules for the inspection are to be negotiated with the agency this summer.

Experts at the symposium also discussed what kind of access to request. As a first step, most would like to see more accurate mapping of the mounds. For now, no one is talking about entering the hallowed imperial burial chambers. Some 2000-year-old secrets are not about to be revealed.

–DENNIS NORMILE

CREDITS: D. NORMILE/SCIENCE

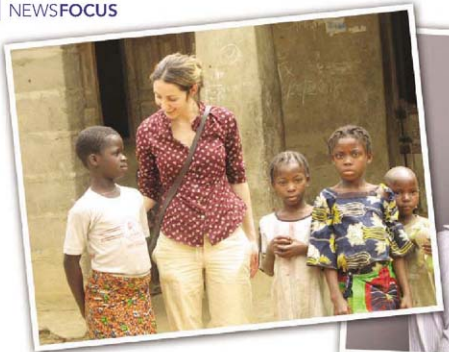

PROFILE: PARDIS SABETI

Picking Up Evolution's Beat

Pardis Sabeti mixes geek cool with hot science as she studies how human populations have evolved to resist malaria and Lassa fever

CAMBRIDGE, MASSACHUSETTS—Over the past 72 hours, Pardis Sabeti has managed only 2 hours of sleep each night, most of them inside a crumpled blue sleeping bag she keeps under a desk at the Broad Institute Center for Genome Research in Cambridge, Massachusetts. Sabeti, who burst on the scientific scene in 2002 with a novel test for natural selection in the human genome, has been racing to meet the submission deadline for a National Institutes of Health (NIH) grant to support her research on the evolution of resistance to malaria and Lassa fever. Also in her schedule this year: serving as a panelist at the World Economic Forum in Davos, Switzerland; a research trip to Africa; speaking to young women about careers in science; and writing songs and recording for her pop/rock band.

To manage all this, Sabeti, 32, has been sleeping under desks for much of her relatively short career. The petite Iranian-American with a toothy smile has cut a wide swath through the research world, racking up awards and honors at a dizzying pace: a Rhodes scholarship at Oxford University, a L'Oreal Women in Science award, and summa cum laude honors at Harvard Medical School, to name a few. She's also made a name in the wider world: The London *Daily Telegraph* recently called her one of the "top 100 living geniuses" (she tied for 49th place with Henry Kissinger, Richard Branson, Stevie Wonder, and Meryl Streep), and CNN named her one of eight "geniuses who will change your life."

Sabeti also seems to have a genius for raising money. While still a postdoc, her own grants totaled more than $600,000, and she is currently a co-investigator on a $2 million Bill and Melinda Gates Foundation grant. She was recently hired as a Harvard assistant professor, turning down offers from several other leading universities.

And then there's the band: She's the lead singer in the Boston-based alternative group Thousand Days, which plays gigs up and down the East Coast and has released three albums. Sabeti's singing voice is "sweet and sexy," wrote one music reviewer, adding wryly that "it's nice to know she has a successful back-up career in case her attempts at winning the Nobel Prize don't pan out."

The band may boost Sabeti's visibility, but it's her scientific drive that elicits enthusiasm from her colleagues. Broad Institute geneticist David Reich, who has worked closely with Sabeti, sums her up this way: "She is a very cool person but also sort of a nerd."

Sabeti was born in Tehran, Iran, where her father was a high-ranking official in the Shah's government. He sought asylum in the United States shortly before the 1979 revolution, and Sabeti grew up in Orlando, Florida, with a large extended family.

She traces her academic success to her early life in this close-knit clan. "My mother created a summer camp in our house, where she would teach the children and make us do book reports. And my sister, who is 2 years older than me, would teach me and my cousin what she had learned in school." Sabeti says mathematics was her first love. Her high-energy personality, she adds, appeared in those early years. "I'm a hyper person," she says. "My parents always told me to relax."

Reich, who met Sabeti when they were both grad students at Oxford, says she has always been "very driven." Her habit of pulling all-nighters was well-established by then, recalls Hans Ackerman, a fellow Rhodes scholar who is now a medical fellow at NIH in Bethesda, Maryland. "I would come into the lab and find her asleep under her desk after a full night of doing PCRs."

Why does she work so hard? "I guess I just want to make my parents proud of me," she says.

Although Sabeti's workaholic ways have brought her scientific success, Broad Institute Director Eric Lander and others also note her charisma and her efforts to reach out to the community. For example, as an undergrad at the Massachusetts Institute of Technology, Sabeti founded a still-thriving program to help incoming freshmen develop leadership skills. She also worked with RNA pioneer David Bartel, who recalls only one glitch in their association: "She gave out the lab phone number as the contact" for the leadership program. So many students called, "we had to change the

CREDITS: LEFT TO RIGHT: NISHA BROOKE, CHUN-KAI SHIH, BRIAN BERNER

Hyperactive. Pardis Sabeti—malaria researcher, role model for young scientists, and rock performer—keeps on the move.

number," says Bartel.

Sabeti also took the lead at Harvard Medical School, producing a lighthearted orientation video for first-year students, featuring prancing, juggling, balloon-wielding students and faculty. She now presents this video in person to each entering class. In fact, she's still making videos. One will be shown during a *NOVA* profile of her to be aired in July, featuring appearances by researchers including Lander, as well as Sabeti's music.

Sabeti's band, Thousand Days—which describes itself on MySpace as a "love child" between the rock group U2 and the pop band Mazzy Star—has been a regular presence on the New England music scene for several years. Sabeti writes her own songs, including one called "Coming Up" that seems a metaphor for her career. She says she "loves the creative spirit" in both music and science but is "more at home" in science. Given her scientific schedule, she hasn't found time to perform in recent months.

She continues to focus on the research she began at Oxford: teasing out signs of selection in the human genome. At Oxford, Sabeti focused on genetic susceptibility to malaria, zeroing in on two alleles that conferred resistance to the parasite. Most researchers assumed that these genetic variants had been favored by selection, but there was little evidence to prove it.

Over the previous 20 years, researchers had developed dozens of tests for detecting "signatures" of natural selection in the genome (*Science*, 16 June 2006, p. 1614), but they had very low power to detect more recent evolutionary changes, particularly during the last 10,000 years, when many of the diseases that afflict humankind, including malaria, arose.

Working with Reich and with her doctoral adviser, Dominic Kwiatkowski of Oxford University in the U.K., Sabeti hit on a novel way of combining two types of genetic information to create a more powerful test: the frequency of a particular variation and the structure of the genome surrounding it. Normally, variants are shuffled in a random fashion across the genome. But if a particular variant is the target of recent natural selection, its rapid increase in frequency can create so-called haplotype blocks, groups of genes that have "hitchhiked" along for the Darwinian ride (see graphic, below). Some earlier selection tests looked at both variant frequencies and haplotypes in humans, but they weren't very sensitive. Sabeti used her math skills to devise a genetic "clock," based on haplotype structure, that could reveal whether recent, high-frequency variants were due to selection or just chance—greatly strengthening the power to detect evolution's hand.

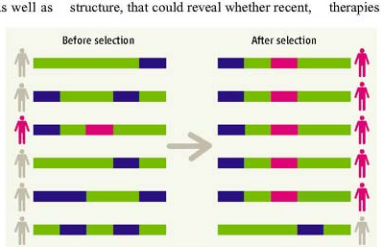

Hitchhikers. When a genetic variant favored by selection (pink bar) spreads rapidly in a population, other variants linked to it come along for the ride.

In collaboration with Kwiatkowski, Lander, Reich, and others, Sabeti then applied the new approach to the protective malaria variants. "We saw a whopping signal" of positive selection, Sabeti says. When these results were published in *Nature* in 2002, her scientific reputation was made. "This test is one of the most exciting developments in the field in the past few years," says Chris Tyler-Smith, a genome researcher at the Wellcome Trust Sanger Institute in Hinxton, U.K. Evolutionary biologist Martin Kreitman of the University of Chicago, who had developed a similar test but was beaten into print by a few months, says he has "nothing but praise for her contributions." He adds that Sabeti's most recent contribution, a genome-wide search for selected genes in collaboration with Lander, the International HapMap Project, and others, "is a beautiful piece of work."

Lander says Sabeti's test anticipated the detailed information that the HapMap would later make available. "Pardis has a very energetic imagination," he says. "Not many people think about what they would do if they had data they don't yet have."

The genome-wide study, published in *Nature* last October, identified two genes called *LARGE* and *DMD* that are involved in Lassa fever infection and show strong signals of natural selection in West Africans. Despite striking about 300,000 people each year and killing 20,000 of them, Lassa fever has been neglected by public health experts. Sabeti hopes to use her test to identify variants protective against the disease, which could eventually help in the search for new therapies and a vaccine. Looking at Lassa's evolutionary history is "a very innovative approach" that "might breathe some new life into field research" into the disease, says Lassa fever expert Joseph McCormick of the University of Texas School of Public Health in Brownsville, who is a consultant to Sabeti on the project.

At the moment, Sabeti seems to be flying high. But some colleagues are concerned that her fame could set her up for a big fall if her hyper pace slackens. "I worry that too many expectations are being put on Pardis," says one researcher. But Nancy Oriol, Harvard Medical School's dean of students, isn't worried. "If you are motivated by serving others and doing good work, as is Pardis, you won't get burned out," she says.

Indeed, despite all the attention she attracts, Sabeti says she feels more at home with her inner nerd: "Even though I am gregarious, I interact more with [scientific] papers than with people. Deep down, I am just a math geek." **–MICHAEL BALTER**

SOURCE: PARDIS SABETI

Special skills. The orangutans of Suaq Balimbing are renowned for their distinctive behavior, including using tools to open fruit.

CONSERVATION BIOLOGY

A Renowned Field Station Rises From the Ashes

After a frustrating hiatus, wildlife researchers are returning to a swamp in war-torn Aceh Province for a chance to study some of the world's smartest apes

SUAQ BALIMBING, INDONESIA—After an hourlong ride wending up the Lembang River through dense tropical rain forest, the speedboat sputters up to a rickety plywood dock. At the top of steps carved into the riverbank is a pair of shacks. Soaked clothes hang outside, drying. The Suaq Balimbing research station may look like hillbilly central, but inside it is buzzing with scientific life: 15 researchers and assistants jostling for space alongside generators, laptops, and cans of food.

No one is complaining about the cramped quarters. Suaq shot to fame in the mid-1990s, when researchers discovered tool use among orangutans here in Sumatra's Gunung Leuser National Park. Apart from humans and chimpanzees, no other primates have demonstrated such abilities, and Suaq remains the only location where orangutans regularly use stick tools to crack fruits and hunt for termites and honey. More recently, a landmark paper in *Science* (3 January 2003, p. 102) demonstrated that orangutan populations possess distinct traditions, skills, and social quirks: their own cultures. These orangutans "do things that we haven't seen orangutans do in other sites," explains Cheryl Knott, a primatologist at Harvard University. "[Suaq] helped change our views and understanding of these animals."

For the better part of a decade, this unique window into orangutan culture was shuttered. At the end of the 1990s, an upsurge of violence in Aceh Province's long-running civil war forced wildlife researchers to abandon their work in the province. The Suaq team, led by primatologist Carel van Schaik of the University of Zürich, Switzerland, pulled out in September 1999, after insurgents murdered the station's head assistant. When van Schaik and his colleagues returned for a brief survey in 2006, they found that the Indonesian army had razed the station's two sturdy buildings. "The rebels had been using our camp, so the military didn't burn it down for nothing," he says. Boardwalks that traversed the research site—a 500-hectare swamp—had rotted away.

After the warring parties signed a peace treaty in 2005, researchers began to trickle back to Aceh. "The bad times are over," proclaims van Schaik. "People are getting back into the field."

Nowhere has the homecoming been more anticipated than at Suaq. Last year, van Schaik's crew and a Switzerland-based nonprofit, PanEco, built a modest replacement station and hacked a 46-kilometer trail grid for observing orangutans night and day. The collection of behavioral data resumed last September. Scientists couldn't be happier. "We were all waiting for this place to reopen," says Andrea Gibson, a Ph.D. student at the University of Zürich who had to delay her fieldwork for 3 years because of the hiatus.

Cultured apes

During the rainy season, which lasts from October to March, trails at Suaq are waded, not walked. The knee-deep, pungent red mud has a powerful suction. "You can disappear in these waters," says Ellen Meulman, another Zürich University Ph.D. student. Leeches are ubiquitous, and king cobras and tigers lurk unseen. Among primatologists, says van Schaik, Suaq is known as "human hell" but "orangutan heaven." The shaggy apes are undisturbed—the nearest village is dozens of kilometers away—and food is plentiful, with some 70 kinds of fruit for the picking.

Meulman and her colleagues head out from the field station in the wee hours of the morning and slog for nearly 2 hours across perilous terrain to get to the orangutan nesting site before dawn. They don't get back to camp for their rations of rice and canned mackerel until after dark. In between, they track orangutan behavior in minute detail: Is a subject playing with a neighbor? Eating, and if so, what? Vocalizing? Using a tool?

The orangutans have some remarkable skills. For example, they know how to fashion a stick to crack open the razor-sharp shell of *Neesia* fruit. Van Schaik hypothesizes that they learned this skill after using simpler tools to dig for honey, fish for termites, and scoop for water. But it's unknown how these skills are acquired and transferred. "There's still a lot of doubt in the literature on this," he says. "We would really like to nail it."

One clue may be the friendliness of the lowland orangutans, who frequently gather in small groups known as "parties." "There are a lot of opportunities for social learning," says Meulman. "We're looking at what they're doing when they're together. We've seen teaching and cultural learning." Curious adults, for instance, will observe neighbors making umbrellas or gloves out of leaves and imitate those behaviors. Juveniles learn to build mosquito-repellent nests out of terentang leaves by watching their mothers.

Even simple nests, perhaps used for

CREDIT: UNIVERSITY OF ZÜRICH

afternoon naps, suggest the presence of culture. "It was always assumed they randomly break sticks together and build nests the same way," says Gibson. "But there are definite differences in the arrangement of branches [among groups]." For her research, Gibson has been scaling trees to examine old nests and plans to sleep in one of the 30-meter-high beds for a night. This has never been attempted, she says, apparently due to the possibility of attack from a reticulated python. But it's worth the risk, she says: The data could answer basic questions, such as why orangutans sleep in nests rather than just out on a sturdy branch. "There are some things you have to experience firsthand," she says with a smile.

With the return of primatologists to Aceh, research on orangutan culture is gathering momentum. Although Suaq has stolen the show, the research requires extensive collaboration with other study sites. Case in point: Van Schaik didn't make the jump from observing tool use at Suaq to concluding that orangutans hold a deep cultural repertoire until he compared notes with scientists at five other field stations. Likewise, a 1999 *Nature* paper that first presented evidence for chimp culture required data from seven sites across central Africa to document the full range of their behavioral repertoire. "You can't say anything about culture if it's just one site," says Knott. "You need the comparative perspective."

Knott's orangutan field station at Gunung Palung in Borneo also resumed work last year. She had shuttered it in 2003, after the staff became concerned that hostile loggers might become violent. Knott is studying differences in diet, vocalization, and reproduction to determine whether these behaviors have cultural or ecological origins. Much of this research will be in collaboration with other sites, including Suaq and the Ketambe Research Center, the longest running orangutan field site in Sumatra. Take, for instance, the differences in foraging behavior. "Is this variation purely due to optimal foraging or social learning?" says Ketambe manager Serge Wich, a researcher with the Great Ape Trust in Des Moines, Iowa. "We want to know which kinds of food prompted cultural innovation."

CREDIT: JERRY GUO

Losing time

Because fieldwork stopped for several years across Aceh, it has been difficult to quantify the impact of the civil war on a biodiversity hot spot that is home to elephants, rhinoceroses, leopards, sun bears, tigers, and some 6500 orangutans. "Only now are many studies restarting," says Wich. Although the fighting at Ketambe, in the island's interior, was not as fierce as on the west coast near Suaq, researchers had to evacuate in 2002 and only returned 2 years ago. After compiling a 37-year data set, says Wich, "it was sad to have the gap."

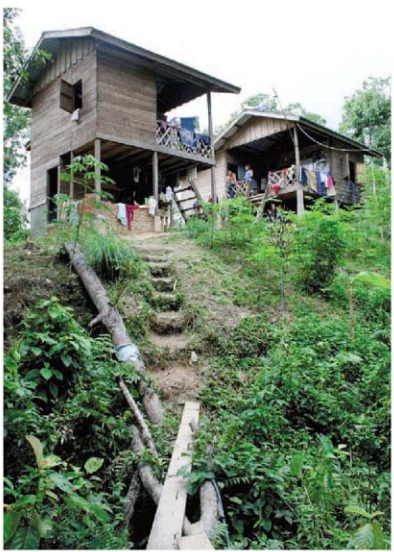

Up and running. The research center in Sumatra's Gunung Leuser National Park has been rebuilt after being occupied by rebels and destroyed by the army.

Although the primatologists at Suaq lost much more time—8 years' worth of data—the 70 or so orangutans they study haven't missed a beat. The concentration of orangutans here is higher than anywhere else in the world: twice the density of other sites on Sumatra and four times that of Borneo, the only other place where these apes are found in the wild. A vibrant population appears to be the key factor enabling otherwise solitary creatures to "teach" each other skills such as tool use, making Suaq the ideal laboratory for studying the origins of human culture, says van Schaik.

Ironically, the war may have given Leuser's orangutans a reprieve. When Indonesia's former President Suharto was ousted in 1998, illegal loggers were about to overrun the station. "The civil war stemmed that," explains Ian Singleton, director of conservation for PanEco and a manager of Suaq. "The illegal loggers and poachers didn't want to risk being shot, so the civil war was extremely good for conservation." During the past 5 years, when Suaq was offline, Singleton released 100 rehabilitated Leuser orangutans back into the Sumatran rain forest.

But other threats loom large. Faced with expanding oil palm plantations, the resurgence of illegal logging and mining after the peace treaty, highway construction, and a booming pet trade, orangutans may become extinct in the next decade or two, says Singleton. A United Nations Environment Programme report published in February 2007 warned that 98% of the orangutan's habitat—tropical rain forests—would disappear by 2022. Based on satellite imagery, the report listed Leuser as one of the most vulnerable hot spots. Last year, Singleton says, developers began draining swamps and burning forests north of Suaq for oil palm plantations.

Van Schaik knows that he and his colleagues can't afford to lose more time. They plan to build a six-room dormitory, install solar panels for a constant supply of electricity, and build three boardwalks to ease the trip to the research site. They hope to have the station restored to its former glory by fall. In the meantime, van Schaik is hiring assistants for an expanding research agenda. "We only scratched the surface before," says Gibson. "We have the most intelligent and interesting orangutans. There are so many bubbling questions to be answered." **–JERRY GUO**

Jerry Guo is a writer in New Haven, Connecticut.

Green on the screens 450

Tracking genetically engineered crops 452

LETTERS

edited by Jennifer Sills

Parsing the Evolution of Language

WHILE NOAH WEBSTER MAY HAVE PRODUCED THE EARLIEST COMPENDIUM ON AMERICAN English, the divergence from British English dates from much earlier. Long before the publication of Webster's Dictionary in 1806, pronunciation in America and in Britain had begun to differ (*1*, *2*). The Dictionary thus does not mark a fixed point when all Americans shifted abruptly from British to American English. The speciation, rather, was gradual, because individual speakers change gradually, by increments, in their lifetimes; individual changes also spread gradually from speaker to speaker.

In the Brevia "Languages evolve in punctuational bursts" (1 February, p. 588), Q. D. Atkinson *et al.* are right that there has yet to be an experimental demonstration of "punctuational bursts" that mark the evolution of language. However, the idea that language evolution proceeds in "bursts" of change alternating with periods of stasis has long been recognized in linguistics. Although there are periods in language evolution when population-wide changes are less noticeable, this does not mean that when changes are noticed they must have occurred abruptly. They are gradual even if their spread within a population took only a few decades.

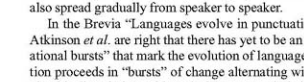

We believe there is a difference between rapid changes, which can still be incremental, and abrupt changes, as when one speaker says "baht" or "bet" when "bat" is intended. When such a change spreads within a population, it does not affect every word that, for instance, has the American vowel sound of bat (such as pat and lack) simultaneously, nor does every member of the relevant population of speakers participate in the process at a given time.

BRIAN D. JOSEPH[1] AND SALIKOKO S. MUFWENE[2]

[1]Department of Linguistics, The Ohio State University, Columbus, OH 43210–1298, USA. [2]Department of Linguistics, University of Chicago, Chicago, IL 60637, USA.

References

1. Henry Louis Mencken, *The American Language* (A. A. Knopf, New York, 1921).
2. P. K. Longmore, *J. Interdisciplinary History* **37**, 513 (2007).

Response

IN OUR BREVIA, WE USED THE EXAMPLE OF Webster's Dictionary—widely regarded as the inaugurating dictionary of American English—to illustrate how the desire for a distinct social identity can motivate language changes, such as spelling. Of course, some changes may have begun much earlier. We are not aware that anyone has measured how rapid or gradual these changes were by using the sorts of quantitative methods we have developed, but it would be informative to do so.

Phylogenies use nodes to summarize the outcome of population-level processes that, working forward in time, give rise to distinct entities, be they species or languages. Our statistical methods can detect whether these events occur relatively abruptly or more gradually (*1*–*3*). They do so by detecting whether an excess of evolutionary divergence arises in association with the number of times a new species or language has emerged on a phylogeny. They do not make assumptions about precisely when these species or languages emerged.

Changes to languages that occur over a few decades may seem gradual at the time but can be relatively abrupt in the lifetime of a language or language family. As an example, the frequency with which meanings are used in everyday language affects their rate of word replacement over thousands of years (*4*). Some words are replaced dozens of times in the history of a language family (such as the word for "bird" in Indo-European) while others may never be replaced (such as the word for "two").

To speakers "on the ground" even these extremes are probably indistinguishable, but over historical time they give rise to very different outcomes.

QUENTIN D. ATKINSON,[1]* ANDREW MEADE,[1] CHRIS VENDITTI,[1] SIMON J. GREENHILL,[2] MARK PAGEL[1,3]†

[1]School of Biological Sciences, University of Reading, Reading RG6 6AS, UK. [2]Department of Psychology, University of Auckland, Private Bag 92019, Auckland 1142, New Zealand. [3]Santa Fe Institute, Santa Fe, NM 87501, USA.

*Present address: Institute of Cognitive and Evolutionary Anthropology, University of Oxford, Oxford OX2 6PN, UK.

†To whom correspondence should be addressed. E-mail: m.pagel@reading.ac.uk

References

1. A. J. Webster *et al.*, *Science* **301**, 478 (2003).
2. M. Pagel *et al.*, *Science* **314**, 119 (2006).
3. C. Venditti *et al.*, *Syst. Biol.* **55**, 637 (2006).
4. M. Pagel *et al.*, *Nature* **449**, 717 (2007).

Inspecting Urban Health

C. DYE'S PERSPECTIVE, "HEALTH AND URBAN living" (8 February, p. 766), provided an excellent overview of the history and trends of health in urban areas but is silent on some key issues. In addition to comparisons of urban and rural health, the growing urban health research field has benefited from examining health within urban communities (*1*–*5*). These studies have helped expose the wide disparities between the rich and poor not only in environmental health but also in health outcomes (*6*). Wilkinson *et al.*, in a review of more than 150 studies, found that "health is less good in societies where income differences are bigger" (*7*).

The most likely underlying reason for the

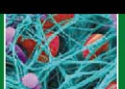
Blood clot elasticity
456
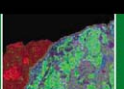
Identifying ancient asteroids
457

disparities in health is not, as Dye suggests, "governance and the organization of civil society," but rather structural problems such as inequality, poverty, debt, globalization, unemployment, and education (*8*). Many of these are indeed governance-related, but others fall squarely in the realm of global and national economics. In contrast to Dye's proposal that "a nation may now be judged by the health of its urban majority," I suggest that nations be judged by the health of their most vulnerable, especially the urban migrants, children, and residents of urban slums and informal settlements.

ELIZABETH THOMAS

Medical Research Council South Africa, WHO Collaborating Centre for Urban Health, University of the Witwatersrand, Johannesburg, South Africa.

References

1. T. Harpham, M. Tanner, Eds., *Urban Health in Developing Countries: Progress and Prospects* (Earthscan, London, 1995).
2. T. Harpham, C. Molyneux, *Prog. Dev. Stud.* **1**, 113 (2001).
3. I. M. Timaeus, L. Lush, *Health Trans. Rev.* **5**, 163 (1995).
4. E. P. Thomas *et al.*, *Health Place* **8**, 251 (2002).
5. S. Mercado *et al.*, *J. Urban Health* **84** (suppl. 1), 7 (2007).
6. M. Marmot, R. G. Wilkinson, Eds., *Social Determinants of Health* (Oxford Univ. Press, London, 2005).
7. R. G. Wilkinson, K. E. Pickett, *Soc. Sci. Med.* **62**, 1768 (2006).
8. World Health Organization Commission on Social Determinants of Health (www.who.int/social_determinants/en/).

Response

MY REVIEW OF CHILD MORTALITY CONCLUDED not only that urban inhabitants enjoy better health on average than their rural counterparts but also that the benefits of urban living are greater for the rich than for the poor, thus magnifying the differences between them. The sites included in my review were mostly in low- and middle-income countries, and this picture of better but more uneven urban health may not apply in richer parts of the world. In England, for example, the concentration of relatively poor people now living in London and in other large metropolitan areas means that infant mortality rates are equal to or higher than the national average (*1*).

Among the factors that determine the distribution of ill health in populations, I predict that governance will indeed turn out to be vital in many countries. However, to find out whether this is right or wrong, we need to carry out substantial investigations of the structural causes, which will identify the functional relations between unemployment, education, and poverty (however measured), and how these act as determinants of health.

CHRISTOPHER DYE

Department of Tuberculosis, World Health Organization, Geneva CH-1211, Switzerland.

Reference

1. Office for National Statistics, *Births, Perinatal and Infant Mortality Statistics, 2005*, in *Health Stat. Q.* **31**, 76 (2005).

The Quest for Stronger, Tougher Materials

THE PERSPECTIVE "STRUCTURAL NANOcomposites" (Y. Dzenis, 25 January, p. 419) describes a quest for improved structural materials and indicates that composites with nanoscale reinforcements would have "exceptional mechanical properties." Is this true?

Why would reinforcements that are small in size or volume offer any particular benefit over larger-scale reinforcements? As the Perspective correctly asserts, if the composite material is to be used for a small-volume structure, clearly the reinforcements must also be small. In addition, small-volume reinforcements are stronger, as has been known since the early days of research on whiskers (*1*). In this regard, reinforcement by carbon nanotubes, for example, which are thought of as one of the strongest materials in existence (*2*), would seem ideal.

The problem with this notion is that new materials are not limited by strength, but by resistance to fracture (also known as fracture toughness). It is not by accident that most critical structures, such as bridges, ships, and nuclear pressure vessels, are manufactured from materials that are low in strength but high in toughness. Indeed, the majority of toughening mechanisms mentioned by Dzenis—i.e., crack deflection, plastic deformation, and crack bridging—are promoted by increasing, not decreasing, reinforcement dimensions [e.g., (*3*)]. Is it any surprise that "results obtained so far are disappointing"?

ROBERT O. RITCHIE

Materials Sciences Division, Lawrence Berkeley National Laboratory, and Materials Science and Engineering, University of California, Berkeley, CA 94720, USA. E-mail: roritchie@lbl.gov

References

1. A. Kelly, *Strong Solids* (Clarendon Press, Oxford, UK, 1966).
2. B. G. Demczyk *et al.*, *Mater. Sci. Eng. A* **A334**, 173 (2002).
3. A. G. Evans, *J. Am. Ceram. Soc.*, **73**, 187 (1990).

Response

RITCHIE'S REJECTION OF STRENGTH IN FAVOR OF toughness is perfectly suitable for ceramics but can be less appropriate when applied to other materials, such as polymers or even metals. Advanced polymer composites—a class of lightweight, strong, and stiff materials based on high-performance continuous fibers—are now being used in a variety of critical applications, such as primary aerospace structures. Unlike metals, these composites do not experience large deformations before failure. Instead, a degree of toughness is provided by multiple damage and crack accumulation and deflection mechanisms, many involving strong fibers. There is high interest in further improving composites' strength and other mechanical properties, as exemplified by the continuous industrial effort to produce stronger reinforcing fibers. For some of the fibers (e.g., carbon, glass, and ceramic fibers), higher strength has been linked, among other factors, to finer fiber diameters.

From a composites perspective, it was only natural to try to use the strength of nanoscale reinforcement, such as carbon nanotubes, in a superstrong and lightweight composite. Early predictions were optimistic (*1*–*3*). However, as Ritchie correctly asserts, the question of whether nanoscale materials will be beneficial to bulk structural materials is still open to discussion. Experience with high-strength polymer composites calls for a strong interface and high volume fraction of nanoreinforcement. Research to date has not uncovered any fundamental drawbacks for achieving these, except for possible deterioration of the intrinsic carbon nanotube strength as a result of covalent bonding, as mentioned in the Perspective. The situation is more complex with regard to toughness. The benefits of larger reinforcement diameters mentioned by Ritchie may not be universal. After all, there are multiple toughening mechanisms in composites, and some of them can be expected to benefit from the enhanced strength and resilience of nanoreinforcement and/or its larger surface-to-volume ratio. There is experimental evidence of improvements in toughness of brittle materials as a result of carbon nanotube nanoreinforcement (*4*, *5*). Continuous nanofibers (*6*) are also expected to produce improvements while removing some of the problems associated with discontinuous nanomaterials. Yet, clearly more studies are needed to elucidate the fundamentals of fracture in the nanoreinforced materials, including possible limiting effects of small scale.

Finally, toughness and strength are not always mutually exclusive. True, for the intrinsically ductile materials, such as metals, improvements in strength usually come at the expense of toughness. However, for brittle materials, such as ceramics, in the presence of flaws that individually cause fracture, strength can be proportional to toughness. In the example used in the Perspective, we used nanoscale reinforcement to toughen the thin interfacial layers in advanced composites. We expect this to result in improvements in composite strength, as well as fatigue durability and impact resistance. Similar effects can be predicted for other medium-term applications described in the Perspective. We will continue to hope for a time when we can demonstrate the existence of bulk supernanocomposites (defined as nanocomposites exceeding the performance of modern advanced fiber-reinforced composites).

YURIS DZENIS

Department of Engineering Mechanics, Nebraska Center for Materials and Nanoscience, University of Nebraska, Lincoln, NE 68588, USA. E-mail: ydzenis@unl.edu

References

1. P. Calvert, *Nature* **399**, 210 (1999).
2. E. T. Thostenson *et al.*, *Comp. Sci. Technol.* **61**, 1899 (2001).
3. J. N. Coleman *et al.*, *Adv. Mater.* **18**, 689 (2006).
4. A. Peigney, *Nat. Mater.* **2**, 15 (2003).
5. B. W. Sheldon, W. A. Curtin, *Nat. Mater.* **3**, 505 (2004).
6. Y. Dzenis, *Science* **304**, 1917 (2004).

TECHNICAL COMMENT ABSTRACTS

COMMENT ON "Eddy/Wind Interactions Stimulate Extraordinary Mid-Ocean Plankton Blooms"

Amala Mahadevan, Leif N. Thomas, Amit Tandon

McGillicuddy *et al.* (Reports, 18 May 2007, p. 1021) proposed that eddy/wind interactions enhance the vertical nutrient flux in mode-water eddies, thus feeding large mid-ocean plankton blooms. We argue that the supply of nutrients to ocean eddies is most likely affected by submesoscale processes that act along the periphery of eddies and can induce vertical velocities several times larger than those due to eddy/wind interactions.

Full text at www.sciencemag.org/cgi/content/full/320/5875/448b

RESPONSE TO COMMENT ON "Eddy/Wind Interactions Stimulate Extraordinary Mid-Ocean Plankton Blooms"

Dennis J. McGillicuddy Jr., James R. Ledwell, Laurence A. Anderson

The alternative mechanism proposed by Mahadevan *et al.* is an unlikely explanation for our observations because their model predicts a bloom at the periphery of the eddy, whereas the observations show it located at the eddy center, and because the vertical displacements caused by the nonlinear Ekman effect are too small to lead to an extraordinary biological response in this eddy.

Full text at www.sciencemag.org/cgi/content/full/320/5875/448c

Letters to the Editor

Letters (~300 words) discuss material published in *Science* in the previous 3 months or issues of general interest. They can be submitted through the Web (www.submit2science.org) or by regular mail (1200 New York Ave., NW, Washington, DC 20005, USA). Letters are not acknowledged upon receipt, nor are authors generally consulted before publication. Whether published in full or in part, letters are subject to editing for clarity and space.

ENVIRONMENTAL HISTORY

Cultivating a New Nation

Sharon Kingsland

Fruits and Plains adopts a novel approach to the history of contemporary restoration ecology and modern concerns about invasive species in America. Rather than view these practices as new developments in ecology and conservation biology, Philip Pauly shows how they can be seen as the culmination of a 200-year history of horticultural practice in the United States. Pauly (a historian at Rutgers University who died early this month) depicts these horticultural practices as involving science but also as tied to a craft tradition, one linked closely to an evolving American debate about how to acquire culture. His ambitious goal is to use horticulture to connect environmental, agricultural, scientific, and art histories with the history of national development.

Fruits and Plains
The Horticultural Transformation of America

by Philip J. Pauly

Harvard University Press, Cambridge, MA, 2008. 350 pp. $39.95, £25.95, €30. ISBN 9780674026636.

Pauly charts the tension between three attitudes (the "desires for the exotic, enthusiasms for the native, and fears of the alien") that characterize American debates through two centuries. Americans could warmly embrace a cosmopolitan perspective, welcoming new species into the landscape and experimenting with the creation of new forms. In the nation's early years, enriching its flora was a means of improving American culture, raising it to the level of western Europe by creating a better place and a better people. On the other hand, Americans might champion the virtues of American plants, seeking to Americanize the landscape by promoting the spread of desirable species, while abhorring the destructive power of imported species and their attendant pests. The Hessian fly that plagued American wheat crops in the late 18th century prefigured a future fraught with dangers from other invaders. Rejecting cosmopolitanism in preference to a nativist stance, Americans called for quarantine and eradication of pests as they confronted the specter of enemy aliens descending from abroad and consuming native vegetation.

Pauly examines these shifting attitudes through profiles of key individuals working in various contexts. He discusses not only famous visionaries like Thomas Jefferson but also many lesser-known individuals who were nonetheless important historical actors. Eighteenth-century naturalists worried about how Americans should settle their new lands and what kinds of horticultural practices would make for a successful adaptation. Pauly shows how organized horticulture developed in the United States; how societies, nurserymen-entrepreneurs, and the gardening press interacted; and how new institutions for the promotion of horticulture were created. Historical examples drawn from such different activities as fruit cultivation and landscape architecture collectively impress on us how much energy and enthusiasm Americans invested in this pioneer form of biotechnology.

Importing species or extending the ranges of native plants unleashed new pests, however. The late 19th and early 20th centuries saw the professionalization of agricultural sciences and the emergence of new ideas about quarantine and eradication of insect pests along with development of chemical weapons against such invaders as the gypsy moth, San José scale, and Mediterranean fruit fly. The cosmopolitan passions of botanical collectors such as David Fairchild clashed with the nativist views of people such as Charles Marlatt, who escalated the war on nature through the Plant Quarantine and Control Administration. As an object lesson illustrating the dangers of imported pests and the courageous activism of the U.S. Department of Agriculture, Fairchild's collection of Japanese ornamental cherry trees, meant for Washington, was condemned and burned in 1909 on Marlatt's order. Pauly supports the idea that the action had deeper significance, resonating with contemporary arguments about the Yellow Peril and Japanese treachery.

Two landscapes draw Pauly's special attention. Southern Florida's rapid development from the late 19th century illustrates the tensions evident throughout American history between exoticism, Americanism, and fear of the alien. So do the prairie grasslands, where horticulturists debated ideas about restoring "primitive" forests, expanding the ranges of useful American trees, and importing foreign species for a cosmopolitan effect. Pauly sees the prairies as the locus of new ideas, for in these environments Americans had to grapple with difficult questions about why the prairie lacked trees: was this a primeval condition or an accident of history? The prairie landscape demanded substantial rethinking of the relationship between nature and culture.

Following this history into the 20th century, Pauly uses the prairie landscape to explore modern ecological restoration work, as in Aldo Leopold's re-creation of the prairie at the University of Wisconsin in the 1930s, the development of the Konza Prairie Research Natural Area in the 1970s, and the inclusion of Konza in the Long-Term Ecological Research Network in the 1980s. Pauly sees modern ecologists and restoration scientists as the true inheritors of the legacy of horticultural science and craftsmanship. He understands this legacy as extending well beyond the adoption of horticultural practices by modern ecologists. On a more profound level, ecologists have come to recognize the extent to which North American ecology has been shaped by millennia of human occupation and disturbance, and in drawing that conclusion they also are led to realize that management is inevitable. Modern restoration ecologists have taken over the professional and social niches occupied by horticulturists in the past. Thus we see that restoration ecology and concern with invasive species is the latest stage of a quintessentially American story that extends back to the birth of the nation.

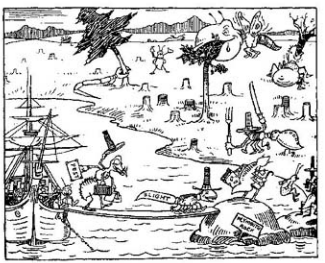

Alien pests. This cartoon accompanied a piece by the president of the American Forestry Association supporting Charles Marlatt's November 1918 ban on the entry of foreign nursery stock, seeds, and bulbs.

The reviewer is at the History of Science and Technology Department, Johns Hopkins University, 3505 North Charles Street, #203, Baltimore, MD 21218, USA. E-mail: sharon@jhu.edu

10.1126/science.1156769

CREDIT: AAI, FOR 25, 1953 (1919)

FILM: ENVIRONMENT

Seeing Green on the Silver Screen

In March, the 16th annual Environmental Film Festival in the Nation's Capital brought 115 movies—documentaries, features, animations, shorts, and children's films—to Washington, DC. Here are our reviewers' reactions to five of them.

Most Dangerous Catch. David Elisco, Director. Sea Studios, Monterey, CA. 2008. 57 minutes. National Geographic's *Strange Days on Planet Earth*.

"Follow a fish and you can end up in some unexpected places," says actor Edward Norton at the beginning of a new episode of *Strange Days on Planet Earth*. The show explores two indirect effects of overfishing that are both surprising and dramatic (although one is highly speculative). Along the way, it provides an entertaining view of how scientists stumble into mysteries and then solve them. Twice it proves the point that archives can be places of important discovery.

Throughout, Norton offers commentary that is intelligent, if sometimes stilted and breathless. The real star is Justin Brashares, a young ecologist who went to Ghana in the 1990s to study antelope and was struck by their scarcity. After hearing a lecture by a former government official about the importance of marine fish throughout the national economy, Brashares and his colleagues studied rural markets and found a striking correlation: When fish are scarce, more bushmeat is for sale [J. S. Brashares *et al.*, *Science* **306**, 1180 (2004)]. Research in the archives of Mole National Park revealed that a long-term decline in 41 African species matches the decline of the fishery in the Gulf of Guinea. One note to viewers: although a booming population of marauding baboons hikes the tension, the connection to overfishing isn't clear in the show. In fact, Brashares's baboon numbers have increased because their predators have been hunted.

The show then cuts to the coast of Namibia, where Bronwen Currie works for the Ministry of Fisheries. She is surprised when her town is fouled by the stench of rotten eggs and dead fish wash up on the beach as in a horror movie. (This is just one of several instances when the film lapses into juvenile cinematography.) Currie searches through local records and finds past mass kills, then teams up with oceanographers. They discover the role of hydrogen sulfide from rotting phytoplankton, as well as explosive releases of methane. Satellites capture a fish kill in action, stretching up the coast for hundreds of kilometers [S. J. Weeks, B. Currie, A. Bakun, *Nature* **415**, 493 (2002)]. By then, I was wondering what this story has to do with overfishing. Andrew Bakun, an oceanographer at Namibia's National Marine Research and Information Center, proposes that the massive overfishing of sardines has led to a surfeit of phytoplankton, perhaps increasing the frequency of the submarine eruptions. That conclusion feels tenuous, as does Bakun's suggestion that overfishing may be contributing to global warming, but the story of the discovery is well told.

So much for the unexpected problems caused by fishing. The last third of the show races through several attempts to relieve the pressure, including marine reserves in California and more ecologically benign approaches to aquaculture. After the two narratives, this part seems jam-packed and rushed. These are worthy, but not unexpected, places to end up. Perhaps a lesson from the fishing industry would have helped: less can be more. —**Erik Stokstad**

FLOW: For Love of Water. Irena Salina, Director. Water Project, USA. 2008. 93 minutes. www.flowthefilm.com

In Cochabamba, Bolivia, soldiers in riot gear fire tear gas into crowds hurling rocks and stones in a fight over access to clean water. Such access, Irena Salina's film *FLOW: For Love of Water* tells us, will become a major political and economic flash point in the 21st century. The film's two principal themes—affordable access to clean water and "ownership" of water rights—take us into the heart of towns and villages in India, South Africa, the United States, and the aforementioned Bolivia, where the first skirmishes in the latest water wars are taking place. On affordable access to clean water, the film's message is clear: many rural solutions can be low-tech and local, putting control of water resources directly in the hands of the people who use them. Salina approaches ownership of water rights mainly through the proxy of a protracted legal dispute between concerned citizens and a Nestlé water bottling plant in Stanwood, Michigan. Here the message is muddled, as we learn

CREDIT: FLOW: FOR LOVE OF WATER/THE WATER PROJECT LLC

little of what reasonable limits on water harvesting activities might be.

The film's strength is its passionate call to arms to those concerned about the global trend in privatization of water treatment and delivery systems and with the potential consequences for the poorest and most vulnerable members of society. The intimate connection Salina gives us with the women sitting in silent protest outside a Coca-Cola bottling plant in Plachimada, India, is both moving and motivating. Indeed, throughout the documentary, determined individuals and local communities are seen pitted against "villainous" multinational water and bottling companies (Thames Water, Vivendi, Suez, Coca-Cola, Nestlé, etc.) and the World Bank (one of whose number I am married to). Yet, with this relentless portrayal of multinationals (in connivance with the World Bank) as heartless profiteers, an opportunity is missed to both nuance the arguments—how water can be provided equitably in ever-expanding urban areas in the developing world—and engage the "enemy" in a more constructive, and ultimately productive, dialogue. —**Guy Riddihough**

Building the Future—Energy. Nicolas Brown, Director. UK. 2007. 54 minutes.

In *Building the Future—Energy*, Nicolas Brown provides vignettes of projects aimed at new, sustainable energy sources and the challenges faced by the individuals (described as heroes) working on them. Although frozen methane brings to mind the moons of Jupiter, investigators are diving in search of underwater fissures close to outcrops of gas hydrates. They believe that there could be enough such methane under the Gulf of Mexico to power the United States for years if it can be extracted safely.

Next, the film describes the hazards involved in building the Netherlands' first off-shore wind farm, at Egmond aan Zee. It compares assembling blades half the size of a football field and their platforms in the

midst of the North Sea to balancing a semi-truck on four basketballs.

The film then turns to a place not known for high winds: Roosevelt Island, adjacent to Manhattan. In 2007, Verdant Power and the New York State Research and Development Authority conducted an experiment to see whether the tides of the East River could be harnessed to provide electricity for a grocery store, with the dream of eventually using tides to provide as much as 10% of the power needed by New York City. Although the potential is great, strong tides have destroyed underwater turbine blades, and the effects of such turbines on the ecosystem remain to be fully explored

Others are focusing on the Sun's power. Brown highlights Roger Davey of EnviroMission, whose goal has been to build a commercial solar-thermal power plant in Australia (where there are 300 or more days of sunshine a year). In the United Kingdom, the Joint European Torus is re-creating the power of the sun in a large fusion reactor. It is clean energy (no radioactivity) but a risky process that could take decades to develop.

This unabashedly upbeat film offers an antidote for anyone afflicted with a sense of fatalism about the future of clean energy. **–Barbara Jasny**

Gimme Green. Isaac Brown and Eric Flagg, Directors. Jellyfish Smack, USA. 2006. 27 minutes. www.gimmegreen.com

The ubiquitous American lawn is a facade requiring the use of scarce water resources and the application of carcinogenic chemicals. At least that is the image presented in Isaac Brown and Eric Flagg's documentary *Gimme Green*. The film offers a scattered look at the pros (mainly aesthetics) and cons (the work, pesticides, and water use) of having a well-maintained lawn.

Brown and Flagg note that in the early 20th century most people didn't own their home and there were no yards. With home ownership, they imply, came community standards for tidy turf. They interview several people who suggest that unkempt yards mark less-community-minded individuals and who pass judgments on those lacking neat lawns. The film shows the absurdity to which some take this standard and how the desire for green leads to the use of water that we can't spare. It also touches on the potential risks of the insecticides and herbicides used to treat lawns, commenting that children living in homes with treated lawns are more likely to develop leukemia and that some of these chemicals are carcinogens that have made their way into our groundwater. These facts are presented (without referencing sources) as breaks between interviews.

Lighthearted and fun, the film races along making its main, rather depressing, points about why we should consider other ways to decorate our properties. Unfortunately, it presents few such alternatives—and those all too quickly: a brief scene touching on the natural look, a short scan of books on gardening with native plants, and a presentation of artificial turf as a substitute. The filmmakers demonstrate an aptitude for the style of other recent documentaries that entertain while informing. *Gimme Green* skewers a familiar aspect of our lives and, hopefully, forces the audience to rethink their obsession with turf.

–Laura M. Zahn

Scarred Lands and Wounded Lives: The Environmental Footprint of War. Alice Day and Lincoln Day, Directors. Video Takes, USA. 2008. 60 minutes. www.fundforsustainabletomorrows.org/film.htm

I began watching *Scarred Lands and Wounded Lives* with some skepticism—if the world fails to act to prevent the deaths of men, women, and children during war, will it pay any attention to a discussion of the accompanying damage to the Earth? However, the extensive research and skillful presentation by sociologists Alice and Lincoln Day make the film a surprisingly moving experience. Interviews of scientists, war veterans, and others are carefully interspersed with footage that makes vivid the long-term damage to the planet that has resulted from military conflicts and activities: e.g., cluster-bombs from as long ago as the Vietnam War that are still killing children and hindering efforts to restore agriculture, possibly toxic seepage from the more than 4000 ships sunk near South Pacific reefs during World War II, war-related deforestation in such places as Afghanistan and Vietnam, and contamination by radioactive wastes associated with nuclear weapons in many parts of the world. The filmmakers also address other themes such as the limited ability of ecosystems to survive damages caused by military actions, the extent to which problems could be addressed if resources were not being diverted to planned and ongoing wars, and the need to transition to environmental sustainability. **–Barbara Jasny**

10.1126/science.1158876

CREDITS: (TOP) GIMME GREEN/JELLYFISH SMACK PRODUCTIONS; (BOTTOM) JONAS JORDAN, US ARMY CORPS OF ENGINEERS

ECOLOGY

Harvesting Data from Genetically Engineered Crops

More than a billion acres have been planted with genetically engineered crops in the USA since 1996, but we do not fully know their ecological costs and benefits.

Michelle Marvier,[1]* Yves Carrière,[2] Norman Ellstrand,[3] Paul Gepts,[4] Peter Kareiva,[1,5] Emma Rosi-Marshall,[6] Bruce E. Tabashnik,[2] L. LaReesa Wolfenbarger[7]

Agricultural output must keep pace with a steadily increasing human population, yet must do so without destroying critical habitat for biodiversity or severely impairing ecosystem services. Genetically engineered (GE) crops may help meet these demands. However, a full accounting of the relative costs and benefits accrued from the widespread planting of GE plants is still unavailable. Uncertainties about the long-term, large-scale effects of GE crops are fueling a polarized debate. One side perceives that excessive regulation is slowing the delivery of benefits (*1*); the other is concerned that adoption is proceeding hastily and without adequate safeguards (*2*). The widespread planting of GE crops in the United States since 1996 represents a grand experiment that could provide the information necessary to resolve much of this debate. Unfortunately, this experiment cannot be analyzed because we lack well-documented maps depicting the varying prevalence of crops with specific GE traits each year.

Data documenting acreage planted to various crop species are annually collected by the U.S. Department of Agriculture's (USDA) National Agricultural Statistical Service (NASS) in all 50 states (*3*), and a more extensive census of U.S. agriculture is conducted every 5 years (*4*). Since 2000, a randomly selected subset of farmers has been asked annually if they planted GE varieties of corn, cotton, or soybean, the most widely planted of the GE crops in the United States. Although the NASS annually interviews >125,000 farmers about their land use, the data regarding acreage devoted to various GE crops are aggregated to the level of individual states—a spatial resolution too crude to allow assessments of the environmental consequences, either positive or negative, of GE crops.

Data on the geographic distribution of GE crops would be more informative and useful if it were aggregated and publicly released at the spatial scale of counties, of which two-thirds are <2000 km^2. In western states such as Arizona, with some counties >10,000 km^2, townships would be a more appropriate spatial scale (see figure, above). Annual data regarding crop acreage are already available at the scale of counties for the entire nation. We are proposing that the NASS also report the proportion of acres planted to GE varieties at this scale. This would permit analyses that could illuminate the trade-offs associated with alternative agricultural practices, while maintaining farmer pri-

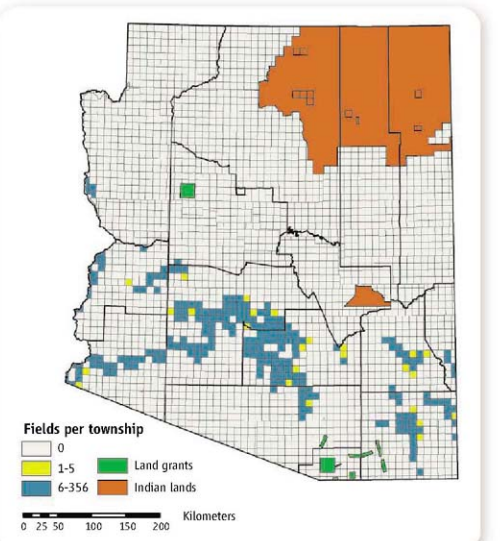

Distribution of agricultural fields in 2005 in Arizona counties and townships. Counties are delimited by thick lines (mean area = 19,700 km^2), and townships by thin black lines (mean area = 85.2 km^2). With some exceptions, land grants and Indian lands are not divided into townships. The mean number of fields per township for the 261 townships with at least one field was 96; 25 had 1 to 5 fields (yellow), 236 had 6 to 356 fields (blue). Privacy would be preserved by mapping the distribution of GE crops by county, or in many cases by townships with >5 fields. [Mapped data are from the Arizona Geographic Information Council and the Arizona Cotton Research and Protection Council.]

CREDIT: C. ELLERS-KIRK, CARTOGRAPHER

[1]Environmental Studies Institute, Santa Clara University, Santa Clara, CA 95053, USA. [2]Department of Entomology, University of Arizona, Tucson, AZ 85721–0036, USA. [3]Department of Botany and Plant Sciences, University of California at Riverside, Riverside, CA 92521–0124, USA. [4]Department of Plant Sciences, University of California at Davis, Davis, CA 95616–8780, USA. [5]The Nature Conservancy, Seattle, WA 98105, USA. [6]Department of Biology, Loyola University Chicago, Chicago, IL 60626, USA. [7]Department of Biology, University of Nebraska, Omaha, NE 68182–0040, USA.

*Author for correspondence. E-mail: mmarvier@scu.edu

vacy (see figure). If generating these estimates at the scale of counties should prove too costly, the relevant information could be obtained from seed sale records. For example, the U.S. Environmental Protection Agency (EPA) requires corporations to report annual sales of certain insect-resistant GE varieties by county as a condition of registration (*5*, *6*).

In addition, finer resolution is needed about the characteristics of the GE crops. The NASS annually reports acreages for GE crops lumped into four crude categories: insect-resistant, herbicide-resistant, stacked (meaning resistant to both insects and herbicides), and "all biotech varieties." However, this classification masks substantial variation. For example, 12 different combinations of one to three insecticidal proteins that kill caterpillars, beetles, or both are produced by different varieties of GE corn and cotton currently registered in the United States (*7*). It is essential to discern whether a particular transgenic variety and its traits are associated with environmental patterns such as changes in water quality, biodiversity, or pest resistance. Therefore, we recommend that the NASS keep and make available to environmental scientists records regarding the specific transgenic varieties planted. For completeness, GE field trial locations (again, at the county level, to avoid vandalism of plots) and accidental releases of GE organisms should also be included in a spatially explicit database.

Analyses of the consequences of GE crops must be interpreted in the context of other farming practices. Fortunately, information regarding agricultural practices such as the use of insecticides and herbicides is already being collected on a sufficiently fine scale in several states (*8*–*10*), and such efforts could be merged into national maps. Although cause-and-effect relationships would be difficult to determine, the prevalence of GE crops varies widely among counties within states (*11*), which produces spatial and temporal contrasts that can be analyzed as large-scale experiments. More nuanced investigations are possible by drawing on regularly monitored environmental attributes such as water quality, soil erosion, and land-use patterns, which are reported by the USDA, EPA, and other federal and state agencies (see table, above).

Some important lessons have already been learned from analyses similar to those proposed here. For example, cotton growers in Arizona have collaborated with researchers (under an agreement preserving farmers' privacy) by providing detailed statewide maps of fields of conventional and GE cotton. These maps have allowed researchers to show that insect-resistant GE cotton has fostered long-term suppression of a major insect pest and has helped to reduce insecticide use while maintaining crop yield (*12*, *13*). Diversity of nontarget insects was decreased by insecticide use, but was not directly affected by cultivation of GE versus conventional cotton.

By linking maps of agricultural practices with existing monitoring of birds, fish, and amphibians, one could also examine associations between agricultural practices and trends in species abundances across both space and time (see table). Agriculture is the dominant land use in the USA and in most of the world. Regulations, public policy, and financial incentives are often aimed at making agriculture more sustainable or more productive (*14*, *15*). Yet, rarely do we have data to know the actual consequences of different farming practices. GE crops are a new technology that promises to revolutionize agriculture for the good of humankind. To inform our choices about agricultural options, we must seize the chance to collect and assess data that are relatively easily obtained. The key will be to balance the rights of privacy for individual farmers and corporate concerns regarding confidential business information with the public good that can come from analyzing these data.

Variable	Frequency	Spatial scale	Agency or organization
Use of insecticides, herbicides, and fungicides*	Annually Every 5 years Annually	States Counties Counties	USDA NASS† USDA NASS State agencies
Use of chemical fertilizers and manures‡	Every 5 years	Counties	USDA NASS
Other farming practices§	Annually	States	USDA NASS
Water quality‖	Approx. hourly to every 4 years	Site, watersheds, basins	USGS NAWQA, EPA¶
Aquatic organism surveys**	Every 3 to 4 years	Site, watersheds, basins	USGS NAWQA, EPA
Amphibian research and monitoring	Annually	Nested catchment	USGS
Breeding bird survey	Annually	Site	USGS
Christmas bird count	Annually	Site	USGS
Endangered species distributions	Irregular	Counties	NatureServe

*By active ingredient and crop. †See www.pestmanagementinfo/naxs/. ‡By crop. §Includes summer fallow vs. continuous cropping, irrigated vs. not, crop rotations (for specific crops). ‖Includes pesticide residues, suspended sediments, physical and chemical attributes. ¶See http://water.usgs.gov/nawqa/ and www.epa.gov/storet. **Biomonitoring of macroinvertebrates and fishes.

Examples of existing public information. When integrated with spatially explicit data on the use of GE crops, such information could allow assessment of the benefits and drawbacks of these crops. Although these data are not all at the spatial scale of counties or townships and data quality is variable, this list provides a starting point for the types of analyses we envision. Many relevant spatially explicit datasets can be downloaded from http://water.usgs.gov/lookup/getgislist. "Site" refers to a transect, river segment, or other relevant sampling unit. In all cases, sites are smaller than the scale of counties (or townships), and therefore, data from sites could potentially be aggregated to the scale of counties (or townships).

The approach we advocate will help us identify which agricultural practices maximize benefits to farmers and society while minimizing environmental risks. The United States has the world's most extensive history of using GE crops and one of the world's best continental-scale programs in environmental monitoring. Combining these two sources of information provides an opportunity to lead the world in identifying agricultural pathways for the future that best serve people and the environment. Providing scientists access to data on GE crop use at the county scale is a small and relatively inexpensive step with enormous scientific and public benefits.

References and Notes

1. K. J. Bradford, A. Van Deynze, N. Gutterson, W. Parrott, S. H. Strauss, *Nat. Biotechnol.* **23**, 439 (2005).
2. D. E. Ervin, R. Welsh, S. S. Batie, C. L. Carpentier, *Agricult. Ecosyst. Environ.* **99**, 1 (2003).
3. NASS, "Acreage data" (2007); www.nass.usda.gov.
4. USDA agricultural census data, www.agcensus.usda.gov.
5. B. D. Siegfried *et al.*, *Am. Entomol.* **53**, 208 (2007).
6. EPA, *The Environmental Protection Agency's White Paper on* Bt *Plant-Pesticide Resistance Management* (EPA Publ. 739-S-98-001, EPA, Washington, DC, 1998); www.epa.gov/EPA-PEST/1998/January/Day-14/paper.pdf.
7. Registered plant-incorporated protectants, www.epa.gov/pesticides/biopesticides/pips/pip_list.htm.
8. California Department of Pesticide Regulation (DPR), "An overview of California's unique full reporting system" (California DPR, Sacramento, CA, 2000).
9. A. Fournier, P. C. Ellsworth, V. M. Barkley, in *Cotton, A College of Agriculture Report* (Series P-151, Univ. of Arizona, Tucson, AZ, 2007), pp. 155–165.
10. "New York State Pesticide Reporting Law (PRL)," Environmental Conservation Law Article 33, Title 12 (1996).
11. Y. Carrière *et al.*, *Pest Manag. Sci.* **61**, 327 (2005).
12. M. G. Cattaneo *et al.*, *Proc. Natl. Acad. Sci. U.S.A.* **103**, 7571 (2006).
13. Y. Carrière *et al.*, *Proc. Natl. Acad. Sci. U.S.A.* **100**, 1519 (2003).
14. USDA-ERS, *Adoption of Bioengineered Crops, AER-810* (USDA-ERS, Washington, DC, 2002); www.ers.usda.gov/publications/aer810/aer810.pdf.
15. EPA, *EPA's Report on the Environment (ROE): Science Report* (EPA, Washington, DC, 2007); http://cfpub.epa.gov/roe/.

10.1126/science.1154521

LEARNING THEORY

The Advantage of Abstract Examples in Learning Math

Undergraduate students may benefit more from learning mathematics through a single abstract, symbolic representation than from learning multiple concrete examples.

Jennifer A. Kaminski,* Vladimir M. Sloutsky, Andrew F. Heckler

Abstract knowledge, such as mathematical knowledge, is often difficult to acquire and even more difficult to apply to novel situations (*1*–*3*). It is widely believed that a successful approach to this challenge is to present the learner with multiple concrete and highly familiar examples of the to-be-learned concept. For instance, a mathematics instructor teaching simple probability theory may present probabilities by randomly choosing a red marble from a bag containing red and blue marbles and by rolling a six-sided die. These concrete, familiar examples instantiate the concept of probability and may facilitate learning by connecting the learner's existing knowledge with new, to-be-learned knowledge. Alternatively, the concept can be instantiated in a more abstract manner as the probability of choosing one of n things from a larger set of m things.

The belief in the effectiveness of multiple concrete instantiations is reasonable: A student who sees a variety of instantiations of a concept may be more likely to recognize a novel analogous situation and apply what was learned. Learning multiple instantiations of a concept may result in an abstract, schematic knowledge representation (*1*, *4*), which, in turn, promotes knowledge transfer, or application of the learned concept to novel situations (*1*, *5*). However, concrete information may compete for attention with deep to-be-learned structure (*6*–*8*). Specifically, transfer of conceptual knowledge is more likely to occur after learning a generic instantiation than after learning a concrete one (*7*).

Therefore, we ask: Is learning multiple concrete instantiations the most efficient route to promoting transfer of mathematical knowledge? Here, we tested a hypothesis that learning a single generic instantiation (that is, one that communicates minimal extraneous information) may result in better knowledge transfer than learning multiple concrete, contextualized instantiations.

In experiment 1, undergraduate college students learned one or more instantiations of a simple mathematical concept. They were then presented with a transfer task that was a novel instantiation of the learned concept. The to-be-learned concept was that of a commutative mathematical group of order three. This concept is a set of three elements, or equivalence classes, and an operation with the associative and commutative properties, an identity element, and inverses for each element. This concept was chosen because it involves the most basic properties of the real number system, yet it is simple, novel to the study participants, and can be easily instantiated in different ways.

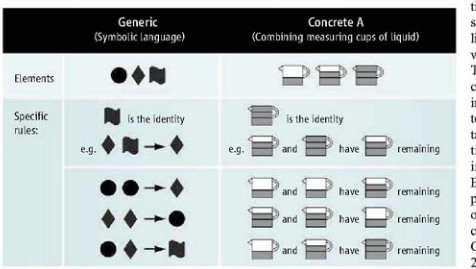

Generic and concrete instantiations of a mathematical group.

One instantiation used in this research was generic. This instantiation was described as a written language involving three symbols (see figure, above) in which combinations of two or more symbols yield a predictable resulting symbol. Statements were expressed as *symbol 1, symbol 2 → resulting symbol.* Three other instantiations (Concrete A, B, and C) were concrete, contextualized, and involved elements that might appear meaningful in the context. The Concrete A instantiation was shown in previous research to facilitate quick learning of the rules of the mathematical group (*6*). The elements were three images of measuring cups containing varying levels of liquid (see figure, below). Participants were told they needed to determine a remaining amount when different measuring cups of liquid are combined. Concrete B and C instantiations were constructed similarly, with story lines and elements that would assist learning. The same mathematical rules were presented in slices of pizza or tennis balls in a container, rather than portions of a measuring cup of liquid (*9*). Eighty study participants were assigned to one of four learning conditions: Generic 1, Concrete 1, Concrete 2, or Concrete 3, with participants learning one generic instantiation, one concrete instantiation, two concrete instantiations, or three concrete instantiations, respectively.

Training was equated across conditions; all participants were presented with the same rules and the same number of examples, questions with feedback, and test questions. After this learning phase, all participants were presented with the same transfer task, which was a novel concrete instantiation of the same group structure that was presented during learning. The transfer instantiation involved perceptually rich elements, as do many real-world instantiations of mathematics, and was described as a children's game involving three objects (*9*). In the game, children sequentially pointed to objects; and a child who was "it" pointed to a final object. If the child pointed to the correct final object, then he or she was the winner. The correct final object was specified by the rules of the game (rules of the mathematical group). Participants received no explicit training in the transfer domain. Instead, they were told that the rules of the game were like the rules of the system(s) they had just learned and that they could figure out these rules by using their newly acquired knowledge. After being asked to study

Center for Cognitive Science, Ohio State University, Columbus, OH 43210, USA.

*Author for correspondence. E-mail: kaminski.16@osu.edu

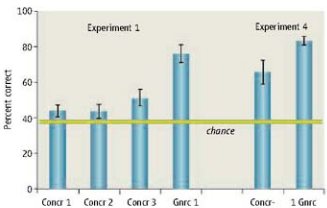

Transfer test scores across learning conditions (means ± SEM).

a series of examples, from which the rules could be deduced, they received a 24-question multiple-choice test isomorphic to the questions they answered during the learning phase.

In all conditions of this experiment (as well as the other experiments reported here), participants successfully learned the material with no differences in learning scores ($F_{3,68} < 1$) or learning times ($F_{3,68} < 1.5$). However, there were significant differences in transfer (see experiment 1, in the figure above). Participants in the Generic 1 condition performed markedly higher than participants in each of the three concrete conditions ($F_{3,68} = 11.9$, $P < 0.001$; post hoc Tukey's test, P values < 0.002). Furthermore, transfer in the Generic 1 condition was above chance ($t > 7$, $P < 0.005$), whereas transfer in the concrete conditions did not reliably exceed chance (t values < 1.7, P values > 0.35; $t = 2.8$, $P = 0.06$ for Concrete 3).

These results indicate that learning one, two, or three concrete instantiations resulted in little or no transfer, whereas learning one generic instantiation resulted in significant transfer. If transfer from multiple instantiations depends on whether the learner abstracts and aligns the common structure from the learned instantiations (*1*, *4*), then transfer failure suggests that participants may have been unable to recognize and align the underlying structure.

In two additional experiments, we assisted structural alignment. In experiment 2, 20 participants learned Concrete A and Concrete B instantiations and were given the alignment of analogous elements across the learning instantiations. To our surprise, this assistance yielded no improvement in transfer; scores were not above chance (means ± SD: 41% ± 16.7%, $t_{19} = 0.94$, $P > 0.35$). In experiment 3, we asked 20 participants after learning Concrete A and Concrete B instantiations to compare them, by matching analogous elements and writing any observed similarities. Explicit comparisons have been shown to facilitate transfer (*5*, *10*). All participants correctly matched elements, but the distribution of transfer scores was bimodal. Approximately 44% of our participants scored highly on the transfer test (95% ± 4.7%). However, the remaining participants did not do well (51% ± 11.6%). Therefore, the act of explicit comparison may help some, perhaps high-performing, learners transfer, but may not help others (*11*).

Overall, concrete and generic instantiations have different advantages. Concrete instantiations may be more engaging for the learner and may facilitate initial learning (*6*), but do not necessarily promote transfer. At the same time, generic instantiations can be learned and do promote transfer. On these grounds, one could argue that presenting a concrete instantiation and then a generic instantiation may be an optimal learning design for promoting transfer. One could also argue that the concrete instantiations used in experiments 1 to 3 are very similar to each other and that successful transfer might require instantiations that are more diverse.

We address these issues in experiment 4. Forty participants were assigned to one of two learning conditions: One-Generic (participants learned the generic instantiation) or Concrete-then-Generic (participants learned the Concrete A instantiation then the Generic instantiation). The results were that participants who learned only the generic instantiation outperformed those who learned both concrete and generic instantiations (see experiment 4 in the figure above; $t_{31} = 2.7$, $P < 0.02$).

Our findings suggest that giving college students multiple concrete examples may not be the most efficient means of promoting transfer of knowledge. Moreover, because the concept used in this research involved basic mathematical principles and test questions were both novel and complex, these findings could likely be generalized to other areas of mathematics. For example, solution strategies may be less likely to transfer from problems involving moving trains or changing water levels than from problems involving only variables and numbers. Instantiating an abstract concept in a concrete, contextualized manner appears to constrain that knowledge and to hinder the ability to recognize the same concept elsewhere; this, in turn, obstructs knowledge transfer. At the same time, learning a generic instantiation allows for transfer, which suggests that such an instantiation could result in a portable knowledge representation. Compared with concrete instantiations, generic instantiations present minimal extraneous information and hence represent mathematical concepts in a manner close to the abstract rules themselves.

Because the difficulty of transferring knowledge acquired from concrete instantiations may stem from extraneous information diverting attention from the relevant mathematical structure, concrete instantiations are also likely to hinder transfer for young learners who are less able than adults to control their attentional focus. We have evidence that 11-year-olds transferred successfully from a generic instantiation, but not from a concrete one (*12*).

If a goal of teaching mathematics is to produce knowledge that students can apply to multiple situations, then presenting mathematical concepts through generic instantiations, such as traditional symbolic notation, may be more effective than a series of "good examples." This is not to say that educational design should not incorporate contextualized examples. What we are suggesting is that grounding mathematics deeply in concrete contexts can potentially limit its applicability. Students might be better able to generalize mathematical concepts to various situations if the concepts have been introduced with the use of generic instantiations.

References and Notes

1. M. L. Gick, K. J. Holyoak, *Cogn. Psychol.* **15**, 1 (1983).
2. L. R. Novick, *J. Exp. Psychol. Learn. Mem. Cogn.* **14**, 510 (1988).
3. S. K. Reed, A. Dempster, M. Ettinger, *J. Exp. Psychol. Learn. Mem. Cogn.* **11**, 106 (1985).
4. L. R. Novick, K. J. Holyoak, *J. Exp. Psychol. Learn. Mem. Cogn.* **17**, 387 (1991).
5. R. Catrambone, K. J. Holyoak, *J. Exp. Psychol. Learn. Mem. Cogn.* **15**, 1147 (1989).
6. J. A. Kaminski, V. M. Sloutsky, A. F. Heckler, in *Proceedings of the 27th Annual Conference of the Cognitive Science Society*, B. Bara, L. Barsalou, M. Bucciarelli, Eds., Stresa, Italy, 21 to 23 July 2005 (Lawrence Erlbaum, Mahwah, NJ, 2005), pp. 1090–1095.
7. V. M. Sloutsky, J. A. Kaminski, A. F. Heckler, *Psychonom. Bull. Rev.* **12**, 508 (2005).
8. R. L. Goldstone, Y. Sakamoto, *Cogn. Psychol.* **46**, 414 (2003).
9. Materials and methods are available as supporting material on *Science* Online.
10. D. Gentner, J. Loewenstein, L. Thompson, *J. Educ. Psychol.* **95**, 393 (2003).
11. Learning scores differed between participants who transferred and those who did not (means ± SD: 93% ± 4.4% and 84% ± 12.9%, respectively), independent sample t test, $t_{34} = 1.97$, $P = 0.066$.
12. J. A. Kaminski, V. M. Sloutsky, A. F. Heckler, in *Proceedings of the 27th Annual Conference of the Cognitive Science Society*, R. Sun, N. Miyake, Eds., Vancouver, BC, 26 to 29 July 2006 (Lawrence Erlbaum, Mahwah, NJ, 2006), pp. 411–416.
13. Supported by the Institute of Education Sciences, U.S. Department of Education, through grants R305H050125 and R305B070407. The opinions expressed are those of the authors and do not represent views of the Institute or the U.S. Department of Education.

10.1126/science.1154659

Supporting Online Material
www.sciencemag.org/cgi/content/full/320/5875/454/DC1

BIOPHYSICS

Enigmas of Blood Clot Elasticity

Biophysical studies are beginning to elucidate the molecular mechanisms that lead to the unique viscoelastic properties of blood clots.

John W. Weisel

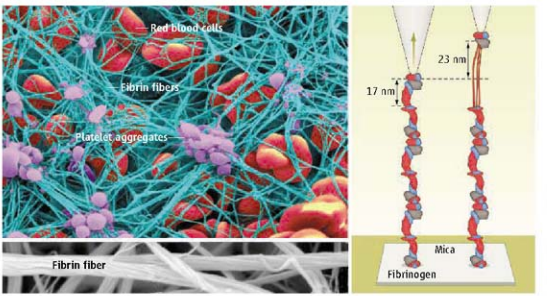

Structure and mechanical properties of fibrin. (Upper left) A whole blood clot is made up of a branched network of fibrin fibers (blue), platelet aggregates (purple), and red blood cells. **(Lower left)** Fibrin fibers have been visualized by scanning electron microscopy. **(Right)** The unfolding of domains of fibrinogen has been studied by pulling with the tip of an atomic force microscope.

Fibrin is the primary structural protein of the blood clot, and its mechanical characteristics are essential to stop bleeding. Yet, although clotting is vital to the preservation of life, blood clots that impede the flow of blood in vivo—called thrombi—are responsible for most heart attacks and strokes and complicate other pathological conditions, including many types of cancer and peripheral vascular disease. Recent studies have begun to shed light on the molecular origins of the mechanical properties of fibrin clots.

The soluble precursor protein of fibrin in blood is fibrinogen, which is converted by cleavage of small peptides to fibrin. Initially a monomer, fibrin then polymerizes to form the fibrin clot, a gel or network of fibers (see the figure, upper left panel). Formation of this clot generally accompanies aggregation of platelets at the site of injury to form a plug that stems leakage of blood from the blood vessels.

The fibrin clot is a viscoelastic polymer, which means that it displays the elastic properties of a spring and the viscous properties of a typical fluid (*1*). Fibrin's viscoelastic properties determine whether a thrombus will have a tendency to become occlusive or to break apart so that fragments block smaller blood vessels, as well as the likely response of the thrombus to common clinical treatments, including angioplasty or thrombolysis. The clinical significance of clot mechanical properties is illustrated by the fact that the stiffness of clots formed from the blood of patients who have had heart attacks at an early age is 50% greater than that of controls, indicating that these clots are abnormal (*2*).

Since the first large-scale purification of fibrinogen more than 60 years ago, scientists have learned a great deal about fibrinogen's structure, the process of fibrin polymerization, and the structure and mechanical properties of clots (*3*, *4*). Yet, we still know relatively little about the origin of the viscoelastic properties of fibrin clots. Its viscoelastic properties are similar to those of a lightly cross-linked rubber, but its structure is very different. The fibrin in a typical physiological clot will occupy only about 0.25% of the total volume of blood, and a stable gel can be formed with fibrin polymer comprising just 0.0025% of the volume. Clots are made up of a coarse network of branching fibers instead of the random-coil network of thin, highly flexible strands found in typical rubbers. The extent of our ignorance of the origin of fibrin's mechanical properties is so great that straightforward calculations of branch point density from clot stiffness are off by ~6 orders of magnitude (*5*).

Some clues to the origin of clot elasticity have come from examination of correlations between the structures and mechanical properties for a wide variety of clots (*6*). The long, thin fibers that make up fibrin clots are stiffer with respect to stretching than bending, implying that clot elasticity likely involves fiber bending (*5*). Indeed, bending of fibers and reorientation of fibers in the direction of the stress accompanies the deformation of clots (*7*). By pulling with optical tweezers on beads attached to individual fibers, the stiffness and elastic moduli of fibrin fibers in a clot have been measured (*8*).

At large strains, clot stiffness increases, which is uncommon and may be important physiologically—especially under the high stresses of arterial blood flow—if it affects clot strength. Theoretical work is beginning to shed light on the molecular basis for this unusual behavior (*9*). At the microscopic level, individual fibers have been stretched by as much as a factor of six with the tip of an atomic force microscope before rupture, making them the most highly extensible biological polymers known (see the figure, lower left panel) (*10*). Extending the earlier optical tweezers results on the elastic properties of fibers (*8*) to different strains should provide some clues to the microscopic origin of the viscous properties of fibrin clots.

Molecular mechanisms accounting for clot mechanical properties are emerging. It now seems clear that some domains of fibrin molecules unfold with stress. Unfolding experiments on single fibrinogen molecules and naturally occurring fibrin polymers yield results that are nearly impossible to interpret, because the structures are so complex that many unfolding events are possible. Tandem repeats of individual domains would aid interpretation but are difficult to prepare. To get around these problems, single-stranded fibrinogen polymers have been prepared and

Department of Cell and Developmental Biology, University of Pennsylvania School of Medicine, Philadelphia, PA 19104, USA. E-mail: weisel@mail.med.upenn.edu

the unfolding of fibrin(ogen) domains has been measured by single-molecule atomic force microscopy (see the figure, right panel) (*11*). These results suggest that the α-helical coiled-coils unfold first, acting as a molecular source of clot resilience, which may be the first clearly demonstrated biological function for protein unfolding.

Molecular dynamics simulations can help clarify experimental results (*12*, *13*), but simulations on appropriate time scales for this large and complex molecule may require the use of coarse-grained methods. Knowing which fibrin domains are mechanically stable and which domains unfold might one day help to clarify the associations between molecular and clot properties and suggest novel sites for drug targeting.

Better understanding of the molecular origins of clot elasticity should make it possible to relate mechanical properties of different clots to their structures. Studies of clots made from recombinant or naturally occurring fibrinogen mutants are likely to be useful for these efforts. Clots including platelets are more complex, because the platelets control fibrin polymerization, and the structure of thrombi is also determined by the forces and transport of blood flow. Furthermore, platelets are filled with actin and myosin and thus generate large contractile stresses on fibrin clots, somewhat like other active-gel systems, such as actin filaments with myosin (*14*) or microtubules with kinesin or dynein (*15*).

The challenges to determining the microscopic and molecular properties of fibrin are manifold, but overcoming them will lead to an understanding of the clot mechanical properties at the molecular, fiber, and whole-clot levels. These insights may enable us to prevent many life-threatening maladies and develop new treatments.

References

1. J. W. Weisel, *Biophys. Chem.* **112**, 267 (2004).
2. J.-P. Collet *et al.*, *Arterioscleros. Thromb. Vasc. Biol.* **26**, 2567 (2006).
3. J. W. Weisel, in *Advances in Protein Chemistry*, D. A. D. Parry, J. Squire, Eds. (Elsevier, San Diego, 2005), vol. 70, pp. 247–299.
4. S. T. Lord, *Curr. Opin. Hematol.* **14**, 236 (2007).
5. J. D. Ferry, in *Biological and Synthetic Polymer Networks*, O. Kramer, Ed. (Elsevier, Amsterdam, 1988), pp. 41–55.
6. E. A. Ryan *et al.*, *Biophys. J.* **77**, 2813 (1999).
7. M. F. Müller, H. Ris, J. D. Ferry, *J. Mol. Biol.* **174**, 369 (1984).
8. J.-P. Collet, H. Shuman, R. E. Ledger, S. Lee, J. W. Weisel, *Proc. Natl. Acad. Sci. U.S.A.* **102**, 9133 (2005).
9. C. Storm, J. J. Pastore, F. C. MacKintosh, T. C. Lubensky, P. A. Janmey, *Nature* **435**, 191 (2005).
10. W. Liu *et al.*, *Science* **313**, 634 (2006).
11. A. E. X. Brown, R. I. Litvinov, D. E. Discher, J. W. Weisel, *Biophys. J.* **92**, L39 (2007).
12. M. Sotomayor, K. Schulten, *Science* **316**, 1144 (2007).
13. B. Lim *et al.*, *Structure* **16**, 449 (2008).
14. D. Mizuno, C. Tardin, C. F. Schmidt, F. C. MacKintosh, *Science* **315**, 370 (2007).
15. T. Surrey, F. Nedelec, S. Leibler, E. Karsenti, *Science* **292**, 1167 (2001).

10.1126/science.1154210

PLANETARY SCIENCE

Identifying Ancient Asteroids

Remote spectroscopy has identified the oldest asteroids in the solar system.

Thomas H. Burbine

More than 400,000 asteroids have been identified in the solar system to date. These objects are thought to be the surviving remnants of the planetesimals that formed the planets about 4.6 billion years ago. The ages and mineralogical characteristics of these planetesimals can be estimated through high-precision laboratory analyses of the compositional and isotopic properties of meteorites, of which more than 30,000 samples exist. Until now there has been no way to estimate when an asteroid formed, other than assuming that its age was similar to that of most meteorites. On page 514 of this issue, Sunshine *et al.* (*1*) present results of a remote spectroscopic study to show that a number of asteroids are enriched in the oldest known objects in the solar system (calcium-aluminum inclusions or CAIs) (see the figure), thereby making them the most ancient asteroids currently known.

CAIs are common components of the most primitive meteorites, carbonaceous chondrites, which have not undergone significant heating and are thought to be representative of the composition of the solar nebula. CAIs are predicted to be the first condensates that formed out of the solar nebula and can have ages as old as ~4.567 billion years (*2*). Also commonly found in carbonaceous chondrites are chondrules, cooled molten droplets that formed during the rapid heating and then cooling of solid precursor material. On average, chondrules appear to have formed 2 million to 3 million years after CAIs (*3*). This age difference between CAIs and chondrules indicates that CAIs were removed from the innermost regions of the protoplanetary disk, where they are assumed to have first formed, soon after they first condensed. Without this early removal, the isotopes of the CAIs would have been reset during the heating and cooling period of chondrule formation and the ages of the CAIs would resemble chondrules. Thus, the identification of a CAI-rich asteroid would date its formation at ~4.567 billion years ago.

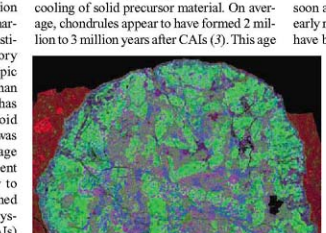

Ancient asteroids. False-color x-ray elemental map (*10*) of a calcium-aluminum inclusion (CAI) in the Allende meteorite. The predominantly greenish, circular object is the CAI and spinel minerals are the violet areas in the CAI. Red, areas enriched in Mg; green, areas enriched in Ca; blue areas enriched in Al.

In the early 1990s, spinel ($MgAl_2O_4$) was shown to be abundant on the surfaces of some asteroids (387 Aquitania and 980 Anacostia) (*4*). Near-infrared data (*5*) indicated that these objects have a very strong absorption feature centered at wavelengths around 2 μm, which is indicative of spinel with at least a small concentration of Fe^{2+}. Pyroxene, a likely suspect as the most common mineral with an absorption band centered near 2.0 μm, could be ruled out because it also has a strong absorption at ~0.9 μm, which was not present in the spectra of these asteroids. CAIs, the only component in meteorites that contain spectrally significant abundances of

Department of Astronomy, Mount Holyoke College, South Hadley, MA 01075, USA. E-mail: tburbine@mtholyoke.edu

spinel, were the most likely source of the absorption, but a spinel-rich surface due to igneous processes could not be ruled out.

In a study that should be the template for future analyses of asteroids because of its combination of telescopic observations, meteoritic characterization, and spectral modeling, Sunshine *et al.* can now precisely link spinel-rich asteroids and CAIs. A visible spectroscopic survey of more than 1000 asteroids (*6*) identified possible spinel-rich objects in the visible-wavelength region due to their strongly reddish (reflectance increasing with increasing wavelength) spectra below ~0.75 μm and their featureless flat spectra from ~0.75 to 0.92 μm. Near-infrared measurements using SpeX (*7*), a medium-resolution infrared spectrograph located at the NASA Infrared Telescope Facility on Mauna Kea, found that these objects had the strong absorption characteristic of spinel. To determine the best compositional analog for these asteroids, CAIs and CAI-free matrix material from the CV chondrite Allende were separated out and characterized. Spectral modeling of the components was then done to best match the spectra of the asteroids and to narrow down the mineralogical interpretation.

One unanswered question is why these asteroids did not melt, which would have obliterated the spectral signature of the CAIs. If these asteroids contained the typical, initial $^{26}Al/^{27}Al$ ratios found in CAIs, their high aluminum contents should have caused melting. Perhaps these objects contained much lower abundances of $^{26}Al/^{27}Al$ and therefore constitute evidence for heterogeneous distribution of ^{26}Al in the solar nebula, or perhaps they contained very high abundances of ice (*8*) that acted as a buffer against full-scale melting and differentiation.

Sample return from an asteroid has been attempted only by the Japanese Hayabusa mission (*9*) from a near-Earth object (NEO), whereas the objects identified by Sunshine *et al.* reside in the main asteroid belt. If a spinel-rich NEO can be identified, it surely would be an attractive target for a sample return mission: obtaining for laboratory analysis some of the most primitive material still remaining in the solar system.

References

1. J. M. Sunshine, H. C. Connolly Jr., T. J. McCoy, S. J. Bus, L. M. Croix, *Science* **320**, 514 (2008).
2. Y. Amelin, A. N. Krot, I. D. Hutcheon, A. A. Ulyanov, *Science* **297**, 1678 (2002).
3. J. N. Connelly, Y. Amelin, A. N. Krot, M. Bizzarro, *Astrophys. J.* **675**, L121 (2008).
4. T. H. Burbine, M. J. Gaffey, J. F. Bell, *Meteor. Planet. Sci.* **27**, 424 (1992).
5. J. F. Bell, P. D. Owensby, B. R. Hawke, M. J. Gaffey, *Lunar Planet. Sci. Conf.* **19**, 57 (1988).
6. S. J. Bus, R. P. Binzel, *Icarus* **158**, 106 (2002).
7. J. T. Rayner *et al.*, *Pub. Astron. Soc. Pac.* **115**, 362 (2003).
8. R. E. Grimm, H. Y. McSween Jr., *Icarus* **82**, 242 (1989).
9. H. Yano *et al. Science* **312**, 1350 (2006).
10. T. J. Fagan, Y. Guan, G. J. MacPherson, *Meteor. Planet. Sci.* **42**, 1221 (2007).

10.1126/science.1157604

CELL BIOLOGY

A One-Sided Signal

Changes in the distribution of a lipid within the plasma membrane affect normal cell function and virus infection.

Gregory D. Fairn and Sergio Grinstein

Lipids are increasingly recognized as essential for cells to transduce signals. Phosphoinositides—the phosphorylated derivatives of the membrane lipid phosphatidylinositol—control diverse cellular processes, including cell proliferation and survival, cytoskeletal organization, and vesicle trafficking. Similarly, the membrane lipid phosphatidylserine is key to initiating processes as important and dissimilar as blood coagulation and the clearance of dead cell remnants (apoptotic bodies). Defects in phosphatidylserine metabolism can lead to serious disorders including Scott's syndrome (a rare hemorrhagic disease) and autoimmune diseases such as systemic lupus erythematosus (*1*). Yet despite its importance, little is known about how phosphatidylserine functions during signal transduction. On pages 528 and 531 of this issue, Darland-Ransom *et al.* (*2*) and Mercer and Helenius (*3*) provide new insights into the biology of phosphatidylserine and reveal an unappreciated role in viral infection.

Unlike other phospholipids, the signals conveyed by phosphatidylserine do not entail metabolic conversion but are instead encoded by its subcellular localization. Phosphatidylserine is enriched in the plasma membrane. In healthy cells at rest, virtually all the phosphatidylserine is found in the inner leaflet of this lipid bilayer, where it serves as a molecular beacon for proteins that contain a structural motif called the C2-domain. Moreover, because phosphatidylserine is very abundant (≥20 mol % of the inner leaflet) and is anionic, it contributes substantially to the negative charge of the cytoplasmic face of the plasma membrane and promotes the recruitment of positively charged, polycationic proteins.

The mechanism that generates the striking asymmetry in the transmembrane distribution of phosphatidylserine has been debated extensively, but recent evidence suggests that a class IV P-type ATPase may be the long-sought enzyme (aminophospholipid translocase) that maintains this unequal distribution in the membrane bilayer (*4*, *5*). However, because the mammalian genome encodes at least 14 potential class IV ATPases, definitive genetic confirmation has been lacking. The likelihood that multiple isoforms of this lipid translocase (ATPase) would display redundant function has made removing or silencing the endogenous encoding genes in mammalian cells a daunting task. To circumvent this complication, Darland-Ransom and colleagues took advantage of the model nematode *Caenorhabditis elegans*, which contains only six homologs of these ATPases, also referred to as transbilayer amphipath transporters. Systematic gene silencing using RNA interference revealed that only the ATPase encoded by the gene *tat-1* is required to maintain phosphatidylserine asymmetry. Furthermore, cells that exposed phosphatidylserine on the outer (exofacial) leaflet of their plasma membrane, due to the elimination of *tat-1*, were subject to phagocytosis (internalization) by other cell types, even though the engulfed cells were not overtly undergoing cell death (apoptosis). Interestingly, the phagocytosis of cells exposing phosphatidylserine at the outer surface of their plasma membrane was not exhaustive and appeared to be random. This raises the possibility that engagement of cell surface receptors for phosphatidylserine, such as PSR-1 in *C. elegans* or Tim-1 and Tim-4 in mammalian cells (*6*), may not suffice to trigger phagocytosis, and that other signals

Cell Biology Program, Research Institute, The Hospital for Sick Children, Toronto, Ontario M5G 1X8, Canada. E-mail: sga@sickkids.ca

may contribute to the removal of apoptotic cells. In this regard, the cell surface protein CD36 recognizes oxidized forms of the phospholipid (*7*). A second alteration, such as the oxidation of exofacial phosphatidylserine, may be required for effective clearance of apoptotic bodies.

As reported by Mercer and Helenius, loss of phosphatidylserine asymmetry in the plasma membrane is also important for some viral infections. Like other viruses with a lipid bilayer coating, vaccinia virus acquires its membrane envelope as it buds off of the infected host cell. Because the infected cells undergo apoptosis, and thus experience scrambling of plasma membrane lipids, the budding virus also acquires an envelope that exposes phosphatidylserine on its external surface (see the figure). The authors found that, although not required for the virus to bind to the surface of the host cell, the presence of exofacial phosphatidylserine is required for viral entry. The nature of the internalization pathway is particularly intriguing because like other poxviruses, vaccinia virus is large (≥200 nm in diameter), exceeding the size accommodated by endocytosis, the engulfment process that uses specialized minute invaginations to internalize only a small area of the cell surface. Using a series of pharmacological agents, the authors showed that vaccinia enters cells by a process akin to macropinocytosis, a less specific internalization process that is more generally involved in the uptake of surrounding fluids. The sensitivity of vaccinia entry into cells to inhibitors of tyrosine kinases suggests the involvement of a transmembrane receptor for phosphatidylserine, as well as the existence of separate binding determinants on the receptor for the virus and for phosphatidylserine. This is consistent with a "tether and tickle" mechanism in which a separate attachment site is required for phosphatidylserine receptors to effectively bind and internalize apoptotic cells (*8*). The involvement of phosphatidylserine may not be limited to infection by vaccinia viruses. Papuamide B, a natural compound with anti-HIV properties, also binds to phosphatidylserine (*9*). It is therefore conceivable that HIV similarly requires phosphatidylserine for infection and that papuamide B interferes by occluding the lipid on the viral surface. The role of phosphatidylserine in the entry of HIV and other viruses will surely be explored in greater detail now.

The site(s) where membrane phosphatidylserine asymmetry is generated merit consideration. In eukaryotic cells, phosphatidylserine is synthesized primarily on the cytosolic aspect of the endoplasmic reticulum, an organelle through which secreted proteins pass. However, probes for phosphatidylserine failed to detect significant amounts of this lipid on the cytosolic surface of the endoplasmic reticulum or of the Golgi complex, another organelle of the secretory pathway (*10*, *11*). It is possible that phosphatidylserine fails to accumulate in the secretory pathway organelles because it is rapidly exported through this pathway following its biosynthesis. It may also be that newly synthesized phosphatidylserine is preferentially translocated to the luminal leaflet of these organelles, and thus is inaccessible to specific probes (*10*, *11*). Accordingly, the few studies analyzing phosphatidylserine sidedness in vesicles derived from the endoplasmic reticulum suggest that a vast majority of the lipid is in the luminal leaflet of the membrane (*12*). If these observations are validated, phosphatidylserine and other aminophospholipids could initially be delivered to the external aspect of the plasma membrane upon secretion, and would have to be rapidly "flipped" inward by specific enzymes (flippases). This speculation is lent some credence by the observations that phosphatidylethanolamine accumulates transiently within the membrane of yeast at sites of localized exocytosis and that this effect is accentuated when plasma membrane flippases are inactive (*13*).

Asymmetry in the distribution of plasma membrane phosphatidylserine clearly has functional importance, and the asymmetry may extend to other organelles. Yet our

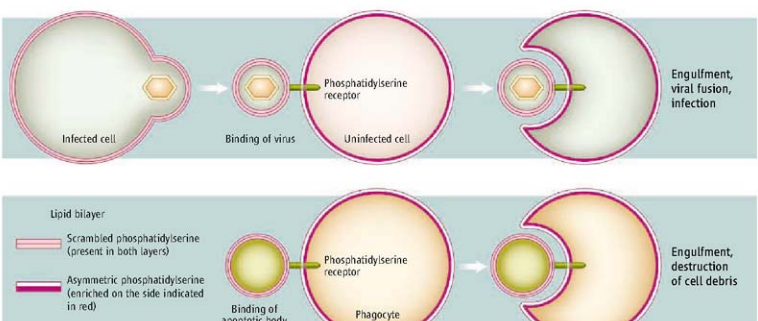

Flipping lipids. A cell undergoing apoptosis exposes phosphatidylserine at its cell surface, a signal for a phagocytic cell to engulf the dying cell (or smaller pieces of the dying cell, called apoptotic bodies). Similarly, in the late stage of vaccinia virus infection, a host cell undergoes apoptosis and externalizes phosphatidylserine in its plasma membrane. A virus budding from this cell thus acquires a membrane envelope that exposes phosphatidylserine on its outer surface. This lipid serves as a signal for viral uptake by a noninfected cell through a mechanism similar to macropinocytosis.

understanding of the molecular mechanisms that generate and maintain phosphatidylserine asymmetry is still in its infancy. The recent identification of phosphatidylserine-specific receptors and the development of genetically encoded biosensors to detect phosphatidylserine in live cells will accelerate discovery in this field.

References and Notes

1. R. F. Zwaal, P. Comfurius, E. M. Bevers, *Cell. Mol. Life Sci.* **62**, 971 (2005).
2. M. Durland-Ransom *et al.*, *Science* **320**, 528 (2008).
3. J. Mercer, A. Helenius, *Science* **320**, 531 (2008).
4. X. Tang *et al.*, *Science* **272**, 1495 (1996).
5. G. Lenoir *et al.*, *Curr. Opin. Chem. Biol.* **11**, 654 (2007).
6. M. Miyanishi *et al.*, *Nature* **450**, 435 (2007).
7. M. E. Greenberg *et al.*, *J. Exp. Med.* **203**, 2613 (2006).
8. P. R. Hoffmann *et al.*, *J. Cell Biol.* **155**, 649 (2001).
9. A. B. Parsons *et al.*, *Cell* **126**, 611 (2006).
10. T. Yeung *et al.*, *Science* **319**, 210 (2008).
11. F. Calderon, H. Y. Kim, *J. Neurochem.* **104**, 1271 (2008).
12. A. Zachowski, *Biochem. J.* **294**, 1 (1993).
13. K. Saito *et al.*, *Dev. Cell* **13**, 743 (2007).

14. Supported by grant 7075 of the Canadian Institutes of Health Research (CIHR) and the Heart and Stroke Foundation of Ontario (S.G.) and a CIHR postdoctoral fellowship (G.D.F.).

10.1126/science.1158173

CLIMATE CHANGE

Carbon Crucible

What are the data and modeling requirements for gauging the success of mitigation strategies in reducing greenhouse gas emissions?

Melinda Marquis[1,2]* and Pieter Tans[2]

Atmospheric measurements show that the carbon dioxide (CO_2) concentration in the atmosphere is currently ~385 parts per million (ppm) and rising fast. But this value is a global average that tells us nothing about the regional distribution of greenhouse gas emissions. As the world embraces myriad mitigation strategies, it must gauge which strategies work and which do not. Gaining such understanding will require a greenhouse gas monitoring system with enough accuracy and precision to quantify objectively the progress in reducing emissions, including regional efforts like those in California, New England, and elsewhere.

The current sparse network of observation sites across North America and elsewhere allows us to resolve annual continental fluxes of CO_2. But successful mitigation requires fluxes to be resolved within much smaller regions—on the order of the size of a European country such as France or a U.S. state such as Kansas. Current ground-based measurement technology can provide the required precision, but the number of measurements is insufficient. Data are collected by numerous agencies around the world, yet an integrated system is needed that uses all available data and ensures rigorous quality control for data collection and data analysis.

A powerful way to use all these data is in a data assimilation system, which combines diverse (and often sparse or incomplete) data and models into a unified description of a physical/biogeochemical system consistent with observations. Components of such systems include models of terrestrial photosynthesis (removal of CO_2, called a sink) and respiration (a source of CO_2), models of ecosystem emissions and uptake of other greenhouse gases, models of gas exchange between atmosphere and oceans, and models of gas emissions from wildfires—all grounded in observations.

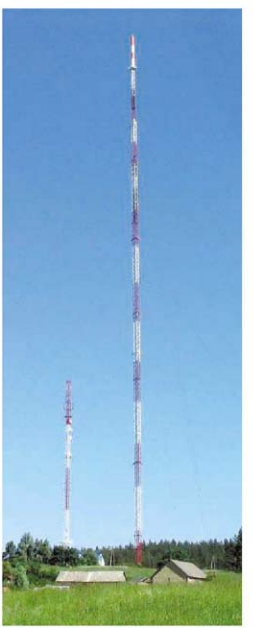

The advantages of height. Atmospheric measurements are made on the tall tower (300 m). The tower, located near Bialystok in eastern Poland, is part of the CarboEurope tall tower network. Similar networks exist in North America and more sparsely in other parts of the world.

CREDIT: MAX PLANCK INSTITUTE FOR BIOGEOCHEMISTRY

The current grid scale for such assimilation systems—such as CarbonTracker, the first data assimilation system to provide CO_2 flux estimates (*1*, *2*)—is limited to ~100 km or larger, primarily due to computer resource limitations. Currently sparse atmospheric greenhouse gas data force us to make the assumption that source variations are coherent over very large spatial scales. More observation sites would make the systems more strongly data-driven. Data assimilation systems also need more refined estimates of fossil fuel emissions, and better process understanding to provide greater detail in emission patterns. Lastly, better models of atmospheric transport will increase the resolution and decrease biases of the data assimilation system. Our ability to distinguish between distant and nearby sources and sinks is limited by how accurately transport models reflect details of the terrain, winds, and atmospheric mixing near the observation sites.

National emissions inventories (which are required by the U.N. Framework Convention on Climate Change) are key data sets for assimilation systems. Inventories are mostly based on economic statistics, which are used to estimate how much of each greenhouse gas enters or leaves the atmosphere (*3*). They are reasonably accurate for CO_2 from fossil fuels (within ~10%) in many developed countries but less so in developing countries and on regional scales. Inventory emission estimates are much less reliable for other CO_2 sources, such as deforestation, and for other major greenhouse gases; for example, the contributions of natural wetlands, rice farming, and cattle to the global methane

[1]Cooperative Institute for Research in Environmental Sciences, 216 UCB University of Colorado, Boulder, CO 80309-0216, USA. [2]National Oceanic and Atmospheric Administration, Earth Systems Research Laboratory, 325 Broadway, Boulder, CO 80305, USA.

*To whom correspondence should be addressed. E-mail: melinda.marquis@noaa.gov

burden are each uncertain to ~30% (*4*). When comparing emission inventories with atmospheric data, substantial errors in the former have been documented (*5*).

The greatest hurdle to rapid progress, however, is the sparseness of atmospheric data. Current measurements include air sampled in flasks, in situ continuous measurements on tall transmitter towers (see the figure), and data from aircraft. Measurements from tall towers are particularly useful. The trace gas concentration observed on a tall tower provides information from a radius of several hundred kilometers. To provide meaningful observation-driven quantification of greenhouse gas sources, the number of sites must be increased from today's ~100 to ~1000, distributed in a suitable global network, and a substantial proportion of these should be tall towers. This could be achieved by placing greenhouse gas measurement instruments on existing communication towers around the world. Vertical-profile observations from aircraft are essential to improve simulation of air exchange between the boundary layer at Earth's surface and the free troposphere above in atmospheric transport models.

Satellite-based instruments can also provide information about CO_2 concentration in the atmosphere, but no current satellite-borne instrument comes close to providing the accuracy, precision, and continuity required to determine regional CO_2 concentrations and local fluxes. Future satellites, including the Orbiting Carbon Observatory (OCO) (*6*) and the Greenhouse Gases Observing Satellite (GOSAT) (*7*), are expected to provide more accurate CO_2 measurements than do today's satellites.

A key component of an improved monitoring system will be simultaneous observations of isotopic ratios and other chemical species characteristic of different source processes. For example, ^{14}C is absent from fossil fuels; recent emissions of fossil-fuel–derived CO_2 reduce the $^{14}C/C$ ratio of CO_2, which can be accurately measured in a few liters of ambient air.

The accuracy requirements for all of these measurements are challenging. For instance, fossil fuel burning in the U.S. adds, on average, less than 1 ppm to the background level of 385 ppm each year. This helps to explain the demanding goal for accuracy of 0.1 ppm for CO_2, and similar goals for CH_4 and N_2O, set by the Global Atmospheric Watch Programme (*8*) of the World Meteorological Organization (WMO). Meeting this goal will require consistent and rigorous application of quality-control and quality-assurance procedures to measurements, analysis, and data handling. Currently, participants in the WMO network can achieve an accuracy of 0.2 ppm, too imprecise by a factor of 2.

Satellite measurements are indispensable in achieving global coverage, but sensor drift (due to temperature effects, aging electronic sources, and the like) and potential artifacts with CO_2 retrieval will be an enduring concern for developing long-term records. The current mission specifications for the OCO satellite require a precision of 1 to 2 ppm, which would be an enormous improvement over that of previous satellites, but may still be too imprecise for regional flux estimates. Satellite retrievals will need continuing validation by comparison to optical absorption spectra that provide CO_2 averaged from the top of the atmosphere to the Earth's surface, and to in situ measurements; the latter will in turn need ongoing duplication by independent methods and laboratories.

Achieving the monitoring system described above will require a global increase in the number of observation sites by roughly a factor of 10, requiring the political will to implement these sites. Further, the success of such a system will require an international framework and support at national levels worldwide, as part of the Global Earth Observation System of Systems (GEOSS). The challenge of creating such a system is a defining test, a critical crucible.

References

1. W. Peters *et al.*, *J. Geophys. Res.* **110**, D24304 (2005).
2. W. Peters *et al.*, *Proc. Natl. Acad. Sci. U.S.A.* **104**, 18925 (2007).
3. U.S. statistics are primarily from the Energy Information Administration, a statistical agency of the U.S. Department of Energy, and from the Environmental Protection Agency.
4. I. Fung *et al.*, *J. Geophys. Res.* **96**, 13033 (1991).
5. P. Bergamaschi *et al.*, *Atmos. Chem. Phys.* **5**, 2431 (2005).
6. D. Crisp *et al.*, *Adv. Space Res.* **34**, 700 (2004).
7. T. Hamazaki, Y. Kaneko, A. Kuze, *Proc. of the XXth ISPRS Congress* (Istanbul, Turkey, 12 to 23 July 2004), pp. 225–227.
8. *Report of the 13th WMO/IAEA Meeting of Experts on Carbon Dioxide Concentration and Related Tracers Measurement Techniques*, (Boulder, CO, USA, 19 to 22 September 2005), WMO Global Atmosphere Watch report no. 168, WMO TD no. 1359.

10.1126/science.1156451

CELL BIOLOGY

RNA Metabolism and Oncogenesis

Regulating the production of RNAs involved in protein synthesis can induce the transformation of cells to an oncogenic state.

Deborah L. Johnson and Sandra A. S. Johnson

The transformation of cells to a malignant state involves the deregulation of protein synthesis. Transfer RNAs (tRNAs) and ribosomal RNAs (rRNAs) are essential components of the cell's protein synthesis machinery. A hallmark of neoplastic transformation is the enhanced accumulation of rRNAs and tRNAs and the increased size of the nucleolus, the site for rRNA synthesis in the nucleus. Underlying these changes is the increased activity of RNA polymerase III, which synthesizes tRNAs, 5*S* rRNAs, and other RNAs that play essential roles in protein synthesis. Although tumor suppressor proteins and oncogenic proteins regulate RNA polymerase III activity (*1*–*5*), a causal connection between rRNA and tRNA metabolism and malignancy has been elusive. Now, a study by Marshall *et al.* (*6*) provides compelling evidence that enhanced activity of this polymerase is indeed essential for cellular transformation.

The transcription of eukaryotic genes requires a set of proteins that specify the placement of RNA polymerase for proper initiation of RNA synthesis to occur. These transcription initiation factors have long been viewed as "housekeeping" proteins. That their activity may be regulated, and that such regulation could be responsible for differential gene expression, once seemed implausible. But, for example, the transcription factor complex TFIIIB, which specifies RNA polymerase III transcription, is indeed controlled by various tumor suppressors and oncogenic proteins (see the figure), suggesting that changes in the complex's activity are associated with malignancy. Because transcription factor complexes are multiprotein structures, their regulation can involve modifications of a single component that can affect interactions among multiple proteins in the complex.

TFIIIB consists of three proteins: the RNA polymerase III–specific components Brf1 and

Department of Biochemistry and Molecular Biology, University of Southern California, Los Angeles, CA 90033, USA. E-mail: johnsond@hsc.usc.edu

Bdp1, and the TATA box–binding protein (TBP), which is required by all nuclear RNA polymerases to initiate transcription. Several tumor suppressor proteins and oncogenes bind directly to TFIIIB constituents. The tumor suppressor retinoblastoma protein binds to Brf1 (*7*), whereas the tumor suppressor p53 associates with TBP (*5*). These interactions disrupt the association of TFIIIB with the transcription factor complex TFIIIC and RNA polymerase III, thereby preventing formation of a functional initiation complex. In contrast, the oncogenic protein c-Myc associates with Brf1 to activate transcription by RNA polymerase III (*2*). Interestingly, TBP not only is regulated by oncogenic stimuli, but also has oncogenic properties (*8*).

Many cell signaling pathways implicated in cell transformation also modify components of transcription factor complexes, affecting their interactions and transcription activity. The extracellular signal–regulated kinase (ERK), which is activated in numerous signaling pathways, phosphorylates Brf1, enhancing TFIIIB-TFIIIC interaction (*9*). Activation of a Ras–mitogen activated protein kinase (MAPK) pathway by epidermal growth factor (EGF) receptor 1 induces the expression of TBP, thus increasing RNA polymerase III–dependent transcription (*10*). In contrast, Maf1 (*11*) and Jnk2 (*10*) are proteins that repress TBP expression. And by inhibiting the phosphatidylinositol 3-kinase (PI 3-kinase)–Akt–mammalian target of rapamycin–S6 kinase signaling pathway, the phosphatase PTEN controls Brf1 and Bdp1 phosphorylation and consequently, the association between TBP and Brf1 (*3*). Despite these findings, it is not known whether specific alterations in the cellular amounts or phosphorylation state of the TFIIIB components are associated with the increased RNA polymerase III–dependent gene activity observed in human cancers.

Marshall *et al.* examined the role of RNA polymerase III–dependent transcription in oncogenic transformation. They selectively activated RNA polymerase III transcription by overexpressing Brf1 in cultured mouse fibroblast and epithelial cells. This increased cell proliferation and promoted anchorage-independent growth (characteristic of transformed cells) and tumorigenesis, indicating that increasing RNA polymerase III activity can lead to oncogenic transformation. These results fit with previous studies revealing that oncogenic signaling pathways induce TBP expression, which alone can induce cellular transformation and tumorigenesis (*8*). Although transcription initiation factors, such as TBP and Brf1, may not be oncogenes in the traditional sense in that they do not necessarily need to be mutated to become oncogenic, it is clear that they serve as critical sites for integrating signals emanating from oncogenic stimuli.

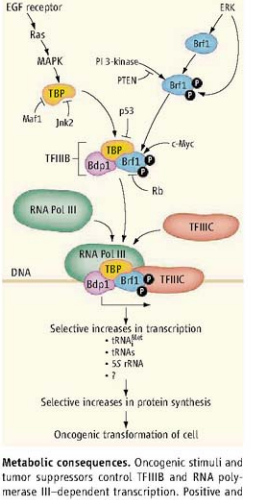

Metabolic consequences. Oncogenic stimuli and tumor suppressors control TFIIIB and RNA polymerase III–dependent transcription. Positive and negative regulators of TFIIIB may alter the expression or function of TBP or Brf1. Alterations in TFIIIB produce differential changes in RNA polymerase III–dependent transcription, resulting in altered expression of specific products. This results in selective changes in protein translation, contributing to oncogenic transformation of a cell.

How might changes in RNA polymerase III–dependent transcription affect the transforming property of cells? Overexpression of the translation initiation factor eIF-4E increases protein production and cell proliferation, suppresses cell death (apoptosis), and promotes malignant transformation (*12*). Unexpectedly, it also results in the preferential translation of mRNAs that encode growth-promoting proteins (*13*). The results of Marshall *et al.* fit with these findings in that changes in the amount of Brf1 do not uniformly increase transcription or resultant protein synthesis, but instead, selectively increase the translation of mRNAs encoding growth-promoting proteins (c-Myc and cyclin D1). Intriguingly, overexpression of $tRNA_i^{Met}$, the tRNA that initiates polypeptide synthesis, mimics the effect of Brf1 overexpression and drives cell proliferation and oncogenic transformation. Thus, $tRNA_i^{Met}$ appears to be rate limiting for the initiation of protein synthesis, pointing to a clear role for tRNA metabolism in dictating the oncogenic state.

How increased expression or enhanced function of TFIIIB components selectively regulate RNA polymerase III–dependent genes remains to be determined. In addition to the increased expression of many RNA polymerase III products, there are also qualitative changes in these products that drive the formation of a transformed cell phenotype. For instance, tissue-specific and developmental regulation of RNA polymerase III–dependent transcription is more common than initially thought (*14*). This opens the possibility that genes transcribed by RNA polymerase III are differentially regulated under various physiological states. It will be interesting to elucidate how Brf1-mediated changes in RNA polymerase III activity potentially alter the pool of various tRNAs to influence the translation of specific mRNAs. Although RNA polymerase III is well known for transcribing tRNAs and 5S rRNAs, recent studies have expanded the repertoire of non–protein-encoding RNAs generated by this enzyme, including microRNAs (*14*). Future work will assess how selective changes in these and other RNA polymerase III gene products influence the oncogenic state.

The finding that the protein synthetic machinery is deregulated in cancer has prompted the investigation of potential cancer therapeutic agents that target components of the translational apparatus (*15*). The study by Marshall *et al.* opens the possibility of targeting components involved in RNA metabolism for generating novel anticancer drugs.

References

1. H. D. Wang, A. Trivedi, D. L. Johnson, *Mol. Cell. Biol.* **17**, 6838 (1997).
2. N. Gomez-Roman, C. Grandori, R. N. Eisenman, R. J. White, *Nature* **421**, 290 (2003).
3. A. Woiwode *et al.*, *Mol. Cell Biol.* 10.1128/MCB.01912-07 (2008).
4. R. J. White, D. Trouche, K. Martin, S. P. Jackson, T. Kouzarides, *Nature* **382**, 88 (1996).
5. D. Crighton *et al.*, *EMBO J.* **22**, 2810 (2003).
6. L. Marshall, N. S. Kenneth, R. J. White, *Cell* **133**, 78 (2008).
7. C. G. Larminie *et al.*, *EMBO J.* **16**, 2061 (1997).
8. S. A. Johnson *et al.*, *Mol. Cell. Biol.* **23**, 3043 (2003).
9. Z. A. Felton-Edkins *et al.*, *EMBO J.* **22**, 2422 (2003).
10. S. Zhong, C. Zhang, D. L. Johnson, *Mol. Cell. Biol.* **24**, 5119 (2004).
11. S. S. Johnson, C. Zhang, J. Fromm, I. M. Willis, D. L. Johnson, *Mol. Cell* **26**, 367 (2007).
12. A. Lazaris-Karatzas, K. S. Montine, N. Sonenberg, *Nature* **345**, 544 (1990).
13. A. De Benedetti, J. R. Graff, *Oncogene* **23**, 3189 (2004).
14. G. Dieci, G. Fiorino, M. Castelnuovo, M. Teichmann, A. Pagano, *Trends Genet.* **23**, 614 (2007).
15. S. C. Thumma, R. A. Kratzke, *Cancer Lett.* **258**, 1 (2007).

10.1126/science.1158680

SCIENCE POLICY

AAAS Works to Raise Science Visibility in 2008 Campaigns

With important science and technology issues receiving only superficial attention in the 2008 U.S. presidential campaigns, AAAS is engaged in a broad effort to raise the profile of S&T in the months leading up to November's election.

The association's efforts reflect a consensus among U.S. science organizations and officials: With the nation at a decisive juncture for addressing future challenges and taking advantage of exciting science-related opportunities, voters need an opportunity to understand each candidate's vision and policy ideas.

"Year by year, the quality of American science looms larger in the overall perspective of our lives," said AAAS Board Chair David Baltimore, who shared the 1975 Nobel Prize in Physiology or Medicine. "Whether in maintaining our economic growth or our personal health or our military strength, science is a key driving force. And yet its importance is rarely discussed in political campaigns."

"AAAS has broad expertise in science policy, and its authority and nonpartisan approach are well-known and respected among policymakers," added former U.S. Representative John Edward Porter, who now serves as chairman of Research!America and as a partner in the Washington, D.C., law firm of Hogan & Hartson. "That puts AAAS in a strong position to promote discussion of science-related issues in this year's campaigns."

AAAS is using a variety of tools to give science an impact on the campaign: Web sites, newspaper columns, debates, and seminars.

Baltimore, writing with fellow Nobel laureate Ahmed Zewail, published an op-ed on 17 April in *The Wall Street Journal* calling for a renewed U.S. commitment to science and technology. Alan I. Leshner, the association's CEO and executive publisher of *Science*, authored commentaries in *The Des Moines Register* and *The Philadelphia Inquirer*, urging the candidates to more forcefully address science issues.

Past and current AAAS officials have been prominent among the supporters of Science Debate 2008, a proposed presidential debate on S&T policy also backed by the National Academy of Sciences, the National Academy of Engineering, the U.S. Institute of Medicine, the Council on Competitiveness, and more than two dozen Nobel laureates—plus thousands of other groups and individuals.

But when the candidates did not respond favorably to a debate proposed for 18 April, just before the Pennsylvania primary, the organizers issued a new invitation to debate in Oregon, offering three possible dates before the state's 20 May primary.

CREDIT: MICHAEL J. COLELLA

(left to right) Thomas Kalil, S&T adviser to the campaign of Senator Hillary Clinton; moderator Claudia Dreifus of the *New York Times*; and Alec Ross, S&T adviser to the campaign of Senator Barack Obama, during a debate at the AAAS Annual Meeting in Boston.

"AAAS joined with other organizations to try to raise the visibility of science-related issues in the presidential campaign by encouraging a science debate," Baltimore explained. "Thus far we have not been successful, but at least we have been able to get some publicity for our concern about the place of science in the next administration."

A preview of a possible debate played out in February during the AAAS Annual Meeting in Boston, when S&T advisers for Democratic candidates Hillary Clinton and Barack Obama appeared on the same stage to discuss the issues. (The campaign of Republican candidate John McCain was invited, but was unable to send anyone to the event.)

Scientists and journalists jammed the hall for the debate between Alec Ross, Obama's adviser on technology, media and telecommunications, and Thomas Kalil, Clinton's adviser for science, technology and innovation.

The advisers shared much common ground. Each said his candidate would reduce political pressures on federal research, double the amount of federal funding for basic science, push for increased information technology to streamline health care, and help build a 21st-century workforce by supporting science, technology, engineering, and mathematics education.

But Kalil argued that Clinton has been "a lot more specific" about her proposals for using S&T investment to restore American economic competitiveness. Ross countered that Obama has produced a "dense," detailed platform on technology issues in particular.

Details about all of the candidates' positions and other election resources can be found at Science and Technology in the 2008 Election—http://election2008.aaas.org—a Web site developed and managed by the AAAS Center for Science, Technology and Congress.

To help raise the profile of S&T issues in other elections, AAAS has joined with eight other scientific societies in cosponsoring the first annual Campaign Education Workshop on 10 May in Washington, D.C. The nonpartisan workshop, organized by Scientists & Engineers for America (SEA), will focus on the practical considerations of running for office as well as specific ways that scientists can become more involved in political campaigns.

The event is an outgrowth of a workshop organized last July by AAAS and SEA as part of the professional development program for AAAS Science & Technology Policy Fellows.

PUBLIC ENGAGEMENT

Workshops Build Story-Telling Skills of Scientists

More than 100 researchers seeking to sharpen their communication skills attended free workshops in San Jose, California, and Raleigh, North Carolina, this spring, as part of an initiative by AAAS to encourage researchers to engage with the public on science and technology topics.

Like many of the participants, Rikke Kvist Preisler had personal and professional reasons for attending the 14 March San Jose seminar. "I often find myself in a situation where school groups, my friends or family, or acquaintances ask me what I do," the University of California-Santa Cruz doctoral student said, admitting that she "often has difficulties explaining what I do in a clear, concise manner, without oversimplifying everything."

The "Communicating Science" workshops, sponsored by the AAAS Center for Public

Engagement with Science and Technology and the National Science Foundation, are one way to break down "the us-versus-them" barrier that can exist between scientists and the public, said Tiffany Lohwater, AAAS's public engagement manager. "The idea with these workshops is to

Allison Leidner at the Raleigh, N.C., workshop.

give scientists tools for communicating research in a way that the public can become involved and interested," she explained.

In small, interactive groups, the participants learned to distill their data into short, meaningful, and memorable messages: prepare for media interviews; reach new audiences through social networking groups such as Facebook; and even rehearse prop use and gestures for their talks.

Igor Gorodezky, a graduate student at the Center for Applied Mathematics at Cornell University who attended the 3 April Raleigh seminar, was interested especially in the perspectives offered by the workshop's panel of reporters and editors. "Getting such a completely candid perspective on how science gets presented to the public from people who do it for a living was really eye-opening," he said.

Stuart Wooley, an assistant professor of biological sciences at California State University-Stanislaus who attended the San Jose workshop, considers public outreach "part of my job responsibilities." But he acknowledged some wariness about the press, recalling several colleagues who have been "misquoted and embarrassed" by news stories. "I think I have something to offer," he said, "but I want to make sure what I offer is correct and that it is transmitted to the reader or listener correctly."

Wooley, who talks about his botanical research in front of K–12 students, farmers, and city government officials, was glad to have more information on engaging all kinds of audiences. Similarly, Allison Leidner, a Ph.D. student in zoology at North Carolina State University, told her group at the Raleigh workshop that her audience would include everyone from the families she meets on the beach while collecting butterflies to members of Congress.

According to Lohwater, many of the researchers seemed glad to find out that they were not alone in their desire to become better communicators. "We knew this kind of networking would be a side benefit, but we had people saying that it was one of the most powerful things about the workshops," she said.

Lohwater and her colleagues expect to offer more workshops around the country beginning this September, at the start of a new academic year. In the meantime, the project's Web site, www.aaas.org/communicatingscience, offers a variety of tools, background materials, and even short "webinars" that can help scientists become better storytellers.

—*Becky Ham*

SCIENCE & SECURITY

Briefing Offers Defense Lessons from Biology

When U.S. Navy submarine designers wanted to improve the hydrodynamics of their sub designs to create a powerful vessel that could cruise the seas for long distances, they found inspiration in the steamlined body shape of the globe-circling skipjack tuna.

The now-decommissioned Skipjack submarines are just one example of how international analysts can look to nature for help in developing nontraditional ways to defend against security threats, according to natural defense expert and Duke University researcher Raphael Sagarin. He spoke at a 10 April briefing sponsored by the AAAS Center for Science, Technology and Security Policy.

"Thinking about the problem holistically may help us understand where and how to intervene, and nature has given us numerous examples of how this can be done," said Center project director Kavita Berger, who organized the briefing.

The natural defenses lecture was the latest in a series of briefings this spring that focused on the nexus of science and security. The Center also gathered experts in Washington, D.C., to analyze the U.S. Navy's February shoot-down of a crippled spy satellite and to discuss the potential diversion of civilian nuclear materials into weapons manufacture.

Speakers at the 18 March satellite briefing focused on the data necessary to determine whether the dangers posed by toxic hydrazine fuel on the plummeting satellite were significant enough to justify the shoot-down, or whether the U.S. government used the satellite's demise as a pretext for testing anti-satellite systems in the wake of a similar shoot-down by the Chinese government last year.

Geoffrey Forden, a senior research associate in the Securities Studies Program at the Massachusetts Institute of Technology, said that even if the satellite's fuel tank did explode during reentry, there was only a 3.5% chance that an individual on the ground would be injured or killed as a result. Forden and Jeffrey Lewis, an arms control specialist at the nonprofit New America Foundation, urged the Pentagon to release its own risk assessment and simulation data to clarify why the agency considered the satellite too risky to leave alone.

At a 25 March briefing on Capitol Hill, speakers warned that the International Atomic Energy Agency (IAEA) "needs to be greatly improved" if it is to safeguard an expected proliferation of nuclear power plants around the world.

The IAEA's monitoring capabilities are stretched to their limit, according to Henry Sokolski, executive director of the Nonproliferation Policy Education Center. He said nearly 800 of the IAEA's 1200 surveillance cameras—placed in nuclear facilities worldwide to monitor suspicious activity—can't provide real-time video feeds to the agency headquarters in Vienna.

Funded by the MacArthur Foundation, the AAAS Center for Science, Technology and Security Policy promotes the integration of science into international and national security policy, including biosecurity, cybersecurity, and nuclear issues.

—*Earl Lane, Benjamin Somers, and Becky Ham*

EDUCATION

AAAS's Summers Receives Lifetime Achievement Award

Laureen Summers, a program associate in Education and Human Resources at AAAS, has received the Lifetime Achievement Award from Science Education for Students with Disabilities (SESD) for her efforts to make science accessible for all children in school classrooms.

In addition to mentoring undergraduate and graduate students on course work and internships, Summers manages NASA's involvement in the AAAS ENTRY POINT! program, which provides competitive, paid summer internships in top government and private research institutions around the country to promising science and math students with disabilities.

"Through her mentorship, Laureen has made significant contributions to increasing the number of people with disabilities who have entered science, technology, engineering, and mathematics programs and the workforce," said Babette Moeller, a past SESD president.

Summers, who has cerebral palsy that affects her speech and muscular coordination, said she was honored to be recognized by SESD, and stressed the importance of the organization's work. "Science education is tremendously exciting, and every student should have access to every aspect of science," she said. "To deny it to anyone is a huge loss."

Summers received the award on 29 March at the National Science Teachers Association's national conference in Boston.

—*Benjamin Somers*

CREDIT: PHOTO COURTESY OF STEVEN R. MCCAW

INTRODUCTION

Green Genes

THE FINISHED SEQUENCES OF THE FLOWERING plants *Arabidopsis*, rice, poplar, and grape; the moss *Physcomitrella*, and the algae *Chlamydomonas* have begun to allow us to understand how plant genomes share common ground with the genomes of other organisms and how they differ. In this special section, along with an online collection (www.sciencemag.org/plantgenomes), we see how current knowledge of plant genomes lends insights to investigations from biochemistry to ecosystems. Taking a comparative view of plant genomes, DellaPenna and Last (p. 479) consider how metabolic pathways are encoded in the genomes and are derived from a complex evolutionary history. Leitch and Leitch (p. 481) discuss why polyploidy is so common in plants and its evolutionary and ecological consequences. Gaut and Ross-Ibarra (p. 484) examine the evolutionary constraints on a plant's genome, with a particular focus on how genomes enlarge or shrink without changing their number of chromosomes. Tang *et al.* (p. 486) look at the consequences of these changes over time and how to uncover genomic changes through the examination of synteny and collinearity. Zhang (p. 489) examines the genomic landscape of epigenetics in plants. In an ecological context, Whitham *et al.* (p. 492) explore how the genome of a single keystone species affects interactions across communities and ecosystems. Benfey and Mitchell-Olds (p. 495) examine gene regulation from a systems network perspective and consider how natural variation and environmental inputs affect the phenotype of an individual.

Online
sciencemag.org
Explore an interactive feature about plant genomes, from evolutionary insight to crop development.

Plant genomics also brings the promise of improving crops through transgenic manipulations. But genetically modified (GM) plants have teetered between success and failure, with ethical and regulatory challenges, as well as public concerns. On p. 466 and in the online collection, Youngsteadt lays out the stats on the world's GM harvests. While GM corn and soybeans have proliferated, golden rice, engineered to combat malnutrition, has languished, Enserink reports (p. 468). As Stokstad points out (p. 472), GM papaya still struggles for worldwide acceptance, even after 10 years on the market.

Two teams have deciphered the grape's genetic code, but whether GM wine will be accepted is a lingering question, says Travis (p. 475). Kintisch explores how plant genomics can advance biofuel agriculture (p. 478). Finally, Kaiser describes how some researchers bent on using GM plants to make human proteins and other pharmaceutical products are moving indoors to allay safety concerns (p. 473).

In addition to these overviews, see the associated Editorial by Fedoroff and the *Science* Careers article by Williams, as well as reports by Field and Osbourn (p. 543), Baerenfaller *et al.* (www.sciencemag.org/cgi/content/full/1157956/DC1), and Dinneny *et al.* (www.sciencemag.org/cgi/content/full/1153795/DC1). Given what has been learned so far from a variety of plant genomes, we eagerly look ahead to a growing field.

–LAURA M. ZAHN, PAMELA J. HINES, ELIZABETH PENNISI, JOHN TRAVIS

CREDIT: K. KRAUSE/SCIENCE

Plant Genomes

CONTENTS

News

466 GM Crops: A World View
468 Tough Lessons From Golden Rice
472 GM Papaya Takes on Ringspot Virus and Wins
473 Is the Drought Over for Pharming?
475 Uncorking the Grape Genome
A Life With Grapes
478 Sowing the Seeds for High-Energy Plants

Perspectives

479 Genome-Enabled Approaches Shed New Light on Plant Metabolism
D. DellaPenna and R. L. Last
481 Genomic Plasticity and the Diversity of Polyploid Plants
A. R. Leitch and I. J. Leitch
484 Selection on Major Components of Angiosperm Genomes
B. S. Gaut and J. Ross-Ibarra
486 Synteny and Collinearity in Plant Genomes
H. Tang et al.
489 The Epigenetic Landscape of Plants
X. Zhang
492 Extending Genomics to Natural Communities and Ecosystems
T. G. Whitham et al.
495 From Genotype to Phenotype: Systems Biology Meets Natural Variation
P. N. Benfey and T. Mitchell-Olds

See also related Editorial page 425; Science Careers article page 419 or go to www.sciencemag.org/plantgenomes; Report page 543; and Science Express Reports by Baerenfaller et al. and Dinneney et al. page 415.

Science

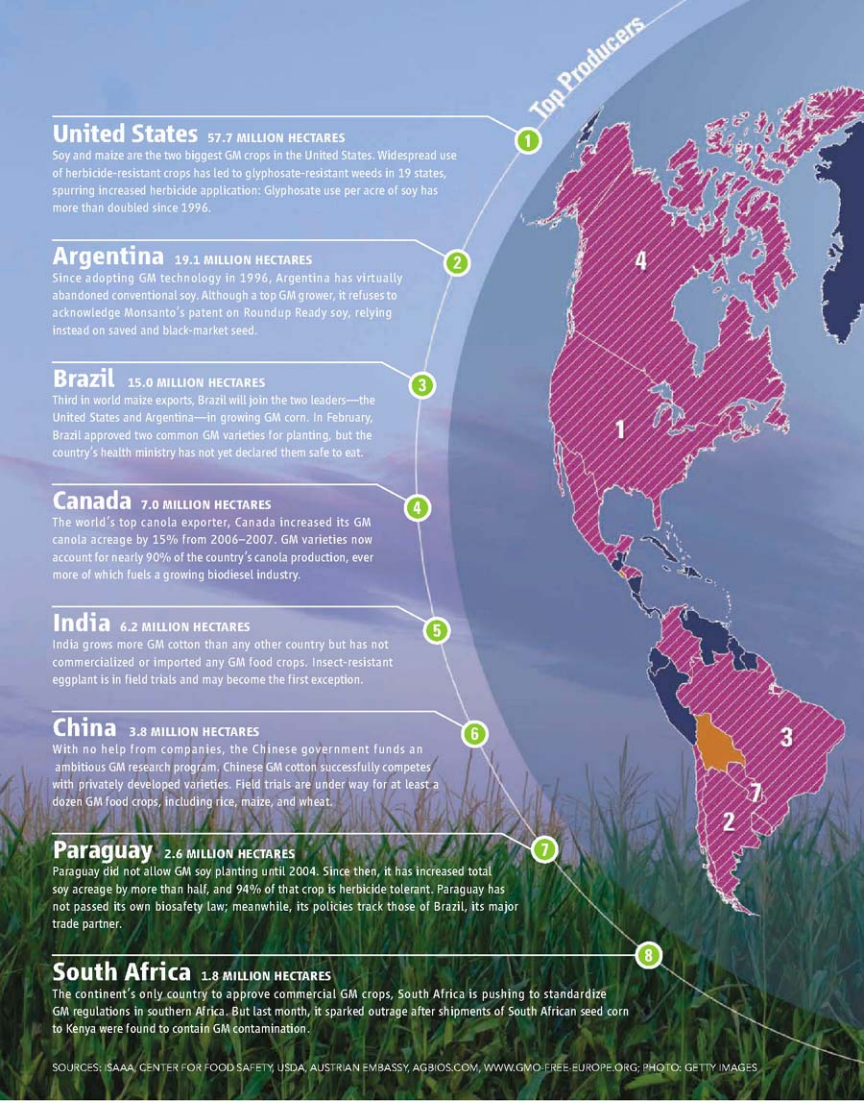

United States 57.7 MILLION HECTARES

Soy and maize are the two biggest GM crops in the United States. Widespread use of herbicide-resistant crops has led to glyphosate-resistant weeds in 19 states, spurring increased herbicide application: Glyphosate use per acre of soy has more than doubled since 1996.

Argentina 19.1 MILLION HECTARES

Since adopting GM technology in 1996, Argentina has virtually abandoned conventional soy. Although a top GM grower, it refuses to acknowledge Monsanto's patent on Roundup Ready soy, relying instead on saved and black-market seed.

Brazil 15.0 MILLION HECTARES

Third in world maize exports, Brazil will join the two leaders—the United States and Argentina—in growing GM corn. In February, Brazil approved two common GM varieties for planting, but the country's health ministry has not yet declared them safe to eat.

Canada 7.0 MILLION HECTARES

The world's top canola exporter, Canada increased its GM canola acreage by 15% from 2006–2007. GM varieties now account for nearly 90% of the country's canola production, ever more of which fuels a growing biodiesel industry.

India 6.2 MILLION HECTARES

India grows more GM cotton than any other country but has not commercialized or imported any GM food crops. Insect-resistant eggplant is in field trials and may become the first exception.

China 3.8 MILLION HECTARES

With no help from companies, the Chinese government funds an ambitious GM research program. Chinese GM cotton successfully competes with privately developed varieties. Field trials are under way for at least a dozen GM food crops, including rice, maize, and wheat.

Paraguay 2.6 MILLION HECTARES

Paraguay did not allow GM soy planting until 2004. Since then, it has increased total soy acreage by more than half, and 94% of that crop is herbicide tolerant. Paraguay has not passed its own biosafety law; meanwhile, its policies track those of Brazil, its major trade partner.

South Africa 1.8 MILLION HECTARES

The continent's only country to approve commercial GM crops, South Africa is pushing to standardize GM regulations in southern Africa. But last month, it sparked outrage after shipments of South African seed corn to Kenya were found to contain GM contamination.

SOURCES: ISAAA; CENTER FOR FOOD SAFETY; USDA; AUSTRIAN EMBASSY; AGBIOS.COM; WWW.GMO-FREE-EUROPE.ORG; PHOTO: GETTY IMAGES

GM Crops
A World View

In 2007, farmers grew more than 114 million hectares of GM crops—mainly soy, maize, cotton, and canola. Here we show who grows them, who imports them, and who avoids them, and highlight the top eight countries that together produce more than 99% of the world's biotech plants.

Compiled by: Elsa Youngsteadt and Erik Stokstad
Design: Kelly Krause
Illustration: Preston Huey

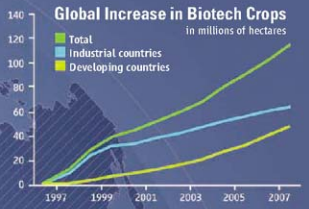

Science

Explore the interactive online map » www.sciencemag.org/plantgenomes/map.html

6

5

8

Grows GM crops commercially

Prohibits commercial growth of GM crops

Allows import of GM crops for food and/or feed

Making a GM crop

1. Identify gene for desired trait, e.g., insect toxicity in *Bacillus thuringiensis* (Bt) bacteria.
2. Create plasmid DNA that contains the Bt transgene and insert into carrier bacteria.
3. Infect corn cell culture with carrier bacteria to transfer gene.
4. Grow cell culture into adult plants, using their seeds to create GM insect-resistant strain.

TOUGH LESSONS FROM GOLDEN RICE

It was supposed to prevent blindness and death from vitamin A deficiency in millions of children. But almost a decade after its invention, golden rice is still stuck in the lab.

IT'S EASY TO RECOGNIZE INGO POTRYKUS AT the train station in Basel, Switzerland. Quietly waiting while hurried travelers zip by, he is holding, as he promised, the framed and slightly yellowed cover of the 31 July 2000 issue of *Time* magazine. It features Potrykus's bearded face flanked by some bright green stalks and a bold headline: "This Rice Could Save A Million Kids A Year."

The story ran at a time when Potrykus, a German plant biotechnologist who has long lived in Switzerland, was on a roll. In 1999, just as he was about to retire, Potrykus and his colleagues had stunned plant scientists and biotechnology opponents alike by creating a rice variety that produced a group of molecules called pro-vitamin A in its seeds. The researchers thought this "golden rice"—named for the yellow hue imparted by the compounds—held a revolutionary promise to fight vitamin A deficiency, which blinds or kills thousands of children in developing countries every year.

Almost a decade later, golden rice is still just that: a promise. Well-organized opposition and a thicket of regulations on transgenic crops have prevented the plant from appearing on Asian farms within 2 to 3 years, as Potrykus and his colleagues once predicted. In fact, the first field trial of golden rice in Asia started only this month. Its potential to prevent the ravages of vitamin A deficiency has yet to be tested, and even by the most optimistic projections, no farmer will plant the rice before 2011.

The delays have made Potrykus, who lives in Magden, a small village in an idyllic valley near Basel, a frustrated man. For working on what he considers a philanthropic project, he has been ridiculed and vilified as an industry shill. Relating the golden rice saga at his dinner table while his wife serves croissants and strong coffee, he at times comes off as bitter.

There's more at stake than golden rice and personal vindication, he says. In his view, 2 decades of fear-mongering by organizations such as Greenpeace, his prime nemesis, have created a regulatory climate so burdensome that only big companies with deep pockets can afford to get any genetically modified (GM) product approved. As a result, it has become virtually impossible to use the technology in the service of the poor, Potrykus says.

Not everybody is so gloomy. Potrykus's co-inventor and main partner, plant biochemist Peter Beyer of the University of Freiburg in Germany, agrees that it's been a difficult decade. But a more cheerful character by nature, Beyer believes rules are just something to be dealt with; complaining about them does little, he says. A handful of other researchers working on GM crops to fight malnutrition also feel confident that their work will eventually pay off.

Many scientists agree with Potrykus, however, that GM technology has become so controversial that for now, there's little point in harness-

Fields of gold. The only field studies of golden rice to date took place in Louisiana in 2004 and 2005.

CREDITS (TOP TO BOTTOM): HORDEIN INTERNATIONAL IMAGES LIMITED / ALAMY; GOLDEN RICE HUMANITARIAN BOARD

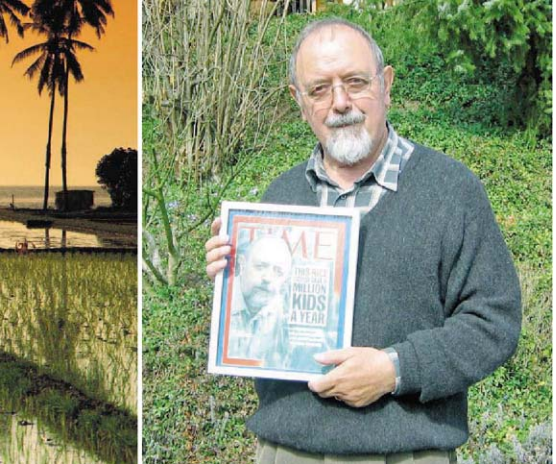

Time flies. The hope expressed in a 2000 *Time* cover story about Ingo Potrykus remains unfulfilled.

CREDIT: MARTIN ENSERINK/SCIENCE

ing it for the world's poorest. HarvestPlus, a vast global program at public research institutes aimed at creating more nutritious staple crops, is forgoing GM technology almost entirely and using conventional breeding instead, despite its built-in limitations. GM products just might end up on the shelf, says HarvestPlus Director Howarth Bouis.

Potrykus, now 75 years old, worries that he may not live to see his invention do any good. "It's difficult for me not to get upset about this situation," he says.

A dream takes root

The idea for golden rice was born at an international agricultural meeting in the Philippines in 1984, says Gary Toenniessen of the Rockefeller Foundation, a philanthropy in New York City. It was the early days of genetic engineering, and over beers at a guesthouse one evening, Toenniessen asked a group of plant breeders how the technology of copying and pasting genes might benefit rice. "Yellow endosperm," one of them said.

That odd answer alluded to the fact that a quarter-billion children have poor diets lacking in vitamin A. This deficiency can damage the retina and cornea and increase susceptibility to measles and other infectious diseases. The World Health Organization (WHO) estimates that between 250,000 and 500,000 children go blind every year as a result, and that half of those die within 12 months. Vegetables such as carrots and tomatoes, as well as meat, butter, and milk, can provide the vitamin or its precursors, but many families in poor countries don't have access to them. A rice variety producing precursors to vitamin A in its endosperm, the main tissue in seeds, might provide a solution—and it would have yellow kernels.

Classical breeding cannot produce such a rice, however, because although pro-vitamin A is present in the green parts of the rice plant, no known strain makes it in its seeds. The only option is to tinker with rice's DNA to produce the desired effect. Throughout the 1980s, the Rockefeller Foundation funded several exploratory studies, but the plan didn't gel until a brainstorming meeting in New York City in 1992, at which scientists discussed the bold idea of reintroducing the biochemical pathway leading to beta carotene, the most important pro-vitamin A, into rice but putting it under control of a promoter that's specific to endosperm.

Potrykus, then a pioneer in rice transgenics at the Swiss Federal Institute of Technology (ETH) in Zürich, attended, as did Beyer, who specialized in carotenoid biochemistry and molecular biology. The two met on the plane to New York and hit it off; their fields of expertise were complementary, and the fact that Zürich is less than 2 hours from Freiburg was helpful. They soon had a proposal written up.

Beyer admits he barely believed in the idea himself, and the Rockefeller's scientific advisory board was equally skeptical. Introducing an entire genetic pathway into rice seemed like a stretch. Still, the foundation rolled the dice and supported the project.

It took 7 years, but Potrykus and Beyer eventually succeeded in making golden rice by splicing two daffodil genes and a bacterial gene into the rice genome. The eureka moment arrived late one night in Freiburg, Beyer recalls. He was analyzing the molecular content of seeds produced in Potrykus's lab, as he often did, using a technique called high-performance liquid chromatography. This time, peaks showed up on the screen where they had never appeared before—the signals of carotenoids. When Beyer went back to look at the batch of seeds, he noticed something he had missed: The grains had a faint yellow hue. Golden rice had been born.

The battle begins

Potrykus says he always knew golden rice—a Thai businessman suggested the catchy name—would be controversial. As a professor in Switzerland, one of the most fiercely anti-GM countries in Europe, he had been confronted with angry students since the 1980s. To protect his plants, ETH spent several million dollars on a grenade-proof greenhouse. For Beyer, unofficial road signs declaring the Upper Rhine Valley a "GM technology-free region" are a twice-daily reminder that the climate in Germany isn't much better.

But golden rice posed a special dilemma to GM crop opponents, admits Benedikt Haerlin, who coordinated Greenpeace's European campaign at the time and now works for the Foundation on Future Farming. Unlike the existing GM crops that primarily helped farmers and pesticide companies, it was the first crop designed to help poor consumers in developing countries. It might save lives. The decision whether to oppose it weighed heavily on him, Haerlin says, which is why he consulted with WHO experts on vitamin A and why he traveled to Zürich to spend a day at Potrykus's lab to talk. Potrykus, impressed by Haerlin's intelligence, hoped to convince his fellow countryman.

He failed. Although Greenpeace pledged not to sabotage field trials, it did launch an aggressive campaign against golden rice. It argued that the crop was an industry PR ploy—seed company Syngenta was involved in the project, the group pointed out—designed to win over a skeptical public

Seeds of discontent. Although Potrykus has retired, Peter Beyer is still working on golden rice at the University of Freiburg.

and open the door to other GM crops. Golden rice did not attack the underlying problem of poverty, Greenpeace said; besides, other, better solutions to vitamin A deficiency existed.

Perhaps Greenpeace's most effective argument, however, was that golden rice simply wouldn't work. The most successful strain created in 2000 produced 1.6 micrograms of pro-vitamin A per gram of rice. At that rate, an average 2-year-old would need to eat 3 kilos of golden rice a day to reach the recommended daily intake, Greenpeace said, and a breastfeeding mother more than 6 kilos. To drive the point home, an activist in the Philippines sat down behind a giant mound of golden rice during a press conference. "Fool's gold," Greenpeace called it.

A photo of the event, which quickly found its way around the world, still makes Haerlin chuckle—and it still makes Potrykus angry. Greenpeace assumed that children had to get *all* of their vitamin A from rice, which was unrealistic; it also ignored the fact, says Potrykus, that even half the recommended intake may prevent malnutrition. And Greenpeace assumed that the uptake of beta carotene by the human gut and its conversion into vitamin A were quite inefficient, resulting in one vitamin molecule for every 12 molecules of beta carotene. Nobody knew the true rate at the time, but a recent, soon-to-be-published study among healthy volunteers who ate cooked golden rice, led by Robert Russell of Tufts University in Boston, suggests that it's more like one for every three or four. "That's really quite good," says Russell, who supports the golden rice project. (A similar study is planned among people with marginal vitamin A deficiency in Asia.)

Haerlin says his calculations were based on the best data at the time. But even if they were correct, Potrykus says, the first golden rice was just a proof of principle. Greenpeace might as well have blamed the Wright brothers for not building a transatlantic airplane, he says.

Industry gets in

The low beta-carotene yield would eventually be tackled by Syngenta—even though Potrykus resented the way the company got involved. Between 1996 and 1999, Beyer's lab received funding through a European Commission contract that also included agrochemical giant Zeneca (called AstraZeneca after a merger in 1999). Under the program's rules, any benefits had to be shared by the signers. AstraZeneca had not worked on golden rice per se, Potrykus says, but the company claimed a share of that intellectual property anyway; it was interested in developing the technology commercially, for instance in health foods, says Potrykus, who was initially "furious" that a big corporation now had a say in his project.

David Lawrence has a different take on those events: At the time, AstraZeneca primarily wanted to support the humanitarian development of golden rice, says the current head of research at Syngenta; the company didn't have any commercial plans. (AstraZeneca's agribusiness division merged with that of Novartis to form Syngenta in 2000.) But whoever's right, the move proved a blessing in disguise, Potrykus now says. At Syngenta, he found a new partner in Adrian Dubock, a bubbly, fast-talking Brit with experience in patents, product development, regulation, and marketing—subjects Potrykus and Beyer admit they were clueless about.

Dubock helped work out a deal in which Syngenta could develop golden rice commercially, but farmers in developing countries who make less than $10,000 a year could get it for free. He also helped solve patent problems with several other companies. Dubock retired from Syngenta in 2007 but remains involved as a member of the Golden Rice Humanitarian Board, a group Potrykus chairs. "Without him, the project would have ended already," Potrykus says.

But perhaps most important, Syngenta scientists replaced a daffodil gene with a maize gene, thus creating a new version of golden rice, dubbed GR2, that produces up to 23 times more beta carotene in its seeds. Even with the one-in-12 conversion factor, that meant 72 grams of dry rice per day would suffice for a child, the company's scientists said in 2005. A 2006 paper by Alexander Stein of the University of Hohenheim in Stuttgart, Germany, estimated that the rice could have a major public health impact at a reasonable cost.

Those results didn't convince the skeptics. Real-world studies are still lacking, says WHO malnutrition expert Francesco Branca, noting that it's unclear how many people will plant, buy, and eat golden rice. He says giving out supplements, fortifying existing foods with vitamin A, and teaching people to grow carrots or certain leafy vegetables are, for now, more promising ways to fight the problem.

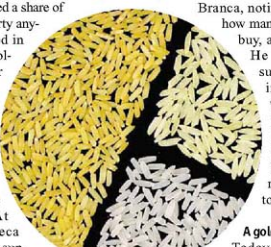

Gold fever. GR2 (*left*) contains more than 20 times more pro-vitamin A than GR1 (*top right*). Ordinary rice (*bottom right*) contains none.

CREDITS: (TOP TO BOTTOM) MARTIN ENSERINK/SCIENCE; GOLDEN RICE HUMANITARIAN BOARD

A golden future?

Today, the debate about golden rice has quieted down, in part because its inventors are keeping a low profile. Syngenta stopped its research on golden rice and licensed the rights to GR2 to the humanitarian board on World Food Day in 2004; given consumers' distrust, there was no money in it, says Lawrence. Most golden rice work is now taking place at six labs in the Philippines, India, and Vietnam, the countries chosen as the best candidates for the crop's launch.

There's a long way to go. Both the original golden rice, now called GR1, and GR2 were created with *Japonica* cultivars that are scientists' favorites but fare poorly in Asian fields. Researchers are now backcrossing seven GR1 and GR2 lines with the long-grained, non-sticky *Indica* varieties popular among Asia's farmers. In early April, researchers at the International Rice Research Institute in the Philippines finally started a field trial with a GR1 backcrossed into a widely used *Indica* variety called IR64—the first field trial ever in Asia. (The only other outdoor studies were two done in Louisiana in 2004 and 2005.) The new varieties must not only produce enough beta carotene but also pass muster in terms of yield, seed quality, and appearance.

The project could have been much further along, Potrykus says, if there weren't so many rules governing GM crops that make little sense. Conventional breeders can bombard plant cells with chemicals and radiation to create useful mutants without having to check how it affects their DNA; a GM insertion must be "clean"—that is, the extra genes must sit neatly in a row without disrupting other genes—which adds months or even years to the lab work. Because field trials take long to get approved, researchers have been confined to greenhouses, in which they have trouble growing the large numbers required for breeding and feeding studies. These requirements have caused "year after year of delays," Potrykus complains.

Even if field trials are successful, there are no guarantees that golden rice will eventually be approved in the target countries. Use of other GM crops, such as Bt cotton, has exploded in Asia in recent years (see infographic, p. 466). But GM rice has languished. In India and China, regulatory agencies have shied away from approving insect-resistant GM rice despite extensive testing. "The expectation is that they will [be approved] eventually," says Toenniessen, "but it's a major decision for any Asian country." Thailand, a major rice exporter, has decided to steer clear of GM rice altogether.

Kavitha Kuruganti of the Centre for Sustainable Agriculture, an anti-GM group in Hyderabad, India, promises a major battle should golden rice head to the market in India. She thinks that the crop is unnecessary and probably unsafe to eat and that a massive switch would reduce diversity and threaten India's food security. "We will try to organize a broad public debate," she says.

Eat your dinner. Greenpeace said more than 3 kilos of golden rice daily were needed to meet dietary standards for vitamin A.

CREDIT: GIL NARTEA/GREENPEACE

Not worth funding?

Whether justified or not, the turmoil over golden rice has shaped other efforts to improve the nutritional value of crops. Take HarvestPlus. With a $14 million annual budget that targets 12 crops, it aims to boost levels of three key nutrients: vitamin A, iron, and zinc. It relies almost entirely on conventional breeding—which has Greenpeace's blessing—because it wants to have an impact fast, says Bouis, the director. What little GM technology HarvestPlus supports is a "hedge," in case the political and regulatory climates shift.

But in plants that have little or no natural ability to produce a nutrient, breeders have nothing to work with. Thus, vitamin A–enriched non-GM rice and sorghum are essentially off the table, says Bouis, as is boosting zinc and iron in sweet potatoes and cassava. Iron in rice is a question mark.

The uncertainty about the future of GM foods also tends to scare off the financial donors on which programs like HarvestPlus depend. Rockefeller, for instance, is frustrated that a GM rice whose field trials it helped pay for in China is stalled, says Toenniessen. "To avoid making the decision to approve it, the Chinese keep asking for more field trials," he says. "In the end, that becomes a foolish use of our funds."

The only charity still investing massively in GM crops with enhanced nutritional value is the Bill and Melinda Gates Foundation. Through its Grand Challenges in Global Health initiative, it is spending more than $36 million to support not only golden rice but also GM cassava, sorghum, and bananas. The foundation declined to comment for this story. But the researchers it supports say that they are optimistic that their products will make it through the pipeline.

James Dale of Queensland University of Technology in Brisbane, Australia, who heads a project to add iron, vitamin A, and vitamin E to bananas, says he has learned several lessons from golden rice, including the importance of local "ownership"—which is why he has teamed up with researchers in Kampala. "This will be a Ugandan banana made by Ugandans," he says.

Not that this mollifies opponents. Greenpeace will fight to keep GM bananas, cassava, and sorghum from poor countries' fields, just as it will keep opposing golden rice, says Janet Cotter of Greenpeace's Science Unit in London.

Battle-scarred, Potrykus says he hasn't given up hope that the regulatory system can be overhauled so that GM technology can benefit the poor. He believes a massive, multimillion-dollar information campaign might help convert the public. He has tried in vain to contact Bill Gates in hopes of tapping his wealth for such a media blitz.

He also wrote the late Pope John Paul II to ask for support for golden rice. "You know the definition of an optimist?" he jokes: "Someone who's asking the church for money." His Holiness declined, but Potrykus was invited to join the Pontifical Academy of Sciences, where he hopes to convene a meeting on golden rice next year—the 10th anniversary of his tarnished invention.

–MARTIN ENSERINK

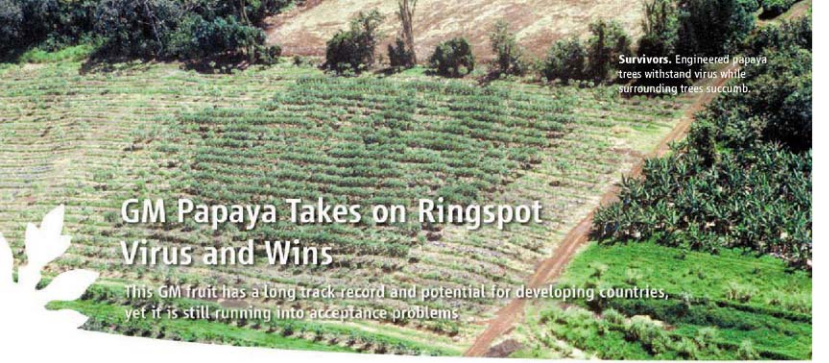

Survivors. Engineered papaya trees withstand virus while surrounding trees succumb.

GM Papaya Takes on Ringspot Virus and Wins

This GM fruit has a long track record and potential for developing countries, yet it is still running into acceptance problems

IF THERE IS AN EXAMPLE OF A SILVER BULLET among genetically modified (GM) crops, it would be virus-resistant papaya trees. They saved the papaya industry in Hawaii from devastation by the ringspot virus, a serious pathogen that deforms fruit and eventually kills conventional trees. "That's a fantastic accomplishment," says George Bruening, a plant pathologist at the University of California, Davis.

As the world's first GM fruit to be successfully commercialized, papaya has a 10-year track record of safety. Yet its future outside Hawaii is far from assured. Although the virus threatens papaya trees almost everywhere they grow, environmental groups are campaigning against its adoption in other countries. "It's really a tragedy," says Sarah Davidson, a Cornell University Ph.D. student, whose analysis of GM papaya in Thailand will appear next month in *Plant Physiology*. "It should have been a model for technology transfer to developing countries."

The story starts in 1978, when Dennis Gonsalves, a young plant virologist at Cornell, returned to his native Hawaii for a visit. The ringspot virus was slowly spreading toward Puna, the main papaya growing region. Gonsalves decided to stand in its path of destruction. By 1991, he and his colleagues had shown that papaya carrying the gene for a viral protein could resist the virus in the greenhouse. Field trials began in April 1992.

Later that spring, the virus started a rampage across Puna. Within 6 years, the papaya harvest had dropped by half, to 11.8 million kilograms. "We were devastated," recalls Loren Mochida, a board member of the Hawaii Papaya Industry Association and manager of Tropical Hawaiian Products, an exporter that suffered two rounds of major layoffs. But the field trials were promising: Whereas conventional trees were infected and nearly barren, the GM trees were large and heavy with fruit.

Richard Manshardt of the University of Hawaii, Manoa, then crossed the GM papaya with a high-yielding variety called Rainbow. Gonsalves says the team showed off the fruit to politicians, schoolchildren, anybody they could interest. "People were rooting us on," he recalls. Today, virus-resistant trees account for about 80% of papaya acreage in Hawaii. "Dennis Gonsalves got there just in time," says Bruening.

The ringspot virus is a problem around the world, and scientists from many countries flocked to Gonsalves's lab to learn how to put the gene into their varieties of papaya. By 1999, Thai scientists had virus-resistant papaya in small field trials. GM papaya is being field-tested or studied in the Philippines, Vietnam, Taiwan, Malaysia, and elsewhere.

GM papaya "is pretty close to an ideal propoor crop," says Davidson. Unlike some GM crops, the technology doesn't require herbicides. And in Thailand, papaya is second only to bananas in importance, with 80% consumed domestically. Many poor farmers cannot afford to eat papaya unless they grow it themselves.

Despite the success in Hawaii, criticism is fierce: In 2005, for example, the Global Justice Ecology Project, based in Hinesburg, Vermont, claimed that GM papaya in Hawaii had caused an "economic and ecological disaster for organic, conventional, and GM papaya farmers alike." It and other opponents are concerned about allergic reactions to the virus coat protein and widespread genetic contamination of conventional papaya. They also assert that GM papaya has become more susceptible to a disease caused by a pathogen called phytophthora.

Most researchers reject these concerns. There is no evidence that the GM plants are allergenic or more vulnerable to phytophthora, says Gonsalves, who now directs the U.S. Department of Agriculture Pacific Basin Agricultural Research Center in Hilo, Hawaii. However, GM papaya can impact conventional growers: In a study of conventional trees published last year, Manshardt and colleagues reported transgenes in 1% of seeds from uninfected, self-pollinating trees planted next to GM papaya. No transgenes were found in seeds from an orchard that was 400 meters downwind.

Ultimately, the acceptance of GM papaya will rest on politics and economics, says Davidson. Countries such as Brazil will likely continue to put up with virus as long as they can profitably export conventional papayas to Europe or Japan, which prohibit GM papaya. In contrast, Mexico may decide to permit the planting of GM papaya, because its major market is the United States, which allows the GM fruit. And although protests by Greenpeace caused the Thai government to ban field tests of GM papaya in 2004, the Thai government may eventually relent in the face of competition from neighbors such as China. Once China deregulates papaya and other GM vegetables, "you won't be able to stop [their spread]," predicts Frank Shotkoski, director of the Agricultural Biotechnology Support Project II at Cornell. "It won't be long before the rest of the world will see it as safe."

–ERIK STOKSTAD

CREDITS: TOP TO BOTTOM: STEVE FERREIRA

In the bag. These cultured carrot cells are engineered to make a human drug.

Is the Drought Over for Pharming?

Despite technological, economic, and social issues, companies are plowing ahead, making drugs and other compounds in plants

MANY A CHILD HAS BEEN TOLD "CARROTS are good for you." That advice could soon take on new meaning for people with Gaucher disease, an inherited metabolic disorder that leads to liver and bone problems. Patients must now be injected every 2 weeks with a manufactured enzyme that costs on average $200,000 a year, making it one of the most expensive drugs ever. If ongoing clinical trials go well, the 5000 Gaucher patients on the therapy could soon have a second option—a cheaper version of the enzyme that stays in the bloodstream longer and can be injected less often.

If the U.S. Food and Drug Administration (FDA) approves recombinant glucocerebrosidase, it will be good news not only for medicine but also for a community far removed from the clinic: plant scientists. Protalix Biotherapeutics in Karmiel, Israel, produces this new version of the protein in giant plastic bags, not in steel vats of mammalian cells like most biologics are. The bags are filled with transgenic carrot cells that are cultured and then processed to extract the drug. "If Protalix gets regulatory approval, that would [make it] the first plant-made pharmaceutical," says plant scientist Charles Arntzen of Arizona State University in Tempe. "For people who work in this field, it will be a very exciting step forward."

Arntzen is chasing an elusive dream: using whole plants as factories to make drugs. Nearly 20 years ago, when researchers first showed that a tobacco plant could be engineered to crank out an antibody, they envisioned harvesting cheap supplies of therapeutic proteins, antibodies, and vaccines from vast fields of crops. For this approach, researchers isolate the target gene and usually insert it into a bacterium called *Agrobacterium* that readily infects the plants and passes on the gene. The gene becomes part of the plant and is passed from one generation to the next, producing foreign protein much as if it were one of the plant's own genes.

However, technological hurdles and a lack of interest from drug companies have hamstrung "pharming," as have worries that pharma crops will escape from their experimental plots and taint the food supply. As a result, many companies have abandoned this research or gone under. And no plant-made drugs for humans have made it to the pharmacy.

But academic scientists and some companies have persisted, improving yields of plant-made drugs and developing innovative ways to keep pharming inside the lab, or the greenhouse. Several plant-made pharmaceuticals (PMPs) are now in patient trials (see chart, p. 474). Moreover, the European Union, the Bill and Melinda Gates Foundation, and the U.S. Department of Defense are fertilizing the field with new funding. "We're actually not doing too bad," says Julian Ma, an immunologist at St. George's University of London in the U.K. "It's just that everyone is in a hurry."

Fields of dreams

The excitement over plant-made pharmaceuticals began with a 1989 paper in *Nature* showing that monoclonal antibodies could be produced in tobacco. The paper "really captured the imagination," says Ma. Monoclonal antibodies were being used to treat a growing number of diseases, from arthritis to cancer, but were expensive to make in mammalian cells. So-called plantibodies appeared to offer a cheaper production method—a kilogram might cost $100 rather than $3 million—and might be simpler to process because they would be free of animal pathogens.

Other discoveries followed. In 1995, for instance, Arntzen's group reported in *Science* that potatoes engineered to make a cholera protein worked as a vaccine when the spuds were fed to mice. Such "edible vaccines" could offer developing countries cheap oral vaccines that didn't require refrigeration, Arntzen suggested (*Science*, 5 May 1995, p. 658).

A company called Large Scale Biology Corp. in Vacaville, California, came up with a shortcut. It didn't bother to create a new tobacco strain when it wanted to produce an antigen for a lymphoma vaccine. It simply sprayed tobacco plants with a tobacco mosaic virus carrying the appropriate gene. The leaves produced useful amounts of the vaccine protein within 14 days. The drug worked in mice, suggesting that vaccines tailored to lymphoma patients' tumors could be made in plants in just weeks. And because the plants carried the foreign gene only until they shed their leaves, they were potentially more acceptable than permanently modified crops.

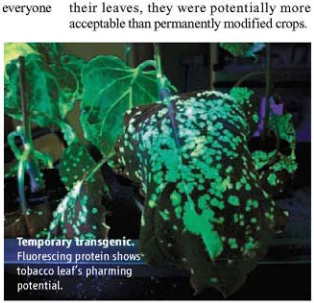

Temporary transgenic. Fluorescing protein shows tobacco leaf's pharming potential.

CREDITS: TOP TO BOTTOM: PROTALIX; BAYER AG

Selected Plant-Made Pharmaceuticals

Company	Plant	Grown in	Drug or product	Disease	Status
Human drugs					
Protalix Biotherapeutics	carrot	cell culture	glucocerebrosidase	Gaucher disease	Phase III trial*
Biolex Therapeutics	duckweed	indoor chambers	alpha interferon	hepatitis C	Phase II trial*
SemBioSys Genetics	safflower	field	insulin	diabetes	Phase I/II trial †
Meristem Therapeutics	corn	field	lipase	cystic fibrosis	Phase III trial †
Other products					
Ventria Bioscience	rice	field	lactoferrin, lysozyme	diarrhea	Efficacy trial §
Cobento	*Arabidopsis*	greenhouse	human intrinsic factor	Vitamin B-12 deficiency	Approved ††
Planet Biotechnology	tobacco	field	secretory antibody vaccine	tooth decay	E.U. approved
Dow AgroSciences	tobacco	cell culture	poultry vaccine	Newcastle disease	USDA approved
CIGB, Cuba	tobacco	greenhouse	vaccine purification antibody	hepatitis B	On market

* Ongoing; † Projected late 2008; § Completed; †† In Ukraine.

Steps along the way. No plant-made human drug has made it through final clinical trials, but several "pharmed" proteins are close to or on the market as supplements, a vaccine reagent, and a medical device.

Scores of biotech companies sprang up to commercialize these discoveries, and some big agbiotech companies got involved as well. By the mid-1990s, more than 180 companies and organizations were working on pharming, according to the Biotechnology Industry Organization.

The companies soon ran into technological snags, however. Biotechnologists couldn't always get plants to express enough protein and had trouble purifying the protein product. Efforts to make edible vaccines stalled after researchers realized that the amount of antigen fluctuated widely from plant to plant. Arntzen thinks that oral vaccines made from dried plant material could work for developing countries, but a vaccine without a strictly controlled dose "would never be approved" in the United States, he says.

Another reality check: lukewarm interest from the big drug companies. They didn't much care that plant-made drugs would be cheaper to make because production is a small chunk of the cost of drug development; the big-ticket item is clinical trials. The companies were also leery of the regulatory hurdles, because both the drug and the new production process would have to clear FDA. "Most pharmaceutical companies aren't willing to take a chance on a drug produced in plants," says Roger Beachy, president of the Donald Danforth Plant Science Center in St. Louis, Missouri.

Also, like other genetically modified crops (see pp. 468, 472), pharma plants can be a public relations nightmare. In 2002, leftover corn plants engineered by ProdiGene Inc. to make a pig vaccine sprouted in a soybean field in Nebraska. For this and an Iowa mishap, the U.S. Department of Agriculture (USDA) fined the company $250,000 and made it pay $3 million to buy and destroy tainted soybeans. The incident stoked opposition from farmers and activists worried about "drugs in your cornflakes."

Other companies underestimated the public's concerns. A company called Ventria Bioscience that wanted to conduct field trials of rice containing two breast-milk proteins useful in combating diarrhea drew the ire of rice growers in California, then Missouri. It wound up in Kansas, where no other rice is grown.

USDA tightened its rules for field trials of pharma plants in 2003 to prevent mistakes like the ProdiGene episode. But skeptics were not assuaged. Bill Freese of the Center for Food Safety in Washington, D.C., says enforcement is "horrendous." As a result, "we don't think [drugs] should be in any food crops, indoors or outdoors," he adds. Many ecologists and some plant scientists are also leery of using food crops for pharma. "It's too dangerous," says Kenneth Palmer, former director of the vaccine program at Large Scale Biology.

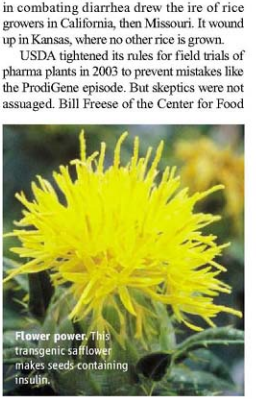

Flower power. This transgenic safflower makes seeds containing insulin.

These concerns drove many companies away from using food crops such as corn for pharmaceuticals. A few big companies, such as Monsanto, dropped PMP research altogether. Stung by bad press and lack of interest from drug companies, many leading plant pharma companies have folded, including ProdiGene and Large Scale Biology. As Palmer puts it, "the field imploded."

Close to the clinic

Despite the setbacks, a handful of companies in the United States and Europe haven't given up. A few have plowed ahead with food crops, grown outdoors, for their pharma products; others have focused on other plants or on unconventional growing schemes.

Meristem Therapeutics in Clermont-Ferrand, France, plans to start final clinical trials for a corn-grown gastric lipase for cystic fibrosis patients by the end of the year. And the Canadian company SemBioSys Genetics Inc. uses transgenic safflower—"much less of a lightning rod than some other crops," says CEO Andrew Baum—to produce insulin, which should be in clinical trials this year. Companies such as Protalix and Biolex Therapeutics sidestep the growing of crops altogether: the former with its carrot-cell culture to make a Gaucher disease enzyme, and the latter by producing interferon using duckweed, tiny clonal plants grown as a layer in clear plastic bags. "We are careful *not* to be associated with whole-plant transgenic technology," says Protalix CEO David Aviezer.

New technologies are attracting attention. To boost expression, the German biotech Icon Genetics relies on bacteria to get transgene-laden viruses into tobacco plants. The company dips the plants into a solution of *Agrobacterium* that carries the DNA for a deconstructed tobacco mosaic virus, which in turn contains the gene for the desired drug. The bacterial bath, followed by a few seconds in a vacuum, gets far more of the virus into plant-leaf tissue than conventional spraying.

In a 2006 paper in the *Proceedings of the*

CREDITS: (TOP TO BOTTOM) ISTOCKPHOTO.COM; KEVIN MAGALA/SCIENCE (SOURCE); INDIVIDUAL COMPANIES AND MOLECULARFARMING.COM; SEMBIOSYS

National Academy of Sciences (*PNAS*), they reported that this method, combined with other techniques, increases the amount of antibody by up to 100-fold, reducing the size of the crop needed and making it feasible to grow plants commercially indoors. Compared with making a transgenic plant, which takes a year or two to develop, this "magnifection" can go from gene to grams of protein in a couple of weeks. "It's incredibly promising technology," says Ma, who, like other academic researchers, is trying out magnifection.

With help from the drug giant Bayer, which bought the company in 2006, Icon Genetics will open a clinical-grade manufacturing plant in June. It expects to begin trials with a cancer vaccine tailored to individual patients in 2009, says CEO Yuri Gleba.

Bayer's move is a healthy sign of regrowth for the pharming field, Ma and others say. And other new sources of support are helping too. Last month, Pharma-Planta, a €12 million, 5-year, European Union–funded project co-coordinated by Ma, described in *PNAS* an anti-HIV microbicide grown in corn or tobacco that could be ready for testing next year. The Defense Department and other U.S. government agencies have provided the Fraunhofer USA Center for Molecular Biotechnology in Newark, Delaware, nearly $14 million to use a technique like magnifection to make vaccines. It has tested anthrax and plague vaccines in nonhuman primates and a pandemic flu vaccine in ferrets. "[We] can do things much faster than any other technology," says Executive Director Vidadi Yusibov, slashing in half the 6 months it now takes to make flu vaccine the traditional way, in chicken eggs. The organization also has $8 million from the Gates Foundation for plant-based vaccines for malaria, sleeping sickness, and flu.

As visions of endless fields of pharma crops have faded, so have unrealistic expectations for pharming. Scientists say they now realize that they need to be smarter about the marketability of the drugs they develop in plants. They think the best bets—Protalix aside—may be high-volume biologics, such as microbicides, monoclonal antibodies, and vaccines, particularly for use in developing countries. Getting these first low-hanging fruits through clinical trials and FDA approval should allay concerns about safety and environmental risks. Says Palmer, now at the University of Louisville in Kentucky, "Once two or three products [win approval], the field should really take off." **–JOCELYN KAISER**

CREDITS (TOP TO BOTTOM): CHARLES O'REAR/CORBIS; HOLT STUDIOS INTERNATIONAL LTD / ALAMY

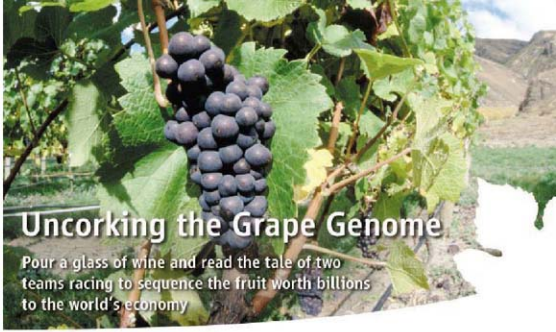

Uncorking the Grape Genome

Pour a glass of wine and read the tale of two teams racing to sequence the fruit worth billions to the world's economy

AMONG WINE CONNOISSEURS, OPINIONS differ about whether 2007 will prove a good year for Pinot Noir. But among plant geneticists, it's the finest vintage ever: Last year, two European teams published high-quality drafts of two Pinot Noir–derived genomes.

Plant biologists are toasting the genomic double-header. This is the first fleshy fruit and just the fourth flowering plant to have its genome decoded. And in economic terms, grapes top the world's fruit crops: We consume them fresh or dried, crush them into juice, and use them to make wine that can sell for many thousands of dollars a bottle. "The contributions of these sequencing efforts are enormous and historical," says grape researcher Steven Lund of the University of British Columbia in Vancouver, Canada.

Wine woes. Powdery mildew (*above*) and other fungal diseases can devastate vineyards.

The story behind the grape genome is one in which a worldwide scientific community came together, then partially splintered into rival camps; money to support sequencing was hard to come by; and success has brought both new insights and delicious questions. The rivalry provided the drama of the story. For a while, a French-Italian grape genome alliance called Vigna/Vigne looked like it was going to be beaten by a disgruntled researcher who started his own genome effort. "Undoubtedly, competition was a driver here, perhaps in a microcosm of the human genome sequence drama of years past," says Lund, referring to the bitter contest between public and private programs to decipher our genetic code. Recently, however, at a workshop* in Udine, Italy, the two grape genome groups began to put aside their rivalry. "I'm hopeful there will be more collaboration now," says Vigna/Vigne member David Horner of the University of Milan in Italy. "It's cool there are two cultivars done. It allows more comparative work."

A key motivation for deciphering the grape genome is to prevent a repeat of the economic devastation that struck the European wine industry in the late 1800s. At that time, phylloxera, sap-sucking insects from North America, ravaged European grapevines. Today, winemakers and grape researchers are struggling to combat new threats, particularly downy and powdery mildew, diseases that have made their way to Europe from the United States over the past century. These fungi are an environmental as well as an economic nightmare: Although only about 5% of Europe's farmland is dedicated to wine vineyards, they account for about 70% of the region's fungicide use.

The new genome information should speed the creation of hardier vines, which has been slow going. "The target now is clearly resistance genes," says Vigna/Vigne member Michele Morgante from the Institute of Genomic Applications (IGA) in Udine. New insights into the locations of these genes can assist breeders as they try to develop better varieties, for example. And identifying genes in the few grapes that are resistant to drought

*Tuning the Taste of Wine, 7 March 2008, Udine, Italy.

or pests may pave the way for genetically modifying common wine grapes to have the same attributes.

But as viticulturists enter the genomic age, many wonder whether the wine industry, particularly the conservative European sector, would dare bypass conventional breeding for genetically modified (GM) grapevines. Scientists have for years been experimenting with GM grapes—usually putting nongrape genes into the fruit's genome—but most winemakers have shied away from public association with such efforts. "For a lot of consumers of wine, especially high-end ones, history and tradition is a very important part of their experience. If you produce wine from a genetically engineered grape, you strike at the heart of that," says Carole Meredith, a former grape geneticist who now runs a vineyard (see sidebar, below).

Taking root

Although there's a dazzling variety of wines produced around the world, the great majority flow from the juices of a single species, *Vitis vinifera*, commonly called vinifera. Indeed, in Europe, this grape is the only source of fine wines—other grapes are limited to fruit, juice, or so-called table wines. Thanks to centuries of breeding, 7000 cultivated varieties, or cultivars, of vinifera now provide an incredible diversity of flavors, from hearty reds to light whites.

A vinifera genome project began to take root in the mid-1990s, largely through the instigation of Meredith, who was then conducting grape research at the University of California, Davis. Meredith and others wanted to use genetics to identify various grape cultivars—Chardonnay, Cabernet Sauvignon, and so on—that can be tricky to distinguish in other ways. In a business in which wines made from different cultivars can vary enormously in price, correct identification is critical.

The researchers proposed to "fingerprint" grapes based on variable DNA sequences called microsatellite markers. Back then, however, identifying such markers "was expensive and laborious, and no one lab was ever going to develop enough to make their efforts worthwhile," Meredith recalls. "So I approached all the people I knew and suggested working together."

From that suggestion arose an international consortium that amassed hundreds of such markers within several years. The researchers were thirsty for more. In 2001, many of them, including Meredith, formed the International Grape Genome Program, arguing for a full-fledged sequencing of a vinifera cultivar.

But who would pay for it? It was well-known that grapes weren't on the U.S. genomics menu. In 2001, Enrico Pè of the Sant'Anna School of Advanced Studies in Pisa proposed a grape genome program in Italy, sponsored by the private sector. But bank foundations and winemakers declined.

Finally, in 2005, the French research agencies INRA and Genoscope joined with various Italian groups, including IGA and universities in Verona and Udine, to form Vigna/Vigne, which means vine in French and vineyard in Italian, respectively. This time, researchers did not ask winemakers for money, only political support, says Pè, who now leads the Italian side of the collaboration. France ultimately contributed about €8.5 million, Italy, about €12 million.

The race is on

Except when discussing European football—their national teams are bitter rivals—the French and Italian groups meshed smoothly. Still, agreeing on what to sequence wasn't easy. Compared with many plants, vinifera grapevines are extremely heterozygous: The female and male versions of the plant's chromosomes differ significantly. This complicates the sequencing and assembly of an accurate genome. The Italian scientists first considered a Sangiovese grape, then a Pinot Noir. Their French counterparts lobbied for a Cabernet Sauvignon grape, but after studying its DNA further, the team decided it was too challenging as well.

Finally, an almost-forgotten grapevine growing in a French greenhouse provided a solution. In the 1980s, a French viticulturist hoping to develop a better vine for winemakers began inbreeding a Pinot Noir. Several generations of selfings produced a few lines with simplified genomes but also stunted their growth and made them unappealing for wine production. Vigna/Vigne decided one of those, PN40024, would offer the best potential for sequencing, even if it was, as Pè jokes, "pathetic, hardly a grape."

Just months after Vigna/Vigne began its PN40024 sequencing effort, Pè and his colleagues were shocked to learn of a rival effort. In March 2006, Riccardo Velasco and his colleagues at the Istituto Agrario San Michele

CREDIT: STEPHEN LAGIER

A Life With Grapes

CAROLE MEREDITH SPENT 3 DECADES STUDYING grape genetics, and she helped start the grape genome efforts that bore fruit last year. But in 2003, she traded her lab bench for a life of winemaking in California's Napa Valley.

Before that career shift, Meredith had earned fame for using genetic fingerprinting to resolve the origins of some of the world's great wines, including Chardonnay and Cabernet Sauvignon (*Science*, 3 September 1999, p. 1562). She and her colleagues garnered the most attention by tracing the roots of the iconic American wine grape Zinfandel to an ancient Croatian grape called Crljenak kastelanski. Such research, Meredith says, "was very attractive to the popular press and wine-geek consumers."

It didn't pay the bills, however. Her grapevine sleuthing was never directly funded, and Meredith argues that there is a bias in the United States against supporting grape research despite the fruit's economic importance. "I think that, in large part, it's due to our history of Prohibition, and there's still the feeling in Washington that research related to the alcoholic beverages is not the best use of taxpayer money."

To Meredith, it's fitting that Europeans sequenced the grape genome. "In Europe, grapes for wine are a fundamental part of their agricultural heritage and modern economy," she says.

Burned out from the bureaucracy of research and the constant search for grants, Meredith retired and joined her husband, Stephen Lagier, who had been working for the Robert Mondavi Winery, to make their own wine using land they purchased in 1986. Doing almost everything themselves—vineyard work, winemaking, bottling, sales—the

all'Adige (IASMA) in Trentino, Italy, announced that they were almost done sequencing the genome of a Pinot Noir grape used in many countries to make red and sparkling wines. Velasco had been involved in some of the original genome planning efforts, including Pè's Italian proposal, but he disagreed with the initial decision to switch from sequencing an outbred Pinot Noir to a Cabernet Sauvignon. His institute then lobbied the Trentino regional government for about €10 million to pursue its own grape genome. IASMA initially kept quiet about the true scope of the project, says Velasco, because "the possibility of failure was high." Unlike Vigna/Vigne, which kept sequencing in-house, IASMA contracted with Myriad Genetics in Salt Lake City, Utah, to sequence and help assemble most of the genome.

After the IASMA bombshell, Anne-Francoise Adam-Blondon of INRA says that the French-Italian effort ground to a halt for several months as members discussed whether to spend their governments' money on something that had apparently already been accomplished. But IASMA hadn't published its genome, so Vigna/Vigne decided to press on.

The race ended with Vigna/Vigne winning by a nose. It published the PN40024 genome online 27 August in *Nature* (sciencenow.sciencemag.org/cgi/content/full/2007/827/1). Velasco's Pinot Noir genome appeared online 19 December in *PLoS One*. Some Vigna/Vigne members felt that Velasco initially downplayed their feat, by, for example, reminding the media that PN40024 wasn't a real Pinot Noir or used for wine. But Velasco attended last month's workshop, which focused on Vigna/Vigne's results, and he was greeted warmly. "The two projects are fully complementary," he says.

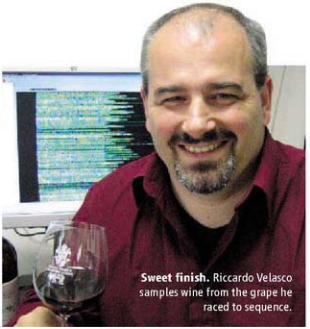

Sweet finish. Riccardo Velasco samples wine from the grape he raced to sequence.

CREDIT: IASMA COLLECTION

Decanting the genome

It's already clear that the two genomes vary significantly. Although both efforts predict that the vinifera genome contains about 30,000 genes, the Pinot Noir sequenced by Velasco's team has about 270 members of a gene family associated with disease resistance, whereas the inbred PN40024 strain has almost 360, Adam-Blondon reported at the workshop. The two grapes also differ in the number of the many hundreds of genes related to the production of polyphenols, flavenoids, and resveratrols—all of which contribute to a wine's color, aroma, and taste.

Several of the talks in Udine centered on how genomic data could aid the breeding of disease-resistant grapevines. Gabriele Di Gaspero of IGA, for example, is trying to harness the powers of a Central Asian grape that is used for raisins. It is the first vinifera shown to stand up to powdery mildew, a discovery by a Hungarian group that electrified grape biologists a few years ago. Di Gaspero and colleagues have been crossbreeding the grape with a mildew-vulnerable vinifera and have used DNA markers identified through the genome projects to pinpoint the chromosomal location of a disease-resistance gene.

In theory, researchers can now—even without identifying the exact gene—breed resistance into popular wine grapes such as Chardonnay and Pinot Noir. After crossing the Central Asian grape with their favorite wine grape, they can select and continue to breed just the seedlings whose DNA contains the markers bracketing the mystery resistance gene. Ultimately, such marker-assisted selection could result in a disease-resistant grape that retains most of the qualities needed to make a good wine, instead of raisins. Still, bringing a new grape to market can take decades—and scientists have to be sure the transferred resistance gene is stable in its new genetic surroundings. "When you plant a grape field, it's for 30 years, so you really need durable resistance," notes Adam-Blondon.

Grape researchers are also using the new genome data to probe the interplay of genes, environment, and wine flavors in a variety of cultivars. In Udine, Mario Pezzotti of the University of Verona detailed genetic studies of the unusual process that produces the Italian red wine Amarone. The grape involved typically produces a sweet wine, but decades ago winemakers realized that if those same grapes dry for several months after harvest, the withered fruit make a more intense and bitter wine that has since become highly valued. Although some of his colleagues predicted that genetics had little to do with the withering process, Pezzotti revealed that large numbers of genes are active during this period, including many that influence a wine's taste and aroma. Amarone makers are now following the research with intense interest, he says.

The Vigna/Vigne and the IASMA teams are now on more cordial terms, but they do have some scientific disagreements. Both have found evidence of whole-genome duplications in vinifera's past—a common feature of plant evolution in which new species arose after an ancestral plant accidentally duplicated its genome or hybridized with another to expand its gene set (see p. 481). Velasco and his colleagues argue that such an event happened relatively recently, after grapes had split off from the branches on which *Arabidopsis* and poplar belong. Vigna/Vigne, on the other hand, has concluded that the grape genome did not undergo any recent expansion. It instead suggests that vinifera derives from an ancient hybrid that once had six sets of chromosomes. Because each team used different strategies for discerning and dating duplications, says Velasco, "who knows who's right?"

Indeed, Pè ended the Udine workshop with the reminder that having a grape genome—or two—in hand merely provides a foundation for future work. "Most of the data still have to be digested," he notes. A glass or two of vinifera's valuable juices, perhaps a nicely aged Cognac, should speed the process. **–JOHN TRAVIS**

couple now produce a well-regarded Syrah.

Although she may have helped pave the way for genetically modified (GM) vines, Meredith says she wouldn't plant them herself, for practical reasons. She has no concerns about the safety of GM grapes and believes vines engineered to resist disease could be useful. But Meredith predicts "tremendous consumer resistance" to GM wines. "I'm a realist," she says. "The only thing that would convince me to switch to a genetically engineered grape … is if my alternative was a dead vineyard."

Meredith loved her research career, particularly the historical studies of wine grapes. But today, sitting in her house on a Napa mountainside watching birds fly over her vineyards, she's content making delicious wine with grapes from her own land. "It's a lovely existence," she says. **–J.I.**

Sowing the Seeds for High-Energy Plants

New crops and improved genetics could be key to successful biofuel agriculture

Carpet sale. Test plots assess corn, *Miscanthus*, and switchgrass (below) as biofuels.

ONCE, PLANT BREEDERS DREAMED OF plumper tomatoes, heartier soybeans, and juicier corn kernels. These days, visions of squat poplars and earless corn stalks are dancing in their heads. They are hoping these newfangled crops will make cost-effective biofuels.

The dominant method of making biofuels today, converting sugars from crops such as corn or sugarcane to ethanol, threatens the food supply and imposes environmental costs. Ultimately, processing cellulose from the cell walls of stems and leaves, which are generally discarded, would make better use of agricultural acreage, as would increasing the oil content of oil-producing crops. In the United States, both government-supported genomicists and privately funded plant scientists are expanding plant genomics research and field studies to figure out the species with the best biofuel potential and how to wring more energy out of each acre planted.

Many researchers are looking at well-known species whose genomes have already been sequenced for clues to making other plants better energy crops: *Arabidopsis*, rice, poplar, and now, corn (*Science*, 7 March, p. 1333). Others plan to tackle sequencing projects for species few had cared about until a few years ago. These include perennials such as switchgrass (*Panicum virgatum*) and *Miscanthus*, both considered good candidates for energy crops because of their high cellulose content. And some scientists are breeding a wide variety of candidate crops around the world, hoping to find optimal varieties. "The spotlight is on this underdeveloped field," says plant biochemist Kenneth Keegstra of Michigan State University in East Lansing, part of the Great Lakes Bioenergy Research Center.

Humans have been growing food crops for 10,000 years, but the effort to produce fuel down on the farm is in its infancy. Studies of the genetic factors that control cell walls are just revving up, and key finds have often occurred serendipitously. "We're at such a basic stage," says Great Lakes center biologist Richard Amasino. For example, in examining why certain varieties of maize showed sugar-rich yellow splotches—researchers dubbed them "tie-dyed" mutants—plant geneticist David Braun of Pennsylvania State University in State College found abnormal amounts of cellulose accumulating in the mutants' cell walls—a potentially useful feature in biofuel crops. Braun hypothesizes that the genes involved could be used in grasses to boost their cellulose content. And last year, Keegstra and colleagues described a gene that likely encodes the enzyme that makes one of four hemicelluloses, which along with cellulose and lignin, make up cell walls, in *Arabidopsis*. Keegstra believes a cell wall engineered to include more hemicellulose might be more easily digestible by biofuel-processing enzymes.

Keegstra and Amasino's institute is one of three centers established by the U.S. Department of Energy (DOE), which is providing each $135 million over 5 years to bring genomics to bear on biofuels. Another, the Joint BioEnergy Institute, led by Lawrence Berkeley National Laboratory, will try to find other relevant genes in *Arabidopsis* and rice. The BioEnergy Science Center at Oak Ridge National Laboratory in Tennessee will focus on poplar and switchgrass. (Each includes enzyme scientists and microbiologists chasing better techniques of breaking cellulose down into fermentable sugars.) In addition, the DOE Joint Genome Institute (JGI) in Walnut Creek, California, is training its sequencing firepower on energy crops.

"There's nothing like having a genome," says JGI Director Edward Rubin. Take poplar, the first tree sequenced (*Science*, 15 September 2006, p. 1596). Before its code was completed in 2006, researchers knew of only 23 genes for proteins called auxin response factors, which control growth. Scientists have now identified 40 in poplar and shown in experiments with mutants that they can manipulate the genes to grow tall, fat, or short varieties. Making shorter branches, for example, could allow foresters to plant trees closer together and maximize biomass density.

Private companies are also chasing after biofuel genes. Synthetic Genomics in San Diego, California, co-founded by geneticist J. Craig Venter, is looking for genes to increase oil yield, drought tolerance, and disease resistance in oil palm, used to make biodiesel in Southeast Asia and Africa. BP's Energy Biosciences Institute at the University of California, Berkeley, a $500 million center started last year, is mapping the genes in the fast-growing *Miscanthus*, a 1.5-meter-high perennial that has been tested as a cellulosic ethanol crop in European trials for 15 years.

The BP institute is also using traditional breeding to study *Miscanthus* in Illinois, sugarcane in Brazil, and sweet sorghum in China, among other projects. It's important to cast a wide net for biofuel crops, says Christopher Somerville, the institute's director. "There's still a lot of uncertainty about what the optimal species are."

–ELI KINTISCH

CREDITS: (TOP TO BOTTOM) ANDREW LEAKEY 2006; THE GARDEN PICTURE LIBRARY / ALAMY

PERSPECTIVE

Genome-Enabled Approaches Shed New Light on Plant Metabolism

Dean DellaPenna[1]* and Robert L. Last[1,2]

Plant metabolism research has experienced a second golden age resulting from synergies between genome-enabled technologies and classical biochemistry. The rapid rate at which genomics data are being accumulated creates increased needs for robust metabolomic technologies and fast and accurate methods for identifying the activities of enzymes.

Plants are unrivaled in the natural world in both the number and complexity of metabolites they produce. Recent estimates are that a single plant species can produce 5000 to 25,000 different compounds and that the >100,000 known chemical structures represent a fraction of the total in the plant kingdom (*1*). This number will increase substantially as analytical methods improve (*2*) and more diverse species are analyzed in detail. Given this diversity, an understanding of plant metabolic networks sufficient to permit predictable modification of metabolism is exceedingly challenging (*3*). Although daunting, the potential payoffs will include balancing the diet of the world's population for optimal health, production of renewable chemical feedstocks by green chemistry, and the generation of biofuels. An increased fundamental understanding of plant biochemistry is essential for addressing these and many other problems confronting humanity in the coming decades.

To devise novel strategies for rapidly advancing plant metabolism research, it is useful to first consider past progress (Fig. 1). The last century was marked by periods of remarkable advancements, principally driven by new technologies. The development of modern chromatographic techniques in the 1940s and 1950s led to an explosion of information about metabolic end products and the realization that there are common themes in central metabolism shared by all organisms. The combination of chromatography and radiolabeled tracers from the 1950s to the 1970s ushered in the first golden age of plant metabolism, during which a single generation of plant biochemists was able to propose pathways for the major plant compound classes. This created opportunities to purify and study novel enzyme activities, although this was typically limited to a small group of proteins that were abundant, stable, and soluble and for which substrates were commercially available. Unlike the situation with microorganisms, the plants selected as amenable for biochemical study often had poorly developed genetics. Starting in the early 1980s (*4*), the ability to isolate mutant plants defective in multiple steps of biochemical pathways, along with the expression of plant cDNAs to complement existing mutations in microorganisms (primarily *Escherichia coli* and *Saccharomyces cerevisiae*), allowed hundreds of plant metabolic enzymes to be identified and cloned. These mutants allowed evaluation of the roles of specific enzymes in plant biosynthetic pathways and the functions of pathway end products for the organism (*5*, *6*). Once full-length cDNAs became available, the problem of obtaining enough protein for detailed enzymatic analysis could be circumvented by expression and purification of target proteins in microbes and animal cells. For example, activity of the previously recalcitrant intrinsic membrane potassium transporter KAT1 was assayed in *Xenopus* oocytes (*7*).

Publication of the first two bacterial genomes in 1995 marked the beginning of the genomic era and presaged a second golden era for research in plant metabolism. As with the introduction of chromatography and radiolabeled tracers, the current public availability of draft or completed genomes for >1000 bacteria and >140 eukaryotes creates unprecedented opportunities to study individual plant enzymes, pathways, and metabolic networks (*8*, *9*).

Genomic resources facilitate connecting plant genes with metabolic functions (*10*–*12*). In addition to identification by overall primary sequence similarity, encoded proteins can be grouped into families based on the presence of conserved domains, motifs, or only a few amino acids (from three-dimensional structures) defined as being essential for substrate binding, catalysis, or regulation. The power of this approach is that it allows direct comparison of proteins with shared properties between organisms that may be separated by hundreds of millions of years of evolution. Typically, the function of only a small fraction of the identified proteins is known (often from studies of model organisms), but this information is sufficient to suggest catalytic properties and inspire functional analysis of other family members or related proteins in other organisms (*11*, *13*–*15*).

Comparative genomics information from the several hundred sequenced bacterial genomes can also be leveraged to characterize biosynthetic processes that are shared between plants and bacteria. A powerful and relatively underused approach takes advantage of the observation that genes encoding proteins of related physiological function are often colocalized on bacterial chromosomes, in operons, in gene fusions forming multifunctional enzymes, or simply in close proximity (*8*–*11*). The depth of such bacteria-derived contextual data makes it more robust and accurate for predicting gene function and pathway associa-

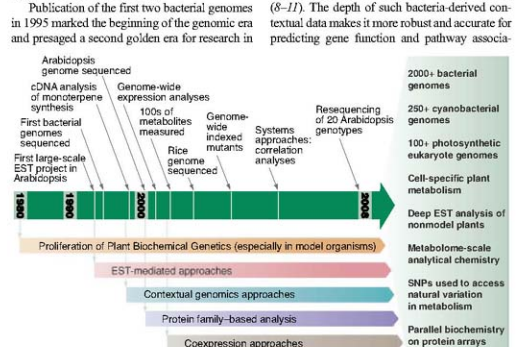

Fig. 1. Time line of genomics-enabled plant biochemistry. Selected major advances to date are indicated above and below the time line. Some approaches and tools likely to further understanding of plant biochemistry during the coming decade are indicated to the right of the time line.

[1]Department of Biochemistry, Michigan State University, East Lansing, MI 48824, USA. [2]Department of Plant Biology, Michigan State University, East Lansing, MI 48824, USA.

*To whom correspondence should be addressed. E-mail: dellapen@msu.edu

tions than simple homology-based search results. Such contextual information has been important for identifying missing pathway steps, and in some cases entire pathways, in plants, such as isopentenyl pyrophosphate synthesis by the methylerythritol phosphate pathway (*16*) and vitamin synthesis (*10*–*12*, *15*).

Our understanding of vitamin biosynthesis in plants was influenced by the availability of genomic resources and demonstrates the range of evolutionary mosaics in plant metabolic pathways. The synthesis of pantothenate (vitamin B_5) and biotin (vitamin B_7) is identical in plants and bacteria, and orthologous enzymes were readily identifiable by homology, contextual information, or mutant complementation (*12*). Tocopherols (vitamin E) are only synthesized by photosynthetic eukaryotes and some cyanobacteria. Four of five plant tocopherol biosynthetic genes have clearly recognizable sequence similarity to cyanobacterial orthologs, whereas the fifth is an unrelated methyltransferase of archeal origin (*17*, *18*). The evolutionary origins of thiamine (vitamin B_1) biosynthesis in plants (Fig. 2) are even more diverse (*12*).

Some of the most interesting biochemistry carried out by plants has no known parallel in microbes, requiring plant-specific approaches to gene and enzyme discovery. Specialized plant metabolites (historically referred to as "secondary metabolites") often are produced at high levels in specific tissues or cell types of individual species or groups of taxonomically related species. Alkaloids (e.g., morphine and codeine) and latex in laticifer cells in poppy and rubber trees, terpenes and saponins in epidermal cells of many plant families, and resins in trees are economically important examples of such compounds.

The cell-type-specific production of secondary metabolites was exploited to purify and then clone the first monoterpene synthases by first purifying the secretory cells from trichomes of peppermint leaves that make the compound. Expressed sequence tag (EST) analysis of these same cells led to the discovery of many of the enzymes of this pathway (*13*, *19*). This approach was feasible because epidermal "hair" trichome cells are particularly amenable to bulk isolation, unlike many other plant cell types that also produce high levels of specialized metabolites (*20*). However, recent breakthroughs in laser microdissection technology in plants (*21*) and use of fluorescence-activated cell sorting of specific cell types (*22*) should make the isolation of such previously unobtainable cell types tractable for genomics-enabled approaches.

The plant cell wall is the most complex polymer in nature, and enzymes involved in its biosynthesis are notoriously uncooperative. Improving our understanding and ability to manipulate cell wall composition has taken on renewed urgency in relation to cellulosic ethanol production from crops. Two novel classes of cell wall biosynthetic enzymes were identified using genomic techniques in nonmodel organisms that were specifically selected because of their active synthesis of particular classes of cell wall polymers during seed development. Mannan synthase was identified from guar bean (*14*), which produces high levels of galactomannan, and a beta-1,4 glucan synthase involved in xyloglucan biosynthesis was cloned from developing nasturtium seeds (*23*), which make large amounts of xyloglucan. Both sequences were then used to annotate certain *Arabidopsis* genes that resemble cellulose synthases. These studies represent an increasingly common approach in which genomics data from model species are leveraged in nonmodel organisms that have characteristics especially suitable from a biochemistry perspective, and in turn the results obtained further enrich our understanding of metabolism in the model organisms.

Approaches using large-scale, publicly available transcript profiling data to identify genes coexpressed with known pathway genes or with the accumulation of specific metabolites are increasingly being used to discover new pathway regulators and enzymes. Sulfur-containing glucosinolates function as defense compounds in plants and have cancer-preventive properties in animals. Many mustard-family plants synthesize glucosinolates, including *Arabidopsis*, in which the biosynthetic pathway has been largely elucidated (*24*). mRNA accumulation of two R2R3-Myb transcription factors (of 125 in the *Arabidopsis* genome) was found to have strong positive correlation with known glucosinolate biosynthetic genes, suggesting that they might regulate the expression of the pathway. When expressed in plant cell cultures, each positively regulated glucosinolate accumulation, confirming their roles as transcriptional regulators of the pathway. As data and tools for transcriptome, proteome, and metabolome profiling become available for a wider range of plants, correlation analysis and other systems biology approaches should increasingly aid discovery of pathways and the dynamic ways in which they are regulated (*25*).

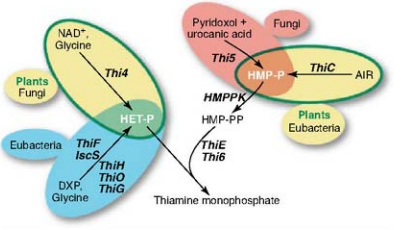

Fig. 2. Plant thiamine monophosphate (TMP) synthesis is an evolutionary mosaic. Organisms that synthesize TMP do so by condensation of HMP-PP and HET-P, which are synthesized by unrelated pathways and enzymes in fungi and eubacteria. Plant TMP synthesis (green-outlined ellipses) is an evolutionary hybrid of the fungal and eubacterial pathways. For clarity, not all genes, steps, or metabolites are shown. Enzymes without color highlighting are common to all three taxa. Bacterial nomenclature (e.g., *ThiC* and *ThiE*) refers to *E. coli* genes while fungal nomenclature (e.g., *Thi4*, 5 etc.) are *S. cerevisiae* genes (*21*). AIR, aminoimidazole ribonucleotide; DXP, deoxy-D-xylulose 5-phosphate; HET-P, hydroxyethylthiazole phosphate; HMP, hydroxymethylpyrimidine; HMP-P, HMP phosphate; HMP-PP, HMP pyrophosphate; HMPPK, HMP-P kinase.

Although the future of research in plant metabolism in the coming decade is exceedingly bright, the success of genome-based approaches is creating a resurgence of some of the traditional challenges in the field. Advances in DNA sequencing throughput is increasing the phylogenetic breadth of plant and microbial genomic and cDNA sequences useful to plant biochemists at an impressive rate [for examples, see (*26*)]. The combination of rapid, deep EST sequencing (through DNA sequencing by synthesis methods such as 454 pyrosequencing) and proteomics combined with methods for isolating biologically intact molecules from single cells or specific cell types is allowing study of specialized biochemistry of nonmodel organisms previously unapproachable by genetics or genomics. The treasure trove of DNA and protein sequences creates an urgent need to expand our ability to identify and quantify small molecules to permit rapid association of gene expression and end products (*2*). As it becomes easier to identify DNA sequences that encode candidates for specific enzymes, the decades-old problem of synthesizing substrates, optimizing enzyme assays, and measuring products becomes more acute. This creates new opportunities for collaboration between biochemists, chemists, and genome scientists in discovering new pathways and engineering plants with currently unimagined roles for the good of humanity.

References and Notes

1. R. N. Trethewey, *Curr. Opin. Plant Biol.* **7**, 196 (2004).
2. R. L. Last, A. D. Jones, Y. Shachar-Hill, *Nat. Rev. Mol. Cell Biol.* **8**, 167 (2007).
3. L. J. Sweetlove, D. Fell, A. R. Fernie, *Biochem. J.* **409**, 27 (2008).
4. C. R. Somerville, W. L. Ogren, *Proc. Natl. Acad. Sci. U.S.A.* **77**, 2684 (1980).

5. P. L. Conklin, E. H. Williams, R. L. Last, *Proc. Natl. Acad. Sci. U.S.A.* **93**, 9970 (1996).
6. H. Maeda, D. DellaPenna, *Curr. Opin. Plant Biol.* **10**, 260 (2007).
7. D. P. Schachtman *et al.*, *Science* **258**, 1654 (1992).
8. A. Osterman, R. Overbeek, *Curr. Opin. Chem. Biol.* **7**, 238 (2003).
9. R. Overbeek *et al.*, *Nucleic Acids Res.* **33**, 5691 (2005).
10. V. de Crecy-Lagard, A. D. Hanson, *Trends Microbiol.* **15**, 563 (2007).
11. D. DellaPenna, B. J. Pogson, *Annu. Rev. Plant Biol.* **57**, 711 (2006).
12. M. E. Webb *et al.*, *Nat. Prod. Rep.* **24**, 988 (2007).
13. R. B. Croteau, E. M. Davis, K. L. Ringer, M. R. Wildung, *Naturwissenschaften* **92**, 562 (2005).
14. K. S. Dhugga *et al.*, *Science* **303**, 363 (2004).
15. D. Tholl, *Curr. Opin. Plant Biol.* **9**, 297 (2006).
16. M. Rodriguez-Concepcion, A. Boronat, *Plant Physiol.* **130**, 1079 (2002).
17. Z. Cheng *et al.*, *Plant Cell* **15**, 2343 (2003).
18. A. L. Van Eenennaam *et al.*, *Plant Cell* **15**, 3007 (2003).
19. B. M. Lange *et al.*, *Proc. Natl. Acad. Sci. U.S.A.* **97**, 2934 (2000).
20. A. L. Schinmeller *et al.*, *Plant J.*, in press; doi: 10.1111/j.1365-313X.2008.03432.x
21. T. Nelson, S. L. Tausta, N. Gandotra, T. Liu, *Annu. Rev. Plant Biol.* **57**, 181 (2006).
22. K. Birnbaum *et al.*, *Science* **302**, 1956 (2003).
23. J. C. Cocuron *et al.*, *Proc. Natl. Acad. Sci. U.S.A.* **104**, 8550 (2007).
24. B. A. Halkier, J. Gershenzon, *Annu. Rev. Plant Biol.* **57**, 303 (2006).
25. M. Naoumkina *et al.*, *Proc. Natl. Acad. Sci. U.S.A.* **104**, 17909 (2007).
26. U.S. Department of Energy, Joint Genome Institute, http://genome.jgi-psf.org/euk_cur1.html
27. This work was supported by funding from the Michigan State University Foundation, Harvest Plus, the Grand Challenges in Global Health Initiative, and NSF MCB 0519740 to D.D.P.; and by NSF DBI 0604336, MCB 0519740, and DBI 0619489 to R.L.L.

10.1126/science.1153715

PERSPECTIVE

Genomic Plasticity and the Diversity of Polyploid Plants

A. R. Leitch[1] and I. J. Leitch[2]

Polyploidy, a change whereby the entire chromosome set is multiplied, arises through mitotic or meiotic misdivisions and frequently involves unreduced gametes and interspecific hybridization. The success of newly formed angiosperm polyploids is partly attributable to their highly plastic genome structure, as manifested by tolerance to changing chromosome numbers (aneuploidy and polyploidy), genome size, (retro)transposable element mobility, insertions, deletions, and epigenome restructuring. The ability to withstand large-scale changes, frequently within one or a few generations, is associated with a restructuring of the transcriptome, metabolome, and proteome and can result in an altered phenotype and ecology. Thus, polyploid-induced changes can generate individuals that are able to exploit new niches or to outcompete progenitor species. This process has been a major driving force behind the divergence of the angiosperms and their biodiversity.

Polyploidy occurs in many animals (e.g., in fishes, insects, and amphibians) and plants (e.g., ferns and mosses) but is particularly widespread in the flowering plants (angiosperms), including many major crops (Fig. 1). Molecular analyses suggest that the genomes of most (>90%) extant angiosperms retain evidence of one or more ancient genomewide duplications (*1*) and that numerous species have undergone more recent polyploidy (*2*). For example, the polyploid *Arabidopsis suecica* is considered to have formed from "diploid" parents circa (ca.) 12,000 to 300,000 years ago, whereas each of the parental genomes retain evidence of more ancient duplications estimated to have arisen ca. 101 to 168 million years ago (Ma), 66 to 109 Ma, and 24 to 40 Ma (*3*). Polyploidy often occurs in association with interspecific hybridization, a condition called allopolyploidy, that can result in the generation of new species. It is not clear why polyploidy is so abundant in angiosperms, particularly when its occurrence in gymnosperms, considered to be sister to angiosperms, is so low (<5% are polyploid). Nevertheless we wish to know the origin, evolution, and consequences of polyploidy to reveal how it has contributed to the diversity of angiosperms seen today (estimated to be 250,000 to 400,000 species) (*4*–*10*).

Polyploids commonly arise from unreduced gametes by nondisjunction of chromosomes in the germ line. Unreduced gametes occur widely in both animals and plants, but there are differences in the survival of the derived triploid offspring. For example, in humans diploid gametes occur 0.2 to 0.3% of the time, but they rarely lead to triploid young and these do not survive to adulthood. In angiosperms, unreduced gametes occur with a mean frequency of about 0.56%, with interspecific hybridization, herbivory, and disease stress, among others, elevating their occurrence (*11*). However, in contrast to humans, derived triploid angiosperms frequently survive and can be important in establishing higher ploidy levels (*12*). Furthermore, ongoing chromosome

Fig. 1. A sample of agricultural crops that are polyploid, showing oil from oilseed rape (*Brassica napus*, $2n = 4x = 38$), bread from bread wheat (*Triticum aestivum*, $2n = 6x = 42$), rope from sisal (*Agave sisalana*, $2n = 5x = 180$), coffee beans (*Coffea arabica*, $2n = 4x = 44$), banana (*Musa* triploid hybrids, $2n = 3x = 33$), cotton (*Gossypium hirsutum*, $2n = 4x = 52$), potatoes (*Solanum tuberosum*, $2n = 4x = 48$), and maize (*Zea mays*, $2n = 4x = 20$).

[1]School of Biological and Chemical Sciences, Queen Mary, University of London, London E1 4NS, UK. (E-mail: a.r.leitch@qmul.ac.uk) [2]Jodrell Laboratory, Royal Botanic Gardens, Kew, Richmond, Surrey TW9 3AB, UK. (E-mail: i.leitch@kew.edu)

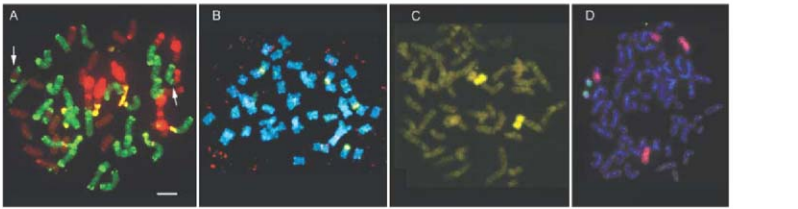

Fig. 2. Differences in genomic plasticity between angiosperms and mammals revealed by chromosome labeling patterns using fluorescent in situ hybridization. (**A**) Genome painting distinguishes parental genomes in polyploid synthetic tobacco ($2n = 4x = 48$, 1C = 5.4 pg). Chromosomes were labeled with both red and green fluorescent markers that identify the parental origin of the chromatin by color. Chromosomes with red and green segments carry translocations (arrows). [Image reproduced with permission from (*24*). Copyright 2006, Botanical Society of America] (**B**) The differential labeling of parental chromatin is lost in a related allopolyploid, *Nicotiana nesophila* ($2n = 4x = 48$, 1C = 5.0 pg), because of near-complete genome turnover occurring over ca. 5 million years. [Image reproduced with permission from (*25*). Copyright 2005, *New Phytologist*] In contrast, the conserved genome structure of mammals is illustrated by the ability of human chromosome paints to label chromosomes of (**C**) orangutan ($2n = 2x = 48$, 1C = 3.6 pg), which diverged from humans more than 15 Ma, and (**D**) horse ($2n = 2x = 64$, 1C = ca. 3.2 pg), which diverged over 55 Ma. [Image in (C) reproduced with permission from (*26*). Copyright 1992, National Academy of Sciences. Image in (D) reproduced with permission from (*27*). Copyright 2004, Springer-Verlag] Scale bars indicate 10 μm [(A) and (B)], ca. 3.5 μm (C), and 4.5 μm (D).

nondisjunction can give rise to complex aneuploid and polyploid series (e.g., *Cardamine pratensis* L., with reported chromosome numbers of $2n =$ 16, 24, 28, 30, 33 to 38, 40 to 46, 48, 52 to 64, and 67 to 96). Newly formed allopolyploids may be particularly common in angiosperms, given the abundance of unreduced gametes and the general lack of targeting in pollen delivery (e.g., via insects or wind) to the female receptive organ in the flower (the stigma). However, few successfully establish. Indeed, the allopolyploid plant York groundsel (*Senecio eboracensis*, Asteraceae) probably arose naturally in the 1970s through allopolyploidy involving a native and introduced species. It now grows as a weed of industrial wastelands, but redevelopment of the area is destroying its habitat, and unless it can disperse to similar sites elsewhere it will go extinct. Thus, in less than 50 years from its birth, this species is now nearing extinction, illustrating the precarious nature of early polyploid establishment (*5*). Nevertheless polyploid species are highly numerous, and even in the past 150 years several new species are known to have evolved and established (*6*).

Genomic Plasticity in Polyploids

Angiosperms are remarkable in their ability to tolerate the considerable genomic impact of polyploidy arising from the accommodation of divergent genomes in the same nucleus, intraspecific chromosome number variations, unbalanced parental chromatin contributions, and chromosomal rearrangements, for example, inversions and translocations (*13*) (examples of intergenomic translocations are arrowed in Fig. 2A, which shows a chromosome spread at metaphase of a polyploid species). This remarkable plasticity of the genome is also evident from the diverse and often rapid genetic and epigenetic changes associated with polyploidy [e.g., (retro)transposon mobility, sequence rearrangements and losses, gene silencing, DNA methylation changes, and chromatin remodeling (*2*, *6*, *8*)]. Many chromosomal changes are induced by multivalent formation and aberrant segregation of chromosomes at meiosis in early generation polyploids (*10*). These abnormalities can reduce fertility, but sexual selection will favor the most fertile and viable individuals and remove those that are maladapted. Little is known about how regular chromosome pairing is restored, although pairing genes may enhance bivalent formation in some polyploid wheats and mustards. Meiosis may therefore dually impact the evolution of many newly formed polyploids by (i) enabling sexual propagation and (ii) generating, through meiotic errors, large-scale chromosomal variation upon which genetic drift and/or selection can act. Overall, we surmise that the high frequencies of unreduced gametes provide a constant evolutionary pressure toward polyploidy in angiosperms, whereas genomic plasticity relaxes the genetic and developmental constraints against polyploid formation.

Studies of synthetic allopolyploids, aiming to mimic natural species, have been valuable in providing insights into the nature of angiosperm genome plasticity. They reveal that the genomic response to polyploidy can be fast, targeted, but highly variable between species (*8*). Nevertheless, changes in the epigenetic profile appears to be a universal response that can lead to partitioning of the expression of duplicated ancestral genes to specialized tissue-specific activity or function (subfunctionalization) (*2*). Duplicate genes can, however, also be lost, and over longer time frames this contributes to genome diploidization, an ongoing process that returns the genome to a diploidlike form (*14*).

In angiosperms, genomewide turnover of nongenic and/or repetitive sequences leads to further diploidization through the erosion of differences between parental genomes in the polyploid. Over time frames of 5 to 10 million years there can be near-complete retroelement turnover (*15*) and tandem repeat replacement, resulting in the loss of many genome-specific sequences (*16*) (Fig. 2, A and B). This genome plasticity contrasts markedly with mammalian genomes, in which single chromosome losses or gains are usually detrimental, polyploidy is rare or absent, and large-scale genome organization remains conserved over tens of millions of years (Fig. 2, C and D).

With high-throughput DNA sequencing technologies, it is now feasible to determine the parental origin of sequences in both the genomic DNA and the transcriptome and to compare profiles between natural and synthetic polyploids and related diploids. Such approaches will inform the extent to which differential sequence losses are targeted at specific genomes, chromosomes, or chromosomal regions; the influence of maternal and paternal origins; the role of environmental factors; and the mechanisms and processes involved in the evolution of duplicated alleles.

Genome Size Plasticity

Angiosperm genome sizes vary nearly 2000-fold compared with taxa that generally lack polyploidy, such as mammals (genome size varies fivefold) and birds (genome size varies twofold), emphasizing the plasticity in angiosperm genome structure. Polyploidy results in an instantaneous multiplication in DNA content, after which di-

vergence of lineages may be accompanied by genome size increases or decreases, the direction of which reflects a balance between mechanisms that expand genomes (e.g., retroelement insertion) and those which shrink them (e.g., deletions). With the accumulation of extra genome(s), there is an increased demand for nutrients, particularly nitrates and phosphates, that are needed to make nucleic acids and proteins (*17*). Yet phosphorus is often limited in supply, as in Australia, where ancient weathered soils have so little phosphorus that they restrict the distribution of some plant communities (*18*). Such nutrient demands are not a problem for animals that assimilate DNA directly from their food. However, for plants in areas where nutrient levels are limiting, we predict that there will be selection against polyploids or for those that can eliminate excess DNA. This hypothesis is supported by the fact that after polyploidy, genome downsizing in angiosperms is the most common response (*17*). More research is needed to determine the role of nutrient limitation in the establishment and evolution of polyploids in comparison with related diploids and to examine the incidence of polyploidy in those environments, such as bogs and heaths, where nutrient levels are low. One might also predict that similar trends toward genome downsizing would be less apparent in animals for which such nutrients are not limiting, but to date no comparable analyses have been done.

Transcriptome, Metabolome, and Proteome

Genomic plasticity has downstream effects on the transcriptome, proteome, and metabolome that can generate phenotypic variation in polyploids exceeding that found in the parents (*9*). At the transcriptome level, studies on natural and synthetic polyploids have demonstrated genomewide nonadditive, nonrandom changes in gene regulation (e.g., silencing and up- and down-regulation), many of which were tissue and/or species-specific. The reprogramming of the allopolyploid transcriptome has been shown to be triggered predominantly by interspecific hybridization rather than by chromosome multiplication (*9*).

Changes at the transcriptome need not necessarily be reflected in the proteome, given the potential for posttranscriptional and posttranslational modifications. Unfortunately, there are few studies into the effects of polyploidy on the proteome. Nevertheless, research on synthetic *Brassica* allopolyploids showed that 25 to 38% (depending on tissue) of proteins displayed quantitative variation from an expected additive pattern of proteins found in the two parents, with changes being rapid and, in some instances, nonstochastic, reproducible, and organ-specific (less than 1% of changes were qualitative). As with the transcriptome, it was interspecific hybridization that stimulated the most perturbations in expression (*19*). Interestingly, in silico analysis of nonadditive proteins failed to reveal any substantial biological consequences (*20*).

Not surprisingly, allopolyploidy has also been shown to trigger changes to the metabolome. The profile of secondary metabolites manufactured in defense of herbivory were shown to differ substantially in response time, duration, and strength between two *Nicotiana* allopolyploids that share the same parental origins (*21*). Similarly, in synthetic *Nicotiana* allopolyploids differences were observed between individuals and their parents (*22*). In nature, such physiological differences may affect allopolyploid evolution and survival.

The picture emerging from studies of synthetic polyploids is that interspecific hybridization is primarily responsible for triggering extensive and rapid changes and generating variation that may facilitate adaptation and speciation. Given this, one might expect homoploid species, (i.e., those derived from interspecific hybrids without an accompanying genome duplication) to be more common, yet only about 20 have been reported. Homoploids exploit niches unavailable to the parents and may diverge through spatial isolation or rapid genome divergence. In some cases, their success has been attributed to the acquisition of transgressive characters, that is, those characters that fall outside the range found in the parents (*23*). However, interspecific hybridization typically causes gene flow between populations, breaking down species isolation barriers, and does not usually lead to speciation. In contrast, chromosome multiplication can create instant barriers with diploid parents. Thus, both components of allopolyploidy contribute to their widespread occurrence: (i) interspecific hybridization to trigger changes at all levels from the gene to ecology and (ii) chromosome multiplication to establish these changes. We now face the challenge to determine how perturbations to the transcriptome, metabolome, and proteome influence the phenotype and ecology, requiring the transfer of molecular technologies to an ecological setting. Furthermore, better understanding is needed to explain how polyploids establish fertility, necessitating the search for mechanisms driving regular bivalent pairing; certainly if controlling genes are discovered they may find applications in the production of new polyploid crops.

Conclusions and Future Prospects

In angiosperms, allopolyploidy triggers a new steady state for the transcriptome, metabolome, and proteome networks and perhaps enhances network robustness and/or increases network complexity. We suggest it is genomic plasticity that enables step changes in the steady state, equipping newly originated polyploid individuals with novel biochemical pathways and transgressive characters and allowing them to exploit new niches and/or outcompete diploid parents. Although most new polyploid individuals will die, they must have arisen sufficiently often and with sufficient success to have been a major driving force behind the divergence of angiosperms.

Models explaining how genomic reorganization and epigenetic reprogramming causes changes in gene expression after polyploidy are focused on mechanisms that establish locus-specific expression of duplicated alleles in early polyploids (*9*). Such models need to be tested against rigorous statistical analyses of networks of molecular interactions to determine network robustness and the nature and strength of individual links. Network analyses will also reveal how newly formed polyploids differ in their response to the environment compared with their progenitors and provide understanding of the ecological advantages of polyploidy. We will need to distinguish between responses to polyploidy that are specific, stochastic, or ubiquitous at the levels of individuals, populations, and species. Such information will assist crop breeders and lead to an enhanced understanding of polyploid-generated angiosperm diversity.

References and Notes

1. L. Cui *et al.*, *Genome Res.* **16**, 738 (2006).
2. K. L. Adams, J. F. Wendel, *Curr. Opin. Plant Biol.* **8**, 135 (2005).
3. S. De Bodt, S. Maere, Y. Van de Peer, *Trends Ecol. Evol.* **20**, 591 (2005).
4. M. L. Ainouche, A. Baumel, A. Salmon, *Biol. J. Linn. Soc.* **82**, 475 (2004).
5. R. J. Abbott, A. J. Lowe, *Biol. J. Linn. Soc.* **82**, 467 (2004).
6. D. E. Soltis, P. S. Soltis, J. A. Tate, *New Phytol.* **161**, 173 (2003).
7. C. Brochmann *et al.*, *Biol. J. Linn. Soc.* **82**, 521 (2004).
8. K. L. Adams, J. F. Wendel, *Trends Genet.* **21**, 539 (2005).
9. Z. J. Chen, *Annu. Rev. Plant Biol.* **58**, 377 (2007).
10. L. Comai, *Nat. Rev. Genet.* **6**, 836 (2005).
11. J. Ramsey, D. W. Schemske, *Annu. Rev. Ecol. Syst.* **29**, 467 (1998).
12. B. C. Husband, *Biol. J. Linn. Soc.* **82**, 537 (2004).
13. R. T. Gaeta *et al.*, *Plant Cell* **19**, 3403 (2007).
14. B. C. Thomas, B. Pedersen, M. Freeling, *Genome Res.* **16**, 934 (2006).
15. J. X. Ma, K. M. Devos, J. L. Bennetzen, *Genome Res.* **14**, 860 (2004).
16. K. Y. Lim *et al.*, *New Phytol.* **175**, 756 (2007).
17. I. J. Leitch, M. D. Bennett, *Biol. J. Linn. Soc.* **82**, 651 (2004).
18. N. C. W. Beadle, *Ecology* **43**, 281 (1962).
19. W. Albertin *et al.*, *Genetics* **173**, 1101 (2006).
20. W. Albertin *et al.*, *BMC Genomics* **8**, 56 (2007).
21. Y. Lou, I. T. Baldwin, *Proc. Natl. Acad. Sci. U.S.A.* **100**, 14581 (2003).
22. I. S. Pearse, T. Krugel, I. T. Baldwin, *Plant J.* **47**, 196 (2006).
23. L. H. Rieseberg, J. H. Willis, *Science* **317**, 910 (2007).
24. K. Y. Lim *et al.*, *Am. J. Bot.* **93**, 875 (2006).
25. J. J. Clarkson *et al.*, *New Phytol.* **168**, 241 (2005).
26. A. Jauch *et al.*, *Proc. Natl. Acad. Sci. U.S.A.* **89**, 8611 (1992).
27. F. Yang *et al.*, *Chromosome Res.* **12**, 65 (2004).

28. We thank Natural Environment Research Council for support and A. Kovarik, Y. Lim, and two anonymous referees for insightful comments.

10.1126/science.1153585

PERSPECTIVE

Selection on Major Components of Angiosperm Genomes

Brandon S. Gaut* and Jeffrey Ross-Ibarra

Angiosperms are a relatively recent evolutionary innovation, but their genome sizes have diversified remarkably since their origin, at a rate beyond that of most other taxa. Genome size is often correlated with plant growth and ecology, and extremely large genomes may be limited both ecologically and evolutionarily. Yet the relationship between genome size and natural selection remains poorly understood. The manifold cellular and physiological effects of large genomes may be a function of selection on the major components that contribute to genome size, such as transposable elements and gene duplication. To understand the nature of selection on these genomic components, both population-genetic and comparative approaches are needed.

Flowering plants are relative newcomers to the evolutionary stage, appearing for the first time 150 to 200 million years ago. Angiosperms have since radiated across the globe, quickly becoming a dominant life form on the planet. Mirroring their rapid diversification, the size of angiosperm genomes has changed rapidly as well: Higher plants vary ~2000-fold in genome size, from the 64-Mb genomes of *Genlisea* (corkscrew plants) (*1*) to the 124-Gb genomes of *Fritillaria* (the fritillary lilies) (Fig. 1) (*2*). Still, the nature of the relationship between genome size and natural selection is not well understood.

Genome size correlates with broad-scale patterns of plant biology. Plant species with large genomes tend to have large cells and large seeds, factors that are associated with a number of life-history traits. But plants with large genomes also have lower photosynthetic rates, grow more slowly, and are underrepresented in extreme environments (*3*). The ecological costs incurred by large genome size have a parallel evolutionary cost: Plant genera with the largest genomes tend to have the lowest species diversity, suggesting that genome size affects speciation rates (*3*).

Genome size also varies among individuals within a species, and such variation has been linked to selection. Individuals with the same chromosome number can vary as much as 40% in genome size (*4*). This intraspecific diversity correlates with environmental clines and growth characteristics (*5*) and may also respond to indirect selection on other traits (*6*). However, the mechanisms that connect genome size to phenotype remain unclear. One possibility is that DNA content affects cell volume and replication, leading to generally lower growth rates. The accrual of DNA may also have functional effects via gene regulation or copy-number variation (*5*). In any case, the manifold cellular and physiological effects of a larger genome may result in direct selection either on genome size itself or on the major components that contribute to genome size.

The largest contributor to genome size is repetitive DNA, particularly transposable elements (TEs). In fact, it is common for the majority of a plant's genome to consist of transposon-derived DNA (Fig. 2). Much has been learned about TEs from genomic sequence data, including their distribution among species, their genomic locations of accumulation, the mechanisms by which they are purged from genomes, and their rates of proliferation. The last may be particularly impressive; the rice genome has increased >2% in size over the past few hundred thousand years because of TE activity alone (*7*). Individual animal genomes may also be element-rich (*8*), but plant genomes appear to vary more rapidly with respect to their transposon-derived component.

Given the apparently detrimental consequences of a large genome, it follows that the accumulation of transposons is probably deleterious to plant fitness. Many individual transposon insertions—such as those into coding regions—may be strongly deleterious, leading to their rapid loss from the gene pool (*9*). However, understanding the role of natural selection in shaping transposon diversity ultimately requires a population-genetic approach. In *Drosophila*, humans, *Arabidopsis*, and pufferfish, quantitative estimation of the strength of selection from population-genetic data suggests that TE insertions are on average slightly delete-

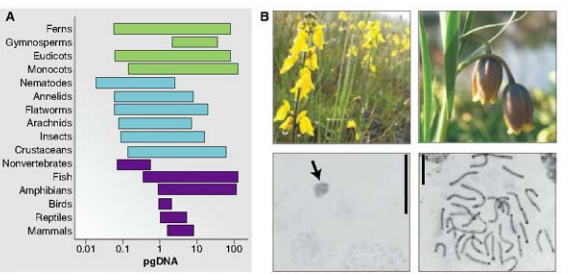

Fig. 1. (A) Despite being among the most recent of the groups depicted, monocots and eudicots encompass the widest range of genome sizes. Data are from (*1*, *2*). pgDNA, picograms of DNA. **(B)** Photos depict the flower and metaphase squashes of *Genlisea* (*1*) on the left and a triploid *Fritillaria* (*30*) on the right. The arrow indicates the dividing *Genlisea* nucleus. Scale bars represent 10 μm. [Photo credit: Fernando Rivadavia (*Genlisea*) and Christine Skelmersdale (*Fritillaria*)]

Department of Ecology and Evolutionary Biology, 321 Steinhaus Hall, University of California Irvine, Irvine, CA 92697–2525, USA.

*To whom correspondence should be addressed. E-mail: bgaut@uci.edu

approach could go a long way toward illuminating the selective forces acting on plant genomes.

Population-genetic approaches have also been useful for identifying adaptive transposon insertions (*13*). This and other evidence suggests that TEs are not just deleterious but also contribute to genome function. In plants, transposons have been domesticated to become functional genes (*14*), have inserted complete exons into expressed genes (*15*), and have facilitated the formation of previously unrecognized genes via reverse transcriptase (*16*). Transposons are also potential sources of cis-regulatory elements and small RNAs. Moreover, transposable element activity can also accelerate the response to selection, presumably by producing genetic variation on which selection can act. An example is selection on bristle number in *Drosophila melanogaster*, where *p* element lines responded rapidly to selection but lines without active *p* elements did not (*17*). This study suggests that natural and artificial selection on a phenotypic trait could drive correlated increases in transposon activity in a manner antagonistic to selection against large genome size.

Gene duplication is another major contributor to plant genome size. The angiosperms sequenced to date contain more gene duplicates than animals (Fig. 2). Much of this duplication is due to polyploid events, which create complete genetic redundancy by copying every gene in the genome. Although many duplicated genes are lost as they accumulate mutations and deletions, this process is nonrandom (*18*). Genes related to transcription, signal transduction, and development are more likely to be retained as duplicates than other functional gene categories. This biased retention may result from variable sensitivity of genes to dosage effects, with selection acting to maintain proper stochiometric ratios (*18*). Retention biases can also be taxon specific, perhaps explaining the high abundance of aromatic proteins in grapes (*19*).

Tandem duplication is another potent source of gene duplication. Tandemly duplicated genes represent ~15% of genes in angiosperm genomes (*20*); curiously, this proportion closely mirrors the 10 to 17% range of tandem duplicates found across animal genomes (*21*). Tandemly duplicated genes are probably subjected to different selection pressures than genes duplicated by polyploidy, on the basis of four lines of evidence: (i) First, tandem events tend to duplicate only one component of a genetic network, as opposed to entire networks. (ii) Second, tandemly duplicated genes are biased toward a different set of genes; tandem duplicates are overrepresented for membrane proteins and abiotic response genes (*20*). These genes tend to be at the end of biosynthetic pathways, suggesting that tandem duplicates are retained more readily if they do not perturb key branch points of networks. (iii) Third, differences between tandem and polyploid duplicates extend to patterns of gene expression, because tandem duplicates diverge more rapidly in expression (*22*). (iv) Lastly, tandem duplication events are ongoing and common. It has been estimated conservatively that 1 out of ~700 *Arabidopsis thaliana* seeds contain a copy-number variant caused by unequal crossing over between tandem duplications (*23*).

Tandem duplication is common enough to occur on an ecological time scale and may thus be a particularly potent source of genetic innovation for local adaptation. Tandem duplications have been shown to mediate boron tolerance in barley (*24*), submersion tolerance in rice (*25*), and diversification of secondary metabolites in *A. thaliana* (*26*). However, there is not yet a great deal of information as to the extent of copy-number variation in plants, the role of copy-number variants in local adaptation, and the contribution of copy-number variants to genome-size variation among individuals. Careful characterization in humans indicates that up to 12% of the genome may vary in copy number (*27*), but even this impressive number is unlikely to account for the 40% difference in genome size among some plant populations.

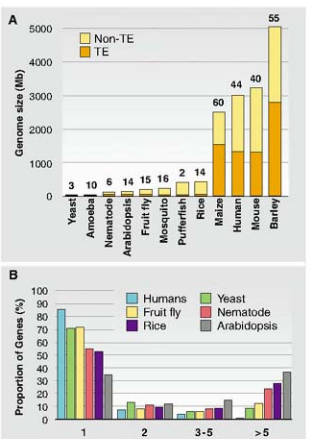

Fig. 2. TE content and gene-family size for representative sets of eukaryote genomes. **(A)** Genomic TE content [from (*8*)]. Numbers above each bar represent the percentage of each genome made up of TEs. **(B)** Percent of the genome made up by gene families of varying sizes (single copy at left to greater than five copies at right) [from (*31*)].

Our discussion underscores the need for genome-wide assessments of all types of genetic variation (including nucleotide polymorphism, copy-number variation, and TEs) at the population level. Such information is a necessary precursor for characterizing recent selection on plant genomes and also for understanding the mechanisms that contribute to genome-size variation. Population genomic data can address the relative strengths of purifying, balancing, and directional selection; the genomic components that contribute to adaptation; and the identification of genes that have been targets of selection. These diversity assessments eventually need to include explicit multipopulation sampling so that diversity patterns can be evaluated to detect signatures of local adaptation. Thus far, the only genome-level polymorphism surveys in plants have targeted *A. thaliana* (*28*, *29*), yielding insights about selection on coding regions and revealing unexpected trends (such as high levels of diversity in genes that mediate interactions with the biotic environment). Unfortunately, technological limitations inherent to these studies have prevented a comprehensive assessment of the relative frequency and amount of copy-number versus transposon polymorphism, and thus these important components of genome size and function remain poorly characterized.

Population genomic data provide information about recent selection, but inter-species comparisons may uncover selection manifested over longer time periods. Yet, there has been shockingly little comparative analysis of plant genomes, owing to the substantial evolutionary distances among the four angiosperm genome sequences published to date. This lack of analysis has highlighted the need for dense sequencing within recently diverging clades. For example, the *A. lyrata* and sorghum genome sequences will provide fitting contrasts to those of *A. thaliana* and maize, respectively. These contrasts will yield information about the type and strength of selection on coding regions, molecular-evolutionary patterns that characterize species divergence, and basic dynamics of plant genome evolution. We do not yet know, for example, whether plant genomes contain large, conserved intergenic regions like those of animals and whether such intergenic regions constrain the lower limits of genome size. Similarly, we do not have a clear picture of the evolution of gene

complement, particularly over modest (intrafamilial) evolutionary distances. Comparative data will also facilitate a broader understanding of the dynamics of gene duplication and TE accumulation.

Nevertheless, additional comparative and population-genetic data alone will not yield a complete understanding of selection on plant genomes or on the processes that govern genome-size variation. There is first a pressing need for additional theoretical advances to provide a conceptual framework to interpret polymorphism data, especially in the context of demographic change in structured populations. Similarly, the theory of the population genetics of gene duplication is in its infancy, as is our understanding of whether standing genetic variation commonly contributes to adaptation. In addition, we need to better understand biological factors that affect the process of selection but are usually not included in molecular-evolutionary or population-genetic models; such factors include paramutation, methylation, epistasis, and gene conversion. Finally, there is always a need to complement inferences about selection with functional assays, particularly if the goal is to correctly identify the genetic variants that have been targeted by selection. With the need for additional data and theoretical models, we clearly are only beginning to understand the complex interplay among phenotypic diversity, genome size, and natural selection.

References and Notes

1. J. Greilhuber *et al.*, *Plant Biol. (Stuttgart)* **8**, 770 (2006).
2. T. R. Gregory *et al.*, *Nucleic Acids Res.* **35**, D332 (2007).
3. C. A. Knight, N. A. Molinari, D. A. Petrov, *Ann. Bot. (London)* **95**, 177 (2005).
4. A. L. Rayburn, H. J. Price, J. D. Smith, J. R. Gold, *Am. J. Bot.* **72**, 1610 (1985).
5. T. R. Meagher, C. Vassiliadis, *New Phytol.* **168**, 71 (2005).
6. A. L. Rayburn, J. W. Dudley, D. P. Biradar, *Plant Breed.* **112**, 318 (1994).
7. J. Ma, K. M. Devos, J. L. Bennetzen, *Genome Res.* **14**, 860 (2004).
8. M. G. Kidwell, *Genetica* **115**, 49 (2002).
9. K. Naito *et al.*, *Proc. Natl. Acad. Sci. U.S.A.* **103**, 17620 (2006).
10. S. I. Wright, Q. H. Le, D. J. Schoen, T. E. Bureau, *Genetics* **158**, 1279 (2001).
11. D. E. Neafsey, J. P. Blumenstiel, D. L. Hartl, *Mol. Biol. Evol.* **21**, 2310 (2004).
12. M. Lynch, J. S. Conery, *Science* **302**, 1401 (2003).
13. Y. T. Aminetzach, J. M. Macpherson, D. A. Petrov, *Science* **309**, 764 (2005).
14. M. E. Hudson, D. R. Lisch, P. H. Quail, *Plant J.* **34**, 453 (2003).
15. J. D. Hollister, B. S. Gaut, *Mol. Biol. Evol.* **24**, 2515 (2007).
16. W. Wang *et al.*, *Plant Cell* **18**, 1791 (2006).
17. A. Tarkamanzehi, C. Moran, F. W. Nicholas, *Genetics* **131**, 73 (1992).
18. G. Blanc, K. H. Wolfe, *Plant Cell* **16**, 1679 (2004).
19. O. Jaillon *et al.*, *Nature* **449**, 463 (2007).
20. C. Rizzon, L. Ponger, B. S. Gaut, *PLoS Comput. Biol.* **2**, e115 (2006).
21. V. Shoja, L. Q. Zhang, *Mol. Biol. Evol.* **23**, 2134 (2006).
22. T. Casneuf, S. De Bodt, J. Raes, S. Maere, Y. Van de Peer, *Genome Biol.* **7**, R13 (2006).
23. B. S. Gaut, S. I. Wright, C. Rizzon, J. Dvorak, L. K. Anderson, *Nat. Rev. Genet.* **8**, 77 (2007).
24. T. Sutton *et al.*, *Science* **318**, 1446 (2007).
25. K. Xu *et al.*, *Nature* **442**, 705 (2006).
26. D. J. Kliebenstein, V. M. Lambrix, M. Reichelt, J. Gershenzon, T. Mitchell-Olds, *Plant Cell* **13**, 681 (2001).
27. R. Redon *et al.*, *Nature* **444**, 444 (2006).
28. R. M. Clark *et al.*, *Science* **317**, 338 (2007).
29. J. O. Borevitz *et al.*, *Proc. Natl. Acad. Sci. U.S.A.* **104**, 12057 (2007).
30. L. F. La Cour, *Philos. Trans. R. Soc. London Ser. B Biol. Sci.* **285**, 61 (1978).

31. S. Lockton, B. S. Gaut, *Trends Genet.* **21**, 60 (2005).
32. We thank the Gaut lab for discussions. This work was funded by NSF grants to B.S.G.

10.1126/science.1153586

PERSPECTIVE

Synteny and Collinearity in Plant Genomes

Haibao Tang,[1] John E. Bowers,[1] Xiyin Wang,[1] Ray Ming,[2] Maqsudul Alam,[3] Andrew H. Paterson[1]*

Correlated gene arrangements among taxa provide a valuable framework for inference of shared ancestry of genes and for the utilization of findings from model organisms to study less-well-understood systems. In angiosperms, comparisons of gene arrangements are complicated by recurring polyploidy and extensive genome rearrangement. New genome sequences and improved analytical approaches are clarifying angiosperm evolution and revealing patterns of differential gene loss after genome duplication and differential gene retention associated with evolution of some morphological complexity. Because of variability in DNA substitution rates among taxa and genes, deviation from collinearity might be a more reliable phylogenetic character.

Eukaryotic genomes differ in the degree to which genes remain on corresponding chromosomes (synteny) and in corresponding orders (collinearity) over time (*1*). For example, most eutherian (placental mammal) orders have incurred only moderate reshuffling of chromosomal segments since descent from common ancestors ~130 million years ago (*2*). Indeed, karyotype evolution along major vertebrate lineages appears to have been slow since an inferred whole-genome duplication occurred ~500 million years ago (*3*). Accordingly, accurate identification of orthologs across eutherian taxa is relatively routine, and deduction of synteny and collinearity is often straightforward with best-in-genome criteria (*4*), identifying one-to-one best matching chromosomal regions in pairwise genome comparisons.

Angiosperm (flowering plant) genomes fluctuate remarkably in size and arrangement even within close relatives, with recurring whole-genome duplications occurring over the past ~200 million years accompanied by wholesale gene loss that has fractionated ancestral gene linkages across multiple chromosomes (*5*). Angiosperm genome sizes span more than 1000-fold (*6*), with much of the difference between some well-studied genomes in heterochromatin (*7*). Additionally, the reshuffling of short DNA segments by mobile elements nearly eliminates large-scale collinearity in heterochromatic regions (*7*).

Despite recurring whole-genome duplications, angiosperm chromosome numbers are more static than genome size, mostly within a range of less than 50-fold (*6*). Condensation of two chromosomes into one is known in many lineages; a particularly striking case involved the demonstration that $n = 10$ (chromosome number) members of the *Sorghum* genus are ancestral to $n = 5$ members of the genus (*8*). Indeed, *Sorghum bicolor* (sorghum) and *Zea mays* (maize) have the same chromosome number ($n = 10$), although maize has been through a whole-genome duplication since their divergence (*9*), whereas the most recent duplication in sorghum is shared with all other cereals (*10*). The occurrence of several condensations may explain why single arms of several maize chromosomes (10 and 5) correspond to entire sorghum chromosomes (6 and 4) (*11*).

Fully sequenced genomes promise to improve deductions of correspondence, toward a unified framework for comparative evolutionary analysis.

[1]Plant Genome Mapping Laboratory, University of Georgia, Athens, GA 30602, USA. [2]Department of Plant Biology, University of Illinois at Urbana-Champaign, Champaign, IL 61801, USA. [3]Advanced Studies in Genomics, Proteomics, and Bioinformatics Unit, University of Hawaii, Honolulu, HI 96822, USA.

*To whom correspondence should be addressed. E-mail: paterson@uga.edu

In angiosperms, analysis of synteny and paleopolyploidy are inextricably intertwined because comparative genomics in angiosperm sequences require strategies to mitigate the effects of genome duplication and fractionation. For example, *Arabidopsis thaliana* (thale cress) has undergone three paleo-polyploidies, including two doublings (*5*) and one tripling (*12*), resulting in ~12 copies of its ancestral chromosome set in a ~160-Mb genome. Further complicating the comparison of *A. thaliana* to other angiosperms are an additional 9 to 10 chromosomal rearrangements in the past few million years since its divergence from *A. lyrata* (rock cress) and *Capsella rubella* (pink shepherd's purse), including condensation of six chromosomes into three, bringing the chromosome number from $n = 8$ to $n = 5$ (*13*). In *Carica* (*14*) argues against an alternative interpretation on the basis of an analysis of a second *Vitis* genome (*16*), which suggested that β occurred in a common ancestor of *Arabidopsis-Populus*.

Synteny can be identified through the clustering of neighboring matching gene pairs; however, differences in gene density and tandem gene arrays among species may cause statistical artifacts. Collinearity, a more specific form of synteny, requires common gene order. Collinearity and synteny have traditionally been identified by looking for one-to-one (pairwise) conservation between species. To take better advantage of new genomic resources as they become available, multiway collinearity analyses are needed, with progressive alignments accompanied by statistical evaluation and iterative refinement (*4*). In

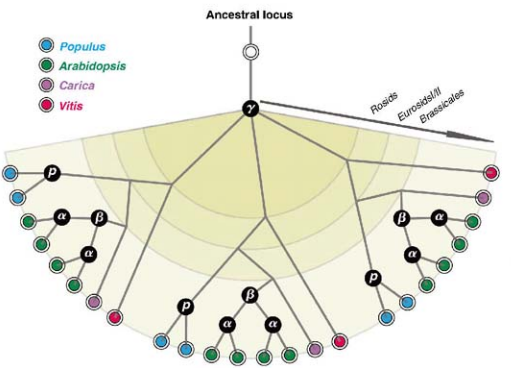

Fig. 1. Idealized gene tree that contains multiple orthologs and paralogs in *Populus*, *Arabidopsis*, *Carica*, and *Vitis*. For illustration purpose, this has assumed equal evolutionary rates along all branches and no gene loss following polyploidy. The polyploidy events are represented as black circles and labeled α and β within the *Arabidopsis* lineage (*5*), salicoid duplication *ρ* in *Populus* (*15*), and γ, which is shared by all four species (*12*, *14*).

Other eudicot genomes show less-complicated genome architectures than *Arabidopsis*. Although still controversial, the two most recent paleopolyploidies affecting *Arabidopsis* [α and β, following the usage in (*5*)] now appear to have occurred within the crucifer lineage (*12*, *14*). *Populus trichocarpa* (poplar) underwent a duplication specific to its own salicoid lineage (*15*) and shares only one of the three paleo-polyploidies (γ) affecting *Arabidopsis*. *Vitis vinifera* (grape) (*12*) and *Carica papaya* (papaya) (*14*), the latter within the same taxonomic order (Brassicales) as *Arabidopsis*, each have only γ and no subsequent polyploidies (Fig. 1). Indeed, the absence of the β event angiosperms, such multiple alignments offer the further advantage of helping to unravel the consequences of genome duplications.

One partial solution for inferring ancestral gene orders in angiosperms has been a bottom-up approach, in which the most recently duplicated segments are interleaved to generate hypothetical intermediates that are further recursively merged (*5*). However, this approach requires an additional cycle of deductions for each duplication event and compounds any errors. An alternative top-down approach requires only one cycle of deduction by simultaneously searching for and aligning all structurally similar segments across multiple genomes and subgenomes. The top-down approach should be more sensitive because it can incorporate transitive homology (*17*), in which segments A and B have undergone reciprocal gene loss and no longer show correspondence to each other but both correspond with a third segment, C. Relationships among such degenerated duplicated regions, easily missed by a bottom-up approach, can often be resolved by comparison to another genome that does not have the duplication or that underwent independent gene loss. Such comparisons have clarified synteny among yeast species (*18*).

Top-down analyses show a high degree of collinearity between *Arabidopsis*, *Carica*, and *Populus* (*14*). For example, we identified three branches each containing orthologous segments from up to four *Arabidopsis*, one *Carica*, and two *Populus* genomic region(s), suggesting paleohexaploidy in a common ancestor of these species (Fig. 2A). Applying these methods to the *Vitis* (grape) genome validated the reconstructed order and inferred triplicated structure of a common *Arabidopsis-Carica-Populus* ancestor. *Vitis* is a eudicot outside of the two eurosid clades that contain *Arabidopsis-Carica* (eurosids II) and *Populus* (eurosids I) (*19*), therefore providing an independent lineage suitable to test the gene order alignments. Paleo-hexaploidy (triplication) has also been suggested over 94.5% of the *Vitis* genome (*12*). When the *Arabidopsis-Carica-Populus* consensus is aligned to *Vitis*, the two independently inferred triplication patterns correspond closely (Fig. 2B). Thus, top-down gene order alignment revealed genome triplication that eluded prior detection in *Arabidopsis* (*5*) and *Populus* (*15*) and also supported the conclusion that the triplication occurred in a common ancestor of *Vitis*, *Arabidopsis*, *Carica*, and *Populus* (*12*).

The emerging unified framework for comparative evolutionary analysis of angiosperm genes and genomes will improve in power and precision as more genomes are sequenced. However, the current framework remains bipolar because we can identify extensive synteny and collinearity within core eudicots and grasses, respectively, but much less between the two groups because of longer evolutionary distance and more genome rearrangements. Collinear orthologs between rice (*Oryza sativa*) and the four core eudicots account for only ~15% of *Oryza* genes distributed over about half of the genome. The longest *Oryza-Arabidopsis* collinear segment contains 23 orthologous gene pairs but is improved twofold, to 47, by incorporating *Vitis*. Additional monocot sequences from noncereal genomes such as *Musa acuminata* (banana) or *Ananas comosus* (pineapple), along with sequences of basal eudicots such as *Eschscholzia california* or *Papaver somnifera* (California or opium poppy) and *Aquilegia formosa* (columbine), and basal angiosperms such as *Amborella trichopoda* (no common name), may further

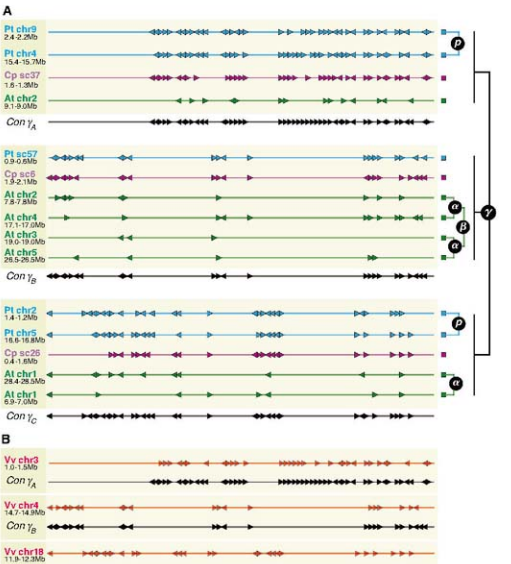

Fig. 2. Typical view of multiple collinear regions among several eudicot genomes. Triangles represent individual genes and their transcriptional orientations. Genes with no syntenic matches to the selected regions are not plotted. **(A)** Alignment among *Arabidopsis* (green), *Carica* (magenta), and *Populus* (blue) chromosomal regions. The whole alignment reveals four distinct duplications, illustrated in Fig. 1. The regions are grouped into three consensus γ-subgenomes (Con γ_A, γ_B, γ_C) on the basis of parsimony. Aligned genes within each γ subgenome are merged into an inferred order by consensus. **(B)** The inferred γ partitions are validated with the *Vitis* genome (red) because each γ subgenome clustered in (A) has only one closely matching *Vitis* chromosomal region.

improve detection of collinearity and synteny across major angiosperm clades.

Pan-angiosperm genome comparisons show correlated patterns of gene retention and loss in paleo-polyploid lineages. Alignments of multiple descendant chromosomes after polyploidy events reveal cases in which ancestral genes were deletion-resistant, consistently being preserved in syntenic subgenomes (*20*). Such preferential conservation of genes from particular families such as MADS-box genes (*21*) and other transcription factors may contribute to increasing morphological complexity (*22*). The opposite case is that of gene functional groups for which members have been consistently restored to one copy after multiple polyploidy cycles, suggesting that there are advantages in having only single copies of these genes (*20*).

Because of variability in DNA substitution rates among plants, deviation from collinearity might be a more reliable phylogenetic character. DNA substitution rates can be highly variable among seed plant lineages, with extreme cases showing 100-fold variation within the same genus on the basis of a study of mitochondrial genes (*23*). Analysis of rare changes (when compared to DNA substitutions) in genomic structure—such as specific rearrangements of gene order, insertions, or deletions—provides an informative and robust way to resolve relationships among many lineages (*24*). In retrospect, early inferences on polyploidy in angiosperms and vertebrates were initially confused by gene phylogenies but later resolved with synteny (*12*, *25*).

Improved synteny and collinearity alignments emerging from top-down approaches applied to multiple genomes and subgenomes are a potential foundation for reconstruction of the ancestral state(s) of angiosperm genomes. Consensus gene orders within syntenic blocks can be approximated on the basis of top-down alignments. Ordering among the syntenic blocks themselves on the macrolevel is more difficult; however, several combinatorial algorithms exist to reconstruct ancestral genomes under a most-parsimonious rearrangement scenario (*26*). The resulting orders would reveal not only shared but also divergent genes inserted into novel locations, underlining lineage-specific changes. Additional genome sequences will improve power to resolve gene orders at the microlevel and also contribute to identifying functionally important DNA, such as the evolutionarily constrained elements among 28 vertebrate genomes (*4*).

References and Notes

1. A. Coghlan, E. E. Eichler, S. G. Oliver, A. H. Paterson, L. Stein, *Trends Genet.* **21**, 673 (2005).
2. M. A. Ferguson-Smith, V. Trifonov, *Nat. Rev.* **8**, 950 (2007).
3. Y. Nakatani, H. Takeda, Y. Kohara, S. Morishita, *Genome Res.* **17**, 1254 (2007).
4. W. Miller *et al.*, *Genome Res.* **17**, 1797 (2007).
5. J. E. Bowers, B. A. Chapman, J. Rong, A. H. Paterson, *Nature* **422**, 433 (2003).
6. M. D. Bennett, J. B. Smith, *Philos. Trans. R. Soc. Ser. B* **334**, 309 (1991).
7. J. E. Bowers *et al.*, *Proc. Natl. Acad. Sci. U.S.A.* **102**, 13206 (2005).
8. R. Spangler, B. Zaitchik, E. Russo, E. Kellogg, *Syst. Bot.* **24**, 267 (1999).
9. Z. Swigonova *et al.*, *Genome Res.* **14**, 1916 (2004).
10. A. H. Paterson, J. E. Bowers, B. A. Chapman, *Proc. Natl. Acad. Sci. U.S.A.* **101**, 9903 (2004).
11. J. E. Bowers *et al.*, *Genetics* **165**, 367 (2003).
12. O. Jaillon *et al.*, *Nature* **449**, 463 (2007).
13. K. Yogeeswaran *et al.*, *Genome Res.* **15**, 505 (2005).
14. R. Ming *et al.*, *Nature*, in press.
15. G. A. Tuskan *et al.*, *Science* **313**, 1596 (2006).
16. R. Velasco *et al.*, *PLoS One* **2**, e1326 (2007).
17. Y. Van de Peer, *Nat. Rev. Genet.* **5**, 752 (2004).
18. M. Kellis, B. W. Birren, E. S. Lander, *Nature* **428**, 617 (2004).
19. D. E. Soltis, P. S. Soltis, P. K. Endress, M. W. Chase, *Phylogeny and Evolution of Angiosperms* (Sinauer, Sunderland, MA, 2005).
20. A. H. Paterson *et al.*, *Trends Genet.* **22**, 597 (2006).
21. J. Nam, C. W. dePamphilis, H. Ma, M. Nei, *Mol. Biol. Evol.* **20**, 1435 (2003).
22. M. Freeling, B. C. Thomas, *Genome Res.* **16**, 805 (2006).
23. J. P. Mower, P. Touzet, J. S. Gummow, L. F. Delph, J. D. Palmer, *BMC Evol. Biol.* **7**, 135 (2007).
24. A. Rokas, P. W. Holland, *Trends Ecol. Evol.* **15**, 454 (2000).
25. P. Dehal, J. L. Boore, *PLoS Biol.* **3**, e314 (2005).
26. E. E. Eichler, D. Sankoff, *Science* **301**, 793 (2003).

27. Funded by NSF MCB-0450260 to A.H.P. and J.E.B., DBI-0421803 to R.M. and A.H.P., the U. Hawaii to M.A., and U.S. Department of Defense W81XWH0520013 to M.A.

10.1126/science.1153917

PERSPECTIVE

The Epigenetic Landscape of Plants

Xiaoyu Zhang

In plants, DNA methylation, histone modifications, and RNA interference play critically important roles in regulating chromatin structure, thereby profoundly affecting transcription and other molecular events. Recent advances in microarray and high-throughput sequencing technologies have enabled genome-wide studies of these pathways in great detail. The vast amounts of "epigenomic" data generated so far have provided new insights into the mechanisms and functions of these pathways and have broadened our understanding of the structure and organization of plant chromatin as a whole.

The genomes of several plants have been sequenced, and those of many others are under way. But genetic information alone cannot fully address the fundamental question of how genes are differentially expressed during cell differentiation and plant development, as the DNA sequences in all cells in a plant are essentially the same. Numerous studies in the past decade have unveiled the importance of several mechanisms in regulating transcription by affecting the structural properties of the chromatin. These mechanisms, including DNA cytosine methylation, covalent modifications of histones, and certain aspects of RNA interference (RNAi), are referred to as "epigenetic" because they direct "the structural adaptation of chromosomal regions so as to register, signal or perpetuate altered activity states" (*1*).

The components and the mechanistic aspects of plant epigenetic pathways as well as their functions in regulating plant development have been the subjects of several excellent recent reviews (*2*–*6*). My goal here is to summarize the results from genome-wide profiling studies of DNA methylation, histone modifications, and the aspects of RNAi that are relevant to chromatin modifications.

To date, most such epigenomic studies have been performed in *Arabidopsis thaliana*, largely as a result of the availability of powerful high-throughput tools (e.g., high-density whole-genome microarrays). The compact genome (~120 Mb) of *Arabidopsis* has been completely sequenced (*7*). Most of the repetitive sequences (~20 Mb; mostly transposons and their relics) cluster in the pericentromeric regions, whereas the majority of the ~27,000 protein-coding genes are distributed on the arms of the five chromosomes (Fig. 1).

DNA Methylation

Three distinct DNA methylation pathways with overlapping functions have been characterized in *Arabidopsis*. The mammalian DNMT1 homolog METHYLTRANSFERASE 1 (MET1) primarily maintains DNA methylation at CG sites (CG methylation) (*8*). The plant-specific CHROMOMETHYLASE3 (CMT3) interacts with the H3 Lys^9 dimethylation (H3K9me2) pathway to maintain DNA methylation at CHG sites (CHG methylation, H = A, C, or T) (*9*, *10*). The DNMT3a/3b homologs DOMAINS REARRANGED METHYLASE 1 and 2 (DRM1/2) maintain DNA methylation at CHH sites (CHH methylation), which requires the active targeting of small interfering RNAs (siRNAs) (*11*, *12*).

The genome-wide pattern of DNA methylation has been the subject of several waves of microarray studies (*13*). Methylated and unmethylated DNA can be distinguished by three major types of experimental approaches: sodium bisulfite treatment that converts cytosine (but not methylcytosine) to uracil, enzymatic digestion (using methylation-specific endonucleases or methylation-sensitive isoschizomers), and affinity purification or immunoprecipitation (with methyl-cytosine binding proteins and antibodies to methyl-cytosine, respectively). The methylated fraction of the genome is then visualized by hybridizing treated DNA to microarrays (*14*–*20*). Results from these microarray studies were largely consistent: About ~20% of the *Arabidopsis* genome is methylated, with transposons and other repeats comprising the largest fraction, whereas the promoters of endogenous genes are rarely methylated. Surprisingly, methylation in the transcribed regions of endogenous genes is unexpectedly rampant. More than one-third of all genes contain methylation (called "body methylation") that is enriched in the 3′ half of the transcribed regions and primarily occurs at CG sites (Fig. 1 and Fig. 2A).

Most recently, Cokus, Feng, and colleagues combined sodium bisulfite treatment of genomic DNA with ultrahigh-throughput sequencing (>20× genome coverage) to generate the first DNA methylation map for any organism at single-base resolution (*21*). Relative to microarray-based methods, this "BS-Seq" method offers several advantages. First, it can detect methylation in important genomic regions that are not covered by any microarray platform (such as telomeres, ribosomal DNA, etc.). Second, it reveals the sequence contexts of DNA methylation (i.e., CG, CHG, and CHH) and therefore provides important information regarding the epigenetic pathways that function at any given locus. For example, all three types of methylation colocalize to transposons, but gene body methylation occurs exclusively at CG sites. Third, BS-Seq is more effective in detecting light methylation and subtle changes (e.g., in mutants). Fourth, the theoretically unlimited sequencing depth makes it possible to quantitatively measure the percentage of cells in which any particular cytosine is methylated, thereby offering important clues regarding potential cell-specific DNA methylation.

DNA methylation is critically important in silencing transposons and regulating plant development. Severe loss of methylation results in a genome-wide massive transcriptional reactivation of transposons (*14*, *17*, *18*), and quadruple mutations in *drm1 drm2 cmt3 met1* cause embryo lethality (*22*). Interestingly, the role of DNA methylation in regulating transcription appears to depend on the position of methylation relative to genes. Methylation in promoters appears to repress transcription (*18*). Paradoxically, however, body-methylated genes are usually transcribed at moderate to high levels and are transcribed less tissue-specifically relative to unmethylated genes (*16*–*18*). Loss of body methylation does not seem to trigger a systematic and drastic overexpression of body-methylated genes to the same extent as transposon reactivation (*14*, *17*, *18*). However, a moderate up-regulation of body-methylated genes was observed, suggesting that body methylation might be involved in fine-tuning transcription levels (*17*). In addition, differential body methylation patterns in different *Arabidopsis* ecotypes are not preferentially correlated with differential gene expression (*16*). Thus, the exact role of body methylation in regulating transcription remains unknown (*2*). However, erasure of body methylation in the *met1* mutant seems to trigger stochastic redistribution of histone modifications (e.g., H3K9me2) and hyper-CHG and CHH methylation within genes, at least some of which result in ectopic gene silencing (*20*, *23*).

The ability to profile DNA methylation in a high-throughput manner also enables studies of DNA methylation from population genetics and evolutionary perspectives. Much like comparative genomics, a "comparative epigenomics" approach should allow the identification of evolutionarily conserved DNA methylation at specific loci with important functions, as well as differences in DNA methylation that contribute to phenotypic variations. The first such study identified numerous differentially methylated sites between two *Arabidopsis* ecotypes that diverged thousands of years ago (*16*). However, these two ecotypes share DNA methylation patterns at the majority of the sites assayed, indicating that DNA methylation could be stably maintained genome-wide for thousands of years.

Histone Modifications

The patterns of covalent histone modification are highly complex because of the large number of residues that can be modified as well as the multiple, combinatorial modifications (e.g., meth-

Department of Plant Biology, University of Georgia, Athens, GA 30602, USA. E-mail: xiaoyu@plantbio.uga.edu

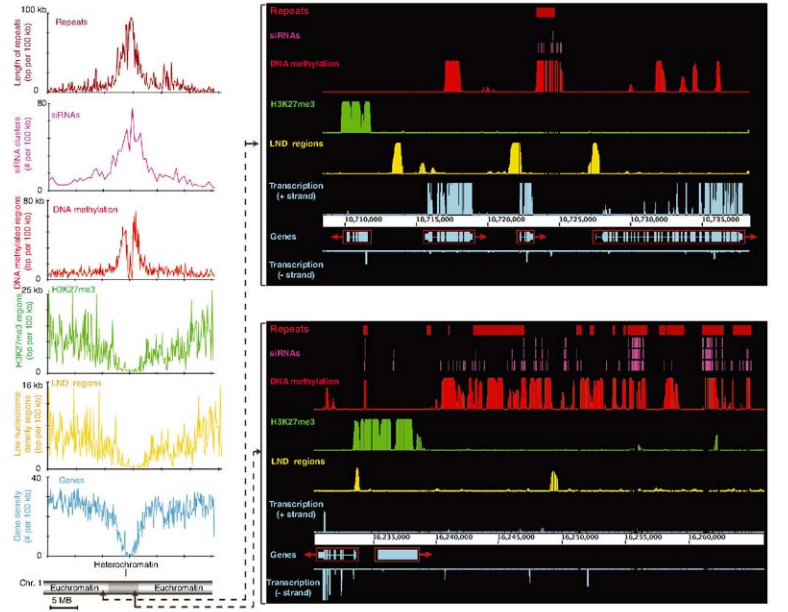

Fig. 1. Distribution of genes, repetitive sequences, DNA methylation, siRNAs, H3K27me3, and low nucleosome density (LND) regions in *Arabidopsis* (*18*, *25*, *31*). The chromosomal distributions are shown on the left, using chromosome 1 as an example. The *x* axis shows chromosomal position. Right panels: detailed distribution patterns and transcription activity (vertical blue bars) in a gene-rich region (top) and a repeat-rich region (bottom). Red boxes indicate genes; arrows indicate the direction of transcription.

ylation, acetylation, phosphorylation, ubiquitination, etc.) (*6*). Some modifications directly alter chromatin structure, whereas others serve as binding platforms to recruit additional effectors.

To date, the genomic distribution patterns of histone H3 methylated at several lysine residues (H3K4me2, H3K9me2/3, and H3K27me3) have been determined in *Arabidopsis* by microarray analysis of samples from chromatin immunoprecipitation (ChIP-chip) (*14*, *24*, *25*). The results are generally consistent with the functions of these modifications inferred from locus-specific studies. H3K4me2 is involved in gene activation and is preferentially localized to endogenous genes but depleted in transposons (*14*). In contrast, H3K9me2 overlaps almost exclusively with transposons and other repeats, consistent with its primary function in transposon silencing (*14*, *24*). A genome-wide profiling of H3K27me3 revealed the presence of this modification at a large number of genes (~4400), most of which are highly tissue-specific and transcriptionally silent in the tissues assayed (young seedling) (Fig. 1 and Fig. 2A) (*24*, *25*). It is possible that H3K27me3-mediated repression may be generally involved in the maintenance of tissue-specific gene expression patterns. The function of H3K9me3 is not yet characterized in plants. Unlike H3K9me2, H3K9me3 appears to be excluded from repetitive sequences and instead localizes to genes, but it does not seem to overlap substantially with either H3K4me2 or H3K27me3 (*24*).

Small RNAs

Four major endogenous RNAi pathways have been described in *Arabidopsis*. The microRNA (miRNA), transacting siRNA (ta-siRNA), and natural-antisense siRNA (nat-siRNA) pathways mainly function at the posttranscriptional level through mRNA degradation and/or translation inhibition (*26*, *27*). In contrast, the siRNA pathway is involved in gene silencing both transcriptionally by directing DNA methylation and posttranscriptionally by guiding mRNA cleavage (*12*).

Millions of 21- to 24-nucleotide (nt) siRNAs have been cloned and sequenced from wild-type *Arabidopsis* plants and siRNA pathway mutants (*28*–*37*). Most of these studies generated not only sequence information necessary to map the siRNAs back to their originating genomic loci, but also the length information of siRNAs that is indicative of the processing enzymes involved (e.g., DICER-LIKE enzymes, DCLs). The majority of the siRNAs (>90%) are produced from double-

stranded RNA (dsRNA) precursors generated by RNA polymerase IV isoform a (Pol IVa) and RNA-dependent RNA polymerase 2 (RDR2). These dsRNA precursors are then processed by DCL3 to 24-nt siRNAs (with partially redundant contributions from DCL2 and DCL4) and become preferentially associated with ARGONAUTE4, which then interacts with Pol IVb to direct DRM1/2-mediated CHH methylation (*28*, *29*, *31*, *36*–*38*). Most of these siRNAs are derived from genomic loci corresponding to transposons with high levels of CHH DNA methylation, and very few are found in protein-coding genes (Fig. 1 and Fig. 2A) (*21*, *29*–*31*).

Independent siRNA profiles generated from the same tissue type (i.e., inflorescence) are remarkably similar (*30*–*37*). In addition, when key components of the siRNA pathway were eliminated and then reintroduced (e.g., Pol IV and RDR2), restoration of a siRNA population with the original composition immediately occurred (*31*, *39*). These observations suggest that the targeting of Pol IVa to its "sites of action" is highly reproducible. On the other hand, important differences exist between the siRNAs that accumulate in seedlings and inflorescence, which suggests that the targeting of Pol IVa may be developmentally regulated (*30*). Specific sequence motif near the boundaries of Pol IVa–transcribed regions (where transcription initiation might occur) has yet to be reported. It is also attractive to speculate that certain epigenetic marks colocalizing with siRNAs might be involved in Pol IVa targeting. However, mutations in other epigenetic pathways that eliminate siRNA production have not been identified.

The majority of the remaining siRNAs (<10%, mostly 21 nt long) are derived from genomic regions corresponding to inverted repeats, independently of Pol IVa and RDR2 (*29*, *31*, *32*, *37*). These siRNAs are most likely processed by DCL1 from single-stranded hairpin RNA precursors generated by Pol II, a process resembling miRNA biogenesis. However, most of these siRNAs are present at relatively low levels, and it is not yet clear whether they target endogenous mRNAs to regulate plant development. Nevertheless, these siRNAs might represent "evolving miRNAs" that could eventually acquire endogenous gene targets (*29*, *31*, *32*, *35*).

Out of *Arabidopsis*?

Most known genes involved in epigenetic pathways are shared between monocots and dicots (many are even present in moss), and loss-of-function mutations in corresponding genes lead to similar molecular defects (*40*). In addition, the chromosomal-level distribution of several histone modifications is similar between maize and *Arabidopsis* (*41*). However, recent data suggest that, unlike in *Arabidopsis*, genic DNA methylation in rice appears to be enriched in the promoter regions of endogenous genes and associated with transcriptional repression (*42*). It is therefore possible that the mechanisms and functions of some epigenetic pathways might have diverged and acquired distinct functions during plant evolution.

The extent to which epigenetic pathways regulate gene expression in a particular species may also be affected by the genetic architecture of its genome. For example, results from *Arabidopsis* suggest that DNA methylation, siRNA, or H3K9me2 primarily regulate genes through nearby repetitive sequences (*14*, *18*, *43*–*46*). The close proximity of repeats to genes, although relatively rare in *Arabidopsis*, may be the norm rather than the exception in larger genomes where genes are commonly embedded in an ocean of repetitive sequences (*47*). This is already apparent in rice, which still has one of the "leanest" genomes in the grasses. As shown in Fig. 2B, relative to *Arabidopsis*, a significantly higher fraction of rice genes are closely associated with repetitive sequences. Consistent with this notion, although the loss of RDR2 (which primarily functions in transposon silencing) does not affect normal development in *Arabidopsis*, mutation of its homolog in maize (*Mediator of Paramutation1*; *MOP1*) leads to a number of development abnormalities (*48*–*50*). Finally, endogenous gene families could be subject to similar epigenetic controls as transposons because of their repetitive nature (*51*, *52*). Such gene families may be present at higher copy numbers in larger plant genomes, particularly in relatively recent polyploids (e.g., *Brassica* or wheat). It therefore might be reasonable to expect that epigenetic silencing pathways play much broader roles in regulating gene expression in plants with larger and more complex genomes.

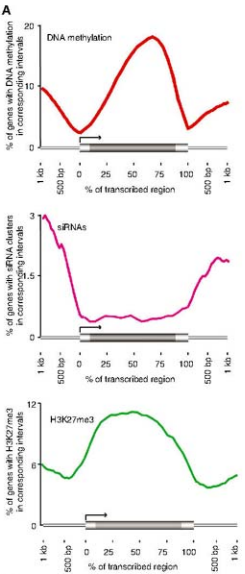

Fig. 2. **(A)** Distribution of DNA methylation, siRNAs, and H3K27me3 relative to *Arabidopsis* genes (*18*, *25*, *31*). One-kilobase regions upstream and downstream of each gene are divided into 50–base pair intervals, each gene is divided into 20 intervals (5% each interval), and the percentage of genes overlapping with each epigenetic mark in the corresponding regions is graphed. Thick and thin horizontal bars represent genes and intergenic regions, respectively. **(B)** Distribution of repetitive sequences relative to genes in *Arabidopsis* (green) and rice (red).

Conclusions

Recent high-throughput profiling studies in *Arabidopsis* have painted a picture of epigenetic compartmentation, where the two major fractions of the genome are associated with and regulated by different epigenetic mechanisms. That is, genes are regulated by pathways such as H3K27me3, H3K4me2, and miRNAs/ta-siRNAs/nat-siRNAs, whereas transposons and other repeats are silenced by DNA methylation, H3K9me2, and siRNAs. Such a functional distinction, however, is blurred when the two genetic fractions overlap, which occurs much more frequently in larger and more complex genomes. The function(s) of DNA methylation that are enriched in different fractions of the gene space in *Arabidopsis* (3′ half of transcribed regions) and rice (promoter regions), as well as DNA methylation by the DEMETER (DME) family of DNA glycosylases (*53*), are not yet understood and warrant further functional studies.

Although increasingly comprehensive, such an epigenomic picture remains static. Relatively little is known about how the plant epigenome changes in response to developmental or envi-

ronmental cues. A particularly interesting question may be how mechanisms that evolved to stably silence transposons could offer the flexibility required for the developmental regulation of endogenous genes. In addition, we do not yet have a clear understanding of the nature and the maintenance of the boundaries separating epigenetically distinct chromatin compartments. In some cases, genetic landmarks (such as the transcription unit) may serve as borders; in other cases, the balancing acts of opposing epigenetic mechanisms may help to stably maintain the epigenetic landscape of plant genomes.

References and Notes.

1. A. Bird, *Nature* **447**, 396 (2007).
2. M. Gehring, S. Henikoff, *Biochim. Biophys. Acta* **1769**, 276 (2007).
3. I. R. Henderson, S. E. Jacobsen, *Nature* **447**, 418 (2007).
4. M. Matzke, T. Kanno, B. Huettel, L. Daxinger, A. J. Matzke, *Curr. Opin. Plant Biol.* **10**, 512 (2007).
5. L. Vaillant, J. Paszkowski, *Curr. Opin. Plant Biol.* **10**, 528 (2007).
6. J. Pflueger, D. Wagner, *Curr. Opin. Plant Biol.* **10**, 645 (2007).
7. Arabidopsis Genome Initiative, *Nature* **408**, 796 (2000).
8. E. J. Finnegan, W. J. Peacock, E. S. Dennis, *Proc. Natl. Acad. Sci. U.S.A.* **93**, 8449 (1996).
9. A. M. Lindroth *et al.*, *Science* **292**, 2077 (2001).
10. L. Bartee, F. Malagnac, J. Bender, *Genes Dev.* **15**, 1753 (2001).
11. X. Cao, S. E. Jacobsen, *Curr. Biol.* **12**, 1138 (2002).
12. S. W. Chan *et al.*, *Science* **303**, 1336 (2004).
13. D. Zilberman, S. Henikoff, *Development* **134**, 3959 (2007).
14. Z. Lippman *et al.*, *Nature* **430**, 471 (2004).
15. R. K. Tran *et al.*, *Curr. Biol.* **15**, 154 (2005).
16. M. W. Vaughn *et al.*, *PLoS Biol.* **5**, e174 (2007).
17. D. Zilberman, M. Gehring, R. K. Tran, T. Ballinger, S. Henikoff, *Nat. Genet.* **39**, 61 (2007).
18. X. Zhang *et al.*, *Cell* **126**, 1189 (2006).
19. J. Reinders *et al.*, *Genome Res.* **18**, 469 (2008).
20. O. Mathieu, J. Reinders, M. Caikovski, C. Smathajitt, J. Paszkowski, *Cell* **130**, 851 (2007).
21. S. J. Cokus *et al.*, *Nature* **452**, 215 (2008).
22. X. Zhang, S. E. Jacobsen, *Cold Spring Harb. Symp. Quant. Biol.* **71**, 439 (2006).
23. S. E. Jacobsen, E. M. Meyerowitz, *Science* **277**, 1100 (1997).
24. F. Turck *et al.*, *PLoS Genet* **3**, e86 (2007).
25. X. Zhang *et al.*, *PLoS Biol.* **5**, e129 (2007).
26. F. Vazquez, *Trends Plant Sci.* **11**, 460 (2006).
27. E. J. Chapman, J. C. Carrington, *Nat. Rev. Genet.* **8**, 884 (2007).
28. Y. Qi *et al.*, *Nature* **443**, 1008 (2006).
29. C. Lu *et al.*, *Genome Res.* **16**, 1276 (2006).
30. C. Lu *et al.*, *Science* **309**, 1567 (2005).
31. X. Zhang, I. R. Henderson, C. Lu, P. J. Green, S. E. Jacobsen, *Proc. Natl. Acad. Sci. U.S.A.* **104**, 4536 (2007).
32. R. Rajagopalan, H. Vaucheret, J. Trejo, D. P. Bartel, *Genes Dev.* **20**, 3407 (2006).
33. M. D. Howell *et al.*, *Plant Cell* **19**, 926 (2007).
34. K. D. Kasschau *et al.*, *PLoS Biol.* **5**, e57 (2007).
35. N. Fahlgren *et al.*, *PLoS ONE* **2**, e219 (2007).
36. I. R. Henderson *et al.*, *Nat. Genet.* **38**, 721 (2006).
37. R. A. Mosher, F. Schwach, D. Studholme, D. C. Baulcombe, *Proc. Natl. Acad. Sci. U.S.A.* **105**, 3145 (2008).
38. M. El-Shami *et al.*, *Genes Dev.* **21**, 2539 (2007).
39. S. W. Chan, X. Zhang, Y. V. Bernatavichute, S. E. Jacobsen, *PLoS Biol.* **4**, e363 (2006).
40. Y. Ding *et al.*, *Plant Cell* **19**, 9 (2007).
41. J. Shi, R. K. Dawe, *Genetics* **173**, 1571 (2006).
42. X. Li *et al.*, *Plant Cell* **20**, 259 (2008).
43. H. Saze, T. Kakutani, *EMBO J.* **26**, 3641 (2007).
44. W. J. Soppe *et al.*, *Mol. Cell* **6**, 791 (2000).
45. R. Martienssen, A. Baron, *Genetics* **136**, 1157 (1994).
46. R. K. Slotkin, R. Martienssen, *Nat. Rev. Genet.* **8**, 272 (2007).
47. K. M. Devos, J. Ma, A. C. Pontaroli, L. H. Pratt, J. L. Bennetzen, *Proc. Natl. Acad. Sci. U.S.A.* **102**, 19243 (2005).
48. J. E. Dorweiler *et al.*, *Plant Cell* **12**, 2101 (2000).
49. M. R. Woodhouse, M. Freeling, D. Lisch, *PLoS Biol.* **4**, e339 (2006).
50. M. Alleman *et al.*, *Nature* **442**, 295 (2006).
51. T. L. Stokes, B. N. Kunkel, E. J. Richards, *Genes Dev.* **16**, 171 (2002).
52. J. Bender, G. R. Fink, *Cell* **83**, 725 (1995).
53. J. Pontvianne *et al.*, *Proc. Natl. Acad. Sci. U.S.A.* **104**, 6752 (2007).

54. I sincerely apologize to authors whose work is not cited here because of space limitations. I thank S. Wessler, K. Dawe, and S. Jacobsen for their critical reading of the manuscript and helpful suggestions, and N. Jiang for sharing unpublished data on rice repeats. Supported by a grant from the University of Georgia.

10.1126/science.1153996

PERSPECTIVE

Extending Genomics to Natural Communities and Ecosystems

Thomas G. Whitham,[1,2] Stephen P. DiFazio,[3] Jennifer A. Schweitzer,[4] Stephen M. Shuster,[1,2] Gery J. Allan,[1,2] Joseph K. Bailey,[4] Scott A. Woolbright[1,2]

An important step in the integration of ecology and genomics is the progression from molecular studies of relatively simple model systems to complex field systems. The recent availability of sequenced genomes from key plants is leading to a new understanding of the molecular drivers of community composition and ecosystem processes. As genome sequences accumulate for species that form intimate associations in nature, a detailed view may emerge as to how these associations cause changes among species at the nucleotide level. This advance could dramatically alter views about the structure and evolution of communities and ecosystems.

The emerging field of community and ecosystem genetics has shown that genetic variation in one species can influence the composition of associated communities (the interacting species that live in a particular area) and the functioning of ecosystems (the biotic community and its abiotic environment) (*1*, *2*). To date, this field has focused mainly on the genetics of foundation plant species—those that structure their ecosystems by creating locally stable conditions and providing specific resources for diverse organisms (*3*). When a foundation species' genotype influences the relative fitness of other species, it constitutes an indirect genetic interaction (*4*), and when these interactions change species composition and abundance among individual tree genotypes, they cause community and ecosystem phenotypes to become statistically distinct from one another (*2*). Figure 1 shows some of the community and ecosystem phenotypes that have been quantified for the foundation tree species, *Populus angustifolia*. These include canopy arthropod communities, soil microbial communities, soil nutrient pools, and interactions between an insect herbivore and its avian predators. Common garden studies show that these phenotypes are all heritable (*4*–*6*) in the broad sense (i.e., additive, dominant, and epistatic genetic effects influence these phenotypes). For example, genes control the susceptibility to the leaf-galling aphid, *Pemphigus betae*, in *P. angustifolia*. The presence or absence of this insect is determined by susceptible or resistant tree genotypes. This interaction predictably affects other trophic levels and alters the composition of a diverse community of fungi, insects, spiders, and avian predators (*2*, *5*). This work suggests that indirect genetic interactions among relatively few species (e.g., a tree, herbivores, mutualists, and/or pathogens) and their environment may structure the composition and abundance of a much larger community of organisms and define ecosystem processes such as nutrient cycling. However, much work needs to be undertaken to understand the genomic components underlying these phenotypes, such as additive genes and epigenetic effects. Here, we examine how a genomics perspective may aid our understanding of communities and ecosystems by focusing on the indirect genetic interactions that arise among a few foundation species rather than attempting to

[1]Department of Biological Sciences, Northern Arizona University, Flagstaff, AZ 86011, USA. [2]Merriam-Powell Center for Environmental Research, Northern Arizona University, Flagstaff, AZ 86011, USA. [3]Department of Biology, West Virginia University, Morgantown, WV 26506–6057, USA. [4]Department of Ecology and Evolutionary Biology, University of Tennessee, Knoxville, TN 37996, USA.

*To whom correspondence should be addressed. E-mail: Thomas.Whitham@nau.edu

understand the interactions among all species in an ecosystem.

Although much progress has been made in obtaining genome sequences for of a few agricultural (e.g., rice) or model plant species (e.g., *Arabidopsis*), extending this knowledge to complex communities and ecosystems in natural systems represents a major frontier. Ecologically important traits with known effects on communities and ecosystems have been mapped in *Populus*, including sex, dormancy, disease resistance, leaf chemistry, and biomass (Fig. 2) (*7*–*10*). Many of these same traits can expand our understanding of community and ecosystem phenotypes among related species in other ecosystems; for example, markers from *Populus trichocarpa* x *P. deltoides* genetic maps (*10*) have been transferred to other *Populus* and *Salix* species (i.e., aspen and willow) (*11*, *12*), thereby bridging genetic resources between these species (Fig. 2). Similar links between *Eucalyptus globulus* and a community of herbivorous arthropods and mammals have been established with the identification of quantitative trait loci (QTLs) involved in plant defensive chemicals (*13*). It is important to note that this line of inquiry is in its infancy, especially as it pertains to interspecific comparisons. However, a focus on the shared and unique aspects driving ecological interactions among many different species with a community genetics perspective justifies genomic investigation of nonmodel foundation species (e.g., *Zostera* and *Solidago* spp.) (*14*, *15*) that support diverse communities but lack the necessary mapping resources or genomics tools.

Community heritability (H^2_C), the tendency of related individuals within a species to support similar communities of organisms and ecosystem processes, provides a bridge linking ecological interactions and genomics (*2*, *4*). For example, regardless of where a replicate clone of an individual tree genotype was planted in a common garden, it accumulated a similar arthropod community that was significantly different from other replicated tree genotypes. Overall, tree genotype accounted for about 60% of the variation in the arthropod community (i.e., $H^2_C = 0.60$) (Fig. 1). Because these analyses confirm a genetic basis for community phenotypes, they link community-level traits with plant genetic maps and genome sequences (Fig. 2), that is, they reveal genomic locations where genes underlying species interactions may reside. For example, foliar arthropod and soil microbial community phenotypes as well as ecosystem phenotypes (e.g., rates of litter decay and soil nitrogen mineralization processes) covary with plant leaf chemistry, especially levels of condensed tannins and phenolic glycosides (*16*–*18*). Given the importance of condensed tannins and lignins in energy flow and nutrient cycling, now that their genes are being identified (*10*), we can extend our understanding of the functional drivers of ecosystem processes in natural forests (*16*, *19*).

A genomics perspective can further add to our understanding of community structure and ecosystem processes by elucidating the specific genes, alleles, and epigenetic mechanisms that underlie community heritability and ecosystem phenotypes (Fig. 1) associated with mapped traits in foundation species (Fig. 2). When interspecific interactions have fitness consequences for one or more species, selection occurs within a community context (*4*). Foundation species imposing selection on other community members are expected to cause genetic differentiation among communities (*20*). This process provides the simplest explanation for significant heritability in community phenotypes (*2*, *4*). It also suggests that when allelic or genomic variation within foundation species with phenotypic effects exhibit population genetic structure, interacting species will also show population level structure to a degree determined by the concordance of their life cycles (*20*). For example, the aphid, *Pemphigus betae*, has evolved two life cycles. In a natural hybrid zone of *Populus angustifolia* x *P. fremontii*, where trees are highly susceptible, aphids alternate between their primary tree hosts and their herbaceous secondary hosts, *Rumex* and *Chenopodium* spp. In contrast, in the adjacent zone of pure *P. angustifolia*, trees are more resistant and aphid survival is lower. In these habitats, aphids live year-round on the roots of their secondary host; this is a simpler life cycle. Reciprocal transfer experiments show that these life cycles are maintained in the field (*21*), which supports the hypothesis that aphids and their tree hosts genetically covary. The theoretical prediction (*20*) that differential population genetic structure arising from these associations should be identifiable by statistical covariance between neutral markers in each species remains to be tested.

Because interspecific interactions and their fitness effects are underlain by the heritable traits of an individual, species within the community undergo continuous evolutionary change (*22*). For example, the mutualism between ectomycorrhizal fungi and trees commonly affects other species, both directly and indirectly. However, little is known about the molecular mechanisms regulating the interactions between the host plant and these fungi. Joint analysis of whole genome sequences and transcriptional profiles of the *Laccaria bicolor* fungus and its *P. trichocarpa* host (*23*) shows that the fungal genome encodes 28 pre-

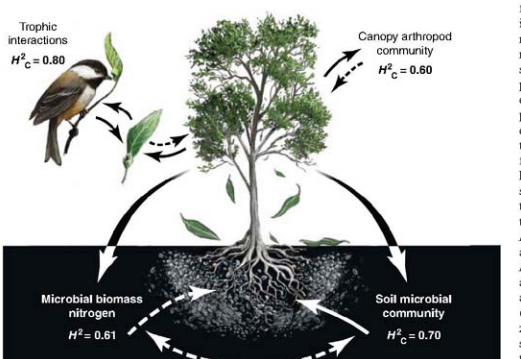

Fig. 1. Community and ecosystem phenotypes of individual tree genotypes of *Populus angustifolia* show broad-sense heritability (H^2). Significant heritability of the canopy arthropod community, soil microbial community, trophic interactions between birds and insects, and soil nutrient pools demonstrate how trait variation in a foundation tree can structure communities and ecosystem processes (H^2_C for community traits; H^2 for single ecosystem trait) (*4*–*6*). Because soil microorganisms mediate many ecosystem processes, including litter decomposition and rates of nutrient mineralization, the formation of these communities may feed back to affect plant fitness. Solid lines indicate known interactions; dashed lines indicate possible interactions. Quantitative genetic patterns such as these argue that genomic approaches will enhance our understanding of how interacting community members influence ecosystem processes.

CREDIT: VICTOR LEMPKE

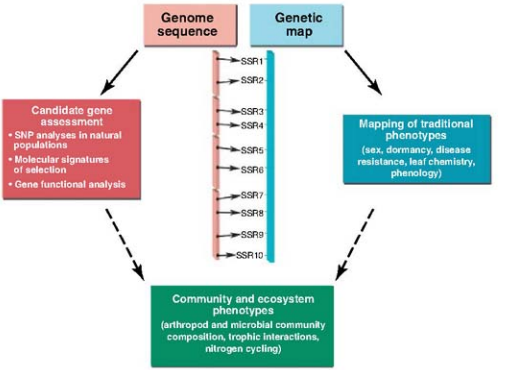

Fig. 2. Traditional phenotypes (i.e., those expressed in the individual or population) can be used as a bridge for uncovering the molecular determinants of community and ecosystem phenotypes. First, genomic regions controlling traditional phenotypes are identified with QTL analysis and/or genetic association studies. Candidate genes from these intervals are identified from the genome sequence and anchored to genetic maps with sequence-tagged markers like simple sequence repeats (SSRs). Second, these candidate genes are assessed for their involvement in traditional phenotypes with high-resolution association mapping in natural populations, searching for signatures of selection such as selective sweeps, enhanced local linkage disequilibrium, and/or rates of synonymous and nonsynonymous polymorphisms. Third, genes with evidence for associations and recent selection are then subjected to functional analysis, including transgenic overexpression and knockouts and transcriptome analysis. Fourth, genes responsible for traditional phenotypes can be linked to community and ecosystem phenotypes through studies in common gardens and natural populations. SNP, single-nucleotide polymorphism.

viously undescribed, small secreted proteins that are highly induced upon establishment of the mycorrhizal mutualism. Similarly, the *P. trichocarpa* genome contains homologs of proteins important in establishing ectomycorrhizal mutualisms in other species (*24*). Identified candidate genes controlling the establishment and maintenance of this relationship allow for detailed studies of genetic covariation among species (*4*, *20*).

A genomics approach to ecosystem processes is especially important because these processes represent the combined effects of interactions among multiple species, environmental variation, and complex feedback mechanisms that can be difficult to partition or understand in an evolutionary context. Understanding the molecular basis (and expression) of plant and subsequent community traits may simplify our understanding of ecological interactions that affect ecosystem processes. In turn, these processes may feed back to have fitness consequences for the individual expressing those traits. For example, the condensed tannins that affect trophic interactions, soil microbial communities, leaf litter decomposition, and soil nitrogen mineralization rates (*6*, *16*) may also feed back to affect the fitness of the host plant itself. The heritability of specific community and ecosystem phenotypes (Fig. 1) suggests that a genomics approach may link the covarying genetic interactions that have resulted in these quantitative patterns.

As the above studies emphasize, quantifying the genetic covariance among species is key to understanding the evolution of communities and ecosystems (*20*). Thus, the information gained by studying multiple interacting genomes will inform larger questions than understanding any one genome alone. With the sequencing of the *Populus trichocarpa* genome (*10*) and with *Eucalyptus* in progress, we are now in a position to understand how genes in these foundation tree species, directly and indirectly, affect the evolution of their associated forest communities and mediate ecosystem processes. Multiple genomes and genomic tools are becoming available for diverse organisms that interact with *Populus*, including the mycorrhizal fungus, *Laccaria bicolor* (*24*), with other mycorrhizal, pathogen, and endophytic bacteria in progress (Table 1). This integrative approach is being used in the study of microbial symbiotic communities in animals. Here, genome sequencing has revealed that these microbial communities undergo evolutionarily convergent reductions in genome size, resulting in obligate associations driven by complementary metabolic pathways (*25*).

Although integrating interactions among foundation species at the genomic level is no small task, it is far less imposing than understanding the interactions of all species in an ecosystem. A focus on genome-based interactions among foundation species provides scientists with a realistic approach for unraveling the ecology and evolution of complex ecosystems. Without such an overview, ecosystems may seem intricate beyond description, except as random or stochastic assemblages of communities. A merger of genomics with community and ecosystem ecology may ultimately provide an understanding of how

Table 1. Links for ongoing and completed genome sequencing projects for *Populus* and other organisms that were specifically selected for sequencing due in part to their ecological associations with *Populus*.

Species	URL for Sequencing Project
Populus trichocarpa	www.ornl.gov/sci/ipgc
Laccaria bicolor	http://mycor.nancy.inra.fr/IMGC/LaccariaGenome/about_laccaria.html
Glomus intraradices	http://repositories.cdlib.org/cgi/viewcontent.cgi?article=3173&context=lbnl
Paxillus involutus	www.jgi.doe.gov/sequencing/why/CSP2008/pinvolutus.html
Melampsora larici-populina	www.jgi.doe.gov/sequencing/why/CSP2006/poplarrust.html
Microbial community in decaying *Populus* biomass	www.jgi.doe.gov/sequencing/lspssseqplans2007.html
Pseudomonas putida w619	http://genome.jgi-psf.org/finished_microbes/psepw/psepw.home.html
Serratia proteamaculans 568	http://genome.jgi-psf.org/finished_microbes/serpr/serpr.home.html
Stenotrophomonas maltophilia R551-3	http://genome.jgi-psf.org/draft_microbes/stema/stema.home.html

complex natural ecosystems are formed and maintained through evolutionary time.

References and Notes

1. J. Antonovics, in *Plant Resistance to Herbivores and Pathogens*, R. S. Fritz, E. L. Simms, Eds. (Univ. of Chicago Press, Chicago, 1992), pp. 426–449.
2. T. G. Whitham *et al.*, *Nat. Rev. Gen.* **7**, 510 (2006).
3. A. M. Ellison *et al.*, *Front. Ecol. Environ.* **3**, 479 (2005).
4. S. M. Shuster, E. V. Lonsdorf, G. M. Wimp, J. K. Bailey, T. G. Whitham, *Evol. Int. J. Org. Evol.* **60**, 991 (2006).
5. J. K. Bailey, S. C. Wooley, R. L. Lindroth, T. G. Whitham, *Ecol. Lett.* **9**, 78 (2006).
6. J. A. Schweitzer *et al.*, *Ecology* **89**, 773 (2008).
7. V. Jorge, A. Dowkiw, P. Faivre-Rampant, C. Bastien, *New Phytol.* **167**, 113 (2005).
8. A. M. Rae, P. J. Tricker, S. M. Bunn, G. Taylor, *New Phytol.* **175**, 59 (2007).
9. T. M. Yin *et al.*, *Genome Res.* **18**, 422 (2008).
10. G. A. Tuskan *et al.*, *Science* **313**, 1596 (2006).
11. S. J. Hamley, M. D. Mallott, A. Karp, *Tree Genet. Genom.* **3**, 35 (2006).
12. S. A. Woolbright *et al.*, *Heredity* **100**, 59 (2008).
13. J. S. Freeman *et al.*, *New Phytol.* 10.1111/j.1469-8137.2008.02417.x (2008).
14. A. R. Hughes, J. J. Stachowicz, *Proc. Natl. Acad. Sci. U.S.A.* **101**, 8998 (2004).
15. G. M. Crutsinger *et al.*, *Science* **313**, 966 (2006).
16. J. A. Schweitzer *et al.*, *Ecol. Lett.* **7**, 127 (2004).
17. B. Rehill *et al.*, *Biol. Syst. Ecol.* **33**, 125 (2005).
18. R. K. Bangert *et al.*, *Heredity* **100**, 121 (2008).
19. S. A. Harding *et al.*, *Tree Physiol.* **25**, 1475 (2005).
20. M. J. Wade, *Nat. Rev. Gen.* **8**, 185 (2007).
21. N. A. Moran, T. G. Whitham, *Evol. Int. J. Org. Evol.* **42**, 717 (1988).
22. J. N. Thompson, *The Geographic Mosaic of Coevolution* (Univ. of Chicago Press, Chicago, 2005).
23. A. Moya, J. Pereto, R. Gil, A. Latorre, *Nat. Rev. Gen.* **9**, 218 (2008).
24. F. Martin *et al.*, *Nature* **452**, 88 (2008).

25. Land for common gardens provided by the Ogden Nature Center; funding provided by NSF DEB-0425908, NSF DEB-0743437, and Reclamation.

10.1126/science.1153918

PERSPECTIVE

From Genotype to Phenotype: Systems Biology Meets Natural Variation

Philip N. Benfey[1,2]* and Thomas Mitchell-Olds[1]

The promise that came with genome sequencing was that we would soon know what genes do, particularly genes involved in human diseases and those of importance to agriculture. We now have the full genomic sequence of human, chimpanzee, mouse, chicken, dog, worm, fly, rice, and cress, as well as those for a wide variety of other species, and yet we still have a lot of trouble figuring out what genes do. Mapping genes to their function is called the "genotype-to-phenotype problem," where phenotype is whatever is changed in the organism when a gene's function is altered.

Substantial progress in identifying gene function has been made. Studying the effects of modifying individual genes in model organisms such as *Drosophila*, *Caenorhabditis*, and *Arabidopsis* has allowed several thousand genes to be associated with phenotypes. Through similarities in the encoded protein sequence, we have also managed to identify the general function of many genes, classifying them as enzymes, receptors, transcription factors, and so forth. Another informative approach has been to compare genes descended from the same ancestor across many different organisms. In bacteria, this comparative genomics approach has been used to map genes shared among organisms that have similar phenotypes, resulting in the assignment of putative function to these genes (*1*). And yet we still do not know the function of a large number of the genes in either plants or animals, and we still cannot predict with any accuracy what the effect will be of modifying the activity of an uncharacterized gene, even when it has been assigned to a functional class. (Indeed, natural selection may act on effects, which are too subtle to be identified by experimental manipulations; hence, it may be impossible to determine the function of some genes.) Equally daunting is starting with a phenotypic variant and trying to predict what genes are likely to be involved. The problem is complicated by the fact that most phenotypes of medical or agricultural interest are "complex," which means that more than one gene, in addition to environmental factors, contributes to expression of the phenotype. Not that single-gene traits are necessarily uninteresting for medicine or agriculture, but these were easier for geneticists to decipher. Now we are left with multigene traits that are harder to work out.

The difficulty in mapping genotype to phenotype can be traced to several causes, including inadequate description of phenotypes, too little data on genotypes, and the underlying complexity of the networks that regulate cellular functions. Recent technical advances for acquiring genome-wide data hold promise for improvements in genotyping and phenotyping. It is particularly exciting to contemplate the application of these advances to the myriad of interesting phenotypes found in nature. This natural variation is generated by additive and epistatic effects of alleles across multiple genes, resulting in many individuals with phenotypes near the population mean, and a minority showing extreme phenotypes. Some combinations result in enhanced traits, whereas other combinations are deleterious to fitness in specific environments. Phenotypic alterations are usually in matters of amount, rather than in the presence or absence of a trait. The field of statistical genetics has developed sophisticated tools to map such quantitative traits to regions of chromosomes. The chromosomal regions are known as quantitative trait loci (QTLs) and are described in terms of the percentage of the variation of a trait that can be attributed to each region.

What has been generally missing is the context in which to place these percentages associated with QTLs. What does it mean, at the cellular or molecular level, that a particular allelic polymorphism has a large or small effect on a trait? This is where the complexity of the underlying cellular networks comes into play. Until recently, most molecular processes occurring within cells were described in terms of linear pathways. A signal received by a cell would be transmitted by a linear series of molecular interactions, ultimately resulting in a response such as a change in gene expression. The field of systems biology is expanding this view, replacing the linear pathways with interconnected networks. These networks frequently look like the "hub-and-spoke" configurations of airline routes. When viewed from the perspective of a network in which there are preferred and alternative routes, the magnitudes associated with quantitative trait loci take on new meaning. Because of the hub-and-spoke organization of the major airline routes, a snowstorm in Chicago can result in disruption of 35% of transcontinental air traffic, whereas a snowstorm in Des Moines might only cause a 2% change.

This analogy illustrates another way in which systems biology is changing the way we think about biological processes. The relative importance of the different cities is a function of the dynamics of transcontinental air traffic, not of the cities' intrinsic size or location. A city that is central for one airline's network is frequently peripheral for another airline's network. Although the dynamics of metabolic networks have been

[1]Department of Biology, Duke University, Durham, NC 27708, USA. [2]Institute for Genome Sciences and Policy–Center for Systems Biology, Duke University, Durham, NC 27708, USA.

*To whom correspondence should be addressed. E-mail: philip.benfey@duke.edu

studied for some time, it is only recently that the dynamics of signaling and transcriptional networks have come under scrutiny. To study the dynamics of a system requires perturbing it and then observing how it reacts to the perturbation. One way of perturbing a biological system is by changing the external stimuli that it perceives. A culture of bacteria can be given a new source of carbon, or a plant can be transferred from dark to light conditions. Alternatively, the genome can be altered and the effects observed. In traditional genetics, a primary goal is to knock out the activity of individual genes and assess the effects on the organism. From a network perspective, the major disadvantage of this approach is that it is often difficult to infer the normal functioning of the system from disruptions that completely remove a gene. Although perturbations with less drastic effects can be identified through traditional genetics (*2*), they are the norm among the alleles that contribute to natural variation. In the past, this has been considered a disadvantage of natural variation: that the genetic variation occurs at multiple loci, each making only a small contribution to the complex trait. However, for understanding the dynamics of a system, these smaller dispersed effects can become a major advantage. Linking genetic changes to small perturbations in the network may allow us to understand how tuning of the network can produce different outcomes (Fig. 1).

It sounds great in theory, but there are issues to be reckoned with before we can bring the insights of systems biology to bear on natural variation and vice versa. In outbred populations such as humans or many wild plants, the variance attributable to each polymorphic locus is influenced by two factors: how frequently the allele appears in the population, and what the allele does to an individual. Also, the genetic loci that contribute variation to a given phenotypic trait may vary from one population to another; hence, quantitative genetic analyses always are specific to a given reference population. Finally, when experiments have limited statistical power to detect QTLs, then the loci that achieve statistical significance will vary from one experiment to another, on a random basis. Ultimately, however, identifying and analyzing the loci that interact to give rise to natural variation will allow us to better understand how networks give rise to phenotypes.

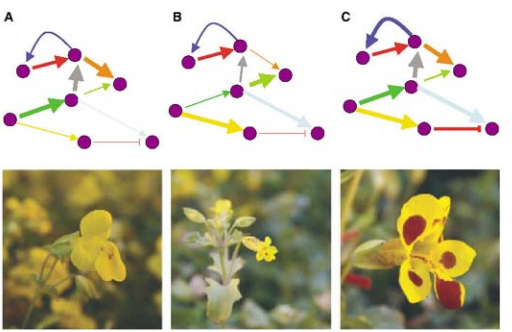

Fig. 1. Ways in which a hypothetical network could control flower form and color among *Mimulus* species. The widespread species *M. guttatus* (**A**) has large, yellow flowers. In contrast, the flowers of *M. laciniatus* (**B**) are typically 75% smaller than those of *M. guttatus*. Other species show elevated expression of red anthocyanin pigments (**C**), as in this hybrid between subspecies of *M. luteus*. Changes at various points in the network (represented by differing widths of the connections [arrows] between network nodes [circles]) could be responsible for this natural variation. [Photos by J. Modliszewski]

Technologies either exist or are visible on the horizon that are likely to make natural variation accessible to systems biology approaches. Methods for sequencing DNA have become much faster and cheaper. A billion bases of DNA (about a third of the human genome) can now be sequenced for under $10,000 and in a matter of days. The goal for human diagnostics is to get to the $1000 genome, and this seems to be attainable within 5 years. For the study of natural variation, inexpensive and rapid DNA sequencing means that we will soon be able to have complete sequence information for all of the genotypes in a population. Hopefully, this does not mean that we will need to sequence every individual in the population; rather, sampling methods will be developed to determine the extent of variation within the population, and then informative genomes can be fully sequenced.

The other major transformation is the use of a host of technologies to improve the precision and breadth of phenotyping. Several studies have shown the value of precise phenotyping in QTL analyses. For example, to identify genes involved in asthma, researchers required highly specific diagnostic guidelines rather than more general ones (*3*). The technologies that are beginning to be applied to natural variation include fine-scale, real-time microscopic and macroscopic imaging (*4*), as well as genome-wide RNA, protein, and metabolite profiling. Together, these technologies are likely to redefine what we call a phenotype. In the past, a phenotype was generally a one-dimensional property: the height of a pea plant, the eye color of a fruit fly, or the glucose level of a human. In the future, phenotype will be a "high-dimensional" entity: the combination of morphological, transcriptional, protein, and metabolic readouts associated with a particular combination of alleles.

How do network models of genotype-phenotype relationships compare with quantitative genetic models of trait variation? Several groups have begun to combine known information on metabolic and regulatory networks with whole-genome expression data, with the goal of predicting organismal phenotypes (*5*–*7*). These mathematical models quantify a causal relationship from genes to gene products to phenotypes, and they can model causal influences of genes that are either monomorphic or polymorphic. In contrast, traditional quantitative genetic models deal only with segregating genetic variation, and thus causal effects of monomorphic loci are invisible to quantitative genetic analysis. There is great potential for a synthesis of network and quantitative genetic modeling to include network topologies and whole-genome expression data.

Can information from genetic networks predict which genes contribute to complex trait variation? Although available information on the genes that underlie QTLs is limited, several studies have examined a related question: the factors that influence rates of protein evolution among species. The best single predictor of the rate of amino acid change in proteins is the level of protein expression (*8*), with highly expressed genes evolving more slowly. Several studies find that genes on the network periphery are more likely to contribute to disease or show patterns of rapid or adaptive evolution (*9*–*13*), suggesting that peripheral proteins may be more likely to influence complex trait variation. However, not all studies support this conclusion (*14*), and there is substantial variation around this trend.

Now we can return to the hub-and-spoke analogy of natural variation in networks. Natural

Fig. 2. Systems biology approaches can be applied to natural variation in wild relatives of *Arabidopsis*, such as this *Boechera* population on the continental divide in Montana (USA).

knockouts of hub proteins often will be lethal, whereas small changes in the function of hub proteins may have pleiotropic effects on multiple traits. For our airline analogy, intermittent thunderstorms in Chicago have a different effect on air traffic than that of a snowstorm that shuts down the airport entirely. Similarly, weakly deleterious alleles may segregate at low frequency in populations and contribute to disease and inbreeding depression (*15*). In contrast, genetic networks may tolerate substantial mutations in peripheral proteins, so natural allelic series at these genes may span a broad range: from small to large effects on phenotypes. Advances in phenotyping technology will increasingly enable saturating QTL screens to identify the natural allelic series that influence network function and that modulate the normal range of network functions we seek to understand in human health and agricultural production.

Analyses of natural variation have great potential to dissect the genetic networks controlling important biological processes. QTL approaches begin with functional polymorphisms influencing complex traits, which can be identified and manipulated via high-throughput techniques. Because these QTLs segregate within extant populations, many of them may be ecologically advantageous in nature. Breeders of both plants and animals long ago discovered that crossing individuals with advantageous traits sometimes results in far greater improvement than predicted (hybrid vigor) but frequently produces the opposite effect: offspring that are not as fit as either parent. This latter outcome has been attributed to epistasis, which traditionally has been interpreted as the effect of genes in a pathway in which the modification of one gene overrides any effect of the modification of a second gene. It is now clear that epistatic interactions among loci play a central role in complex trait variation (*16*, *17*) and indeed can arise from a broad range of network architectures, with or without feedback mechanisms (*18*). As with induced mutations, epistatic interactions involving natural variants may illuminate the function of biological networks (*19*). However, one disadvantage of using natural genetic variation is that we are limited to variants that are polymorphic in the studied populations. As high-throughput technologies advance, future saturating QTL studies of natural populations may be able to reveal most of the ways that network function can be modified.

Although much of the focus on natural variation has been on human diseases, model plant systems are likely to play an important role in the future synthesis of systems biology and quantitative genetics (Fig. 2). Unlike humans and most other mammals, many plants are experimentally tractable and allow easy control and quantification of environmental influences. Plants are amenable to quantitative phenotyping and to dissection of complex phenotypes into their physiological components, which tend to be more robust to experimental manipulations because their physiologies can tolerate more variation than animals. Available natural variation can be augmented by direct crosses, recombinant inbred lines, association panels, and completely sequenced genotypes, which provide a genome-wide catalog of polymorphic alleles.

Between the methods of systems biology and the resources inherent in natural variation, we expect to see insights into the networks that control biological processes such as growth and development. Out of this should come major progress in mapping genotypes to phenotypes. However, much remains to be done. Current methods rarely provide genome-wide analyses at the level of individual cell types or tissues, thus diluting or even losing critical information. This is particularly true when developmentally sensitive phenotypes are analyzed with whole-genome methods such as microarrays. Genes that are expressed highly in a few cell types are not detected when an entire organ or organism is the starting point for these analyses. Nevertheless, the integration of systems biology with quantitative genetic studies of natural variation may fulfill at least part of the promise of genomics to let us know what genes do.

References and Notes

1. N. Slonim, O. Elemento, S. Tavazoie, *Mol. Syst. Biol.* **2**, 10.1038/msb4100047 (2006).
2. A. Friedman, N. Perrimon, *Cell* **128**, 225 (2007).
3. P. Van Eerdewegh *et al.*, *Nature* **418**, 426 (2002).
4. S. G. Megason, S. E. Fraser, *Cell* **130**, 784 (2007).
5. S. M. Welch, Z. S. Dong, J. L. Roe, S. Das, *Aust. J. Agric. Res.* **56**, 919 (2005).
6. H. Jonsson *et al.*, *Bioinformatics* **21**, 1232 (2005).
7. S. K. Sieberts, E. E. Schadt, *Mamm. Genome* **18**, 389 (2007).
8. D. A. Drummond, J. D. Bloom, C. Adami, C. O. Wilke, F. H. Arnold, *Proc. Natl. Acad. Sci. U.S.A.* **102**, 14338 (2005).
9. D. Vitkup, P. Kharchenko, A. Wagner, *Genome Biol.* **7**, R39 (2006).
10. P. M. Kim, L. J. Lu, Y. Xia, M. B. Gerstein, *Science* **314**, 1938 (2006).
11. T. Makino, T. Gojobori, *Mol. Biol. Evol.* **23**, 784 (2006).
12. P. M. Kim, J. O. Korbel, M. B. Gerstein, *Proc. Natl. Acad. Sci. U.S.A.* **104**, 20274 (2007).
13. K.-I. Goh *et al.*, *Proc. Natl. Acad. Sci. U.S.A.* **104**, 8685 (2007).
14. N. N. Batada, L. D. Hurst, M. Tyers, *PLoS Comput. Biol.* **2**, e88 (2006).
15. T. Mitchell-Olds, J. H. Willis, D. B. Goldstein, *Nat. Rev. Genet.* **8**, 845 (2007).
16. J. Kroymann, T. Mitchell-Olds, *Nature* **435**, 95 (2005).
17. B. Kusterer *et al.*, *Genetics* **177**, 1839 (2007).
18. A. B. Gjuvsland, B. J. Hayes, S. W. Omholt, Ø. Carlborg, *Genetics* **175**, 411 (2007).
19. I. Dworkin, A. Palsson, K. Birdsall, G. Gibson, *Curr. Biol.* **13**, 1888 (2003).

20. We thank A. Hartemink, G. Wray, M. Noor, P. Magwene, J. Willis, and members of the Benfey and Mitchell-Olds labs for thoughtful comments on the manuscript, as well as J. Modliszewski and J. Willis for the images of *Mimulus* flowers. Work in the Mitchell-Olds lab on natural variation is funded by a grant from the NSF. Work in the Benfey lab on systems biology is funded by grants from NIH, NSF, and the Defense Advanced Research Projects Agency.

10.1126/science.1153716

Molecular Phylogenetics of Mastodon and *Tyrannosaurus rex*

Chris L. Organ,[1,2] Mary H. Schweitzer,[3,4] Wenxia Zheng,[3] Lisa M. Freimark,[5] Lewis C. Cantley,[5,6] John M. Asara[5,6]*

Protein sequences from bone-derived collagen as old as 68 million years have been detected by using mass spectrometry (*1*, *2*). A BLAST search of the resulting peptide sequences found the highest similarities between the collagen peptides obtained from extracts of *Tyrannosaurus rex* fossil bone and those of birds (*Gallus gallus*) and between mastodon (*Mammut americanum*) and other mammals, including elephant (*Loxodonta africana*). We performed phylogenetic analyses to infer the evolutionary relationships of the *T. rex* [Museum of the Rockies (MOR) 1125] and mastodon (MOR 605). The results extend our knowledge of trait evolution within nonavian dinosaurs into the macromolecular level of biological organization.

We used 21 extant organisms in the analyses. Collagen α1(I) and α2(I) protein sequences from 19 extant organisms (*3*) were obtained from the National Center for Biotechnology Information (NCBI) and ENSEMBL databases. Collagen α1(I) and α2(I) peptide sequences from a metacarpal of *Alligator mississippiensis* were obtained by microcapillary liquid chromatography tandem mass spectrometry (LC/MS/MS) with an ion trap mass spectrometer using the Sequest algorithm (*1*, *2*) and the Paragon algorithm (*4*). Ostrich collagen sequences were determined elsewhere (*1*, *2*). Sequences from alligator (Crocodilia) and ostrich (Aves) represent 63% and 43% of the full-length collagen α1(I) protein available for other organisms, respectively. The collagen α1(I) and α2(I) sequences for elephant (*L. africana*), tenrec (*Echinops telfairi*), and green anole (*Anolis carolinensis*) were obtained by using gene translations from online databases (*5*).

Bayesian, likelihood, parsimony, and distance methods were used to generate evolutionary trees (*6*). In the Bayesian analysis, the posterior distribution of trees reconstructed all extant groups in generally agreed-upon relationships (the posterior probability of clades ranged from 0.80 to 1.00), with the exception of green anole (*A. carolinensis*), which is inferred here to lie at the base of amniotes instead of grouping as the sister taxon to alligator and birds (archosaurs) (Fig. 1). LC/MS/MS from tryptic digests produces fragmentary protein sequence data; however, we found unequivocal support (posterior probability of 1.00) uniting mastodon with elephant as members of Elephantinae, which together group with tenrec (*E. telfairi*) as members of the mammalian group Afrotheria (*7*). Maximum likelihood produces the same groupings, although with less support (approximate likelihood ratio test; aLRT = 0.855 for Elephantinae and 0.872 for Afrotheria). Maximum parsimony analysis also groups mastodon, elephant, and tenrec together (fig. S1, B to D). For the *T. rex* sample, we used five peptide sequences from collagen α1(I) and one from collagen α2(I) (*1*, *2*, *8*) for a total of 89 amino acids (Fig. 1). The *T. rex* clusters within the Archosauria (posterior probability of 0.92), more closely related to birds (chicken and ostrich, 0.9) than alligator, although a lack of informative sites in the ostrich and *T. rex* leaves Dinosauria unresolved. The likelihood tree is identical to the Bayesian tree, except for higher support at these locations in the tree (aLRT = 0.969 for Archosauria and 0.907 for Dinosauria). Branch lengths (expected rates of change per site) indicate a relatively stable and uniform rate of evolution, lacking evidence for a deviation from a molecular clock. Maximum parsimony analysis also groups the *T. rex* with the chicken and ostrich, although bootstrap support is low (fig. S1, B to D). Neighbor joining groups the *T. rex* with the birds, but miscalculates the branching order and misplaces alligator, mastodon, and several extant organisms (fig. S1, B to D).

The slight disagreement between the distance results compared with the Bayesian, likelihood, and parsimony results (all three of which are concordant) are predictable given that distance methods perform poorly for taxa with large amounts of missing data (*9*). Nevertheless, there is congruence between three out of the four methods for the mastodon and four out of four methods for the *T. rex* despite the problem of missing sequence data. The recovered sequences contain informative phylogenetic signal consistent with predictions based on genetic and morphological data for mastodon (*10*, *11*) and on morphological data for *T. rex* (*12*, *13*).

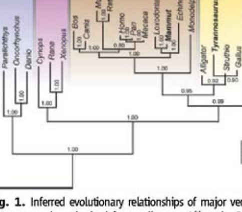

Fig. 1. Inferred evolutionary relationships of major vertebrate groups hypothesized from collagen α1(I) and α2 (I) protein data by using a Bayesian approach. The node (bifurcation) labels are measures of support, which indicate the proportion of trees in the posterior distribution to containing the node. Branch lengths are in expected changes per site.

These results support the endogenous origin of the preserved collagen molecules and confirm the prediction based on morphology that, if biomolecules could be retrieved from a nonavian dinosaur, they would share a higher degree of similarity with birds than with other extant vertebrates. Our findings suggest that molecular data from long-extinct organisms may have the potential for resolving relationships at critical areas of the vertebrate evolutionary tree that have, so far, been intractable. The findings presented here also bolster the use of morphology in phylogenetics because our results are consistent with studies on the evolutionary relationships of fossil forms that rely on morphology (*12*, *13*).

References and Notes

1. J. M. Asara, M. H. Schweitzer, L. M. Freimark, M. Phillips, L. C. Cantley, *Science* **316**, 280 (2007).
2. J. M. Asara *et al.*, *Science* **317**, 1324 (2007).
3. Collagen α1(I) and α2(I) protein sequences were obtained by querying the nonredundant all-taxa protein database from the NCBI and through genome alignments at ENSEMBL (www.ensembl.org).
4. I. V. Shilov *et al.*, *Mol. Cell. Proteomics* **6**, 1638 (2007).
5. The peptide sequence translations for were obtained from ENSEMBL. See (*6*) for accession numbers.
6. Materials and methods are available on *Science* Online.
7. M. S. Springer, W. J. Murphy, E. Eizirik, S. J. O'Brien, *Proc. Natl. Acad. Sci. U.S.A.* **100**, 1056 (2003).
8. J. M. Asara, M. H. Schweitzer, *Science* **319**, 33 (2008).
9. J. J. Wiens, *Syst. Biol.* **52**, 528 (2003).
10. N. Rohland *et al.*, *PLoS Biol.* **5**, 1663 (2007).
11. M. G. Thomas *et al.*, *Proc. R. Soc. London Ser. B* **267**, 2493 (2000).
12. M. J. Benton, in *The Dinosauria*, D. B. Weishampel, P. Dodson, H. Osmólska, Eds. (Univ. of California Press, Berkeley, 2004), pp. 7–19.
13. T. R. Holtz, H. Osmólska, in *The Dinosauria*, D. B. Weishampel, P. Dodson, H. Osmólska, Eds. (Univ. of California Press, Berkeley, 2004), pp. 21–24.
14. M. S. Springer *et al.*, *Syst. Biol.* **56**, 673 (2007).

15. We thank S.V. Edwards, C. Marshall, C. Balakrishnan, M. Baldwin, P. Brito, N. Hobbs, M. Phillips, S. Nagpal, S. Seymour, G. Poulogiannis, B. Zheng, M. Vander Heiden, J. Horner, N. Myhrvold, and C. Hill for assistance. This research was supported by an NIH National Service Research Award Postdoctoral Fellowship granted to C.L.O., the NSF (awards EAR-0634136 and EAR-0541744), the Paul F. Glenn Foundation, and the David and Lucile Packard Foundation.

Supporting Online Material

www.sciencemag.org/cgi/content/full/320/5875/499/DC1
Materials and Methods
SOM Text
Figs. S1 and S2
References and Notes
Appendices 1 and 2

17 December 2007; accepted 25 February 2008
10.1126/science.1154284

[1]Harvard University, Cambridge, MA 02138, USA. [2]Museum of Comparative Zoology, Cambridge, MA 02138, USA. [3]North Carolina State University, Raleigh, NC 27695, USA. [4]North Carolina Museum of Natural Sciences, Raleigh, NC 27601, USA. [5]Beth Israel Deaconess Medical Center, Boston, MA 02115, USA. [6]Harvard Medical School, Boston, MA 02115, USA.

*To whom correspondence should be addressed. E-mail: jasara@bidmc.harvard.edu

Synchronizing Rock Clocks of Earth History

K. F. Kuiper,[1,2] A. Deino,[3] F. J. Hilgen,[1] W. Krijgsman,[1] P. R. Renne,[3,4] J. R. Wijbrans[2]

Calibration of the geological time scale is achieved by independent radioisotopic and astronomical dating, but these techniques yield discrepancies of ~1.0% or more, limiting our ability to reconstruct Earth history. To overcome this fundamental setback, we compared astronomical and $^{40}Ar/^{39}Ar$ ages of tephras in marine deposits in Morocco to calibrate the age of Fish Canyon sanidine, the most widely used standard in $^{40}Ar/^{39}Ar$ geochronology. This calibration results in a more precise older age of 28.201 ± 0.046 million years ago (Ma) and reduces the $^{40}Ar/^{39}Ar$ method's absolute uncertainty from ~2.5 to 0.25%. In addition, this calibration provides tight constraints for the astronomical tuning of pre-Neogene successions, resulting in a mutually consistent age of ~65.95 Ma for the Cretaceous/Tertiary boundary.

Accurate and precise measurement of geological time is a prerequisite for understanding Earth's history. Numerical calibration of the geological time scale (GTS) [for example, GTS2004 (*1*)] is currently based on two independent techniques: astronomical tuning of cyclic sedimentary sequences, which provides a very accurate and high-resolution age model for the youngest Neogene part of the time scale, and radioisotopic dating for older time intervals. However, the various techniques often yield statistically different ages when applied to the same stratigraphic horizons (*2*, *3*).

The radioisotopic dating technique most widely applicable to the late Cenozoic is the $^{40}Ar/^{39}Ar$ method. With careful attention to experimental design, it is possible to achieve analytical precision of 0.2% or better; however, the absolute accuracy of the technique is limited to ~2.5% (*4*, *5*), mainly because of uncertainties in the ages of standards and radioactive decay rates (*6*).

Several attempts have been made to improve the technique's accuracy by calibrating the $^{40}Ar/^{39}Ar$ dating method to the astronomical method. However, these attempts were limited by uncertainties in identifying the location of magnetostratigraphic boundaries and their correlation to the astronomical polarity time scale (*7*), assumptions regarding constancy of sedimentation rates (*7*), complications associated with the use of geochronometers such as biotite (recoil, open-system alteration) and plagioclase (excess argon) (*8*), problems associated with multigrain sanidine experiments (masking complexities in age distributions) (*3*), or uncertainties in astronomical time control (*3*, *9*).

We avoid these drawbacks by applying the single-crystal $^{40}Ar/^{39}Ar$ dating method to sanidine phenocrysts extracted from numerous silicic tephra layers intercalated in an astronomically tuned open marine succession from the Messinian Melilla Basin in Morocco. This basinal succession grades laterally into a marginal carbonate complex; the coarse-grained tephra are derived from the nearby Gourougou volcanic complex (*10*, *11*). The astronomical tuning of the basinal precession–related marl-diatomite cycles is accomplished indirectly, because the sedimentary cycles lack the expression of characteristic details related to precession amplitude and precession-obliquity interference that are common in Mediterranean sapropel sequences (*12*). Selected planktonic foraminiferal bioevents known to be synchronous throughout the Mediterranean have been identified in the Melilla sections and are correlated to well-tuned Mediterranean reference sections (Fig. 1) (*11*) that form the core of the standard Neogene time scale (*12*, *13*). The number of sedimentary cycles at Melilla between these biostratigraphic markers is consistent with the number found in these reference sections (*11*, *12*). This indirect approach allows astronomical dating of each tephra layer (Fig. 1).

Uncertainties in the astronomical ages of the radioisotopically dated tephra horizons are contingent on (i) the applied astronomical solutions, including values for tidal dissipation and dynamical ellipticity; (ii) errors in interpolation resulting from the assumption of a constant sedimentation rate between two astronomically tuned calibration points [in this case, cycles are precession tuned and errors are therefore much less than 21 thousand years (ky)]; and (iii) the lag between the orbital forcing and sedimentary expression (we assume that the lag is zero). No exact error can be calculated, but taking these uncertainties into account and provided that the tuning and correlation itself is correct, we estimate that the uncertainty in the astronomical ages for the volcanic ash layers is ±10 ky.

[1]Faculty of Geosciences, Department of Earth Sciences, Utrecht University, Budapestlaan 4, 3584 CD Utrecht, Netherlands. [2]Faculty of Earth and Life Sciences, Institute of Earth Sciences, Vrije Universiteit Amsterdam, De Boelelaan 1085, 1081 HV Amsterdam, Netherlands. [3]Berkeley Geochronology Center, 2455 Ridge Road, Berkeley, CA 94709, USA. [4]Department of Earth and Planetary Science, University of California, Berkeley, CA 94720, USA.

Table 1. Recalculated ages of K-T boundary and early Paleocene geomagnetic polarity-reversal boundaries, in Ma. The $^{40}Ar/^{39}Ar$ ages of (*36*–*38*) are recalculated relative to the astronomically calibrated age of FCs (28.201 ± 0.046 Ma). An age of 28.02 Ma for FCs (*4*) is adopted in GTS2004. Reversal ages in GTS2004 are based on age calibration by spline fit of selected calibration points, including the K-T boundary with an age of 65.5 Ma. Recalculated radioisotopic ages are given with full error estimate. Details on the revised astronomical tuning are given in Fig. 4. The astronomical ages for the reversal boundaries and K-T boundary are calculated by counting the number of precession cycles from the nearest 100-ky eccentricity maximum/minimum. The age is then calculated by adding or subtracting this number multiplied with the 21-ky precession period to or from the age of the nearest eccentricity maximum or minimum. The astronomical error includes, under the assumption of a correct correlation to the 100-ky eccentricity maximum or minimum, the uncertainty in the 405-ky eccentricity cycle in astronomical solution (±40 ky) (figure 25 in (*35*)) and an additional error of ±15 ky for the uncertainty in the exact position of reversal boundaries. Chron, time interval between polarity reversals of Earth's magnetic field.

Chron / Boundary	GTS2004 (*1*)	Westerhold *et al.* (*39*) Option 1	Westerhold *et al.* (*39*) Option 2	Dinarès-Turell *et al.* (*33*)	Swisher *et al.* (*36*, *37*)	Izett *et al.* (*38*)	Revised tuning (this study)‖
Reversal C28n (o)	64.128	64.028 ± 0.013	64.385 ± 0.013	64.460	64.6		64.698 ± 0.055 (64.663)
Reversal C29n (y)	64.432	64.205 ± 0.014	64.572 ± 0.016	64.670	64.9		64.884 ± 0.055 (64.835)
C29n (o)	65.118	64.912 ± 0.015	65.282 ± 0.016	65.549	65.4		65.724 ± 0.055 (65.702)
K-T	65.50 ± 0.30	65.280 ± 0.010	65.680 ± 0.010	65.777	65.81 ± 0.14* 65.84 ± 0.12† 65.99 ± 0.12‡ 65.84 ± 0.16§	65.98 ± 0.10§	65.957 ± 0.040 (65.940)

*Melt rock of Chicxulub crater. †Sanidine of Z coal. ‡Sanidine of IrZ coal. §Haitian tektites. ‖Bracketed ages tuned to Va03_R7 (*44*).

The $^{40}Ar/^{39}Ar$ dating of the Melilla tephra was performed in parallel at the Berkeley Geochronology Center (BGC) and the Vrije Universiteit Amsterdam (VU) (*14*). In general, $^{40}Ar/^{39}Ar$ ages measured in both laboratories are equivalent within 2σ analytical error (table S1), thus confirming a lack of significant interlaboratory bias at this level of confidence. These results can be converted to an astronomically calibrated age for Fish Canyon sanidine (FCs) by treating the Melilla sanidines as astronomically dated standards and FCs as the unknown (Fig. 2). After incorporating all known sources of error [analytical errors, uncertainty in the astronomical age, and a decay constant of $5.543 \pm 0.020) \times 10^{-10}$ $year^{-1}$ (*15*)], the intercomparison yielded an age of 28.198 ± 0.044 million years ago (Ma). This approach involves the ^{40}K total decay constant, but is insensitive to the value used or its uncertainty. A compilation of the underlying activity data and data updated with new values for other constants led Min *et al.* (*5*) to determine a value of $(5.463 \pm 0.214) \times 10^{-10}$ $year^{-1}$ and showed the conventionally accepted error to be overly optimistic by an order of magnitude. Nonetheless, from this substantially less accurate (but more realistic) value we calculate an indistinguishable age (with negligibly increased uncertainty) of 28.201 ± 0.046 Ma for FCs. We propose that this result should be the age and uncertainty for FCs, rather than the widely used age of 28.02 ± 0.56 Ma (*4*). Our age is 0.65% older than the previous one, although given the larger uncertainty of the earlier value the two ages are statistically indistinguishable.

Comparison of our result with the U/Pb zircon age for the Fish Canyon Tuff is meaningless because of its complex crystallization history, lengthy residence time of zircon, and/or age bias due to Pb loss [for example, see (*16*–*18*)]. Comparison of conventional $^{40}Ar/^{39}Ar$ and U/Pb ages for diverse rock types over more than 3 billion years of geological time demonstrates a systematic offset, in which the U/Pb ages are older by 0 to 1% than the $^{40}Ar/^{39}Ar$ ages for the same rocks (*19*), although scatter in the offset suggests that some of the differences may result from interlaboratory biases or geological complexities. Mundil *et al.* (*20*) presented U/Pb (zircon) and $^{40}Ar/^{39}Ar$ ages for a suite of volcanic rocks between 130 Ma and 2.1 Ga; these results are likely free of detectable bias due to geological complexities (for example, magma residence time of the zircons, differential closure temperatures, or excess ^{40}Ar) or interlaboratory

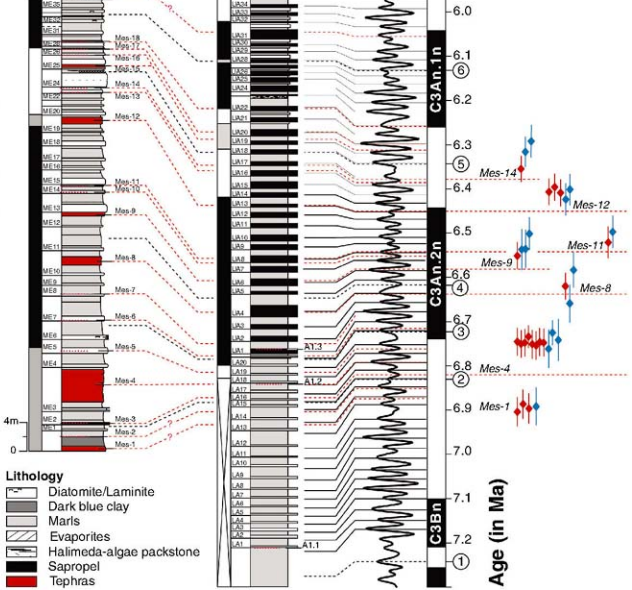

Fig. 1. Astronomical calibration of Messinian Messâdit section in the Melilla-Nador Basin and $^{40}Ar/^{39}Ar$ ages of intercalated tephra. The cycles are tuned to the $La2004_{(1,1)}$ solution (*35*). The main biostratigraphic marker events registered within the studied sections and used for high-resolution correlations are (1) *Globorotalia miotumida* group first regular occurrence (FRO), (2) *G. nicolae* first common occurrence (FCO), (3) *G. nicolae* last occurrence (LO), (4) *G. obesa* FCO, (5) *Neogloboquadrina acostaensis* sinistral/dextral coiling change, and (6) *N. acostaensis* first sinistral influx (*11*, *12*, *43*). The phase relation of the sedimentary cycles to orbital parameters is determined using the exact position of bioevents and characteristic planktonic foraminiferal faunal changes associated with the sedimentary cyclicity in the pre-evaporite Messinian Sorbas basin (*43*). Homogeneous marls in the Moroccan sections correspond to sapropels in Sorbas and other Mediterranean sections (*11*). Astronomical ages for the tephras are derived by linear interpolation between two astronomically tuned points (that is, three-quarters of the height from the base of the homogeneous interval in each cycle is correlated to the insolation maximum). Weighted mean $^{40}Ar/^{39}Ar$ ages of tephra intercalated in the Messâdit section and analyzed in BGC and VU are shown, calculated relative to an age of 28.02 Ma for FCs (*4*) (table S1). The 2σ error bars include only analytical uncertainties of samples and standards.

errors, and yielded an age of 28.28 ± 0.06 Ma for FCs (*21*). Thus, our astronomically tuned FCs age of 28.201 Ma is consistent at the 95% confidence level with normalization of the $^{40}Ar/^{39}Ar$ to the U/Pb system.

Further confirmation of consistency between the $^{40}Ar/^{39}Ar$ and U/Pb systems based on the proposed revised $^{40}Ar/^{39}Ar$ age of FCs comes from comparison of U/Pb and $^{40}Ar/^{39}Ar$ ages of chondritic meteorites, such as Acapulco (*22*) and Allende. A ~0.8 to 1% bias between the most accurate $^{40}Ar/^{39}Ar$ (*23*, *24*) and U/Pb (*25*, *26*) ages has classically been interpreted as evidence for slow cooling after partial melting at 4555.1 ± 1.3 Ma (Acapulco) and formation at 4566.6 ± 1.7 Ma (Allende), as determined by U/Pb dating. With the revised age for the FCs, the K/Ar and U/Pb systems approach concordancy and instead suggest that the parent body of these meteorites cooled rapidly after formation, as suggested by (U+Th)/He (*27*) and I/Xe (*28*, *29*) studies.

The astronomically calibrated FCs age thus eliminates the documented offset of the conventionally calibrated $^{40}Ar/^{39}Ar$ and U/Pb dating systems in many volcanic rocks. It also has implications for ages of geomagnetic polarity reversals over the past 3 million years (My). Numerous studies in the past two decades have demonstrated apparent consistency between the $^{40}Ar/^{39}Ar$ method and the astronomical dating approach in both sedimentary and volcanic settings, starting from a younger age for FCs or other standards (table S3). This implies that the new FCs age is not consistent with many of these results. For example, recalculating some $^{40}Ar/^{39}Ar$ dates for the Matuyama-Bruhnes reversal relative to our age for FCs yields radioisotopic ages older than the astronomical age [table S3 and references in (*14*)]. However, the most recent and comprehensive $^{40}Ar/^{39}Ar$ data (*30*), which suggested that the transition may have been diachronous, are in agreement with our intercalibration.

An important application of the astronomically calibrated $^{40}Ar/^{39}Ar$ method is to provide constraints for the astronomical tuning of pre-Neogene sequences. The prime, first-order target for tuning these older sequences is the 405-ky earth-orbital eccentricity cycle (*31*, *32*). Our method reduces the absolute uncertainty from ~2.5% (or ~1600 ky at 65 Ma) to potentially <0.25% (or <165 ky at 65 Ma), because the uncertainties in absolute amounts of radiogenic ^{40}Ar and ^{40}K in the primary standard and the branching ratio of the ^{40}K decay constant are circumvented using the astronomical age of the Melilla sanidines as the basis for calculating the $^{40}Ar/^{39}Ar$ age. The use of equation 5 of (*4*) enables calculation of the age of an unknown based on an age for the standard determined by means other than the K-Ar system, and requires only knowledge of the total ^{40}K decay constant (that is, not the branching ratio). [Full equations are provided in (*14*)].

We demonstrate the improved age resolution by examining the GTS2004 age of 65.5 Ma for the Cretaceous/Tertiary (K-T) boundary, which marks one of the most important biotic crises in Earth history. The K-T boundary section at Zumaia, Spain, which magnetostratigraphically covers the interval from the younger part of polarity interval C29r well into C26r, has been astronomically tuned and the boundary has been assigned an age of 65.777 Ma (*33*). The astronomical age of (*33*) is uncertain for two reasons: (i) the use of the potentially unstable very-long-period 2.4-My eccentricity cycle as the starting point for the tuning; and (ii) the matching of basic marl/limestone cycle packages [the E-cycles of (*33*)] to successive 100-ky eccentricity minima in the target curve, which is less certain (and stable) than the 405-ky eccentricity minima (fig. S2).

According to (*33*), the 405-ky cycle is not expressed, or only very weakly present at Zumaia. Nevertheless, this cycle can be identified on photographs, in the field, and in the lithologic log of Zumaia of (*33*) through differences in the thickness and expression of marls intercalated between 100-ky limestone beds (Fig. 3 and fig. S3). Details of the cycle pattern confirm the phase relations between the sedimentary cycles and eccentricity as inferred by (*33*). Small-scale precession-related cycles are less well developed in the limestone beds of eccentricity-related cycles, indicating that these beds indeed correspond to eccentricity minima be-

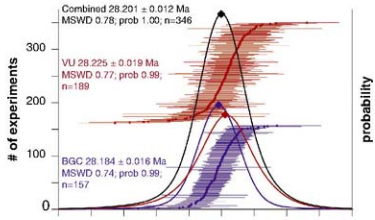

Fig. 2. Astronomically calibrated FCs age. The $^{40}Ar/^{39}Ar$ ages of the ash layers are converted to an astronomically calibrated age for FCs by using the Melilla sanidines as astronomically dated standards and the FCs as the unknown. Instead of doing this exercise for each tephra horizon separately, we included all reliably (both isotopic and astronomical) dated tephra to prevent an a priori bias to one of the astronomically dated tephra. However, the calibrated age is an inverse-variance weighted mean age; thus, tephra mes4, with the highest number of replicate analyses and the most precise data, dominates the final outcome. We include only the single-crystal fusion data (displayed here with 1σ analytical error), and ages with $P > 0.1$. Incremental heating experiments on selected sanidine fractions confirm the thermally undisturbed nature of the samples (*14*). We calculate an astronomically calibrated FCs age for each experiment propagating only analytical uncertainties. The weighted mean FCs age and standard analytical error for BGC and VU data are displayed separately and as a combined-age probability diagram. The 28.201 ± 0.012 Ma age for FCs is converted to an intercalibration factor of R^{FCs}_{astro} of 4.3644 ± 0.0018 for a T_{astro} at 6.500 Ma. This translates to 28.201 ± 0.046 Ma, including decay-constant uncertainties and the uncertainty in the astronomical ages of ±10 ky.

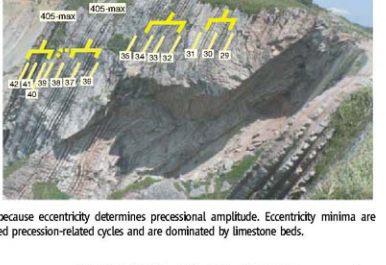

Fig. 3. Photo of the upper part of the Zumaia section below the San Telmo chapel. Both the 100-ky limestone beds 29 to 42 of (*33*) and the large-scale clusters of precession-related basic cycles that mark successive 405-ky eccentricity maxima are indicated (see also figs. S3, a to c). The phase relation with eccentricity is unambiguous: The marly intervals in between the 405- and 100-ky limestone beds often reveal distinct precession-related cycles, which is consistent with eccentricity maxima because eccentricity determines precessional amplitude. Eccentricity minima are marked by weakly developed precession-related cycles and are dominated by limestone beds.

cause eccentricity modulates the precession signal's amplitude.

The K-T boundary at Zumaia lies at the base of a prominent limestone-dominated interval that corresponds to a 405-ky eccentricity minimum. Successive 405-ky minima have ages of ~65.2, ~65.6, ~66.0, and ~66.4 Ma; thus, the challenge is to identify the correlative minimum. The error in the astronomical solution is on the order of 40 ky at 65 Ma [(*34*) and figure 25 in (*35*)]. To pinpoint this minimum, we recalculated published $^{40}Ar/^{39}Ar$ ages for the K-T boundary interval with our astronomical FCs age of 28.201 Ma.

Single-crystal sanidine $^{40}Ar/^{39}Ar$ dates on tephra horizons are available for the same magnetostratigraphic interval in continental sections in Montana (*36*). Haitian K-T boundary tektites and Chicxulub crater melt rock have also been dated by the $^{40}Ar/^{39}Ar$ technique (*37*, *38*). These ages recalculated relative to our FCs age of 28.201 Ma range from 65.8 to 66.0 Ma (Table 1 and table S4). We regard the single-crystal sanidine ages of 65.84 Ma [of Z coal (*36*)] and especially 65.99 Ma [of IrZ coal (*36*)] as the best estimates. These ages are considerably greater than the ages reported in GTS2004, which are based on sea-floor anomaly profiles numerically calibrated by means of a limited number of isotopically dated tie points, including the K-T boundary at 65.5 Ma, using an age of 28.02 Ma for FCs. This approach pins the K-T boundary down to the 405-ky eccentricity minimum around 66.0 Ma. Using this calibration as the starting point, the Zumaia section of (*33*) was retuned, taking the newly recognized 405-ky cycle into account (Figs. 3, 4). The resultant astronomical ages for the K-T boundary and magnetic reversal boundaries are in good agreement with the revised $^{40}Ar/^{39}Ar$ ages (Table 1).

In principle, the revised astronomical age of ~65.95 Ma for the K-T boundary can be shifted upward or downward by one 405-ky eccentricity cycle, resulting in ages of either ~65.56 or ~66.4 Ma (for example, see fig. S4). However, the astronomically recalibrated $^{40}Ar/^{39}Ar$ ages allow us to exclude these ages for the K-T boundary (Table 1 and table S4). Westerhold *et al.* (*39*) similarly linked the K-T boundary to a 405-ky eccentricity minimum using Fe and magnetic susceptibility records of Ocean Drilling Program cores from the Pacific and Atlantic Ocean and including the Zumaia section in their astrochronological framework. Their preferred tuning options result in ages of 65.28 Ma (option 1) or 65.68 Ma (option 2) for the K-T boundary. A third option (66.08 Ma) was added for consistency with our astronomically calibrated age for FCs, but this option is less favored, because it results in a relatively old age of 56.33 Ma for the Paleocene/Eocene boundary, an age that is difficult to reconcile with existing, though limited, radioisotopic constraints, even when recalculated against our astronomical FCs age. However, our Zumaia tuning results in one extra 405-ky cycle compared with (*39*) for the interval between the K-T boundary and the top of the normal polarity interval of C28n. Such differences must be resolved before a tuned Paleocene time scale can be finalized. Nevertheless, our intercalibration firmly links the K-T boundary to the 405-ky eccentricity minimum around 66 Ma.

An age of ~66.0 Ma for the K-T boundary was previously incorporated in the polarity time scale of Cande and Kent (*40*). However, this seemingly identical age was interpreted to be a spurious result from the chemical preparation of volcanic ashes

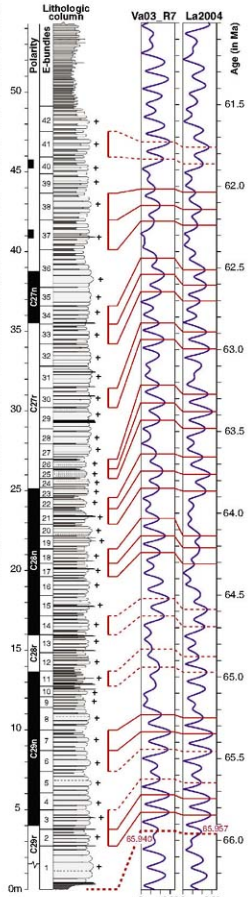

Fig. 4. Tuning of the K-T boundary section at Zumaia. Modified tuning of the Zumaia section following (*33*) that is consistent with the proposed intercalibration and takes the expression of the 405-ky eccentricity cycle into account. Close inspection of the lithologic log suggests that cycle bundles 1 to 14 should be tuned one 100-ky eccentricity minimum older than in (*33*) if the Va03_R7 solution is used for the tuning (note that the differences with the La2004 solution are larger). Crosses to the right of the lithological column mark midpoints of limestone-dominated parts of the 100-ky cycle that correlate with 100-ky eccentricity minima. The boundaries between the 100-ky cycles represent midpoints of the more marly intervals. Solid lines mark correlation lines in intervals in which the identification of the ~100- and 405-ky cycles is rather straightforward; dashed lines mark correlation lines in intervals in which the identification of the 405-ky cycle is less clear but supported by the number of ~100-ky and precession-related cycles. A conservative estimate of the absolute uncertainty in the 405-ky cycle around 65 Ma is ±40 ky (*35*). The estimated uncertainty of ~165 ky in the astronomically calibrated $^{40}Ar/^{39}Ar$ method at the K-T boundary gives a combined estimate of ±200 ky. This is sufficient to pinpoint the correct 405-ky maximum, because the astronomically calibrated $^{40}Ar/^{39}Ar$ ages (Table 1 and table S4) for the K-T boundary correspond closely to a 405-ky eccentricity minimum, leaving no space for tuning the K-T boundary interval one 405-ky eccentricity minimum older (K-T ~66.4 Ma) or younger (K-T ~65.6 Ma). Starting from the eccentricity tuning, the astronomical age of the K-T boundary arrives at 65.957 or 65.940 Ma for the La2004 and Va03_R7 solutions, respectively, using the average precession period (21 ky) at that time and the number of precession-related cycles (2.5) below cycle 2b, the oldest tuned 100-ky eccentricity minimum.

found intercalated in coal beds. Redating of the sanidine in these ash beds (using an age of 27.83 Ma for the FCs) led to a revised age of ~65.0 Ma for the K-T boundary, which was adopted in (*41*). The same single-crystal sanidine dates now provide an age of ~65.95 Ma, relative to our FCs age of 28.201 Ma.

We argue that our astronomically calibrated FCs age of 28.201 Ma should be incorporated in the next standard GTS to recalculate all other $^{40}Ar/^{39}Ar$ ages after it is confirmed by independent (intercalibration) studies. Only in this way is a mutually consistent age calibration of the GTS assured. Moreover, our integrated approach may lead to a stable time scale with unprecedented accuracy, precision, and resolution that will not be forced to undergo any further substantial revisions.

References and notes

1. F. M. Gradstein, J. G. Ogg, A. G. Smith, *A Geologic Time Scale 2004* (Cambridge Univ. Press, Cambridge, 2004).
2. P. R. Renne, D. B. Karner, K. R. Ludwig, *Science* **282**, 1840 (1998).
3. K. F. Kuiper, F. J. Hilgen, J. Steenbrink, J. R. Wijbrans, *Earth Planet. Sci. Lett.* **222**, 583 (2004).
4. P. R. Renne *et al.*, *Chem. Geol.* **145**, 117 (1998).
5. K. W. Min, R. Mundil, P. R. Renne, K. R. Ludwig, *Geochim. Cosmochim. Acta* **64**, 73 (2000).
6. All errors are stated at the 2σ level, unless stated otherwise.
7. P. R. Renne *et al.*, *Geology* **22**, 783 (1994).
8. F. J. Hilgen, W. Krijgsman, J. R. Wijbrans, *Geophys. Res. Lett.* **24**, 2043 (1997).
9. J. Steenbrink, N. Van Vugt, F. J. Hilgen, J. R. Wijbrans, J. E. Meulenkamp, *Palaeogeogr. Palaeoclimatol. Palaeoecol.* **152**, 283 (1999).
10. S. Roger *et al.*, *Earth Planet. Sci. Lett.* **179**, 101 (2000).
11. E. Van Assen, K. F. Kuiper, N. Barhoun, W. Krijgsman, F. J. Sierro, *Palaeogeogr. Palaeoclimatol. Palaeoecol.* **238**, 15 (2006).
12. W. Krijgsman, F. J. Hilgen, I. Raffi, F. J. Sierro, D. S. Wilson, *Nature* **400**, 652 (1999).
13. L. J. Lourens, F. J. Hilgen, J. Laskar, N. J. Shackleton, D. Wilson, in *The Geological Time Scale 2004*, F. M. Gradstein, J. G. Ogg, A. G. Smith, Eds. (Cambridge Univ. Press, Cambridge, 2004), pp. 409–440.
14. Materials and methods are available as supporting material on *Science* Online.
15. R. H. Steiger, E. Jäger, *Earth Planet. Sci. Lett.* **36**, 359 (1977).
16. J. I. Simon, P. R. Renne, R. Mundil, *Earth Planet. Sci. Lett.* **266**, 182 (2008).
17. O. Bachmann *et al.*, *Chem. Geol.* **236**, 134 (2007).
18. M. D. Schmitz, S. A. Bowring, *Geochim. Cosmochim. Acta* **65**, 2571 (2001).
19. B. Schoene, J. L. Crowley, D. J. Condon, M. D. Schmitz, S. A. Bowring, *Geochim. Cosmochim. Acta* **70**, 426 (2006).
20. R. Mundil, P. R. Renne, K. K. Min, K. R. Ludwig, *Eos Transactions American Geophysical Union Meeting Supplement* **87**, Abstract V21A (2006).
21. J. Y. Kwon, K. W. Min, P. J. Bickel, P. R. Renne, *Math. Geol.* **34**, 457 (2002).
22. Acapulco has chondritic chemistry but lacks chondrules owing to early high-temperature metamorphism (*42*).
23. P. R. Renne, *Earth Planet. Sci. Lett.* **175**, 13 (2000).
24. E. K. Jessberger, B. Dominik, T. Staudacher, G. F. Herzog, *Icarus* **42**, 380 (1980).
25. Y. Amelin, V. Pravdivtseva, *Meteorit. Planet. Sci.* **40**, A16 (2005).
26. A. Bouvier, J. Blichert-Toft, F. Moynier, J. D. Vervoort, F. Albarede, *Geochim. Cosmochim. Acta* **71**, 1583 (2007).
27. K. Min, K. A. Farley, P. R. Renne, K. Marti, *Earth Planet. Sci. Lett.* **209**, 323 (2003).
28. R. H. Nichols, C. M. Hohenberg, K. Kehm, Y. Kim, K. Marti, *Geochim. Cosmochim. Acta* **58**, 2553 (1994).
29. T. D. Swindle, *Meteorit. Planet. Sci.* **33**, 1147 (1998).
30. R. S. Coe, B. S. Singer, M. S. Pringle, X. X. Zhao, *Earth Planet. Sci. Lett.* **222**, 667 (2004).
31. L. J. Lourens *et al.*, *Nature* **435**, 1083 (2005).
32. H. Pälike *et al.*, *Science* **314**, 1894 (2006).
33. J. Dinarès-Turell *et al.*, *Earth Planet. Sci. Lett.* **216**, 483 (2003).
34. H. Pälike, J. Laskar, N. J. Shackleton, *Geology* **32**, 929 (2004).
35. J. Laskar *et al.*, *Astron. Astrophys.* **428**, 261 (2004).
36. C. C. Swisher, L. Dingus, R. F. Butler, *Can. J. Earth Sci.* **30**, 1981 (1993).
37. C. C. Swisher III *et al.*, *Science* **257**, 954 (1992).
38. G. A. Izett, G. B. Dalrymple, L. W. Snee, *Science* **252**, 1539 (1991).
39. T. Westerhold *et al.*, *Palaeogeogr. Palaeoclimatol. Palaeoecol.* **257**, 377 (2008).
40. S. C. Cande, D. V. Kent, *J. Geophys. Res.* **97**, 13917 (1992).
41. W. A. Berggren, D. V. Kent, C. C. Swisher, M.-P. Aubry, *Geochronology, Time Scales and Global Stratigraphic Correlation*, *SEPM Special Publication* **54**, 129 (1995).
42. T. J. McCoy *et al.*, *Geochim. Cosmochim. Acta* **60**, 2681 (1996).
43. F. J. Sierro, F. J. Hilgen, W. Krijgsman, J. A. Flores, *Palaeogeogr. Palaeoclimatol. Palaeoecol.* **168**, 141 (2001).
44. F. Varadi, B. Runnegar, M. Ghil, *Astrophys. J.* **592**, 620 (2003).
45. The project was funded by grants 750.198.02 and 814.01.004 of the Netherlands Organisation for Scientific Research to K.K., and supported by NSF grant EAR-9903078 to P.R. and A.D. P.R. and A.D.'s work was also supported by the Ann and Gordon Getty Foundation. Mineral separation facilities at VU were provided by Roel van Elsas.

Supporting Online Material

www.sciencemag.org/cgi/content/full/320/5875/500/DC1
Materials and Methods
SOM Text
Figs. S1 to S4
Tables S1 to S4
References

18 December 2007; accepted 6 March 2008
10.1126/science.1154339

REPORTS

Sign Change of Poisson's Ratio for Carbon Nanotube Sheets

Lee J. Hall,[1] Vitor R. Coluci,[2] Douglas S. Galvão,[2] Mikhail E. Kozlov,[1] Mei Zhang,[1]* Sócrates O. Dantas,[3] Ray H. Baughman[1]†

Most materials shrink laterally like a rubber band when stretched, so their Poisson's ratios are positive. Likewise, most materials contract in all directions when hydrostatically compressed and decrease density when stretched, so they have positive linear compressibilities. We found that the in-plane Poisson's ratio of carbon nanotube sheets (buckypaper) can be tuned from positive to negative by mixing single-walled and multiwalled nanotubes. Density-normalized sheet toughness, strength, and modulus were substantially increased by this mixing. A simple model predicts the sign and magnitude of Poisson's ratio for buckypaper from the relative ease of nanofiber bending and stretch, and explains why the Poisson's ratios of ordinary writing paper are positive and much larger. Theory also explains why the negative in-plane Poisson's ratio is associated with a large positive Poisson's ratio for the sheet thickness, and predicts that hydrostatic compression can produce biaxial sheet expansion. This tunability of Poisson's ratio can be exploited in the design of sheet-derived composites, artificial muscles, gaskets, and chemical and mechanical sensors.

When stretched, most materials contract in both lateral dimensions to decrease stretch-induced volume change. The ratio of percent lateral contraction to percent applied tensile elongation is the Poisson's ratio. Some rubbers have Poisson's ratios of about 0.5 for both lateral directions, so their volume does not appreciably change upon stretching. In very rare materials the sum of Poisson's ratios for lateral dimension changes exceeds unity, so they increase density when stretched and, inversely, expand in at least one direction when hydrostatically compressed (*1*). If a lateral dimension expands during stretching, the associated Poisson's ratio is negative and the material is called auxetic (*2*). Recent interest in this counterintuitive behavior originated from pioneering discoveries that partially collapsed foams and honeycombs (*2*, *3*), fibrillar polymers (*4*), and polymer composites (*5*) can be auxetic.

Poisson's ratio was unknowingly used 2000 years ago in the empirical selection of cork for wine bottle stoppers. Cork stoppers have a near-zero Poisson's ratio for radial directions when subjected to orthogonal uniaxial stress (*6*). A positive Poisson's ratio makes a stopper difficult to insert but easy to remove, and the reverse occurs for a negative Poisson's ratio.

Carbon nanotube sheets (buckypaper) were fabricated (*7*, *8*) by filtration of aqueous dispersions of single-walled nanotubes (SWNTs) (*9*) and multiwalled carbon nanotubes (MWNTs) (*10*) produced by chemical vapor deposition, a technique reminiscent of ancient methods for making writing paper by drying a fiber slurry. The SWNTs are seamless cylinders of graphite

about 1 nm in diameter, and the MWNTs consist of about nine concentric SWNT shells having an outer diameter of about 12 nm (*8*). Scanning electron microscopy shows that bundles of the SWNTs (diameter about 20 nm) and largely unbundled MWNTs are intimately commingled in sheets comprising both nanotube types.

The Poisson's ratios of SWNT and MWNT buckypaper were initially determined by using an optical microscope to measure the change in sheet width as a function of stretch in the sheet length direction. More accurate Poisson's ratio measurements resulted from recording movies of the movements of reflective particles on the sheet surface during constant-rate deformation. Image correlation software was used to derive the relative displacements of about 7000 particles per movie frame and corresponding strains in lateral and tensile directions (*8*). The thickness-direction Poisson's ratio was obtained from scanning electron micrographs showing sheet thickness versus applied in-plane tensile strain (*8*).

The in-plane Poisson's ratio was positive (about 0.06) and little changed until the MWNT content reached 73 weight percent (wt %). Further addition of MWNTs decreased the Poisson's ratio to −0.20. A highly nonlinear dependence of Young's modulus, strength, and toughness on MWNT content was also observed, with maximum density-normalized value between compositional extremes, although electronic conductivity and density were approximately a linear function of MWNT content (Fig. 1, A and B, and fig. S1). Perhaps important for applications, the characterized buckypaper comprising both SWNTs and MWNTs had up to 1.6 times the maximum strength-to-weight ratio, 1.4 times the maximum modulus-to-weight ratio, and 2.4 times the maximum toughness of sheets comprising only SWNTs or MWNTs (Fig. 1, A and B, and fig. S1). Large positive Poisson's ratios were observed for the thickness direction (0.33 and 0.75 for SWNT and MWNT sheets, respectively).

Annealing the nanotube sheets at 1000°C in argon for 15 min did not eliminate the sharp change from positive to negative in-plane Poisson's ratio at 77 to 80 wt % MWNTs, indicating that any residual surfactant in the buckypaper is unimportant. Although hysteretic stress-strain curves were seen upon high-strain unloading and reloading, with hysteresis loop width decreasing with decreasing MWNT content and decreasing strain increment for the loop, the Poisson's ratio was essentially constant over these curves.

The negative in-plane Poisson's ratio of MWNT buckypaper sharply contrasts with that reported previously for ordinary paper, made either commercially or by an ancient method like the one we used, where the experimentally observed in-plane Poisson's ratios are large and positive and theoretical calculations predict the possibility of either positive or negative in-plane Poisson's ratios (*11*–*20*). Although entropy and associated thermally driven deviations from in-plane alignment may produce negative in-plane Poisson's ratios for nanofiber biological membranes and related structures (*17*, *21*), persistence lengths of about 0.1 mm at room temperature for even unbundled SWNTs (*18*) mean that similar entropic effects are not important for determining the Poisson's ratios of buckypaper.

A simple model was developed that predicts the observed negative and positive in-plane Poisson's ratios for sheets of different composition, as well as a much larger positive Poisson's ratio in the thickness direction (Fig. 1C and fig. S2). This model captures key structural features of the carbon nanotube sheets: (i) isotropic in-plane mechanical properties; (ii) nanotubes preferentially oriented in the sheet plane, but positively and negatively deviating from this plane by an average angle γ; and (iii) freedom to undergo stress-induced elongation as a result of straightening meandering nanotubes and changing the angle between intersecting nanotubes. This model can also be applied to other fiber networks having similar structure to buckypaper. Although periodic network models have been previously deployed for fiber sheets (*13*), the model structures have high in-plane anisotropy, so uncertainty in the sign of the Poisson's ratio results from the need to average in-plane properties to obtain those for isotropic sheets.

[1]MacDiarmid NanoTech Institute, University of Texas at Dallas, Richardson, TX 75083, USA. [2]Instituto de Física "Gleb Wataghin," Universidade Estadual de Campinas, Unicamp 13083-970, Campinas, São Paulo, Brazil. [3]Departamento de Física, Universidade Federal de Juiz de Fora, UFJF 36036-330, Juiz de Fora, Minas Gerais, Brazil.

*Present address: Department of Industrial Engineering, Florida State University, Tallahassee, FL 32306, USA.

†To whom correspondence should be addressed. E-mail: ray.baughman@utdallas.edu

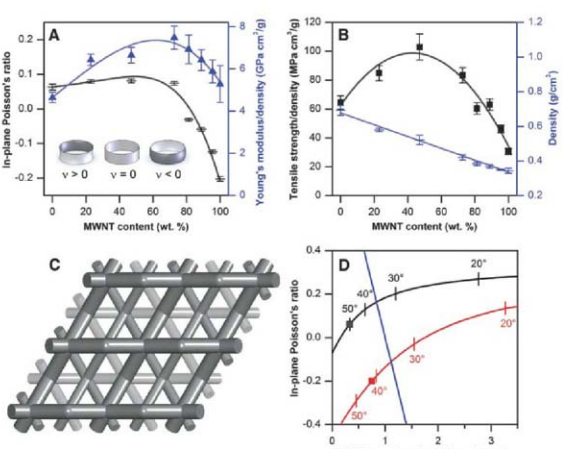

Fig. 1. **(A)** Measured in-plane Poisson's ratio (black dashes) and density-normalized Young's modulus (blue triangles) versus MWNT content in SWNT-MWNT sheets. Inset: Effect of Poisson's ratio sign on transverse curvature for a bent sheet strip. **(B)** Measured density-normalized tensile strength (black squares) and density (blue dashes) versus MWNT content in sheets. **(C)** Model for nanotube sheets, where meandering nanotubes are represented by zigzag chains. **(D)** Relationships between in-plane and thickness-direction Poisson's ratios as a function of indicated average nanotube orientation angle γ for SWNT (black curve) and MWNT (red curve) sheets having the force constant ratios R that yield the measured Poisson's ratios (squares). Poisson's ratios to the right of the blue line provide negative linear compressibilities. The error bars in (A) and (B) correspond to ±SDs of measurements on different samples.

In our model, each meandering nanotube (or nanotube bundle) is represented by a zigzag chain parallel to the sheet plane (with angle of $\pm\gamma$ between the struts and the basal plane). Zigzag chains in one nanotube sheet layer connect via noncovalent interactions with those in adjacent layers at the extremes of the zigs and zags, where torsion about the contact enables change in the angle of intersection between nanotubes. The ratio of the force constant for angle bend to the force constant for changing the inter-nanotube torsional angle is R. These force constants for angle bending at zigzags (k_B) and torsion between contacting nanotubes (k_T) are effective values, arising in the intractable real structure from the energy needed to straighten meandering nanotubes and change the angles between intersecting nanotubes (*22*).

Expressing the total energy needed for a given tensile strain in terms of angle bend and torsional angle changes, and minimizing this energy subject to the constraint that all layers have the same tensile-direction and width-direction strains (*8*), provides in-plane (ν_1) and sheet thickness direction (ν_3) Poisson's ratios of $\nu_1 = [R - 3\sin^2\gamma]/[3(R + \sin^2\gamma)]$ and $\nu_3 = [R + 3\sin^2\gamma]/[3\tan^2\gamma(R + \sin^2\gamma)]$.

These equations predict the observed ν_1 and ν_3 ($\nu_1 = -0.20$ and $\nu_3 = 0.75$ for MWNT sheets; $\nu_1 = 0.06$ and $\nu_3 = 0.33$ for SWNT sheets) for MWNT sheets with $\gamma = 42°$ and $R = 0.67$ and for SWNT sheets with $\gamma = 50°$ and $R = 2.28$. The predicted γ values are consistent with average angles from x-ray diffraction of 41.7° for MWNT sheets and 45.0° for SWNT sheets, as well as previous diffraction measurements for similar SWNT sheets (*23*).

The above equation for the in-plane Poisson's ratio can be expressed as $\nu_1 = (1 - \beta)/(3 + \beta)$, where $\beta = (3\sin^2\gamma)/R = 3(k_T/k_B)\sin^2\gamma$. If the approximation that nanotube struts are rigid is eliminated (δ), we obtain the same dependence of ν_1 on β, but with $\beta = 3k_T/k_{SB}$, where k_{SB} is the force constant for elongation of the nanotube (or nanotube bundles) via a combination of nanotube straightening (changing γ in the present model) and strut deformations. Using a different model, which includes a host of structural and force constant parameters in β, the above dependence of ν_1 on β has been predicted for sheets of ordinary paper (*12*).

Why do cellulose-based paper (*16*), SWNT paper, and MWNT paper provide such different measured in-plane Poisson's ratios (about 0.30, 0.06, and −0.20), even when they are similarly handmade by removing water from sedimented fiber mats? Insights result from first considering the basic types of deformation that lead to extreme positive and negative in-plane Poisson's ratios. Stretch-induced increases in nanotube length without change in the angle between intersecting nanotubes provides the most negative Poisson's ratio (−1, corresponding to an infinite k_T/k_B or k_T/k_{SB} for the above simplified models). Stretch-induced decreases in the angles between intersecting nanotubes increase Poisson's ratio, producing a Poisson's ratio of 1/3 when β vanishes. To visualize this, note that two neighboring nanotube layers in the Fig. 1C model are coupled like the struts of a wine rack. If rotation between struts dominates, as in an ordinary wine rack, the Poisson's ratio is positive. If torsional rotation of struts is blocked and the struts are stretchable but not bendable, increases in strut length produce a negative Poisson's ratio.

To understand the nanoscale origin of the major differences in Poisson's ratio for nanotube fiber mats, consider that beam bending in response to tensile stress has the same effect for increasing Poisson's ratio as does torsional rotation. In the wine rack analog, a positive Poisson's ratio would result if the hinges are welded to struts to prohibit torsional rotation and the struts are much easier to bend than to stretch. Nanotube beam bending in response to a tensile stress within the sheet plane changes the effective angle between intersecting nanotubes and produces a corresponding increase in Poisson's ratio, similar to the response when there are changes in torsional angle for the model of Fig. 1C. If fiber beam bending is the predominant deformation that changes the effective angle between intersecting fibers, and if fiber deviation from in-plane orientation is neglected, then $\beta = 3k_B/k_{SB}$, where the force constants for fiber bending and tensile fiber elongation are k_B and k_{SB}, respectively (*8*). Using this approximation, Perkins (*12*) predicted that the in-plane Poisson's ratio of paper sheets will be positive, with a ν_1 between 0.259 and 1/3, which is consistent with observations.

Why then do we see a negative Poisson's ratio of −0.20 for MWNT sheets and a much smaller positive Poisson's ratio of 0.06 for SWNT sheets? We provide evidence that these large changes in Poisson's ratio arise from changes in the ratio of beam bending to beam stretch force constants. The tubular nanofiber form and the degree of coupling between SWNT walls are important. The MWNTs we used have an outer diameter of about 12 nm, contain about nine walls, and are largely unbundled in the sheets; the SWNTs have an average diameter of about 1.0 nm (*24*, *25*) and a wide distribution in bundle diameters, with an average around 20 nm.

Consider k_B and k_S for a perfectly straight SWNT having strut length L: $k_B = 3\pi C(r/L)^3$ and $k_S = 2\pi Cr/L$, where C is the product of the graphene sheet Young's modulus and sheet thickness, and r is the radius of the SWNT (*18*, *26*). The largest geometrically possible value of r/L is $\sin(60°)/2$, which corresponds to the physically unreasonable case where each layer within the nanotube sheet comprises straight nanotubes that are close-packed within the layer. From $\beta = 3k_B/k_S = (9/2)(r/L)^2$ for the perfect SWNT and $\nu_1 = (1 - \beta)/(3 + \beta)$, this hypothetical buckypaper of perfectly straight, infinitely long, unbundled SWNTs cannot have a Poisson's ratio below 0.04. Because the value of β for buckypaper-like sheets comprising long circular solid fibers is the same as for a SWNT when the effective Young's modulus for bending equals that for tension, the predicted ν_1 is also 0.04 or higher—and likely much higher, because buckypaper-like sheets of ordinary paper do not have fibers that are close-packed in a plane.

Low mechanical coupling between the component SWNTs nested within MWNTs and between SWNTs in bundles within the buckypaper reduces k_B and k_S. Low interwall coupling between outer and inner walls is indicated for MWNTs by the sword-in-sheath type of mechanical failure and the ease of pulling the inner nanotubes from a MWNT (*27*, *28*). Because the following calculations treat only the in-plane Poisson's ratio, we here approximate the structure as comprising successive layers of bundled SWNTs or largely unbundled MWNTs (like that shown in Fig. 1C, but with $\gamma = 0°$), with stretch force constant k_{SB} to accommodate

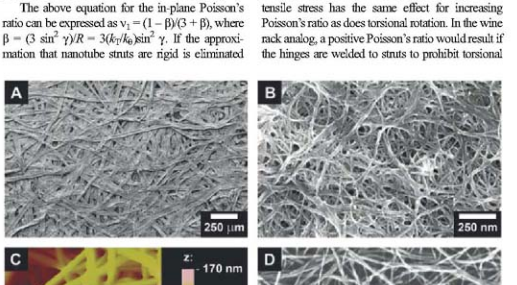

Fig. 2. Scanning electron micrographs of **(A)** ordinary paper made from wood pulp fiber (*19*), **(B)** SWNT buckypaper, and **(D)** MWNT buckypaper. **(C)** An atomic force micrograph (tapping mode, z-range contrast) of MWNT buckypaper.

stretch force reduction due to nanotube meandering. This structure provides a volume per strut of $D'L^2 \sin(120°)$ and a calculated density of $\rho_{calc} = W_L/[D'L \sin(120°)]$, where W_L is the strut weight per unit length and D' is the sum of the covalent diameter of the nanotube and the 0.34-nm van der Waals diameter of carbon (*8*). By equating calculated sheet densities to the observed sheet densities, interjunction lengths of 54.3 nm and 39.5 nm are calculated for the MWNT and SWNT sheets, respectively. Although these distances seem shorter than suggested by the micrographs of Fig. 2, note that the micrographs are for the sheet surface (the face originally in contact with the filter membrane) and do not provide the junction density and corresponding L in the buckypaper interior.

To predict the Poisson's ratio of buckypaper, we calculate the elongation force constant k_{SB} (*8*) from the observed Young's modulus Y according to $k_{SB} = 2D'Y \sin(120°)/(1 - \nu_1)$. Although this little affects the results, ν_1 in this equation is the self-consistently calculated value instead of the measured value. The k_B for the MWNTs is the sum of bending force constants for all component SWNTs nested within the MWNTs, and the k_B for SWNT bundles is derived from the measured average Young's modulus for bending (Y_B) 20-nm-diameter SWNT bundles (50 GPa) (*29*), using the force constant for bending a solid cylindrical rod, $k_B = 3\pi R^4 Y_B/(4L^3)$ (*26*). The predicted Poisson's ratios are –0.17 for MWNT buckypaper (versus the observed –0.20) and 0.17 for SWNT buckypaper (versus the observed 0.06). Increasing Y_B to 81 GPa decreases the calculated ν_1 for SWNT buckypaper to the observed value, and this Y_B is within the range of experimental uncertainty for Y_B (*29*).

These results indicate that large negative Poisson's ratios can be achieved by using large-diameter MWNTs having as many interior walls as possible. Although all nanotube walls contribute additively to k_B, only the outer wall contributes to k_{SB} unless the MWNTs are extremely long. Likewise, decreasing the separation between effectively welded inter-nanotube contacts (such as by increasing sheet density) can decrease Poisson's ratio. However, the effects of these structure changes are not simple, because increasing k_B and decreasing L can decrease nanotube meandering between junctions, and this decrease of meandering can provide a positive contribution to k_{SB}.

Negative Poisson's ratios are sometimes accompanied by much rarer mechanical properties: negative linear compressibilities and negative area compressibility—meaning that a material expands in either one or two orthogonal directions when hydrostatic pressure is applied (*1*). A negative linear compressibility is the inverse of another strange property, increasing density when elongated in a direction where linear compressibility is negative, and both require that $1 - \nu_1 - \nu_3 < 0$. Using the above equations for ν_1 and ν_3 as a function of R and γ for the model of Fig. 1C, negative in-plane compressibility (Fig. 1D), negative area compressibility for the sheet plane, and stretch densification are predicted for $\cos\gamma > (2/3)^{1/2}$, which implies $\gamma < 35.3°$. However, the average γ needed for achieving these properties will decrease as a result of in-plane nanofiber meandering, because only the tensile strain component resulting in thickness change affects ν_3.

The observed continuous tunability of Poisson's ratio, modulus, strength, toughness, density, and electrical conductivity of nanotube sheets could be useful for applications, as could mechanical property optimization using mixtures of nanotubes. However, the change of Poisson's ratio from positive to negative is especially interesting and unexpected. This tunability, which we can now explain, could be exploited in the design of sheet-derived composites, artificial muscles, gaskets, stress/strain sensors, and chemical sensors where analyte absorption induces mechanical stresses. Even shaping processes are affected, because bending a thick nanotube sheet strip will result in either convex or concave lateral deformation (Fig. 1A, inset), depending on the sign of the in-plane Poisson's ratio.

References and Notes

1. R. H. Baughman, S. Stafström, C. Cui, S. O. Dantas, *Science* **279**, 1522 (1998).
2. R. S. Lakes, *Science* **235**, 1038 (1987).
3. L. J. Gibson, M. F. Ashby, *Proc. R. Soc. London Ser. A* **382**, 43 (1982).
4. K. E. Evans, M. A. Nkansah, I. J. Hutchinson, S. C. Rogers, *Nature* **353**, 124 (1991).
5. G. Milton, *J. Mech. Phys. Solids* **40**, 1105 (1992).
6. L. J. Gibson, K. E. Easterling, M. F. Ashby, *Proc. R. Soc. London Ser. A* **377**, 99 (1981).
7. A. G. Rinzler *et al.*, *Appl. Phys. A* **67**, 29 (1998).
8. See supporting material on *Science* Online.
9. P. Nikolaev *et al.*, *Chem. Phys. Lett.* **313**, 91 (1999).
10. M. Zhang, K. R. Atkinson, R. H. Baughman, *Science* **306**, 1358 (2004).
11. H. L. Cox, *Br. J. Appl. Phys.* **3**, 72 (1952).
12. R. W. Perkins, in *Proceedings of the Conference on Paper Science and Technology—The Cutting Edge: Fiftieth Anniversary Year 1929–1979* (Institute of Paper Chemistry, Appleton, WI, 1980), VII, pp. 89–111.
13. M. Delincé, F. Delannay, *Acta Mater.* **52**, 1013 (2004).
14. J. A. Åström, J. P. Mäkinen, H. Hirvonen, J. Timonen, *J. Appl. Phys.* **88**, 5056 (2000).
15. D. H. Boal, U. Seifert, J. C. Shillcock, *Phys. Rev. E* **48**, 4274 (1993).
16. J. P. Benzinski, K. W. Hardacker, *TAPPI J.* **65**, 114 (1982).
17. M. Bowick, A. Cacciuto, G. Thorleifsson, A. Travesset, *Phys. Rev. Lett.* **87**, 148103 (2001).
18. B. L. Yakobson, L. C. Couchman, *J. Nanoparticle Res.* **8**, 105 (2006).
19. C. A. Bronkhorst, *Int. J. Solids Struct.* **40**, 5441 (2003).
20. T. Uesaka, K. Murakami, R. Imamura, *TAPPI J.* **62**, 111 (1979).
21. R. Lakes, *Nature* **414**, 503 (2001).
22. The simplest model that provides these key features of the nanotube sheets has hexagonal space group $P6_222$ and inter-nanotube noncovalent junctions located at (0.5, 0, 0) and equivalent locations in the unit cell. The same mechanical properties result for the intimately related structure in Fig. 1C, in which each successive layer of zigzag chains is equally likely to be added in either of two possible directions.
23. W. Zhou *et al.*, *Appl. Phys. Lett.* **84**, 2172 (2004).
24. M. Yudasaka *et al.*, *Nano Lett.* **1**, 487 (2001).
25. S. M. Bachilo *et al.*, *Science* **298**, 2361 (2002); published online 29 November 2002 (10.1126/science.1078727).
26. C. M. DiBlasio, M. A. Cullinan, M. L. Culpepper, *Appl. Phys. Lett.* **90**, 203116 (2007).
27. M.-F. Yu *et al.*, *Science* **287**, 637 (2000).
28. J. Cumings, A. Zettl, *Science* **289**, 602 (2000).
29. A. Kis *et al.*, *Nat. Mater.* **3**, 153 (2004).

30. We thank R. Raj, S. Shaw, R. Hou, and J. Levinson for their contributions; J. Below for the micrograph of Fig. 2C; and C. A. Bronkhorst for permission to use the micrograph of Fig. 2A. Supported by NSF grant DMI-0609115, Air Force Office of Scientific Research grant FA9550-05-C-0088, Lintec Corporation, and the Brazilian agencies Fundação de Amparo à Pesquisa do Estado de São Paulo and Conselho Nacional de Pesquisas Científicas.

Supporting Online Material

www.sciencemag.org/cgi/content/full/320/5875/504/DC1
Materials and Methods
SOM Text
Figs. S1 and S2
References

28 August 2007; accepted 20 March 2008
10.1126/science.1149815

Stretchable and Foldable Silicon Integrated Circuits

Dae-Hyeong Kim,[1]* Jong-Hyun Ahn,[2]* Won Mook Choi,[1]* Hoon-Sik Kim,[1] Tae-Ho Kim,[1] Jizhou Song,[3] Yonggang Y. Huang,[5]† Zhuangjian Liu,[4] Chun Lu,[4] John A. Rogers[1,3,4]†

We have developed a simple approach to high-performance, stretchable, and foldable integrated circuits. The systems integrate inorganic electronic materials, including aligned arrays of nanoribbons of single crystalline silicon, with ultrathin plastic and elastomeric substrates. The designs combine multilayer neutral mechanical plane layouts and "wavy" structural configurations in silicon complementary logic gates, ring oscillators, and differential amplifiers. We performed three-dimensional analytical and computational modeling of the mechanics and the electronic behaviors of these integrated circuits. Collectively, the results represent routes to devices, such as personal health monitors and other biomedical devices, that require extreme mechanical deformations during installation/use and electronic properties approaching those of conventional systems built on brittle semiconductor wafers.

Realization of electronics with performance equal to established technologies that use rigid semiconductor wafers, but in lightweight, foldable, and stretchable formats would enable many new applications. Examples include wearable systems for personal health monitoring and therapeutics, "smart" surgical gloves with integrated electronics, and electronic eye–type imagers that incorporate focal plane arrays on hemispherical substrates (*1*–*3*). Circuits that use

organic (*4*, *5*) or certain classes of inorganic (*6*–*13*) electronic materials on plastic or steel foil substrates can provide some degree of mechanical flexibility, but they cannot be folded or stretched. Also, with few exceptions (*11*–*13*) such systems offer only modest electrical performance. Stretchable metal interconnects with rigid (*14*) or stretchable (*15*–*17*) inorganic device components represent alternative strategies that can also, in certain cases, provide high performance. In their existing forms, however, none of these approaches allows scaling to circuit systems with practically useful levels of functionality.

We present routes to high-performance, single-crystalline silicon complementary metal-oxide semiconductor (Si-CMOS) integrated circuits (ICs) that are reversibly foldable and stretchable. These systems combine high-quality electronic materials, such as aligned arrays of silicon nanoribbons, with ultrathin and elastomeric substrates, in multilayer neutral mechanical plane designs and with "wavy" structural layouts. High-performance n- and p-channel metal-oxide semiconductor field-effect transistors (MOSFETs), CMOS logic gates, ring oscillators, and differential amplifiers, all with electrical properties as good as analogous systems built on conventional silicon-on-insulator (SOI) wafers, demonstrate the concepts. Analytical and finite element method (FEM) simulation of the mechanics, together with circuit simulations, reveal the key physics. We implement single-crystalline silicon because it provides excellent electronic properties, including high electron and hole mobilities. Commodity bulk silicon wafers (*18*), for cost-sensitive applications, or SOI wafers provide the source of the ultrathin pieces of Si that are required. Vacuum-evaporated materials such as nanocrystalline Si (*19*), which also enable high performance, might offer further advantages in cost. The same approaches to stretchable and foldable integrated circuits reported here can be used with these and other related classes of materials. The strategies reported here are important not only for the Si-CMOS circuits that they enable but also for their straightforward scalability to much more highly integrated systems with other diverse classes of electronic materials whose intrinsic brittle, fragile mechanical properties would otherwise preclude their use in such applications.

Figure 1A schematically summarizes the key steps for forming ultrathin, foldable, and stretchable circuits and presents optical images of representative systems at different stages of the process. The procedure begins with spin-casting a sacrificial layer of poly(methylmethacrylate) (PMMA) (~100 nm) followed by a thin, substrate layer of polyimide (PI) (~1.2 μm) on a Si wafer that serves as a temporary carrier (see supporting online material). A transfer printing process with a poly(dimethylsiloxane) (PDMS) stamp (*20*, *21*) delivers to the surface of the PI organized arrays of n- and p-doped Si nanoribbons (Fig. 1B, inset) with integrated contacts, separately formed from n-type source wafers. Automated stages specially designed for this printing enable multilayer registration with ~2 μm accuracy (*12*). Depositing and patterning SiO_2 (~50 nm) for gate dielectrics and interconnect crossovers, and Cr/Au (5/145 nm) for source, drain, and gate electrodes and interconnects yield fully integrated Si-CMOS circuits with performance comparable to similar systems formed on SOI wafers (fig. S1). Figure 1C shows an image of an array of Si-CMOS inverters and isolated n- and p-channel MOSFETs (n-MOSFETs and p-MOSFETs, respectively) formed in this manner, still on the carrier substrate. In the next step, reactive ion etching forms a square array of small holes (~50 μm diameters, separated by 800 μm) that extend through the nonfunctional regions of the circuits and the thin PI layer into the underlying PMMA. Immersion in acetone dissolves the PMMA by flow of solvent through the etch holes to release ultrathin, flexible circuits in a manner that does not degrade the properties of the devices. These systems can be implemented as flexible, free-standing sheets, or they can be integrated in wavy layouts on elastomeric substrates to provide fully reversible stretchability/compressibility (Fig. 1A). The schematic cross-sectional view at the bottom right illustrates the various layers of this Si-CMOS/PI system (total thickness ~1.7 μm). The ultrathin circuits exhibit extreme levels of bendability, as illustrated in Fig. 1C, without compromising the electronic properties (fig. S2). There are two primary reasons for this behavior. The first derives from elementary bending mechanics in thin films, where the surface strains are determined by the film thickness, t, divided by twice the radius of curvature associated with the bending, r (*22*). Films with $t = 1.7$ μm can be bent to r as small as ~85 μm before the surface strains reach a typical fracture strain (~1% in tension) for the classes of high-performance inorganic electronic materials used here. A second and more subtle feature emerges from full analysis of the bending mechanics in the material stacks of the circuits. The results indicate that the neutral mechanical plane, which defines the position through the thickness of the structure where strains are zero for arbitrarily small r, lies in

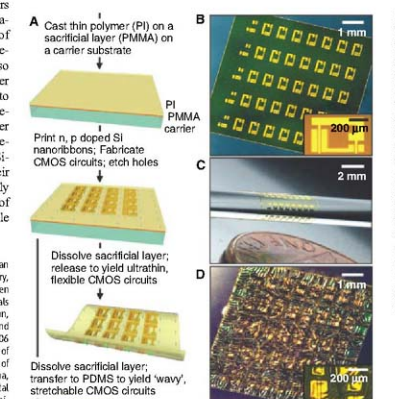

Fig. 1. (A) Overview of the fabrication process for ultrathin CMOS circuits that exploit silicon nanoribbons and enable extreme levels of bendability (third frame from the top) or fully reversible stretchability/compressibility (bottom frame on the left) and schematic cross-sectional view with neutral mechanical plane indicated with a red dashed line (bottom frame on the right). **(B to D)** Optical images of circuits on the carrier wafer and magnified views of a single CMOS inverter (inset) (B), on a thin rod after removal from this carrier (C), and in a wavy configuration on PDMS (D).

[1]Department of Materials Science and Engineering, Beckman Institute, and Frederick Seitz Materials Research Laboratory, University of Illinois at Urbana-Champaign, 1304 West Green Street, Urbana, IL 61801, USA. [2]School of Advanced Materials Science and Engineering, Sungkyunkwan University, Suwon, 440-746, Korea. [3]Department of Mechanical Science and Engineering, University of Illinois at Urbana-Champaign, 1206 West Green Street, Urbana, IL 61801, USA. [4]Departments of Chemistry, Electrical and Computer Engineering, University of Illinois at Urbana-Champaign, 1304 West Green Street, Urbana, IL 61801, USA. [5]Departments of Civil and Environmental Engineering and Mechanical Engineering, Northwestern University, Evanston, IL 60208, USA. [6]Institute of High Performance Computing, 1 Science Park Road, #01-01 The Capricorn, Singapore Science Park II, Singapore 117528.

*These authors contributed equally to this work.
†To whom correspondence should be addressed. E-mail: jrogers@uiuc.edu (J.A.R.); y-huang@northwestern.edu (Y.Y.H.)

the electronic device layers (fig. S3). In other words, the high moduli of the electronic materials move the neutral mechanical plane from the geometric midplane, which lies in the PI, to the device layers. The illustration at the bottom right of Fig. 1 indicates with dashed red lines the approximate locations of this neutral mechanical plane in different regions of the system. This situation is highly favorable because the fracture strains of the materials used in the circuits are substantially lower than those for fracture or plastic deformation in the PI (~7%). Two disadvantages of such circuits are their lack of stretchability and, for certain applications, their low flexural rigidity. These limitations can be circumvented by implementing extensions of concepts that achieve stretchable, wavy configurations of sheets and ribbons of silicon and gallium arsenide (*15*, *16*), in a procedure illustrated in the bottom frame of Fig. 1A. The fabrication begins with removal of the ultrathin circuits from the carrier substrate using a PDMS stamp, evaporating a thin layer of Cr/SiO_2 (3/30 nm) onto the exposed PI surface (i.e., the surface that was in contact with the PMMA), and then generating –OH groups on the surfaces of the SiO_2 and a biaxially prestrained PDMS substrate ($\varepsilon_{pre} = \varepsilon_{xx} = \varepsilon_{yy}$ where the x and y coordinates lie in the plane of the circuit) by exposure to ozone induced with an ultraviolet lamp. Transfer printing the circuit onto the PDMS substrate, followed by mild heating, creates covalent linkages to form strong mechanical bonding between the Si CMOS/PI/Cr/SiO_2 and the PDMS. Relaxing the prestrain induces compressive forces on the circuits that lead to the formation of complex wavy

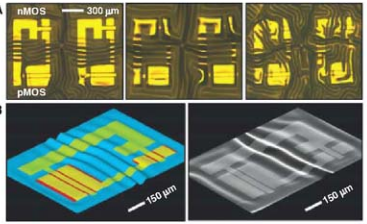

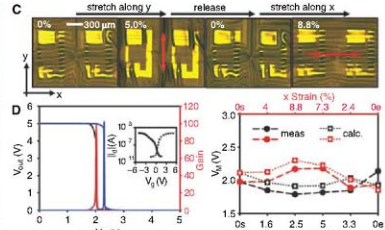

Fig. 2. **(A)** Wavy Si-CMOS inverters on PDMS, formed with various levels of prestrain. (left, ε_{pre} = 2.7%; center, ε_{pre} = 3.9%; right, ε_{pre} = 5.7%.) **(B)** Structural configuration determined by full 3D FEM of a system formed with ε_{pre} = 3.9% (left) and perspective scanning electron micrograph of a sample fabricated with a similar condition (right). **(C)** Optical images of wavy Si-CMOS inverters under tensile strains (*31*) along the x and y directions. **(D)** Measured (red and black) and simulated (blue) transfer characteristics of wavy inverters (left), and n- and p-channel MOSFETs (solid and dashed lines, respectively, in the left inset). Measured (solid circles) and simulated (open squares) inverter threshold voltages for different applied strains along x and y (right).

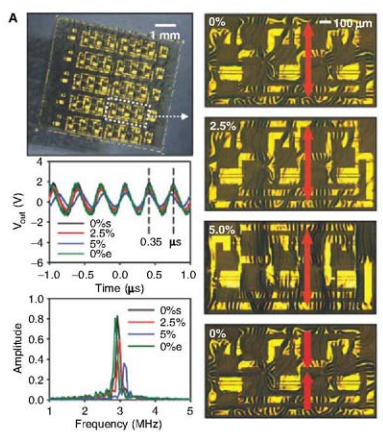

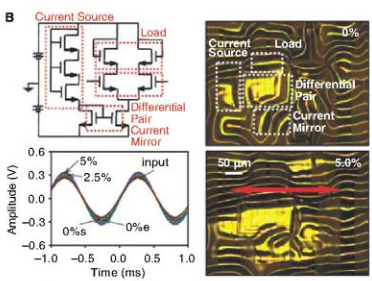

Fig. 3. **(A)** Optical image of an array of stretchable, wavy three-stage CMOS ring oscillators (top left) and magnified views of a typical oscillator at different applied strains (*31*) oriented along the direction of the red arrow (right frames). Measured time and frequency domain responses of an oscillator at different applied strains. **(B)** Circuit diagram of a differential amplifier (top left); output characteristics for various strain values (bottom left); optical images of a wavy differential amplifier in its as-fabricated state (top right) and under applied strain in a direction along the red arrow (bottom right).

patterns of relief by nonlinear buckling processes. The location of the neutral mechanical plane in the device layers, as noted previously, facilitates the nondestructive bending that is required to form these wavy patterns. Circuits in this geometry offer fully reversible stretchability/compressibility without substantial strains in the circuit materials themselves. Instead, the amplitudes and periods of the wave patterns change to accommodate applied strains (ε_{appl}, in any direction in the plane of the circuit), with physics similar to an accordion bellows (*23*). Figure 1D presents an optical image of a wavy Si-CMOS circuit on PDMS, formed with a biaxial prestrain of ~5.7%. The thickness of the PDMS can be selected to achieve any desired level of flexural rigidity, without compromising stretchability.

The left, middle, and right frames of Fig. 2A show optical micrographs of wavy Si-CMOS inverters formed with ε_{pre} = 2.7%, 3.9%, and 5.7%, respectively. The wave structures have complex layouts associated with nonlinear buckling physics in a mechanically heterogeneous system. Three features are notable. First, the waves form most readily in the regions of smallest flexural rigidity: the interconnect lines between the p-MOSFET and n-MOSFET sides of the inverter and the electronically inactive parts of the circuit sheet. Second, as ε_{pre} increases, the wave structures begin to extend from these locations to all parts of the circuit, including the comparatively rigid device regions. Third, the etch holes, representative ones of which appear near the centers of these images, have a strong influence on the waves. In particular, waves tend to nucleate at these locations; they adopt wave vectors oriented tangential to the perimeters of the holes as a result of the traction-free edges at these locations. Cracks form, most commonly in the metal electrodes near the etch holes, when local strains rise to levels ~1 to 2% greater than the local prestrain. The maximum prestrain is ~10% (fig. S4); higher values lead to cracking upon release. The first two behaviors can be quantitatively captured using analytical treatments and FEM simulation, the third by FEM. Analysis indicates, for example, that the p-MOSFET and n-MOSFET regions (SiO_2/metal/SiO_2/Si/PI, ~0.05 μm/0.15 μm/0.05 μm/0.25 μm/1.2 μm) adopt periods between 160 and 180 μm and that the metal interconnects (SiO_2/metal/SiO_2/PI, ~0.05 μm/0.15 μm/0.05 μm/1.2 μm) adopt periods between 90 and 110 μm, all quantitatively consistent with experiment. Figure 2B shows the results of full, three-dimensional (3D) FEM modeling, together with a scanning electron micrograph of a sample. The correspondence is remarkably good, consistent with the deterministic, linear elastic response of these systems. (Slight differences are due to the sensitivity of the buckling patterns to the precise location and detailed shapes of the etch holes and some uncertainties in the mechanical properties of the various layers.) Both the analytics and the FEM indicate that for ε_{pre} up to 10% and 0% < ε_{appl} − ε_{pre} < 10%, the material strains in the device layers remain below 0.4% and 1%, respectively (fig. S4).

Figure 2, C and D, shows images and electrical measurements of inverters under different tensile, uniaxial applied strains, for a wavy circuit fabricated with ε_{pre} = 3.9%. As might be expected, the amplitudes and periods of waves that lie along the direction of applied force decrease and increase, respectively, to accommodate the resulting strains (fig. S5). The Poisson effect causes compression in the orthogonal direction, which leads to increases and decreases in the amplitudes and periods of waves with this orientation, respectively. Electrical measurements indicate that the Si-CMOS inverters work well throughout this range of applied strains. The left frame of Fig. 2D shows measured and simulated transfer curves, with an inset graph that presents the electrical properties of individual n-MOSFET and p-MOSFET devices with channel widths (W) of 300 μm and 100 μm, respectively, to match current outputs, and channel lengths (L_c) of 13 μm. These data indicate effective mobilities of 290 cm^2/Vs and 140 cm^2/Vs for the n- and p-channel devices, respectively; the on/off ratios in both cases are >10^5. The gains exhibited by the inverters are as high as 100 at supply voltages (V_{DD}) of 5V, consistent with circuit simulations that use the individual transistor responses. The right frame of Fig. 2D summarizes the voltage at maximum gain (V_M) for different ε_{appl} along x and y. Tensile strains parallel to the transistor channels (i.e., along y) tend to reduce the compressive strains associated with the wavy structures in these locations (fig. S3). The complex, spatially varying strain distributions and the practical difficulties associated with probing the devices make simple explanations for the associated changes in electrical properties elusive. They also frustrate conclusive statements on the slightly different observed strain sensitivities of the p-channel and n-channel devices (fig. S5). Generally, we speculate that the overall tensile and compressive strains in these systems increase and decrease the electron mobility, respectively, with opposite effects on hole mobility (*24*–*26*), consistent with analysis of measured transistor data using standard long-channel MOS device models (*27*). Tensile strains in the x direction (i.e., perpendicular to the channels) cause opposite mechanical strains, due to the Poisson effect, and therefore also opposite changes in the electrical properties. At the level of the inverters, the changes in the transistors cause decreases and increases in V_M with parallel and perpendicular strains, respectively. Individual measurements of the transistors at these various strain states enable simulations of changes in the inverters (fig. S5); the results, also included in the right frame of Fig. 2D, are consistent with experiment. The devices also show good behavior under mechanical/thermal cycling (up to 30 cycles) (fig. S6).

More complex stretchable circuits can be fabricated using these inverters as building blocks. Figure 3A shows optical images, electrical measurements, and stretching tests on Si-CMOS ring oscillators that use three inverters identical to those in Fig. 2. The mechanical responses are qualitatively consistent with considerations described in the discussion of the inverters. The electrical measurements indicate stable oscillation frequencies of ~3.0 MHz at supply voltages of 10 V, even under severe buckling deformations and strains of 5% and larger. The measured frequencies were 2.9 MHz, 3.0 MHz, 3.1 MHz, and 2.9 Mhz for 0%, 2.5%, 5%, and 0% applied strain, respectively. Formulating detailed explanations for these relatively small shifts is difficult, for reasons similar to those outlined in the discussion of the inverters. The expected strain-induced anisotropy in transport (*28*) must also be considered. More general classes of circuits are also possible. Figure 3B shows a differential amplifier (*29*) for a structural health monitor that integrates four components: a current source (three transistors with L_c = 30 μm and W = 80 μm), a current mirror (two transistors with L_c = 40 μm, W = 120 μm; and L_c = 20 μm, W = 120 μm), a differential pair (two transistors with L_c = 30 μm and W = 180 μm), and a load (two transistors

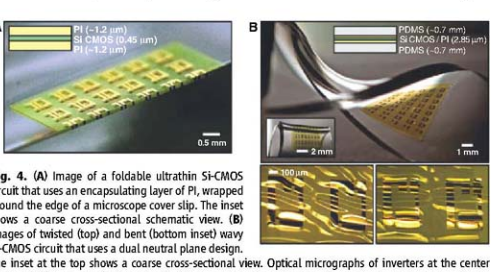

Fig. 4. (A) Image of a foldable ultrathin Si-CMOS circuit that uses an encapsulating layer of PI, wrapped around the edge of a microscope cover slip. The inset shows a coarse cross-sectional schematic view. **(B)** Images of twisted (top) and bent (bottom inset) wavy Si-CMOS circuit that uses a dual neutral plane design. The inset at the top shows a coarse cross-sectional view. Optical micrographs of inverters at the center (bottom left) and edge (bottom right) of the sample in the twisted configuration shown in the top frame.

with $L_c = 40$ μm and $W = 80$ μm). The right frame shows an optical image of the corresponding wavy circuit (fig. S7). This amplifier is designed to provide a voltage gain of ~1.4 for a 500-mV peak-to-peak input signal. Measurements at various tensile strains along the red arrow show gains that vary by less than ~20%: 1.01 without applied strain (0%s, black), 1.14 at 2.5% strain (red), 1.19 at 5% strain (blue), and 1.08 after release (0%e, green).

Although the ultrathin and wavy circuit designs described above provide unusually good mechanical properties, two additional optimizations can enable further improvements. Dominant failure modes observed at high applied strains ($\varepsilon_{appl} - \varepsilon_{pre} > \sim 10\%$) or degrees of bending ($r < \sim 0.05$ mm) are caused by delamination of the device layers and/or fracture of the metal interconnects. A simple design modification that addresses these failures involves the deposition of an encapsulating layer on top of the completed circuits. Figure 4 illustrates a representative layout that includes a thin (~1.2 μm) layer of PI on top of an ultrathin Si-CMOS/PI circuit. The resulting systems are extremely bendable, which we refer to as foldable, as demonstrated in the PI/Si-CMOS/PI circuit tightly wrapped over the edge of a microscope cover slip (thickness ~100 μm) in Fig. 4A. Even in this configuration, the inverters are operational and exhibit good electrical properties (fig. S8). Such foldability is enabled by the good adhesion of the PI layer and its encapsulation of the underlying layers preventing their delamination. Also, the PI layer shifts the metal interconnects at the neutral mechanical plane without moving this plane out of the silicon layers in other regions of the circuits (fig. S8). Such designs can also be incorporated in wavy configurations to enable stretchability/compressibility. The stretchable system presents, however, another challenge. As mentioned previously, the bendability of the Si-CMOS/PI/PDMS is influenced strongly by the thickness of the PDMS. Systems that are both stretchable and highly bendable require the use of thin PDMS. Relaxing the prestrain when using a thin PDMS substrate, however, results in an unwanted, overall bowing of the system rather than the formation of wavy circuit structures. This response occurs because of the very low bending stiffness of thin PDMS, which in turn results from the combined effects of its small thickness and extremely low modulus compared with the PI/Si-CMOS/PI. Neutral mechanical plane concepts that involve the addition of a compensating layer of PDMS on top of the PI/Si-CMOS/PI/PDMS system can avoid this problem. Figure 4B illustrates this type of fully optimized, dual neutral mechanical plane layout (i.e., PDMS/PI/Si-CMOS/PI/PDMS) and its ability to be stretched and bent. The optical micrographs at the bottom left and right of Fig. 4B illustrate the various configurations observed under extreme twisting and stretching of this system.

The strategies presented here demonstrate the degree to which extreme mechanical properties (i.e., stretchability and foldability) can be achieved in fully formed, high-performance integrated circuits by the use of optimized structural configurations and multilayer layouts, even with intrinsically brittle but high-performance inorganic electronic materials. In this approach, the desired mechanical properties are enabled by materials (e.g., PDMS, thin PI, and their multilayer assemblies) that do not need to provide any active electronic functionality. Such designs offer the possibility of direct integration of electronics with biological systems, medical prosthetics and monitoring devices, complex machine parts, or with mechanically rugged, lightweight packages for other devices. Further development of the mechanical concepts to provide, for example, expanded ranges of stretchability (*30*), to extend such electronic systems to other material types, and to exploit them in new classes of devices all appear to represent promising directions for future research.

References and Notes

1. R. Reuss *et al.*, *Proc. IEEE* **93**, 1239 (2005).
2. T. Someya *et al.*, *Proc. Natl. Acad. Sci. U.S.A.* **101**, 9966 (2004).
3. X. Lu, Y. Xia, *Nat. Nanotechnol.* **1**, 163 (2006).
4. A. Dodabalapur, *Mater. Today* **9**, 24 (2006).
5. B. Crone *et al.*, *Nature* **403**, 521 (2000).
6. Y. Sun, J. A. Rogers, *Adv. Mater.* **19**, 1897 (2007).
7. M. Wu, X. Z. Bo, J. C. Sturm, S. Wagner, *IEEE Trans. Electr. Dev.* **49**, 1393 (2002).
8. M. C. McAlpine *et al.*, *Nano Lett.* **3**, 1531 (2003).
9. D. V. Talapin, C. B. Murray, *Science* **310**, 86 (2005).
10. H. O. Jacobs, A. R. Tao, A. Schwartz, D. H. Gracias, G. M. Whitesides, *Science* **296**, 323 (2002).
11. H.-C. Yuan, Z. Ma, M. M. Roberts, D. E. Savage, M. G. Lagally, *J. Appl. Phys.* **100**, 013708 (2006).
12. J.-H. Ahn *et al.*, *Science* **314**, 1754 (2006).
13. T. Serikawa, F. Omata, *Jpn. J. Appl. Phys.* **39**, 1393 (2000).
14. S. P. Lacour, J. Jones, S. Wagner, T. Li, Z. Suo, *Proc. IEEE* **93**, 1459 (2005).
15. D. Y. Khang, H. Jiang, Y. Huang, J. A. Rogers, *Science* **311**, 208 (2006).
16. Y. Sun, V. Kumar, I. Adesida, J. A. Rogers, *Adv. Mater.* **18**, 2857 (2006).
17. Y. Sun, J. A. Rogers, *J. Mater. Chem.* **17**, 832 (2007).
18. S. Mack *et al.*, *Appl. Phys. Lett.* **88**, 213101 (2006).
19. C.-H. Lee *et al.*, *IEEE Int. Electron. Devices Meet.* **2006**, 295 (2006).
20. E. Menard, K. J. Lee, D. Y. Khang, R. G. Nuzzo, J. A. Rogers, *Appl. Phys. Lett.* **84**, 5398 (2004).
21. M. A. Meitl *et al.*, *Nat. Mater.* **5**, 33 (2006).
22. V. D. da Silva, *Mechanics and Strength of Materials* (Springer, New York, 2005).
23. H. Jiang *et al.*, *Proc. Natl. Acad. Sci. U.S.A.* **104**, 15607 (2007).
24. S. E. Thompson *et al.*, *IEEE Trans. Electr. Dev.* **51**, 1790 (2004).
25. S. Maikap *et al.*, *IEEE Int. Electron. Devices Meet.* **2004**, 233 (2004).
26. V. Moroz *et al.*, *Mat. Sci. Semicond. Processing* **6**, 27 (2003).
27. S. G. Streetman, S. K. Banerjee, *Solid State Electronic Devices* (Pearson, New Jersey, 1981).
28. P. Servati, A. Nathan, *Proc. IEEE* **93**, 1257 (2005).
29. J.-H. Ahn *et al.*, *Appl. Phys. Lett.* **90**, 213501 (2007).
30. Y. Sun, W. M. Choi, H. Jiang, Y. Huang, J. A. Rogers, *Nat. Nanotechnol.* **1**, 201 (2007).
31. Here, the tensile strains and applied strains are the global strains defined by the percentage change of substrate length.

32. We thank T. Banks and K. Colravy for help with processing. The materials parts of this effort were supported by the U.S. Department of Energy (DoE), Division of Materials Sciences under award DE-FG02-07ER46471, through the Materials Research Laboratory (MRL). The general characterization facilities were provided through the MRL with support from the University of Illinois and from DoE grants DE-FG02-07ER46453 and DE-FG02-07ER46471. The mechanics theory and the transfer printing systems were developed under support from the Center for Nanoscale Chemical Electrical Mechanical Manufacturing Systems at the University of Illinois (funded by the NSF under grant DMI-0328162).

Supporting Online Material

www.sciencemag.org/cgi/content/full/1154367/DC1
Materials and Methods
Figs. S1 to S8

19 December 2007; accepted 10 March 2008
Published online 27 March 2008;
10.1126/science.1154367
Include this information when citing this paper.

Near-Field Plates: Subdiffraction Focusing with Patterned Surfaces

Anthony Grbic,[1]* Lei Jiang,[2] Roberto Merlin[2]

Using a patterned, grating-like plate to control the electromagnetic near field, we demonstrate focusing well beyond the diffraction limit at ~ 1 gigahertz. The near-field plate consists of only capacitive elements and focuses microwaves emanating from a cylindrical source to a spot of size ≈ λ/20 (half-power beamwidth), where λ is the free-space wavelength. These plates will find application in antennas, beam-shaping devices, nonradiative wireless power-transfer systems, microscopy, and lithography.

Since it was first proposed to use subwavelength apertures to obtain resolutions beyond the diffraction limit (*1*), the electromagnetic near field has enjoyed continued scientific interest. Much of the current attention stems from the work showing that a negative refractive index slab behaves as a perfect lens by focusing both the near- and far-field components emanating from a source (*2*). Following this work, negative refractive index and negative permittivity (*3*–*6*)

superlenses have been experimentally verified at microwave, infrared, and optical frequencies. Recently, a related but alternative approach was introduced, which relies on patterned, grating-like surfaces, to obtain subwavelength resolutions (*7*, *8*). These surfaces, referred to as near-field plates, can be implemented at arbitrary frequencies. We now present a microwave implementation of this approach.

A near-field plate is a subwavelength-structured device that acts as a modulated, nonperiodic surface reactance (it consists of only inductive and capacitive elements). The surface reactance is designed to set up a highly oscillatory electromagnetic field that converges at a prescribed focus in the near field. Depending on their design, near-field plates can focus the field of a plane wave (*8*) or, as shown here, a finite source. Further, they can be tailored to produce focal patterns of various symmetries and shapes. As compared with slabs with negative material parameters, near-field plates only require single-layer processing. The plate reported here was fabricated through standard photolithographic methods.

Given that near-field plates provide strong spatial confinement of electromagnetic waves, they hold promise for near-field sensor and microscopy applications, as well as nonradiative wireless power transference (*9*) and beam-shaping millimeter-wave and optical devices. Methods for confining electromagnetic energy to subwavelength dimensions have been extensively studied in near-field microscopy (*10*–*12*). In particular, near-field probes such as tapered waveguide apertures and metallic and dielectric tips have been used (*13*). Near-field plates offer some distinct advantages over these methods. Unlike conventional probes, the spatial spectrum of the focus can be easily manipulated, because it is determined by the plate's patterned surface. Moreover, near-field plates offer a larger operating distance (a depth of focus) (*7*). The extended spatial spectrum provided by standard near-field probes is only available very close to the small tip or aperture, as a result of the strong divergence of the radiation. In contrast, near-field plates expand the region of the extended spatial spectrum to a length scale, which is, in practice, comparable to that of the resolution. Finally, we note that, similar to slabs with negative material parameters and metallic tips, near-field plates can resonantly amplify the field at the plate's surface and therefore at its focal plane (*8*).

There are four basic steps to design a near-field plate (*8*). The first step is to use back-propagation to find the field at the surface of the plate (aperture field) that produces the desired focal pattern. Back-propagation consists of phase-reversing the propagating spectrum and restoring the evanescent spectrum (*7*, *8*). The second step involves finding the current density on the plate needed to produce the desired aperture field, which is computed by solving an integral equation representing the boundary condition at the plate's surface (*8*). Next, the required surface impedance of the plate is found by taking the ratio of the aperture field to the current density. Lastly, a physical implementation of the surface impedance is realized. This final step requires careful design consideration and the proper choice of material parameters, appropriate to the frequency of operation.

The experimental setup (Fig. 1) results in a field that is two dimensional (2D). In our geometry, the electric field depends on the coordinates y (parallel to the plate) and z (normal to the plate) but does not vary in the x direction (the direction of field polarization, parallel to the antenna). In (*7*), it was shown that an aperture field of the form

$$f(y, z = 0) = M(y)e^{iq_0 y} \qquad (1)$$

can focus in the near field, where $f(y, z = 0)$ is the aperture field, $M(y)$ is a function that has one or more poles with nonzero components in the spatial complex plane, i is the imaginary unit, and q_0 is a constant related to the resolution Δy through

$$\Delta y \sim \frac{2\pi}{q_0} \qquad (2)$$

In the case where $M(y)$ has a single pole, its imaginary component defines the focal length. The aperture field we consider here is given by the following expression

$$f(y, z = 0) = \frac{L[L\cos(q_0 y) + y\sin(q_0 y)]}{[L^2 + y^2]} \qquad (3)$$

This aperture field was shown in (*8*) to produce a focus at a distance $z = L$ from the plate, with the field profile

$$f(y, z = L) \approx e^{-q_0 L} q_0 L \frac{\sin(q_0 y)}{q_0 y} \qquad (4)$$

which has a null-to-null beamwidth of $\Delta y = \frac{2\pi}{q_0}$.

A passive near-field plate was then designed to produce the aperture field of Eq. 4. Specifically, the designed near-field plate focuses the field emanating from s-polarized, electric field components $E_y = E_z = 0$, cylindrical source (the dipole antenna in Fig. 1) oscillating at 1.027 GHz to a subwavelength focus with a full width at half maximum (FWHM) of $\lambda/18$. This value should be compared with $\lambda/2.78$ for the diffraction-limited case. The positions of the focal plane and antenna were both chosen to be at a distance of $L = \lambda/15$ from the near-field plate, as shown in Fig. 1. The near-field plate was designed to operate in a parallel-plate waveguide environment (a 2D scattering chamber). In accordance with image theory, the top and bottom ground planes act as mirrors and make the finite-height near-field plate and the source appear as though they were infinite in the x direction. The microwave source used in the experiments was a coaxially fed thin wire dipole antenna, which acted as a vertical line current. The outer conductor of the coaxial feed was attached to the bottom ground plane, whereas the center conductor, which acted as the dipole antenna, was attached to the top ground plane. The width of the near-field plate, in the y direction,

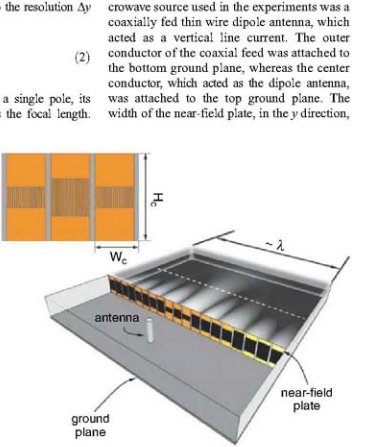

Fig. 1. Schematic showing the experimental setup. The figure shows the coaxially fed dipole antenna (cylindrical source) and near-field plate inside a parallel-plate waveguide. The top ground plane has been removed for clarity. The near-field plate consists of an array of interdigitated capacitors printed on an electrically thin microwave substrate. Also shown is a contour plot of the simulated electric field on the image side (logarithmic scale). The dashed white line denotes the focal plane. The three central elements of the near-field plate are shown in the inset; H_c = 15.0 mm, W_c = 7.5 mm.

[1]Radiation Laboratory, Department of Electrical Engineering and Computer Science, University of Michigan, Ann Arbor, MI 48109–2122, USA. [2]Frontiers in Optical Coherent and Ultrafast Science Center and Department of Physics, University of Michigan, Ann Arbor, MI 48109–1040, USA.

*To whom correspondence should be addressed. E-mail: agrbic@umich.edu

was chosen to be roughly one free-space wavelength: $W = 292.2$ mm.

The current density on the near-field plate was obtained from the aperture field E_{ap} (Eq. 3), by numerically evaluating the integral equation (*14*)

$$E_{ap} = \frac{iM_0|E_{inc}(y=0)|L\cos(q_0 y) + y\sin(q_0 y)]}{[L^2+y^2]} = E_{inc}(y) - \frac{k_0\eta_0}{4}\int_{-W/2}^{W/2} J_x(y')H_0^{(2)}[k_0|y-y'|]dy' \quad (5)$$

which represents the boundary condition at the surface of the near-field plate (*8*). Here, $\eta_0 = 120\pi$ ohms is the wave impedance of free space, $k_0 = 2\pi/\lambda$, J_x is the current density on the plate, M_0 is an amplification factor, and $E_{inc}(y)$ is the electric field incident on the near-field plate from the antenna

$$E_{inc}(y) = \frac{k_0\eta_0 I_x}{4}H_0^{(2)}(\sqrt{y^2+L^2}) \quad (6)$$

where I_x is the current amplitude of the antenna and $H_0^{(2)}$ is the zeroth-order Hankel function of the second kind (a time-harmonic progression of $e^{i\omega t}$ is assumed, where ω is the radial frequency and t is the time). The desired surface impedance, η_{sheet}, was found by taking the ratio of the aperture field to the current density: $\eta_{sheet}(y) = E_{ap}(y)/J_x(y)$.

For this particular near-field plate design, the amplification factor was set to $M_0 = 2$ and $q_0 = 10k_0$ to yield a resolution of $\approx \lambda/20$. To emulate a continuously varying surface impedance, we discretized the plate into $n = 39$ separate elements of width $W_e \approx \lambda/40$ and height $H_e \approx \lambda/20$ (Fig. 1). We determined the impedance of each element (Z_{sheet}) using the properly normalized surface impedance (η_{sheet}) evaluated at the center of each strip from Eq. 5: $Z_{sheet}(n) = \eta_{sheet}(n) \cdot (\frac{H_e}{W_e})$. The impedance elements found through this procedure are all capacitive (*15*). This was expected, given that the mutual impedance matrix defining the electromagnetic interaction between the impedance elements is predominantly inductive for *s*-polarized radiation. These inductive mutual impedances resonate with the capacitive impedances Z_{sheet} and result in an aperture field that is $M_0 = 2$ times higher in amplitude than the field incident on the plate.

The near-field plate was implemented as an array of interdigitated copper capacitors printed on an electrically thin microwave substrate, as shown in Fig. 1 (*15*). The operating frequency of the fabricated near-field plate was 1.027 GHz, which was 2.7% higher than the design frequency of 1.0 GHz. This frequency difference is consistent with etching tolerances associated with the fabrication of the near-field plate, as well as with variations in the parallel-plate waveguide height in which it was tested.

Figure 2, A and B, shows contour plots of the experimental and calculated electric field at the operating (1.027 GHz) and design (1.0 GHz) frequencies, respectively. The electric field amplitude has been normalized to its largest value at a given z. The plots show very good agreement between the measurements and finite element computations, which took into account all electromagnetic interactions as well as the losses associated with the finite conductivity of the capacitors. The relative magnitude of the electric field contour is the same for both plots, and the minima and maxima of the highly oscillatory field between the plate and focal plane show very good agreement between the simulation and the experiment. Figure 2C compares the simulated and measured electric field intensity along the focal plane, located roughly at $\lambda/15$ (2.0 cm) from the near-field plate. The main peaks in the two plots exhibit a FWHM of $\lambda/18$. Fourier transforming the experimental focus reveals that it is composed of spatial frequencies in the range $-10k_0 < k_y < 10k_0$. To emphasize the narrowness of the focus, we plotted an additional curve illustrating what the beamwidth of the electric field would be if the near-field plate were not present. The resolution (FWHM of the focus) was found to decrease from its best value of $\lambda/20.0$ at 1.025 GHz to $\lambda/9.3$ at 1.065 GHz (*15*). At frequencies below 1.025 GHz, the focal pattern exhibited multiple peaks.

This work demonstrates the feasibility of implementing passive surfaces that can focus microwave electromagnetic energy to extreme subwavelength dimensions. At infrared and visible light frequencies, such structures could be implemented with plasmonic (inductive) and dielectric (capacitive) materials (*16*).

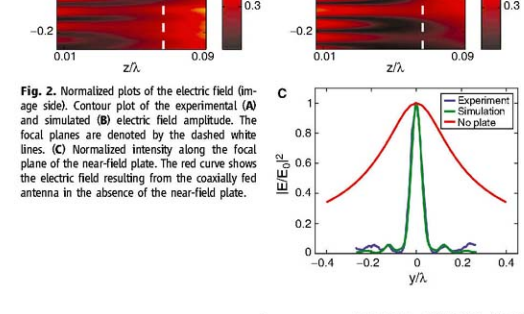

Fig. 2. Normalized plots of the electric field (image side). Contour plot of the experimental (**A**) and simulated (**B**) electric field amplitude. The focal planes are denoted by the dashed white lines. (**C**) Normalized intensity along the focal plane of the near-field plate. The red curve shows the electric field resulting from the coaxially fed antenna in the absence of the near-field plate.

References and Notes

1. E. H. Synge, *Philos. Mag.* **6**, 356 (1928).
2. J. B. Pendry, *Phys. Rev. Lett.* **85**, 3966 (2000).
3. A. Grbic, G. V. Eleftheriades, *Phys. Rev. Lett.* **92**, 117403 (2004).
4. T. Taubner, D. Korobkin, Y. Urzhumov, G. Shvets, R. Hillenbrand, *Science* **313**, 1595 (2006).
5. N. Fang, H. Lee, C. Sun, X. Zhang, *Science* **308**, 534 (2005).
6. D. Melville, R. Blaikie, *Opt. Express* **13**, 2127 (2005).
7. R. Merlin, *Science* **317**, 927 (2007).
8. A. Grbic, R. Merlin, *IEEE Trans. Antennas Propag.*, in press; preprint available at http://arxiv.org/abs/0708.0049.
9. A. Kurs *et al.*, *Science* **317**, 83 (2007).
10. E. A. Ash, G. Nicholls, *Nature* **237**, 510 (1972).
11. D. W. Pohl, W. Denk, M. Lanz, *Appl. Phys. Lett.* **44**, 651 (1984).
12. A. Lewis, M. Isaacson, A. Harootunian, A. Murray, *Ultramicroscopy* **13**, 227 (1984).
13. L. Novotny, B. Hecht, *Principles of Nano-Optics* (Cambridge Univ. Press, Cambridge, 2006).
14. R. F. Harrington, *Field Computation by Moment Methods* (Institute of Electrical and Electronics Engineers, Piscataway, NJ, 1993).
15. The details of the near-field plate design, measurement methods, and frequency-dependent resolution are available as supporting material on *Science* Online.
16. N. Engheta, A. Salandrino, A. Alu, *Phys. Rev. Lett.* **95**, 095504 (2005).

17. The authors thank C. Pfeiffer and S.M. Rudolph for their technical assistance and Saturn Electronics for the fabrication of the printed circuit boards. This work was supported by an Air Force Office of Scientific Research (AFOSR) Young Investigator Research Program Award (FA9550-08-1-0062), a NSF Faculty Early Career Development Award (ECCS-0747623), and AFOSR grants FA9550-07-1-0029 and FA9550-06-01-0279 through the Multidisciplinary University Research Initiative Program.

Supporting Online Material

www.sciencemag.org/cgi/content/full/320/5875/511/DC1
Materials and Methods
SOM Text
Figs. S1 to S3
Table S1
References

2 January 2008; accepted 7 March 2008
10.1126/science.1154753

Ancient Asteroids Enriched in Refractory Inclusions

J. M. Sunshine,[1]* H. C. Connolly Jr.,[2,3,4] T. J. McCoy,[5] S. J. Bus,[6] L. M. La Croix[5,7]

Calcium- and aluminum-rich inclusions (CAIs) occur in all classes of chondritic meteorites and contain refractory minerals predicted to be the first condensates from the solar nebula. Near-infrared spectra of CAIs have strong 2-micrometer absorptions, attributed to iron oxide–bearing aluminous spinel. Similar absorptions are present in the telescopic spectra of several asteroids; modeling indicates that these contain ~30 ± 10% CAIs (two to three times that of any meteorite). Survival of these undifferentiated, large (50- to 100-kilometer diameter) CAI-rich bodies suggests that they may have formed before the injection of radiogenic ^{26}Al into the solar system. They have also experienced only modest post-accretionary alteration. Thus, these asteroids have higher concentrations of CAI material, appear less altered, and are more ancient than any known sample in our meteorite collection, making them prime candidates for sample return.

Calcium- and aluminum-rich inclusions (CAIs) found within all chondritic meteorites are arguably the oldest rocks in our collections and are used to define the start of the solar system (*1*). These millimeter-to-centimeter size objects contain refractory minerals that are the first phases predicted to condense from a gas of solar (or enhanced solar) composition. The highest abundance of CAIs is found in CO chondrites (<13 volume %), but CV3 chondrites contain the most diverse range of CAI types with abundances of up to 10 volume % (*2*). Burbine *et al.* (*3*) identified CAIs on two dynamically related asteroids, 387 Aquitania and 980 Anacostia, that they argued contain CAI abundances of 5 to 10%, similar to that observed in CV3 meteorites. Because the early solar nebula evolved quickly and was spatially heterogeneous, it is reasonable to assume that asteroids with higher concentrations of CAIs should exist. Here, we provide evidence for the existence of several such CAI-rich asteroids from multiple parent bodies.

Near-infrared telescopic spectral surveys have widely been used to identify mafic silicates on the surfaces of asteroids and to infer the composition of the asteroid population as a whole. The only mineral contained in CAIs that has strong absorptions in the 1- to 2-μm region is aluminous spinel ($MgAl_2O_4$, sensu stricto). If aluminous spinel (in solid solution with hercynite, $FeAl_2O_4$) contains as little as tenths of a weight percent of FeO, its spectrum includes a strong, characteristic 2-μm absorption feature. In the absence of abundant mafic minerals, CAIs can thereby be remotely identified on asteroid surfaces (*4*).

CAIs are generally classified, on the basis of petrography and geochemistry, into three major groups: type As, Bs, and Cs (*5*). Of these, only fluffy type As (FTAs) were not melted by a transient heating event before accretion (*6*). Type As and related inclusions are found in all classes of chondrites and are therefore thought to have been well dispersed within the asteroid accretion zone. Refractory minerals similar to those found in FTAs have also been identified in a Stardust sample collected from comet 81P/Wild 2, providing evidence that these materials were widely distributed throughout the solar system (*7*). Recent models of the evolution of protoplanetary disks predict widespread, outward transport of such high-temperature materials around the midplane (*8*). In contrast, type Bs and Cs are restricted to CV3 meteorites and more likely represent localized processing of minerals within restricted portions of the nebula (*9*).

To support our analysis of asteroid spectra, we collected representative spectra from CAIs within the Allende CV3 meteorite (Fig. 1) (*10*). Spectra of three type Bs, three FTAs, and one amoeboid olivine aggregate (AOA) were collected (Fig. 2). The major minerals in FTAs are melilite and spinel, often with abundant alteration phases such as nepheline and hedenbergite, whereas type Bs contain spinel, melilite, fassaite, anorthite, and minor amounts of alteration phases. Both types have minor and varying amounts of perovskite, hibonite, and metal phases. The spectra of both FTA and type B CAIs are dominated by absorptions at 2 μm. However, the spectra of FTAs exhibit much stronger 2-μm absorption features than do the spectra of type Bs. This stronger absorption is consistent with the higher FeO concentrations in aluminous spinels in FTAs: ~3 to 14 weight percent (wt %) compared with < 0.4 wt % in type Bs. Given that abundant FeO is effectively excluded from CAI minerals during condensation, the FeO must have been introduced into the CAIs during an alteration event. Although some FeO can be introduced into type A and B CAIs through gas/solid exchange within the nebula, the observed correlation between FeO content in spinel and the abundance of alteration phases between CAI-types imply that the FeO enrichment is dominantly post-accretionary.

To verify the identifications of Burbine *et al.* (*3*) and locate additional spinel-rich asteroids, we combined visible spectra (*11*, *12*) and near-infrared data obtained with the SpeX instrument at the NASA Infrared Telescope Facility (*13*). SpeX data of Aquitania and Anacostia are

Fig. 1. Smithsonian sample 3509 of the CV3 meteorite Allende sawed into ~1-cm-thick slabs (a centimeter-sized cube marked "1" is included for scale). Refractory inclusions suitable for both thin sectioning and crushing into powders were identified as shown here for slabs 5 and 6. After recording their locations, CAIs were cored out from slabs, and both thin sections and thick butts were produced. Part of the remaining sample was carefully excavated to avoid contamination from matrix materials and crushed into powders for spectral measurements.

[1]Department of Astronomy, University of Maryland, College Park, MD 20742, USA. [2]Department of Physical Sciences, Kingsborough Community College of the City University of New York, Brooklyn, NY 11235, USA. [3]Lunar and Planetary Laboratory, University of Arizona, Tucson, AZ 85721, USA. [4]Department of Earth and Planetary Sciences, American Museum of Natural History, New York, NY 11024, USA. [5]Department of Mineral Sciences, National Museum of Natural History, Smithsonian Institution, Washington, DC 20560, USA. [6]Institute for Astronomy, University of Hawaii, Hilo, HI 96720, USA. [7]Department of Geological Sciences and Engineering, University of Nevada, Reno, NV 89557, USA.

*To whom correspondence should be addressed. E-mail: jess@astro.umd.edu

dominated by a strong 2-μm absorption feature and confirm the previous data (Fig. 3A). On the basis of their unique compositions and general location, it was suggested that these two asteroids (100- and 85-km diameter, respectively) are genetically related (*3*). Shortward of 0.75 μm, the spectra of these two asteroids are also strongly red-sloped, as are a larger number of nearby objects (*14*). This cluster of asteroids, including Aquitania and Anacostia, was proposed as the Watsonia family (*15*). We measured the near-infrared spectra of other members of the Watsonia family. Some, in particular 599 Luisa (Fig. 3B), have spectra that include strong 2-μm absorptions, supporting the hypothesis of a breakup of a larger body.

Visible data also suggest a second group of strongly sloped asteroids, the Henan family (*15*), which was originally identified dynamically (*16*). Near-infrared SpeX data of ~10 much smaller (10 to 15 km), and thus fainter, Henan family asteroids also contain 2-μm absorptions (Fig. 3B), suggesting the existence of a second spinel-rich asteroid family. In addition, we have identified a third spinel-rich body, the 45-km diameter asteroid 234 Barbara (*17*). The spectrum of Barbara is dominated by a strong 2-μm absorption, similar to those of Anacostia and Aquitania (Fig. 3B).

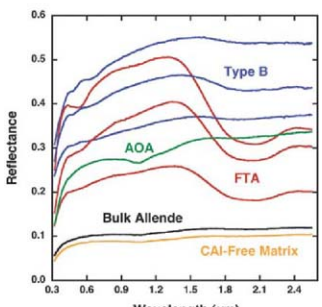

Fig. 2. Spectra of Allende components. CAIs include FTAs (red), type Bs (blue), and an AOA (green). Spectra of CAI-free matrix materials (orange) and a bulk Allende sample (*21*) (black) are also shown. All samples are of <38-μm powders and were measured at RELAB, Brown University's NASA-Keck facility (*40*).

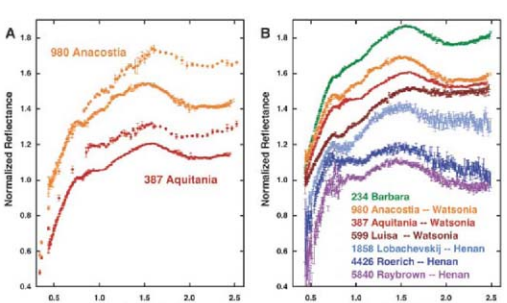

Fig. 3. (**A**) Visible near-infrared spectra of asteroids 387 Aquitania (red) and 980 Anacostia (orange) from Burbine *et al.* (*3*) compared with the current higher–spectral resolution Small Main-Belt Asteroid Spectroscopic Survey (SMASSII) (visible) (*11*, *12*) and SpeX (near-infrared) (*13*) data. (**B**) Combined SMASSII and SpeX data for the asteroid 234 Barbara (green) and representative asteroids from the Watsonia and Henan families (table S1). All spectra are dominated by strong 2-μm absorptions. The observing conditions for these data and other members of the Watsonia and Henan families are given in table S1.

Although they favored a link between spinel-rich asteroids and CAIs, Burbine *et al.* (*3*) could not definitively rule out an alternative spectral interpretation: that the spinel was igneous in origin and due to the spinel group mineral chromite ($FeCr_2O_4$). Spectra of FeO bearing aluminous spinels are distinct from that of chromites (*18*, *19*). Chromite spectra include a strong absorption at 1.3 μm, and the reflectance is lower from 2 to 2.5 μm than it is for FeO-bearing aluminous spinels. Spectra of Watsonia and Henan family members and Barbara lack strong 1.3-μm features and increase in reflectance beyond 2.1 μm. Therefore, we conclude that the asteroids contain FeO in aluminous spinel rather than chromite. The strong 2-μm absorptions in these asteroid spectra do not require that the asteroids are dominated by aluminous spinel but rather that spinel is the only mineral with significant near-infrared absorptions. In meteorites, abundant aluminous spinels are only observed in CAIs, and spinel is the only phase in CAIs that has strong near-infrared absorption features (*20*); yet in Allende, CAIs contain only 10 to 30 volume % aluminous spinels.

To further test the link between CAIs and aluminous spinel-rich asteroids and to determine the abundance of CAI materials on these asteroids, we modeled the asteroid spectra using endmembers collected from Allende. In addition to the spectra of FTAs and type B CAIs (Fig. 2), we measured spectra of a sample of matrix materials extracted from Allende. We first used these CAIs and CAI-free matrix spectral endmembers to model the spectrum of an aliquot taken from the Allende standard reference powder, a homogenized 2.6-kg sample of the bulk meteorite (*21*). Modeling the bulk Allende powder requires the use of radiative transfer theory to account for the multiple scattering among particles that are intimately mixed. This nonlinear effect is addressed with Hapke radiative transfer theory (*22*), which can be used to convert reflectance spectra to single-scattering albedo (*23*). As shown in Fig. 4, we were able to reproduce the spectrum of the Allende bulk powder as a combination of CAI-free matrix and either FTA or type B CAIs (or more likely a combination of both). In the least-squares solution, the bulk Allende spectrum can be modeled with 11% FTA and 89% CAI-free matrix or 10% type B CAIs and 90% CAI-free matrix. These derived abundances of ~10% CAIs are in excellent agreement with the known abundance of CAIs in CV3 meteorites (*2*).

Burbine *et al.* (*3*) argued that the regoliths of Aquitania and Anacostia are relatively immature and that intact CAIs would thus be preserved on their surfaces. With these assumptions, they modeled their asteroid spectra as linear combinations of a CAI and bulk Allende and derived a CAI abundance of 5 to 10%. Recent flybys of several asteroids indicate that a modern regolith is likely to be composed of a highly comminuted mixture of all materials (*24*–*26*). Furthermore, given the similarity in the strengths of CAIs and matrix materials, it is unlikely that intact CAIs could exist in

present-day regoliths. Therefore, to model spectra of asteroids covered in mature intimately mixed regoliths, we used nonlinear radiative transfer theory (*22*), as we did for our laboratory data of Allende (*23*). We estimated the absolute albedos for Barbara, Aquitania, and Anacostia from measurements made by the Infrared Astronomical Satellite (*27*). The relatively small Henan family asteroids have unknown albedos, and thus the abundance of CAIs on their surfaces cannot be reliably determined with radiative transfer theory.

We initially modeled the asteroid data as nonlinear combinations of CAI-free matrix and either FTAs or type B CAIs. However, it is clear even from visual comparisons (Figs. 2 and 3) that the asteroid spectra are sloped relative to the laboratory data (*28*). To account for this slope in our modeling, we used the spectrum of asteroid 2448 Sholokhov, a member of the Watsonia family, which has a generally featureless but sloped spectrum (fig. S1) (*29*). In addition, it is evident that more olivine is needed (compared with Allende) to explain the 1-μm absorptions in the spectra of the asteroids and to brighten the spectra in the 2-μm region. Despite these additional components, no satisfactory fits to the asteroid spectra are achievable with the use of any combination of materials and type B CAIs (Fig. 5A). With type B CAIs, models for all three asteroid spectra include absorptions at 2 μm that are too weak.

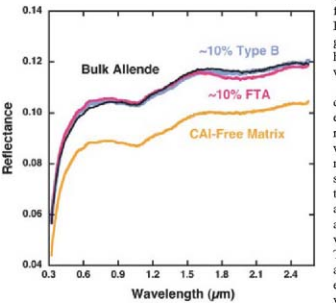

Fig. 4. Spectrally, with the use of radiative transfer theory to account for multiple scattering, bulk Allende (*21*) (black) can be created from the sum of its parts as intimate mixtures of ~90% CAI-free matrix (orange) and ~10% FTA (pink) or ~10% type B CAIs (blue). These spectrally derived abundances are consistent with the percentage of CAIs observed in Allende (*36*).

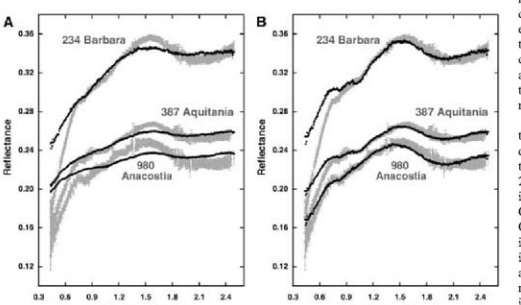

Fig. 5. Radiative transfer models of CAI-rich asteroid spectra using spectral components from Allende (Fig. 4), as described in the text. **(A)** Models using type B CAIs result in poor matches to the asteroid spectra (in particular, the 2-μm absorptions that are too weak). **(B)** Although errors exist in the visible, models with 30 ± 10% FTAs (Table 1) generally match all three asteroid spectra, including the near-infrared absorptions.

Reasonable matches to the spectra of Barbara, Aquitania, and Anacostia—particularly in the near infrared—are achieved with models that include FTAs (Fig. 5B and Table 1). Models of all three asteroid spectra require greater slopes than in the Allende spectra. The relative differences in the slope components among these asteroids, generally well modeled by the spectrum of Sholokhov, probably represent different degrees of space weathering (*28*). The MgO-rich olivine and CAI-free matrix abundances also vary substantially among the asteroids: Barbara has a substantial olivine component, Anacostia requires only CAI-free matrix, and Aquitania has both. Alteration is widespread in almost all primitive planetary materials (*2*), and the variation in olivine content among the asteroids probably reflects differences in their alteration histories. Enrichment in olivine relative to Allende suggests that the asteroids Barbara and Aquitania have experienced less alteration than Allende, whereas Anacostia may be as altered as Allende.

Alteration of most chondrites, which occurs dominantly in accreted bodies and to a lesser extent in gas/solid exchange in the nebula, is also responsible for the enrichments in FeO observed within aluminous spinels in CAIs. FeO in aluminous spinels is essential for producing the observed 2-μm absorptions in their spectra. Whereas the mechanism that mobilized FeO within these apparently unmetamorphosed chondrites remains a mystery, a likely source is the ubiquitous olivine in chondrites that accreted along with CAIs. The specific materials and the timing of accretion affect the extent of such reactions and may explain the variability observed between individual meteorites, even within meteorite groups. This variability also provides a reasonable explanation for the inferred differences in olivine abundance among the CAI-rich asteroids. The FeO enrichment in the CAI minerals within these asteroids is evidence that these objects were aqueously altered and/or thermally metamorphized, although the activity was short-lived and alteration was modest compared with that observed in many chondrites.

Despite these variations in alteration histories that manifest as differences in other spectral components, the near-infrared absorption features of all three asteroids are well modeled with 22 to 39% FTAs. Our modeling therefore indicates that these asteroids contain 30 ± 10% CAIs, substantially more than the 10% seen in CV3 meteorites. Spectrally, these asteroids rich in CAI materials are inconsistent with type B inclusions, which are unique to CV3 meteorites and probably represent localized events in the nebula. Instead, the asteroids appear to be dominated by the minerals contained in type A inclusions, which are ubiquitous in all chondritic classes. The CAI-rich asteroids thus contain both a different distribution and a higher abundance of CAI minerals than CV3 meteorites. Furthermore, we have identified three different CAI-rich parent bodies, including asteroids with diameters of ~50

Table 1. Abundances derived from modeling the spectra of CAI-rich asteroids.

Modeled asteroid	Fluffy type A CAI (hc1)	CAI-free Allende matrix	MgO-rich olivine	Slope (2448 Sholokhov)
234 Barbara	22%	0%	40%	38%
387 Aquitania	25%	16%	26%	33%
980 Anacostia	39%	11%	0%	50%

to 100 km. The CAI-rich asteroids are thus a distinct group of bodies that likely are not represented in our meteorite collection.

The existence of these objects allows us to test hypotheses for the timing of events in the early solar system. If these asteroids had accreted during the first few half-lives of ^{26}Al (~720,000 years) with ~30% CAI material that contains canonical ^{26}Al/^{27}Al ratios, these asteroids would have melted (*30*). Yet melting experiments of carbonaceous chondrites (*31*) show no evidence that aluminous spinel is substantially enriched during melting. This strongly suggests that the CAI-rich asteroids have not undergone substantial melting or differentiation, consistent with their affinity to FTAs. We cannot rule out the possibility that these asteroids accreted with additional materials that prevented igneous differentiation [e.g., abundant ice (*32*)], as the 3-μm spectra of at least one of the asteroids is indicative of minor hydration (*33*). It is also possible that these asteroids experienced an anomalous thermal history related to collisional breakup and reassembly, yet this seems improbable given the number and size of CAI-rich asteroids.

A plausible explanation for the survival of CAI-rich asteroids is that they do not contain canonical ^{26}Al/^{27}Al abundances. Indeed, some refractory inclusions in meteorites contain substantially lower-than-canonical ^{26}Al values or are even devoid of ^{26}Al (*34*), suggesting that ^{26}Al may have been injected into the solar nebula some time after the onset of CAI formation (*35*). The alternative explanation—that the injection of ^{26}Al was spatially variable—is inconsistent with the occurrence of CAI-rich asteroids across the inner mainbelt and the dominance of the ubiquitous FTA-like CAI minerals in these asteroids. If these CAI-rich asteroids accreted from ^{26}Al-poor materials, they may record an early period of solar system history when refractory materials were prevalent but before the injection of ^{26}Al into the solar system. Thus, these asteroids have two to three times more CAI material, appear less altered, and are more ancient than any known sample in our meteorite collection, making them prime candidates for sample return.

References and Notes

1. CAIs have been dated using lead isotopes at 4.566 billion years ago (±2 million years ago)–1 million years ago) by Allègre *et al.* (*36*) and 4.5647 (±0.0006) billion years ago by Amelin *et al.* (*37*).
2. A. J. Brearley, R. H. Jones, in *Reviews In Mineralogy, Vol. 36, Planetary Materials*, J. J. Papike, Ed. (Mineralogic Society of America, Washington, DC, 1998), pp. 3-1–3-398.
3. T. H. Burbine, M. J. Gaffey, J. F. Bell, *Meteorit. Planet. Sci.* **27**, 424 (1992).
4. Other common Fe-bearing silicates that have strong absorptions in the near infrared (*38*). Although pyroxene spectra have absorptions in the 2-μm region, they have even stronger features near 1 μm. Conversely, olivine spectra lack 2-μm absorptions and are instead characterized by a complex feature at 1 μm. It is on this basis (a strong 2-μm absorption in the absence of a stronger 1-μm feature) that spinel is spectrally identified.
5. This nomenclature was primarily designed for use in classifying CAIs from CV3 meteorites. Over the last three decades other descriptive terminology has been developed for other chondrite types (*9*, *39*).
6. H. C. Connolly Jr., S. J. Desch, R. D. Ash, R. H. Jones, in *Meteorites and the Early Solar System II*, D. S. Lauretta, H. Y. McSween Jr., Eds. (Univ. of Arizona Press, Tucson, AZ, 2006), pp. 383–397.
7. M. E. Zolensky *et al.*, *Science* **314**, 1735 (2006).
8. F. J. Ciesla, *Science* **318**, 613 (2007).
9. G. J. MacPherson, D. A. Wark, J. T. Armstrong, in *Meteorites and the Early Solar System*, J. F. Kerridge, M. S. Matthews, Eds. (Univ. of Arizona Press, Tucson, AZ, 1988), pp. 746–807.
10. The Smithsonian Allende sample USNM 3509 was sectioned into large slices, and refractory inclusions were identified and cored. Thin and thick sections were made from half of the objects, and reference materials were preserved for future study. Thin sections were analyzed by the Cameca SX50 electron microprobe at the Lunar and Planetary Laboratory at the University of Arizona to quantify major and minor element abundances. While avoiding contamination from the matrix, material from the other half of the objects was cored out, ground into <38-μm-size powders, and sent to Brown University for spectral measurements at the NASA-Keck Reflectance Experiment Laboratory (RELAB) facility (*40*). All spectra were measured with 5-nm resolution at a standard viewing geometry of 30° incidence, 0° emission.
11. S. Xu, R. P. Binzel, T. H. Burbine, S. J. Bus, *Icarus* **115**, 1 (1995).
12. S. J. Bus, R. P. Binzel, *Icarus* **158**, 106 (2002).
13. J. T. Rayner, P. M. Onaka, M. C. Cushing, C. Michael, W. D. Vacca, *Proc. SPIE* **5492**, 1498 (2004).
14. In the Bus visible asteroid taxonomy, objects with a steep red spectral slope at wavelengths up to 0.75 μm, which are then relatively flat, are classified as L types (*41*).
15. S. J. Bus, thesis, Massachusetts Institute of Technology, (1999).
16. V. Zappalà, Ph. Bendjoya, A. Cellino, P. Farinella, C. Froeschlé, *Icarus* **116**, 291 (1995).
17. Whereas the Henan and Watsonia families are roughly the same distance from the sun, the mean orbits of asteroids making up these two families are markedly different in both eccentricity and inclination. The mean proper elements for the Henan family are ~2.73 astronomical units (AU) (ranging from 2.69 to 2.76 AU), e ~ 0.07, and sin(i) ~ 0.06 (where e is eccentricity and i is inclination), compared with the Watsonia family at ~2.77 AU (ranging from 2.74 to 2.80 AU), e ~ 0.16, and sin(i) ~0.29. This corresponds to a difference in orbital velocity between these families of over 6 km/s, making it highly unlikely these two families can be linked to a single parent body. 234 Barbara is a distinct asteroid located at 2.39 AU.
18. E. A. Cloutis, J. M. Sunshine, R. V. Morris, *Meteorit. Planet. Sci.* **39**, 545 (2004).
19. J. M. Sunshine, E. A. Cloutis, *Lunar Planet. Sci.* **XXXI**, 1640 (1999).
20. E. A. Cloutis, M. J. Gaffey, *Icarus* **105**, 568 (1993).
21. E. Jarosewich, *Meteoritics* **25**, 323 (1990).
22. B. Hapke, *Theory of Reflectance and Emittance Spectroscopy* (Cambridge Univ. Press, New York, 1993).
23. To calculate the single-scattering albedo of each component, we employed Hapke's two-stream approximation assuming no opposition effect, isotropic scattering, and that all components have the same density and particle size (*22*). Once converted to single-scattering albedo, mixing is linear and relative abundances can be estimated using a least-squares solution (*42*, *43*).
24. M. J. S. Belton *et al.*, *Science* **265**, 1543 (1994).
25. J. Veverka *et al.*, *Science* **289**, 2088 (2000).
26. H. Yano *et al.*, *Science* **312**, 1350 (2006).
27. Asteroid spectra are routinely measured relative to a given wavelength, as in Fig. 3, where data are normalized to 0.55 μm. Absolute albedos are obtained from the Infrared Astronomical Satellite (IRAS) Supplemental IRAS Minor Planet Survey database, as archived in the NASA Planetary Data System data set IRAS-A-FPA-3-RDR-IMPS-V6.0.
28. Overall the asteroid spectra are red-sloped; i.e., they increase in reflectance with increasing wavelength. This is typical of asteroid spectra and generally thought to be related to either the presence of opaque phases or weathering in the space environment (*44*, *45*).
29. Although the spectrum of 2448 Sholokhov is not uniquely interpretable, its presence within the same family as several spinel-rich asteroids (the Watsonia family) makes it a stronger candidate for representing spectral slope in modeling these CAI-rich asteroids than any existing theoretical method or potential laboratory analog.
30. A. Das, G. Srinivasan, *Lunar Planet. Sci.* **XXXVIII**, 1338 (2007).
31. A. J. G. Jurewicz, D. W. Mittlefehldt, J. H. Jones, *Geochim. Cosmochim. Acta* **57**, 2123 (1993).
32. R. E. Grimm, H. Y. McSween Jr., *Icarus* **82**, 244 (1989).
33. A. S. Rivkin, D. E. Trilling, J. A. Lebofsky, *Bull. Am. Astron. Soc.* **30**, 1023 (1998).
34. G. J. MacPherson, A. M. Davis, E. K. Zinner, *Meteoritics* **30**, 365 (1995).
35. S. Sahijpal, J. N. Goswami, *Astrophys. J.* **509**, L137 (1998).
36. C. J. Allègre, G. Manhès, C. Göpel, *Geochim. Cosmochim. Acta* **59**, 1445 (1995).
37. Y. Amelin, A. N. Krot, I. D. Hutcheon, A. A. Ulyanov, *Science* **297**, 1678 (2002).
38. J. B. Adams, in *Infrared and Raman Spectroscopy of Lunar and Terrestrial Materials*, C. Karr, Ed. (Academic Press, San Diego, CA, 1975), pp. 91–116.
39. L. Grossman, *Geochim. Cosmochim. Acta* **39**, 433 (1975).
40. C. M. Pieters, T. Hiroi, *Lunar Planet. Sci.* **XXXV**, 1720 (2004).
41. S. J. Bus, R. P. Binzel, *Icarus* **158**, 146 (2002).
42. J. F. Mustard, C. M. Pieters, *J. Geophys. Res.* **92**, E617 (1987).
43. B. E. Clark, *J. Geophys. Res.* **100**, 14443 (1995).
44. B. E. Clark, B. Hapke, C. Pieters, D. Britt, in *Asteroids III*, W. F. Bottke Jr., A. Cellino, P. Paolicchi, R. P. Binzel, Eds. (Univ. of Arizona Press, Tucson, AZ, 2003), pp. 585–599.
45. B. Hapke, *J. Geophys. Res.* **106**, 10039 (2001).

46. This research was funded in part by NASA grants NNX06AH69G (J.M.S.), NNG05GF39G (H.C.C.), and NNG06GF56G (T.J.M. and L.M.L.) and NSF grant AST-0307688 (S.J.B.). We thank T. Hiroi for carefully collecting our spectra of CAIs and Allende samples at RELAB, K. Domanik for assistance with the electron microprobe at Lunar and Planetary Laboratory, and R. Binzel and two anonymous reviewers for suggestions that improved this report.

Supporting Online Material

www.sciencemag.org/cgi/content/full/1154340/DC1
Fig. S1
Table S1
References and Notes

18 December 2007; accepted 6 March 2008
Published online 20 March 2008;
10.1126/science.1154340
Include this information when citing this paper.

Human-Induced Arctic Moistening

Seung-Ki Min, Xuebin Zhang, Francis Zwiers*

The Arctic and northern subpolar regions are critical for climate change. Ice-albedo feedback amplifies warming in the Arctic, and fluctuations of regional fresh water inflow to the Arctic Ocean modulate the deep ocean circulation and thus exert a strong global influence. By comparing observations to simulations from 22 coupled climate models, we find influence from anthropogenic greenhouse gases and sulfate aerosols in the space-time pattern of precipitation change over high-latitude land areas north of 55°N during the second half of the 20th century. The human-induced Arctic moistening is consistent with observed increases in Arctic river discharge and freshening of Arctic water masses. This result provides new evidence that human activity has contributed to Arctic hydrological change.

Arctic and northern subpolar regions play a key role in determining the effects of human-induced forcing of the climate system and are expected to be affected more strongly than other regions. Polar amplification due to meridional heat transport and positive ice-albedo feedback results in more rapid warming at high latitudes than at lower latitudes. Arctic ecosystems, which are very vulnerable to environmental changes, are experiencing the impacts of climate change sooner and more strongly than elsewhere (*1*–*3*). Freshwater inflow into the Arctic Ocean is a critical factor in determining ocean convection in the subarctic seas, affecting the Atlantic Ocean meridional overturning circulation (MOC) and thus the global climate (*4*, *5*).

Observational studies show that precipitation and river discharge have increased in the Arctic region during the past 50 years, together with ocean freshening (*3*, *5*–*7*). Most recent global climate models (GCMs) project northern high-latitude precipitation increases and MOC weakening in the future (*8*). Nevertheless, the question of whether humans have contributed to the observed Arctic precipitation increase has, until now, remained unanswered.

Human influence on the climate has been detected in surface temperature at global and regional scales and in free atmospheric temperature, tropopause height, sea level pressure, ocean heat content, and surface and atmospheric humidity at global scales (*9*–*11*). Detecting precipitation response to external forcing is more challenging for several reasons: The signal-to-noise ratio is lower, global precipitation changes may be constrained by changes in the atmospheric energy balance that results in a smaller precipitation change per unit climate forcing from greenhouse gases than from other agents (*9*, *12*), and the local nature of precipitation makes it more difficult to develop spatiotemporally complete data sets (*12*). Nevertheless, the effects of external forcing on global land precipitation totals (*13*–*15*) and of anthropogenic forcing on the zonal distribution of global land precipitation (*16*) have been detected in observations. Here, we demonstrate a detectable anthropogenic influence on the observed change in Arctic land precipitation over the latter half of the 20th century.

Many Arctic watersheds extend farther south than the area that is traditionally considered as the Arctic region (*3*). The Canadian and Eurasian Arctic flowing watersheds in particular extend to south of 50°N. For the purpose of this analysis, we consider latitude 55°N as the southern boundary for the Arctic. This includes most of the Arctic-flowing river basins in both North America and Eurasia while excluding regions with mid-latitude climate regimes as much as possible.

We used monthly precipitation amounts from the Global Historical Climatology Network (GHCN) data set (*17*), compiled and quality controlled at the National Oceanic and Atmospheric Administration's National Climatic Data Center. Because the availability of station data is limited before 1950, we restricted ourselves to the time period from 1950 to 1999. Canadian stations in the GHCN have many missing values in the 1990s. We therefore replaced Canadian data in the GHCN with 495 adjusted precipitation records (*18*). The resulting combined pan-Arctic data set has reasonably good spatial and temporal coverage and benefits from adjustments for many known precipitation measurement issues (*18*). Nevertheless, uncertainty remains because of the difficulty in measuring precipitation in this region. Monthly precipitation anomalies relative to 1961 to 1990 were subsequently calculated and gridded at the 5° × 5° latitude-longitude resolution before the analyses (*18*).

We used climate simulations obtained from the Coupled Model Intercomparison Project phase 3 (CMIP3) archive and directly from modeling centers. They included ANT simula-

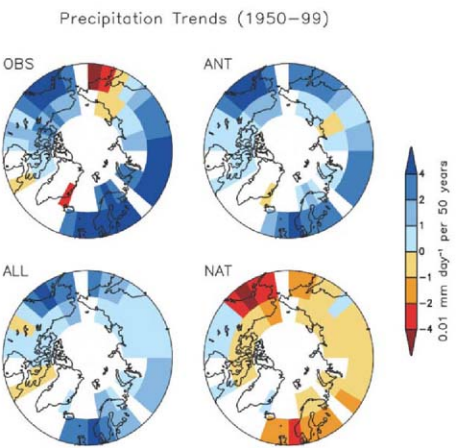

Fig. 1. Large-scale precipitation trends (0.01 mm day^{-1} per 100 years) during 1950 to 1999 from the observations (OBS) and ALL, ANT, and NAT simulations. Large-scale precipitation variation is represented by the first five spatial EOFs of 5-year mean precipitation from the CTL simulations (*18*). Areas with less than 40 years of observations are marked with white space.

Climate Research Division, Environment Canada, Toronto, Ontario M3H 5T4, Canada.

*To whom correspondence should be addressed. E-mail: Francis.Zwiers@ec.gc.ca

tions with historical anthropogenic forcing from greenhouse gases and sulfate aerosols, NAT simulations with reconstructed natural (volcanic and solar) external forcing, and ALL simulations with both anthropogenic and natural external forcing. Control (CTL) simulations were also used when estimating the natural internal variability of precipitation. Details of each group are summarized in table S1. All simulations were interpolated to the same 5° × 5° grid as used for the observations and were masked to mimic the availability of the observational data (*18*).

We used the five leading spatial EOFs (empirical orthogonal functions) computed from the 5-year mean precipitation fields of the multimodel CTL simulations (*18*) to represent the large-scale precipitation variation in the region. These EOFs account for 52% of the total CTL simulation variability of 5-year mean precipitation. We projected 5-year mean precipitation anomalies from the observations and from the ALL, ANT, and NAT simulations onto those EOFs.

Figure 1 shows the large-scale precipitation trends during 1950 to 1999. The observed change is characterized by an overall increasing trend together with a decreasing trend over the easternmost part of Eurasia, as has been previously reported (*3*, *6*, *16*, *19*). The overall multimodel mean trend under ANT forcing resembles that which is observed, but with smaller amplitude. It is also consistent with projected future precipitation change under much stronger greenhouse warming (*8*). The ALL trend has a pattern very similar to the ANT trend, whereas the NAT trend exhibits a pattern of opposite sign.

We compared the observed and simulated space-time variation of precipitation (composed of ten 5-year means, each represented in the five EOF space) using the standard optimal detection approach (*20*–*22*). This method expresses the observations ($\mathbf{y}$) as a sum of scaled response patterns or "fingerprints" ($\mathbf{X}$) estimated from forced GCM simulations plus internal variability ($\boldsymbol{\varepsilon}$): $\mathbf{y} = \mathbf{X}\boldsymbol{\beta} + \boldsymbol{\varepsilon}$. We regressed the observations onto the multimodel mean ALL, ANT, and NAT patterns separately to identify observed precipitation responses to individual forcing factors ("one-signal analysis"). To examine the relative contribution of natural and anthropogenic forcings to the observed precipitation variation, we also conducted a "two-signal analysis" by regressing observations onto the ANT and NAT patterns simultaneously (*20*). These regressions scale the model-simulated fingerprints to best fit the observations. The scaling factors $\boldsymbol{\beta}$ were estimated using the total least squares method (*21*) so as to account for sampling errors in the model-simulated fingerprints.

The two independent estimates of internal variability needed in the estimation and testing of the scaling factors were obtained using both forced and unforced multimodel simulations. Only the multimodel mean values for ALL, ANT, NAT, and CTL simulations respectively were removed from the runs that make up these ensembles when estimating the space-time internal variability covariance matrices, thereby accounting for intermodel variability in the forced response (*18*). Our detection analyses were conducted in a space spanned by the first 14 space-time EOFs of the first of the two 50-dimensional covariance matrices (five principal components for each of ten 5-year periods) obtained in this way. Our detection results are insensitive to reasonable variations in the number of space-time EOFs, as are the results of the residual consistency test (*22*) that was used to compare simulated and observed internal variability. Detection of the response to external forcing is claimed when the 5 to 95% range of the scaling factors $\boldsymbol{\beta}$ lies above zero. The robustness of the detection results is also examined by inflating estimated internal variability by a factor of two.

Figure 2A shows the one-dimensional scaling factors and their 90% confidence ranges estimated with and without doubling model-estimated internal variability. ANT is clearly detected in the one-signal analysis. Although ALL is also robustly detected, NAT is not detectable. The two-signal analysis results indicate that the Arctic precipitation response to ANT forcing can be separated from that of NAT and that the response to ALL forcing in the observations is a manifestation of the response to ANT forcing (also see fig. S1). A two-signal analysis that uses ANT and NAT simulations from the same group of the models produced similar results (fig. S2 and supporting online text). The temporal evolution of the spatial patterns of precipitation change in both observations and simulations (fig. S3) shows similar zonal variations, suggesting that these zonal variations are important contributors to our Arctic domain detection result, just as meridional variation between zonal means is key to detection on the global scale (*16*). Detection results using Arctic average precipitation are less robust (fig. S4). However, detection analyses of precipitation averaged meridionally over three large subregions of the Arctic to retain only very large scale zonal variation in land precipitation yield results similar to those from the full analysis, which underscores the importance of considering the zonal pattern of Arctic precipitation change in the detection analysis (fig. S4 and supporting online text).

It should be noted that for the ANT response, the 5 to 95% scaling factor range lies above 1, with a best-guess value of about 3 (Fig. 2A), suggesting that the multimodel ensemble Arctic precipitation response to ANT

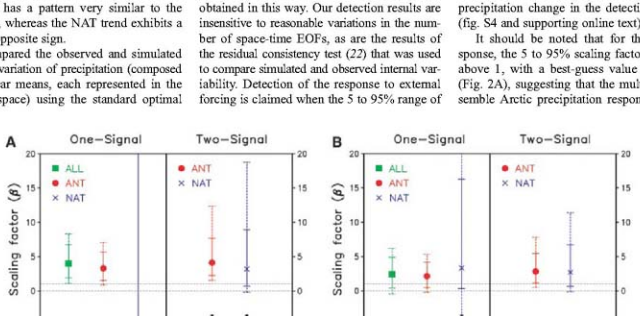

Fig. 2. Best estimates of the scaling factors and their 5 to 95% uncertainty ranges from one-signal and two-signal space-time analyses of 1950 to 1999 Arctic precipitation anomalies with (**A**) raw observations and (**B**) observations from which AO-related variability has been removed. In the one-signal analysis, observed precipitation anomalies are separately regressed onto the multimodel mean precipitation anomalies of all available ALL, ANT, and NAT simulations, respectively. In the two-signal analysis, observed precipitation anomalies are regressed onto the multimodel mean precipitation anomalies from ANT and NAT simulations simultaneously. The first 14 space-time EOFs have been retained in the optimal detection analysis, which explains 55% of total internal variance of the 50-dimensional analysis vector (five principal components for ten 5-year periods). Dashed error bars represent the estimated uncertainty range when model-simulated variability is doubled. The asterisks (*) indicate that the residual consistency test (*22*) is passed only if model-simulated variability is doubled.

forcing is generally underestimated. This is consistent with other studies indicating that models undersimulate precipitation responses to external forcing (*13*–*16*, *23*).

The Arctic Oscillation (AO) is an important contributor to Northern Hemisphere climate variability (*1*, *3*). The prolonged positive AO phase during recent decades is in accord with precipitation changes over Europe and the Arctic (*3*, *24*, *25*). Although modeled AO responses to anthropogenic forcing are generally weaker than observed (*26*, *27*), some studies suggest anthropogenic influences may have been a factor (*9*). To test the sensitivity of our detection results to the possible effect of AO fluctuations, we repeated our detection analyses on observed precipitation series that exclude variability linearly related to the AO. We did so by linearly regressing the observed gridded monthly precipitation anomalies onto the AO index, defined as the first principal component of the monthly mean sea level pressure anomalies north of 20°N (*25*) and by retaining only the regression residuals for detection analyses. The detection results obtained in this way (Fig. 2B) are improved: The scaling factors are closer to one, and model-simulated variability agrees better with observed. This increases confidence in our detection result because it demonstrates human influence on aspects of Arctic precipitation change that are not related to a component of circulation change that has been associated with model structural uncertainty. Nevertheless, it remains difficult to assess the effects of model structural uncertainty, as well as that of observational uncertainty, on our results.

Our results indicate that anthropogenic forcing from greenhouse gases and sulfate aerosols combined has contributed to the observed high-latitude precipitation increase during the latter half of the 20th century. We also find that model-simulated precipitation responses to anthropogenic forcing are weaker than in the observations. This implies that model-projected future precipitation change may also be too weak, which would have important implications for the development of adaptation strategies: It is possible that future Arctic Ocean freshening and MOC slowdown could occur more quickly than indicated by currently available GCM simulations (*7*). Recent studies show that Arctic sea ice is declining substantially faster than indicated by model simulations (*28*, *29*).

References and Notes

1. R. E. Moritz, C. M. Bitz, E. J. Steig, *Science* **297**, 1497 (2002).
2. IPCC, *Climate Change 2007: Impacts, Adaptation and Vulnerability. Contribution of Working Group II to the Fourth Assessment Report of IPCC* (Cambridge Univ. Press, Cambridge, 2007).
3. ACIA, *Arctic Climate Impact Assessment: Scientific Report* (Cambridge Univ. Press, Cambridge, 2005).
4. S. Rahmstorf, *Nature* **419**, 207 (2002).
5. B. J. Peterson *et al.*, *Science* **298**, 2171 (2002).
6. K. E. Trenberth *et al.*, in *Climate Change 2007: The Physical Science Basis. Contribution of Working Group I to the Fourth Assessment Report of IPCC* (Cambridge Univ. Press, Cambridge, 2007), pp. 235–336.
7. B. J. Peterson *et al.*, *Science* **313**, 1061 (2006).
8. G. A. Meehl *et al.*, in *Climate Change 2007: The Physical Science Basis. Contribution of Working Group I to the Fourth Assessment Report of IPCC* (Cambridge Univ. Press, Cambridge, 2007), pp. 747–845.
9. G. C. Hegerl *et al.*, in *Climate Change 2007: The Physical Science Basis. Contribution of Working Group I to the Fourth Assessment Report of IPCC* (Cambridge Univ. Press, Cambridge, 2007), pp. 663–745.
10. K. M. Willett, N. P. Gillett, P. D. Jones, P. W. Thorne, *Nature* **449**, 710 (2007).
11. B. D. Santer *et al.*, *Proc. Natl. Acad. Sci. U.S.A.* **104**, 15248 (2007).
12. M. R. Allen, W. J. Ingram, *Nature* **419**, 224 (2002).
13. F. H. Lambert, P. A. Stott, M. R. Allen, M. A. Palmer, *Geophys. Res. Lett.* **31**, 10203 (2004).
14. N. P. Gillett, A. J. Weaver, F. W. Zwiers, M. F. Wehner, *Geophys. Res. Lett.* **31**, 12217 (2004).
15. F. H. Lambert, N. P. Gillett, D. A. Stone, C. Huntingford, *Geophys. Res. Lett.* **32**, 18704 (2005).
16. X. Zhang *et al.*, *Nature* **448**, 461 (2007).
17. T. C. Peterson, R. S. Vose, *Bull. Am. Meteorol. Soc.* **78**, 2837 (1997).
18. Materials and methods are available as supporting material on *Science* Online.
19. G. Gruza, E. Rankova, V. Razuvaev, O. Bulygina, *Clim. Change* **42**, 219 (1999).
20. G. C. Hegerl *et al.*, *Clim. Dyn.* **13**, 613 (1997).
21. M. R. Allen, P. A. Stott, *Clim. Dyn.* **21**, 477 (2003).
22. M. R. Allen, S. F. B. Tett, *Clim. Dyn.* **15**, 419 (1999).
23. F. J. Wentz, L. Ricciardulli, K. Hilburn, C. Mears, *Science* **317**, 233 (2007).
24. D. W. J. Thompson, J. M. Wallace, *Science* **293**, 85 (2001).
25. D. W. J. Thompson, J. M. Wallace, G. C. Hegerl, *J. Clim.* **13**, 1018 (2000).
26. N. P. Gillett, *Nature* **437**, 496 (2005).
27. R. L. Miller, G. A. Schmidt, D. T. Shindell, *J. Geophys. Res.* **111**, D18101 (2006).
28. M. C. Serreze, M. M. Holland, J. Stroeve, *Science* **315**, 1533 (2007).
29. J. Stroeve, M. M. Holland, W. Meier, T. Scambos, M. Serreze, *Geophys. Res. Lett.* **34**, L09501 (2007).

30. We thank R. Vose and P. Ya. Groisman at the National Climatic Data Centre for the observed precipitation data, and P. Stott and T. Nozawa for the provision of model data. We are grateful to M. Mackay, W. Skinner, and two anonymous reviewers for their helpful comments. We acknowledge the modeling groups, the Program for Climate Model Diagnosis and Intercomparison (PCMDI), and the World Climate Research Programme's (WCRP) Working Group on Coupled Modelling (WGCM) for their roles in making available the WCRP CMIP3 multimodel data set. Support of this data set is provided by the Office of Science, U.S. Department of Energy. S.-K.M. is supported by the Canadian International Polar Year program.

Supporting Online Material

www.sciencemag.org/cgi/content/full/320/5875/518/DC1
Materials and Methods
SOM Text
Figs. S1 to S4
Tables S1 and S2
References

27 November 2007; accepted 18 March 2008
10.1126/science.1153468

Efficient Inhibition of the Alzheimer's Disease β-Secretase by Membrane Targeting

Lawrence Rajendran,[1] Anja Schneider,[2] Georg Schlechtingen,[3,4] Sebastian Weidlich,[4] Jonas Ries,[5] Tobias Braxmeier,[3,4] Petra Schwille,[5] Jörg B. Schulz,[6] Cornelia Schroeder,[4] Mikael Simons,[2] Gary Jennings,[3] Hans-Joachim Knölker,[3,4] Kai Simons[1]*

β-Secretase plays a critical role in β-amyloid formation and thus provides a therapeutic target for Alzheimer's disease. Inhibitor design has usually focused on active-site binding, neglecting the subcellular localization of active enzyme. We have addressed this issue by synthesizing a membrane-anchored version of a β-secretase transition-state inhibitor by linking it to a sterol moiety. Thus, we targeted the inhibitor to active β-secretase found in endosomes and also reduced the dimensionality of the inhibitor, increasing its local membrane concentration. This inhibitor reduced enzyme activity much more efficiently than did the free inhibitor in cultured cells and in vivo. In addition to effectively targeting β-secretase, this strategy could also be used in designing potent drugs against other membrane protein targets.

A key molecule in the pathogenesis of Alzheimer's disease (AD) is the β-amyloid peptide (Aβ), which, either in its soluble oligomeric form or in the plaque-associated version, leads to neurodegeneration (*1*). Aβ is liberated from the membrane-spanning β-amyloid precursor protein (APP) by sequential proteolytic processing using β- and γ-secretases. β-Secretase activity is conferred by a transmembrane aspartyl protease, also termed BACE-1 (β-amyloid cleaving enzyme 1), which catalyzes the rate-limiting reaction in the generation of Aβ (*2*). β-Secretase cleavage of APP occurs predominantly in endosomes, and endocytosis of APP and β-secretase is essential for β cleavage and Aβ production (*3*–*7*). The low pH of endosomes is optimal for β-secretase activity. Conversely, α-secretase cleavage of APP, which precludes production of the toxic Aβ peptide, occurs at the plasma membrane (*8*). Both β- and γ-secretase are thus propitious therapeutic targets (*1*, *9*). However, in

view of the multiple functions of γ-secretase, β-secretase might be the preferred therapeutic target (*10*).

Several transition-state inhibitors have been designed to block the active site of the β-secretase enzyme (*11*, *12*). Many of these have shown potent activity against the purified ectodomain of β-secretase or the reconstituted enzyme (*11*, *13*). Nonetheless, many fail in cellular assays (*14*, *15*). A critical issue in designing inhibitors against the enzyme is to direct inhibition to the subcellular compartment where the enzyme is active. Here, we tested the efficacy of a membrane-tethered version of an otherwise soluble inhibitor that is targeted to endosomes via endocytosis.

Endocytosis is essential for β-secretase activity (*3*–*7*); we thus tested whether the internalization of β-secretase inhibitors was needed for activity. To this end, we assayed the activity of a nonpermeable transition-state peptide inhibitor of β-secretase in a cellular assay, where the production of α-secretase, β-secretase–cleaved ectodomains of APP (sAPPα, sAPPβ, respectively) and Aβ was followed. The free inhibitor inhibited both recombinant and soluble β-secretase (*11*, *13*) (fig. S1) but failed to inhibit β cleavage in cells (Fig. 1 and fig. S2). Because most of the β cleavage occurs in endosomes (*3*–*7*, *16*), sufficient amounts of the free inhibitor might not reach this compartment.

We reasoned that membrane tethering would render the soluble inhibitor competent for endocytosis and deliver the inhibitor to endosomes. Hence, we coupled a sterol moiety as a membrane anchor via a polyglycol linker to the C terminus of the inhibitory peptide (fig. S3) via solid-phase synthesis (see supporting online material). On the basis of the length of the peptide cleavage domain of APP (β/A4 region of APP-770) (*17*), the appropriate length of the linker for inhibition of β-secretase was estimated to be about 89 Å. The sterol-linked inhibitor was more active than the free inhibitor in inhibiting β cleavage (Fig. 1, A and C) and Aβ production (Fig. 1D). Because the free inhibitor coupled to the polyglycol linker but lacking the sterol moiety was inactive, we concluded that the sterol moiety, not the polyglycol linker, was critical for effective β-secretase inhibition (fig. S4). Likewise, another control where the sterol group was N-terminally linked to the inhibitor was also inactive, ruling out a direct influence of the sterol moiety (Fig. 1, A and C). The failure of the N-terminally linked inhibitor to inhibit β-secretase also suggested that proper orientation of the inhibitory peptide was essential for inhibition. Similar results were obtained in a neuroblastoma cell line (fig. S5). Thus, membrane anchoring of an otherwise soluble inhibitor leads to a considerable increase in efficacy.

Having shown that the membrane-anchored inhibitor blocked β-secretase more efficiently than did the free inhibitor in cultured cells, we proceeded to demonstrate that the membrane-anchored inhibitor was indeed transported to the endosomes where β cleavage occurs. For this purpose, we synthesized a fluorescent derivative of both the sterol-linked and the free inhibitor. This labeled inhibitor was equally active against β-secretase (Fig. 2A) and was rapidly endocytosed (Fig. 2B). Inhibition of endocytosis through the use of a mutant dynamin (DynK44A) markedly reduced internalization of the inhibitor (Fig. 2C), whereas overexpression of either soluble green fluorescent protein (GFP; Fig. 2C) or wild-type dynamin (fig. S6) did not alter internalization of the inhibitor. The internalized inhibitor accumulated in endosomes that also harbored APP and BACE-1 (Fig. 2D), which showed that sterol-anchoring efficiently directed the inhibitor to endosomes. Concentrations as low as 0.1 μM were sufficient to block the appearance of the β-cleaved ectodomain of APP in the cells (Fig. 2, E and F) (*6*). In contrast, the free inhibitor was not internalized, nor did it inhibit the production of β-cleaved ectodomain (Fig. 2E). Although sterol-linked inhibitors decreased β cleavage of APP, they concomitantly increased α cleavage (Fig. 1, B and C, and fig. S4). Inhibition of endocytosis also produced the same effect (*3*, *4*, *8*), suggesting that membrane-anchored inhibitor targeted the active β-secretase in endosomes.

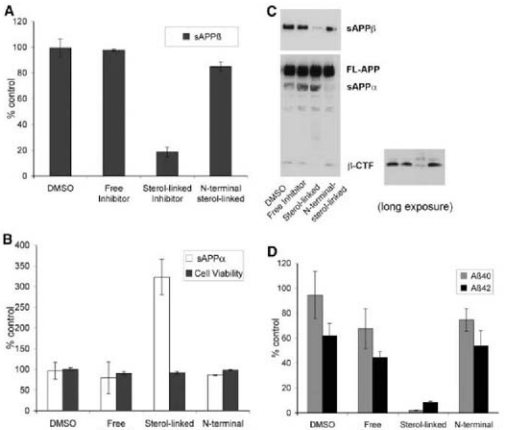

Fig. 1. Sterol-linked inhibitor inhibits β-secretase cleavage of APP and Aβ production. HeLa-swAPP cells were treated with test compounds (200 nM) and the medium was analyzed for (**A**) β cleavage (i.e., the β-cleaved ectodomain, sAPPβ) and (**B**) α cleavage (i.e., the α-cleaved ectodomain, sAPPα) by electrochemiluminescence (ECL) assay (*6*). Cell viability values in (B) are from Alamar Blue assay. (**C**) sAPPβ levels were detected by immunoblotting cell lysates from the samples, using the sAPPβ-specific antibody AN1] (*6*). Full-length APP (FL-APP), sAPPα, and β-cleaved C-terminal fragment (β-CTF) were analyzed by immunoblotting with 6E10 (lower and side panel). Longer exposure (side panel) reveals a clear reduction in β-CTF levels in the sterol-linked inhibitor lane. FL-APP levels serve as the loading control. (**D**) Sterol-linked inhibitor inhibited secretion of Aβ peptides (Aβ40, Aβ42) as measured by ECL assay. Inhibitor data are expressed with respect to DMSO control; DMSO data are expressed as percent-untreated control. ECL results shown are representative of more than four independent experiments and are expressed as means ± SD (sAPPβ, $P < 0.001$; Aβ40, $P = 0.008$; Aβ42, $P = 0.01$; sAPPα, $P = 0.003$).

[1]Max Planck Institute of Molecular Cell Biology and Genetics, Pfotenhauerstr. 108, 01307 Dresden, Germany. [2]Max Planck Institute for Experimental Medicine, 37075 Göttingen, Germany. [3]ADO Technologies GmbH, Tatzberg 47-51, 01307 Dresden, Germany. [4]Department of Chemistry, Technical University of Dresden, Bergstr. 66, 01069 Dresden, Germany. [5]Biotec, Biotechnologisches Zentrum, Tatzberg 47/49, 01307 Dresden, Germany. [6]Center of Neurological Medicine, Waldweg 33, 37073 Göttingen, Germany.

*To whom correspondence should be addressed. E-mail: simons@mpi-cbg.de

An added advantage of using a sterol as a membrane anchor is that the inhibitor not only is inserted into the membrane plane, but may also be enriched in sterol-rich domains. Cholesterol appears to be a risk factor for AD (*18*), and cholesterol-sphingolipid domains in cellular membranes, termed rafts (*6*), function as sites for the amyloidogenic cleavage of APP (*19*, *20*). β-Secretase is enriched in these microdomains (*6*, *19*, *20*). By linking the inhibitor to a sterol, we may have not only targeted it to endosomes, but also enriched the inhibitor in raft domains in these compartments. To determine whether targeting to raft domains promoted the inhibitory effect or was sufficient to simply anchor the inhibitor to the membrane, we synthesized inhibitors with different anchors—palmityl, myristyl, and oleyl (fig. S3)—with different affinities for membranes and raft microdomains (*21*). The oleyl-linked inhibitor was much less active in inhibiting β-secretase than were the saturated chains, the 18-carbon palmitate being intermediate in action between the sterol and the 14-carbon myristate (Fig. 3A).

To test whether this inhibition correlated with raft partitioning, we used scanning fluorescence correlation spectroscopy (sFCS) and avalanche photodiode (APD) imaging on supported bilayers exhibiting a raft-like liquid-ordered (lo)/non–raft-like liquid-disordered (ld) phase separation (fig. S7). Partition coefficient measurements revealed that the sterol-linked inhibitor and the palmityl-linked inhibitor partitioned into raft domains more readily than did the oleyl counterpart (Fig. 3B). Thus, raftophilic anchors of β-secretase inhibitors enhance their inhibitory potential.

To determine whether sterol-linked inhibitors were also effective in vivo, we used triple transgenic *Drosophila* expressing human wild-type APP, β-secretase, and presenilin as a model system. These flies show age-dependent neurodegeneration, a shortened life span, and semilethality and can be rescued by pharmacological treatment with secretase inhibitors (*22*). To study whether the sterol-linked inhibitor attenuated toxicity in these flies, we compared the eclosion rates of transgenic larvae that had been fed the sterol-linked inhibitor to those of solvent-treated controls (Fig. 4A). Treatment of larvae with the sterol-linked inhibitor increased survival rates; hence, the compound not only inhibited β-secretase effectively in cell culture, but also reduced toxicity in vivo. To test whether the sterol-linked inhibitor also efficiently inhibited Aβ production in mammals, we injected the inhibitor stereotaxically into the hippocampus of APPsw/PSΔE9 mice (*23*) and compared the result with mice in-

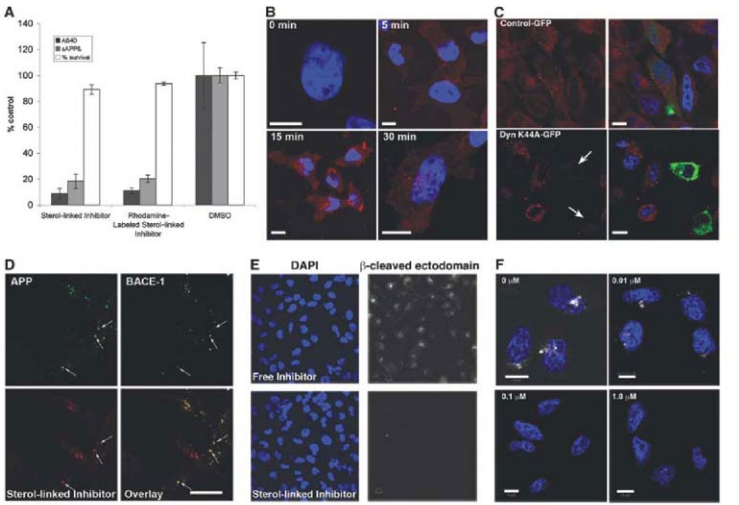

Fig. 2. Sterol-linked inhibitor is internalized into endosomes containing APP/β-secretase. **(A)** Rhodamine-labeled, sterol-linked inhibitor also inhibits β cleavage and Aβ production. Medium of HeLa-swAPP cells treated with inhibitors (2 μM) was analyzed for β cleavage, Aβ40, and cell viability (percent survival) as described for Fig. 1. Results presented are representative of three independent experiments and are expressed as means ± SD (sAPPβ, $P < 0.001$; Aβ40, $P = 0.014$). **(B)** HeLa-swAPP cells were treated with 2 μM rhodamine-labeled, sterol-linked inhibitor (red) for various times indicated. **(C)** Dynamin mutant (DynK44A-GFP), but not control GFP, inhibits internalization of the rhodamine-labeled sterol-linked inhibitor. Arrows indicate reduced internalization of the inhibitor in dynK44A-transfected cells. **(D)** Internalized sterol-linked inhibitor colocalized with internalized APP (green) and β-secretase (white) in endosomes (arrows indicate representative spots). **(E)** β-cleaved ectodomain staining in free inhibitor– or the sterol-linked inhibitor–treated cells (white) (*6*). **(F)** Cells were treated with different concentrations (inset) of the sterol-linked inhibitor as shown. Note that β-cleaved ectodomain (white) levels are already undetectable at 0.1 μM levels. DAPI (4′,6′-diamidino-2-phenylindole) staining (blue) indicates nuclei in (B), (C), (E), and (F). scale bar, 10 μm [(B), (C), (D), and (F)].

jected with either the free inhibitor or the solvent control, dimethyl sulfoxide (DMSO). The sterol-linked inhibitor was indeed more effective than the free inhibitor in inhibiting Aβ production (Fig. 4B).

Thus, membrane anchoring markedly increased the potency of a β-secretase inhibitor. By anchoring the inhibitor to the membrane, we achieved two goals: (i) The inhibitor became endocytosis-competent and gained access to endosomal β-secretase; and (ii) we reduced the dimensionality of the otherwise soluble inhibitor, thereby enhancing the interaction between the inhibitor and the enzyme (*24*). Reaction rates between solutes and membrane receptors can be enhanced by reducing the dimensionality of the solute via nonspecific adsorption (*24*), and here this model has been realized in designing drug candidates. This model also explains why such a membrane-anchored version of the inhibitor would be superior to a soluble but membrane-permeable inhibitor. If tethered molecules (e.g., the enzyme and the inhibitor) were partitioned within microdomains, both the concentration and the interaction times of the components would be increased (*25*), as we have observed. By choosing sterol as a membrane anchor, the inhibitor is enriched in the vicinity of raft-associated β-secretase, thus enhancing their interaction. The increased potency of the sterol-linked inhibitor confirms that the lipid environment and the subcellular localization of β-secretase regulate its activity (*6*, *20*). The concomitant increase in production of the neuroprotective α-cleaved ectodomain highlights the advantage of such an inhibitor, which may explain the efficacy observed in the transgenic fly model (*22*).

This work represents a proof-of-principle for a new approach in the design of more effective β-secretase inhibitors for the treatment of Alzheimer's disease. Because we used a transition-state analog against β-secretase, it was imperative to target the inhibitor to endosomes where it was active. However, this principle could also be used to design strategies to develop inhibitors against other membrane protein targets that are active at the plasma membrane and/or in intracellular compartments.

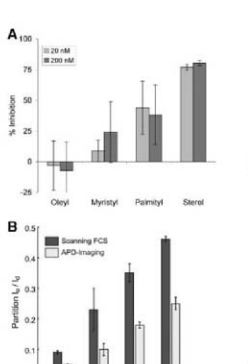

Fig. 3. Raft partitioning of inhibitors enhances their inhibitory potential. **(A)** HeLa-swAPP cells were treated with 20 nM or 200 nM test compounds for 4 hours; medium was harvested and analyzed for sAPPβ (*6*). Percent inhibition of β cleavage is shown as mean ± SD (sterol versus oleyl, $P = 0.009$). Palmityl, Myristyl, and Oleyl represent the anchor modifications of the inhibitors via palmitylation, myristylation, or oleylation, respectively. **(B)** Raft partitioning of oleyl-, palmityl-, and sterol-anchored inhibitors. Partition coefficients of inhibitors with different linkers and BODIPY-cholesterol (Bodipy-ChoL) into non–raft-like liquid disordered (ld) and raft-like liquid ordered (lo) phase were obtained by scanning FCS and APD imaging.

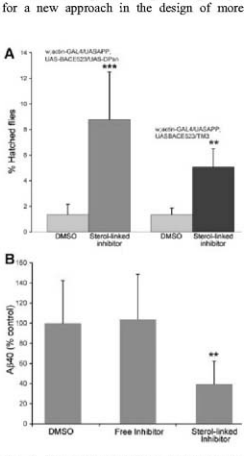

Fig. 4. Sterol-linked inhibitor rescues the lethality of transgenic flies and inhibits the production of Aβ in transgenic AD mice. **(A)** The eclosion numbers of flies, treated with either sterol-linked inhibitor (4 μM) or DMSO, were determined and their ratio versus the total amount of eclosed flies was calculated (percent hatched flies). Results are expressed as means ± SD of four experiments (**$P < 0.01$ for APP/BACE flies, ***$P < 0.001$ for APP/BACE/PRESENILIN flies; χ^2 test). **(B)** Transgenic mice were stereotaxically injected with solvent alone (DMSO), inhibitor without sterol anchor (free inhibitor), or sterol-anchored inhibitor into the hippocampus. Hippocampal Aβ levels were measured after 4 hours. Results are expressed as means ± SD of Aβ values [student *t* test; $P = 0.0068$ for free inhibitor and sterol-linked (**$P < 0.01$) and $P = 0.9389$ for DMSO and free inhibitor].

References and Notes

1. E. D. Roberson, L. Mucke, *Science* **314**, 781 (2006).
2. C. Haass, D. J. Selkoe, *Nat. Rev. Mol. Cell Biol.* **8**, 101 (2007).
3. E. H. Koo, *Traffic* **3**, 763 (2002).
4. S. A. Small, S. Gandy, *Neuron* **52**, 15 (2006).
5. A. Kinoshita *et al.*, *J. Cell Sci.* **116**, 3339 (2003).
6. L. Rajendran *et al.*, *Proc. Natl. Acad. Sci. U.S.A.* **103**, 11172 (2006).
7. X. He, K. Cooley, C. H. Chung, N. Dashti, J. Tang, *J. Neurosci.* **27**, 4052 (2007).
8. E. Kojro, F. Fahrenholz, *Subcell. Biochem.* **38**, 105 (2005).
9. W. Annaert, B. De Strooper, *Annu. Rev. Cell Dev. Biol.* **18**, 25 (2002).
10. R. Vassar, *Adv. Drug Deliv. Rev.* **54**, 1589 (2002).
11. J. S. Tung *et al.*, *J. Med. Chem.* **45**, 259 (2002).
12. L. Hong *et al.*, *Science* **290**, 150 (2000).
13. A. Capell *et al.*, *J. Biol. Chem.* **277**, 5637 (2002).
14. B. Schmidt, S. Baumann, H. A. Braun, G. Larbig, *Curr. Top. Med. Chem.* **6**, 377 (2006).
15. I. D. Hills, J. P. Vacca, *Curr. Opin. Drug Discov. Dev.* **10**, 383 (2007).
16. R. A. Nixon, *Neurobiol. Aging* **26**, 373 (2005).
17. R. Wang, J. F. Meschia, R. J. Cotter, S. S. Sisodia, *J. Biol. Chem.* **266**, 16960 (1991).
18. M. Simons, P. Keller, J. Dichgans, J. B. Schulz, *Neurology* **57**, 1089 (2001).
19. J. M. Cordy, N. M. Hooper, A. J. Turner, *Mol. Membr. Biol.* **23**, 111 (2006).
20. L. Kahodova *et al.*, *J. Biol. Chem.* **280**, 36815 (2005).
21. M. D. Resh, *Subcell. Biochem.* **37**, 217 (2004).
22. I. Greeve *et al.*, *J. Neurosci.* **24**, 3899 (2004).
23. R. Radde *et al.*, *EMBO Rep.* **7**, 940 (2006).
24. G. Adam, M. Delbruck, in *Structural Chemistry in Molecular Biology*, A. Rich, N. Davidson, Eds. (Freeman, San Francisco, 1968), pp. 198–215.
25. B. N. Kholodenko, J. B. Hoek, H. V. Westerhoff, *Trends Cell Biol.* **10**, 173 (2000).

26. We thank G. Yu for the HeLa-swAPP cells; R. Reiffegerste (Evotec, Hamburg, Germany) for the transgenic flies; M. Jucker for the APPsw/PSΔE9 mice; P. Keller for help and advice with the ECL assays; V. Surendranath, W. Zaccharias, D. Lingwood, and R. Klemm for critical reading of the manuscript; and J. Bali and B. Michel for help with cell culture. Supported by Alzheimer Forschung Initiative e.V. (AFI) grant 07855 (L.R.), the European Fund for Regional Development and the State of Saxony (EFRE project 421/206-08) (H.-J.K.), and grant 0314033 from the German Federal Ministry of Education and Research (G.J., G.S., T.B., and C.S.). K.S. is a founder of, holds equity in, and is a member of the advisory board of Jado Technologies, a company that develops novel small-molecule drugs through insights from an emerging area of cell membrane chemistry centered on rafts. H.-J.K. and G.J. are founders of and hold equity in Jado Technologies.

Supporting Online Material

www.sciencemag.org/cgi/content/full/320/5875/520/DC1
Materials and Methods
Figs. S1 to S7
References

18 February 2008; accepted 20 March 2008
10.1126/science.1156609

Plastin 3 Is a Protective Modifier of Autosomal Recessive Spinal Muscular Atrophy

Gabriela E. Oprea,[1,2,3] Sandra Kröber,[1,2] Michelle L. McWhorter,[4] Wilfried Rossoll,[5] Stefan Müller,[3] Michael Krawczak,[6] Gary J. Bassell,[5] Christine E. Beattie,[4] Brunhilde Wirth[1,2,3]*

Homozygous deletion of the survival motor neuron 1 gene (*SMN1*) causes spinal muscular atrophy (SMA), the most frequent genetic cause of early childhood lethality. In rare instances, however, individuals are asymptomatic despite carrying the same *SMN1* mutations as their affected siblings, thereby suggesting the influence of modifier genes. We discovered that unaffected *SMN1*-deleted females exhibit significantly higher expression of plastin 3 (*PLS3*) than their SMA-affected counterparts. We demonstrated that PLS3 is important for axonogenesis through increasing the F-actin level. Overexpression of PLS3 rescued the axon length and outgrowth defects associated with SMN down-regulation in motor neurons of SMA mouse embryos and in zebrafish. Our study suggests that defects in axonogenesis are the major cause of SMA, thereby opening new therapeutic options for SMA and similar neuromuscular diseases.

Spinal muscular atrophy (SMA), a common autosomal recessive neuromuscular disease, is caused by homozygous mutations of the survival motor neuron 1 gene (*SMN1*), whereas the severity of the disease is primarily influenced by the number of *SMN2* copies (*1*). *SMN2*, which usually occurs in one to four copies per genotype, produces insufficient full-length SMN transcript and protein to rescue the SMA phenotype (*2*–*4*). However, a small proportion of individuals homozygous for the absence of *SMN1* are fully asymptomatic despite carrying an identical number of *SMN2* copies as their affected siblings, suggesting the influence of modifier genes (*5*–*8*). Usually, SMA-affected siblings are very similar in terms of their age at onset and the progression of disease (*9*). Between families, however, the SMA phenotype varies between type I (most severe form, patients unable to sit or walk) and type IV (adult form, mild muscle weakness) (*10*, *11*). Reduced levels of SMN cause degeneration of α motor neurons (MNs) in the spinal cord, leading to muscle weakness and atrophy in SMA patients (*10*). Moreover, SMN depletion causes several anomalies, including aberrant MN axon pathfinding, reduced growth velocity, reduced growth cone sizes, and anomalous calcium-channel clustering in the growth cone (*12*–*14*). SMN is a housekeeping protein involved in small nuclear ribonucleoprotein biogenesis and splicing (*15*, *16*) that also plays a role in axonal growth, neuromuscular junction formation, and the transport of RNA along axons (*12*, *17*, *18*). The detailed molecular pathogenesis of SMA, however, is still unknown.

We identified six SMA-discordant families with eight fully asymptomatic females who had inherited the same *SMN1* and *SMN2* alleles as their affected siblings (Fig. 1A and table S1) (*5*, *19*). To identify SMA modifier genes, we first carried out a transcriptome-wide differential expression analysis using total RNA from the lymphoblastoid cell lines (LBs) of four *SMN1*-deleted siblings from family no. 482 (Fig. 1A), together with two unrelated type I and two type III SMA patients. The unrelated type I and III SMA patients were included to exclude differentially expressed transcripts caused by different SMN levels. In total, 18 transcripts showed a greater than threefold dif-

[1]Institute of Human Genetics, University of Cologne, 50931 Cologne, Germany. [2]Institute of Genetics, University of Cologne, 50931 Cologne, Germany. [3]Center for Molecular Medicine Cologne, University of Cologne, 50931 Cologne, Germany. [4]Centre for Molecular Neurobiology and Department of Neuroscience, The Ohio State University, Columbus, OH 43210, USA. [5]Emory University School of Medicine, Department of Cell Biology, Atlanta, GA 30322, USA. [6]Institute of Medical Informatics and Statistics, Christian-Albrechts University of Kiel, 24105 Kiel, Germany.

*To whom correspondence should be addressed. E-mail: brunhilde.wirth@uk-koeln.de

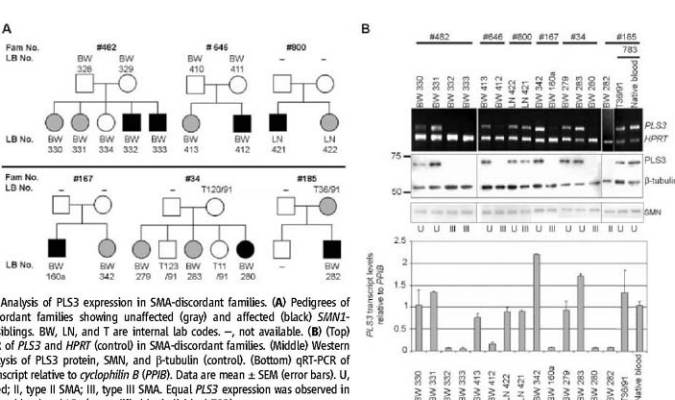

Fig. 1. Analysis of PLS3 expression in SMA-discordant families. **(A)** Pedigrees of SMA-discordant families showing unaffected (gray) and affected (black) *SMN1*-deleted siblings. BW, LN, and T are internal lab codes. –, not available. **(B)** (Top) sqRT-PCR of *PLS3* and *HPRT* (control) in SMA-discordant families. (Middle) Western blot analysis of PLS3 protein, SMN, and β-tubulin (control). (Bottom) qRT-PCR of *PLS3* transcript relative to *cyclophilin B* (*PPIB*). Data are mean ± SEM (error bars). U, unaffected; II, type II SMA; III, type III SMA. Equal *PLS3* expression was observed in both native blood and LBs (exemplified by individual 783).

ference in expression (table S2). However only plastin 3 (*PLS3*, T-plastin or T-fimbrin; MIM 300131, Xq23) exhibited statistically different transcription levels in the affected and unaffected siblings of all SMA-discordant families (Student's t test = 5.560, resampling $P < 10^{-4}$), thereby rendering PLS3 the sole candidate for modifying SMA. All unaffected *SMN1*-deleted siblings revealed high *PLS3* expression (mean ± SEM = 1.298 ± 0.385), whereas all but one affected male showed no expression (Fig. 1B). Previous reports have implied that *PLS3* is not expressed in the hematopoietic system at all, but only in solid tissues, including the spinal cord (*20*). We ruled out the possibility that *PLS3* expression in LBs was induced by Epstein-Barr virus transformation by showing that it was also expressed in native white blood cells (individual 783 in Fig. 1B). The expression of *PLS3* was also confirmed at the protein level (Fig. 1B and fig. S1).

To test whether *PLS3* expression was unique to SMA-discordant families, we used both semi-quantitative reverse transcription polymerase chain reaction (sqRT-PCR) and quantitative RT-PCR (qRT-PCR) to analyze 98 RNA samples from the native blood of healthy controls and 101 RNA samples from LBs of unrelated type I to III SMA patients. *PLS3* was highly expressed in only 5% of the healthy controls (three females and two males), confirming that *PLS3* expression in blood is rare (fig. S2 and table S3A). However, 16% of type I to III SMA patients (six females and ten males) highly expressed *PLS3* (fig. S2 and table S3B), and the difference between controls and SMA patients was highly significant (Fisher's exact $P = 0.0018$). Three of the six highly expressing female patients for whom clinical data were available had only very mild and slowly progressing SMA, despite carrying only two *SMN2* copies (table S4A). In contrast, the disease phenotype of the 10 highly expressing SMA males correlated with the *SMN2* genotype as expected (table S4B). These findings suggest that PLS3 is a gender-specific SMA modifier whose protective effect may not be fully pene-

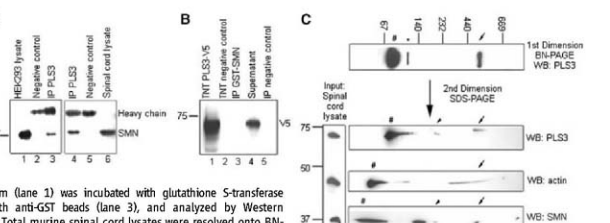

Fig. 2. PLS3 and SMN associate in a large protein complex. **(A)** HEK293 total cell lysates (lane 1 at left) and murine spinal cord (lane 6 at right) were immunoprecipitated (IP) with anti-PLS3 antibody (lanes 3 and 4) and Western blotted with anti-SMN antibody. **(B)** Recombinant PLS3-V5 protein produced in vitro using TnT Quick Coupled Transcription/Translation System (Promega) system (lane 1) was incubated with glutathione S-transferase (GST)–SMN, immunoprecipitated with anti-GST beads (lane 3), and analyzed by Western blotting with anti-V5 antibody. **(C)** Total murine spinal cord lysates were resolved onto BN-PAGE gels and stained with anti-PLS3 antibody. The first-dimension gel was followed by a second SDS-PAGE and Western blot (WB) analysis, allowing the identification of proteins belonging to common protein complexes. Arrows denote the ~500-kilodalton Pls3-Smn-actin complex, and arrowheads denote the ~200-kilodalton Pls3-Smn complex. Number signs indicate monomeric form, and the asterisk indicates putative Pls3 dimer.

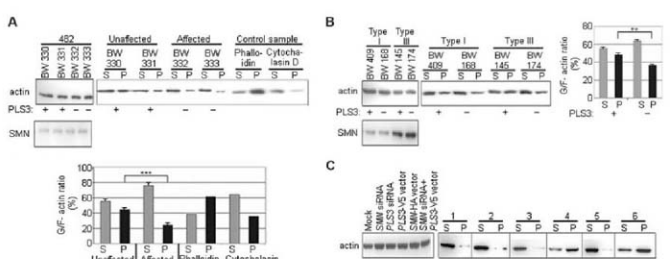

Fig. 3. PLS3 influences the G/F-actin ratio in vivo. G/F-actin levels in **(A)** SMA-discordant family no. 482, **(B)** SMA patients, and **(C)** HEK293 cells after overexpression or knockdown of PLS3 and/or SMN as indicated. (A) to (C) (Left) actin input. (Right) Western blot analysis of G-actin fractions in the supernatant (S) and F-actin fractions in the pellet (P). A phalloidin-treated sample served as a positive control for F-actin; a cytochalasin D–treated sample served as a negative control. +, PLS3 expression; –, no expression. The bar charts show the quantification of G/F-actin levels. Data are mean ± SD (error bars). *P < 0.05; **P < 0.01; ***P < 0.001.

trant, thereby pointing toward an interaction with additional unknown factors.

All our attempts to identify the molecular basis of the differential *PLS3* expression observed in blood (supporting online material text and figs. S3 to S5) provided no unequivocal answer as to whether the expression of *PLS3* in blood is regulated by cis- or trans-acting factor(s).

PLS3 was highly expressed in the human fetal and adult spinal cord (fig. S6). In rat pheochromocytoma 12 (PC12) cells, Pls3 expression significantly increased during neuronal differentiation (fig. S7), suggesting a role for Pls3 in this process. At the protein level, PLS3 and SMN associated in vivo in both human embryonic kidney–293 (HEK293) cells and the mouse spinal cord (Fig. 2A). However, no direct interaction was detected in an in vitro pull-down assay between the recombinant PLS3 and SMN proteins (Fig. 2B), suggesting the involvement of other proteins. Blue-native–polyacrylamide gel electrophoresis (BN-PAGE), followed by a second-dimension SDS-PAGE, from murine spinal cord extracts revealed that Pls3, Smn, and actin are part of a ~500-kilodalton complex and that Pls3 and Smn alone were also present in a second complex of ~200 kilodaltons that was not visible on the Western blot after first-dimension BN-PAGE (Fig. 2C).

PLS3 binds and bundles actin filaments (*21*). Monomeric globular G-actin subunits assemble into filamentous F-actin polymers.

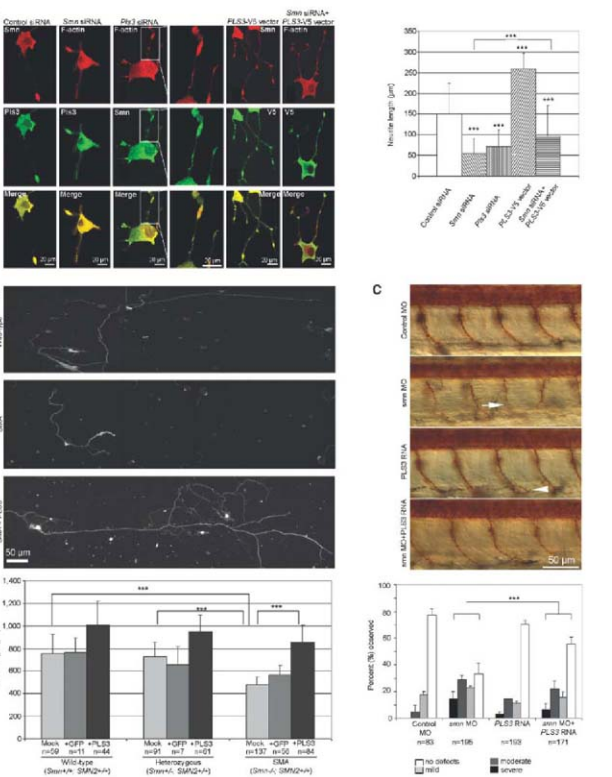

Fig. 4. PLS3 is involved in axonogenesis and rescues the axon length in SMA MNs. **(A)** (Left) Confocal microscopy of neuronal differentiated PC12 cells after transfection as indicated above the panel (see fig. S10 for efficiency). The antibodies that were used are indicated. (Right) Measurements of maximum neurite length in PC12 cells (n = 100 neurites) after transfection and nerve growth factor differentiation for three days. **(B)** (Top) Primary MNs isolated at day E13.5 from WT (*Smn*$^{+/+}$; *SMN2*$^{+/+}$), heterozygous (*Smn*$^{+/-}$; *SMN2*$^{+/+}$), and SMA (*Smn*$^{-/-}$; *SMN2*$^{+/+}$) embryos, cultured for 7 days and immunostained with anti-Tau. (Bottom) The bar chart shows the measurement of axon length from WT, heterozygous, and SMA mouse embryos, which were mock-, GFP-, or PLS3-transduced. **(C)** (Top) Lateral view of zebrafish embryos treated with control MO, *smn* MO, *PLS3* RNA, and *smn* MO + *PLS3* RNA. Motor axons were visualized with znp1 antibody at 36 hours post fertilization. The arrow indicates a severely truncated motor axon in an *smn* morphant, and the arrowhead indicates a mild ventral branch in a *PLS3* injected embryo. The bar chart illustrates that embryos were classified as severe, moderate, mild, or no defects, as previously described (*24*), and the percentage for each group is shown. (A) to (C) Data are mean ± SD (error bars). ***$P < 10^{-4}$.

Bundled F-actin accumulates at the distal extensions of growth cones and filopodia (*22*). Actin cytoskeleton dynamics [G-actin/F-actin (G/F-actin) ratio] plays a major role in axon growth, pathfinding, and branching (*22*). To investigate the potential function of PLS3 in axonal growth and pathfinding, we examined the relation between the G/F-actin ratio and the PLS3 level. Unaffected *SMN1*-deleted siblings who highly expressed PLS3 had significantly increased F-actin levels ($P < 10^{-4}$) in LBs, as compared with their affected siblings who lacked PLS3 expression (Fig. 3A). A comparison between type I and type III SMA patients who either do or do not express PLS3 revealed that only PLS3 (but not SMN) has a significant effect on F-actin levels ($P = 0.0029$) (Fig. 3B). Similar results were obtained by knocking down and/or overexpressing PLS3 or SMN in HEK293 cells (Fig. 3C). These data support the view that PLS3 modifies SMA pathogenesis through stabilizing the growth cones by elevating the F-acting level, as is required for axonogenesis (*22*).

In neuronal differentiated PC12 cells, both endogenous Pls3 and Smn showed diffuse staining in the cytoplasm (especially under the membrane cortex) and accumulated in growth cones and varicosities along the neurites (fig. S8, A and B). Triple-label experiments with Pls3, Smn, and actin in primary murine MNs revealed that endogenous Pls3 and SMN colocalize and are enriched in granules throughout the axons of MNs and accumulate at F-actin–rich growth cones (fig. S8C).

When the functional role of Pls3 was investigated in neuronal-like PC12 cells, both a Pls3 and an Smn knockdown had a dramatic effect on maximum neurite length, compared with control-treated cells (both $P < 10^{-5}$) (Fig. 4A). Overexpression or knockdown of PLS3 in PC12 cells had no effect on SMN expression levels or on the cellular location of SMN (Fig. 4A and fig. S10). Furthermore, the growth cone morphology was affected by Pls3 depletion (column 3 and inset in Fig. 4A). In contrast, PC12 cells overexpressing PLS3 exhibited significantly longer neurites ($P < 10^{-5}$) than did control cells (Fig. 4A). Some 10% of neurites overexpressing PLS3 were markedly elongated, and 30% of them showed cytoplasmic hairlike projections (fig. S9). Simultaneous overexpression of PLS3 and knockdown of Smn led to a highly significant rescue ($P < 10^{-5}$) of average neurite lengths as compared with Smn-deficient cells (Fig. 4A).

To further assess the modifying role of PLS3 in SMA pathogenesis, we used a mouse model for severe SMA carrying two human *SMN2* copies on a null *Smn* background (*23*). MNs were isolated from SMA ($Smn^{-/-}$;$SMN2^{+/+}$), heterozygous ($Smn^{+/-}$;$SMN2^{+/+}$), and wild-type (WT) ($Smn^{+/+}$;$SMN2^{+/+}$) E13.5 embryos, transduced with a lentivirus expressing either green fluorescent protein (GFP) or PLS3-GFP, cultured for 7 days, and assessed for axonal length with antibodies to Tau (anti-Tau) (Fig. 4B). SMA MNs exhibited a significant reduction in axon length compared with cells from either WT or heterozygous embryos (both $P < 10^{-5}$), confirming previous findings (*13*). The detrimental effect of a reduced SMN level on axonal length was significantly rescued ($P < 10^{-5}$) by PLS3 overexpression, and axons reached lengths comparable to nontransduced or Pls3-transduced MNs from WT and heterozygous embryos (Fig. 4B). However, as shown in humans, a certain amount of SMN seems to be required for full rescue.

Finally, we investigated the modifying effect of PLS3 in vivo by knocking down zebrafish smn with antisense morpholino (MO) and by co-overexpression of human PLS3. Human and zebrafish PLS3 are 86% identical. It has been shown that decreased levels of smn result in motor axon–specific outgrowth defects (such as truncations and ectopic branches, that can only be rescued by WT SMN, but not by mutated Δ7SMN) (*12*, *24*), and perturbations due to reduced levels of smn can be clearly visualized (*24*). Whereas PLS3 overexpression in zebrafish embryos using 200 pg of *PLS3* RNA revealed a slight but nonsignificant increase in mild and moderate axon defects compared with controls, the co-injection of *smn* MO (9 ng) and *PLS3* RNA (200 pg) significantly rescued the aberrant axonal outgrowth ($P < 10^{-4}$) in comparison with *smn* MO alone (9 ng) (Fig. 4C), suggesting that PLS3 plays a modifying role in the zebrafish SMA model as well. To further elucidate its functional role, we also knocked down *pls3* in zebrafish embryos. Whereas 9 ng of *pls3* MO resulted in only 40% knockdown, without a phenotypic effect on motor axons, a higher dose of *pls3* MO (12 ng) resulted in 90% lethality. This detrimental effect was partially rescued by co-injection of human *PLS3* RNA, indicating that the knockdown was specific and that pls3 plays an essential role in early zebrafish development. Co-injection of both *smn* and *pls3* MO (9 ng each) also led to full embryonic lethality, suggesting a synergistic effect of the two proteins.

Taken together, our data provide evidence that PLS3 acts as a protective modifier of SMA. The capability of PLS3 to rescue the detrimental effects of reduced SMN levels on axon growth supports the view that axon biology is crucial for SMA pathogenesis and that proteins stabilizing the axon can modify the disease phenotype. As yet, we neither know the cause of the rare PLS3 expression in blood, nor do we understand the gender-specificity of the SMA protective effect of PLS3, but we may speculate that the same regulatory elements that are active in blood are responsible for the modified expression of PLS3 in the spinal cords of unaffected *SMN1*-deleted females. The fact that PLS3 can protect against SMA provides an opportunity to identify regulatory mechanisms that influence the PLS3-SMN complex in MNs. Such knowledge would add insights into the molecular pathogenesis of SMA, as well as that of other related MN diseases, and may help to identify targets for the therapy of these devastating disorders.

References and Notes

1. S. Lefebvre *et al.*, *Cell* **80**, 155 (1995).
2. C. L. Lorson, E. Hahnen, E. J. Androphy, B. Wirth, *Proc. Natl. Acad. Sci. U.S.A.* **96**, 6307 (1999).
3. S. Lefebvre *et al.*, *Nat. Genet.* **16**, 265 (1997).
4. M. Feldkotter, V. Schwarzer, R. Wirth, T. F. Wienker, B. Wirth, *Am. J. Hum. Genet.* **70**, 358 (2002).
5. E. Hahnen *et al.*, *Hum. Mol. Genet.* **4**, 1927 (1995).
6. J. M. Cobben *et al.*, *Am. J. Hum. Genet.* **57**, 805 (1995).
7. C. H. Wang *et al.*, *Hum. Mol. Genet.* **5**, 359 (1996).
8. T. W. Prior, K. J. Swoboda, H. D. Scott, A. Q. Hejmanowski, *Am. J. Med. Genet.* **130A**, 307 (2004).
9. S. Rudnik-Schöneborn, D. Rohrig, G. Morgan, B. Wirth, K. Zerres, *Am. J. Med. Genet.* **51**, 70 (1994).
10. T. Munsat, K. Davies, *Neuromuscul. Disord.* **6**, 125 (1996).
11. K. Zerres, S. Rudnik-Schoneborn, *Arch. Neurol.* **52**, 518 (1995).
12. M. L. McWhorter, U. R. Monani, A. H. Burghes, C. E. Beattie, *J. Cell Biol.* **162**, 919 (2003).
13. W. Rossoll *et al.*, *J. Cell Biol.* **163**, 801 (2003).
14. S. Jablonka, M. Beck, B. D. Lechner, C. Mayer, M. Sendtner, *J. Cell Biol.* **179**, 139 (2007).
15. Q. Liu, U. Fischer, F. Wang, G. Dreyfuss, *Cell* **90**, 1013 (1997).
16. L. Pellizzoni, N. Kataoka, B. Charroux, G. Dreyfuss, *Cell* **95**, 615 (1998).
17. H. L. Zhang *et al.*, *J. Neurosci.* **23**, 6627 (2003).
18. L. M. Murray *et al.*, *Hum. Mol. Genet.*, **17**, 949 (2008).
19. Materials and methods are available as supporting material on *Science* Online.
20. C. S. Lin, A. Lau, T. Huynh, T. F. Lue, *DNA Cell Biol.* **18**, 27 (1999).
21. V. Delanote, J. Vandekerckhove, J. Gettemans, *Acta Pharmacol. Sin.* **26**, 769 (2005).
22. E. W. Dent, F. B. Gertler, *Neuron* **40**, 209 (2003).
23. U. R. Monani *et al.*, *Hum. Mol. Genet.* **9**, 333 (2000).
24. T. L. Carrel *et al.*, *J. Neurosci.* **26**, 11014 (2006).

25. We thank SMA families and genetic counselors, especially S. Rudnik-Schöneborn and K. Zerres; J. L. Schultze, S. Debey, P. Nürnberg, M. Reza-Tollat, F. Rivero-Crespo, and F.G. Hanisch at the Univ. of Cologne for allowing us to use their facilities and for helpful advice; G. Morris (Oswestry, UK) for the mouse anti-survival motor neurons proteins 1 antibody; and B. Wollnik, C. Kubisch, and R. Heller for critical reading of the manuscript. This work was supported by the Center for Molecular Medicine Cologne and the Deutsche Forschungsgemeinschaft (B.W.), families of SMA (W.R. and M.L.M.), and NIH grants RO1NS50414 (C.E.B.) and HD055835 (G.J.B.).

Supporting Online Material

www.sciencemag.org/cgi/content/full/320/5875/524/DC1
Materials and Methods
SOM Text
Figs. S1 to S10
Tables S1 to S4
References and Notes

10 January 2008; accepted 20 March 2008
10.1126/science.1155085

Role of *C. elegans* TAT-1 Protein in Maintaining Plasma Membrane Phosphatidylserine Asymmetry

Monica Darland-Ransom,[1] Xiaochen Wang,[1]* Chun-Ling Sun,[1]* James Mapes,[1] Keiko Gengyo-Ando,[2] Shohei Mitani,[2] Ding Xue[1]†

The asymmetrical distribution of phospholipids on the plasma membrane is critical for maintaining cell integrity and physiology and for regulating intracellular signaling and important cellular events such as clearance of apoptotic cells. How phospholipid asymmetry is established and maintained is not fully understood. We report that the *Caenorhabditis elegans* P-type adenosine triphosphatase homolog, TAT-1, is critical for maintaining cell surface asymmetry of phosphatidylserine (PS). In animals deficient in *tat-1*, PS is abnormally exposed on the cell surface, and normally living cells are randomly lost through a mechanism dependent on PSR-1, a PS-recognizing phagocyte receptor, and CED-1, which contributes to recognition and engulfment of apoptotic cells. Thus, *tat-1* appears to function in preventing appearance of PS in the outer leaflet of plasma membrane, and ectopic exposure of PS on the cell surface may result in removal of living cells by neighboring phagocytes.

Class IV P-type adenosine triphosphatases (ATPases) are putative aminophospholipid translocases (APLTs) that are suggested to promote the inward movement of aminophospholipids such as phosphatidylserine (PS), resulting in the restriction of PS to the inner leaflet of the plasma membrane (*1*–*3*). There are six *Caenorhabditis elegans* homologs of the human aminophospholipid translocases (fig. S1A) (*4*), which were named the *tat* genes as transbilayer amphipath transporters. To investigate the functions of these *C. elegans tat* genes, we used the RNA interference (RNAi) method to reduce their expression and examined whether RNAi treatment of the *tat* genes altered PS distribution in *C. elegans* germ cells with an annexin V–based staining protocol that specifically labels surface-exposed PS in *C. elegans* germ cells (*5*).

In wild-type *C. elegans*, no PS staining was observed on the surface of normal germ cells (Fig. 1A), whereas about 60% of apoptotic germ cells were labeled by annexin V (*5*). In *tat-1*(RNAi)–treated animals, PS staining was observed on the surface of many normal germ cells (Fig. 1B). These PS-stained germ cells appeared not to be

[1]Department of Molecular, Cellular, and Developmental Biology, University of Colorado, Boulder, CO 80309, USA. [2]Department of Physiology, Tokyo Women's Medical University School of Medicine and Core Research for Embryonic Science and Technology (CREST), Japan Science and Technology Agency (JST), Tokyo, 162-8666, Japan.

*These authors contribute equally to this work.

†To whom correspondence should be addressed. E-mail: ding.xue@colorado.edu

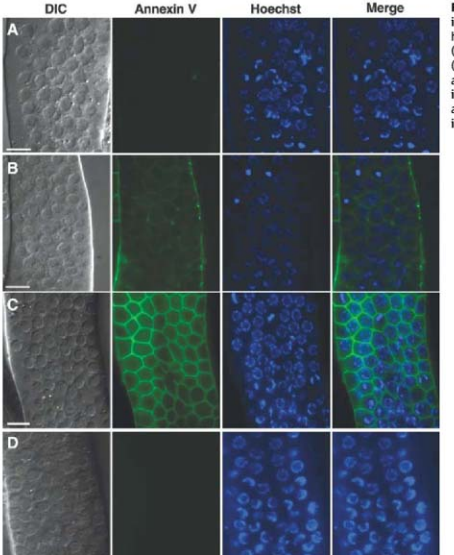

Fig. 1. Exposure of PS on the surface of *C. elegans* germ cells in *tat-1*–deficient animals. Exposed gonads of the following hermaphrodite adult animals were stained with annexin V (*5*): **(A)** wild-type animal (N2), **(B)** *tat-1* RNAi-treated N2 animal, **(C)** *tat-1(tm1034)* animal, and **(D)** *tat-3(tm1275)* animal. Images of differential contrast interference (DIC), annexin V staining, Hoechst 33342 staining, and the merged image of annexin V plus Hoechst 33342 staining are shown. Scale bars indicate 6.5 μm.

apoptotic cells or damaged cells because they lacked the raised buttonlike morphology and the condensed Hoechst 33342 DNA staining pattern that are characteristic of apoptotic germ cells and were not stained by propidium iodide, which stains necrotic or damaged cells (*6*, *7*). RNAi of the other *tat* genes (*tat-2*, *tat-3*, *tat-4*, *tat-5*, and *tat-6*) did not result in PS staining on the surface of living germ cells (table S1). Thus, reduction of the *tat-1* activity alone appears to be sufficient to disrupt asymmetrical PS distribution on the surface of *C. elegans* germ cells.

To confirm the RNAi results, we isolated a deletion allele of *tat-1* (*tm1034*) and a deletion allele of *tat-3* (*tm1275*) (*4*). The *tat-1(tm1034)* mutant contains a 597–base pair (bp) deletion plus a 1-bp insertion in the *tat-1* locus that is predicted to cause a frame shift and an early stop after exon five (fig. S1B) and would remove the ATPase domain as well as 8 of the 10 putative transmembrane domains of TAT-1. The *tat-3(tm1275)* mutant has a 446-bp deletion and a 7-bp insertion that removes parts of the first two exons of the *tat-3* gene and is likely a null allele (fig. S1B).

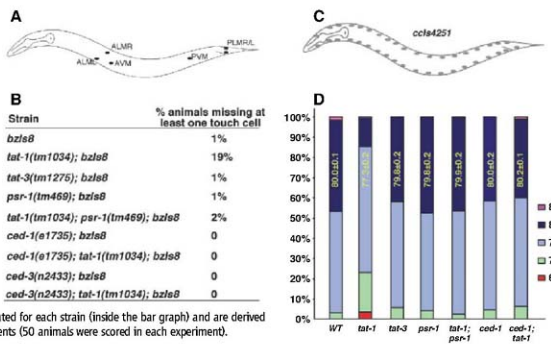

Fig. 2. Random loss of neurons and muscle cells in *tat-1*–deficient animals through a mechanism mediated by *psr-1* and *ced-1*. An integrated GFP reporter line, *bzIs8*, labels six touch-receptor neurons and an integrated GFP reporter line, *ccIs4251*, directs GFP expression in body-wall muscle cells. Neurons or muscle cells that were scored are indicated with black or gray circles (**A** and **C**). The presence of neurons or the number of muscle cells was scored by using a Nomarski microscope with epifluorescence. The percentages of animals missing one or more neurons (**B**) or the percentages of animals with a certain range of muscle cell numbers (**D**) are shown. At least 200 animals were scored for each strain. The average muscle cell number and standard error of mean (SEM) are indicated for each strain (inside the bar graph) and are derived from at least four independent experiments (50 animals were scored in each experiment).

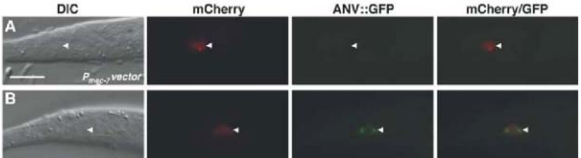

Fig. 3. PS exposure on the surface of the PLM touch cells and PLM cell loss in animals with cell type–specific knockdown of the *tat-1* gene. Animals carrying an integrated transgene harboring P_{hsp}ANV::GFP and an extrachromosomal array containing P_{mec-4}mCherry and P_{mec-7}vector (**A**) or P_{mec-4}mCherry and P_{mec-7}*tat-1IR* (**B**) were subjected to heat-shock treatment at 30°C for 35 min. Two hours later, L2 transgenic larvae were examined with use of a Nomarski (Zeiss, Göttinger, Germany) microscope with epifluorescence. The presence of the PLM cell (indicated by an arrowhead) is revealed by the expression of monomeric Cherry protein (mCherry) from P_{mec-4}mCherry. PS exposure on the surface of the PLM cell is indicated by ANV::GFP labeling. [(A) and (B)] Images of DIC, mCherry, ANV::GFP, and the merged image of mCherry/ANV::GFP are shown. Scale bars indicate 10 μm. (**C**) Quantification of the percentage of the PLM cells showing surface-exposed PS. (**D**) Quantification of the percentage of the PLM cells lost. L1, L2, and L3 indicate three independent transgenic lines for each indicated construct (all contain P_{mec-4}mCherry). Animals carrying these arrays were then crossed into the *ced-1(e1735)* or the *psr-1(tm469)* mutant to generate the mutant strains carrying the same arrays. Numbers in parentheses indicate the number of animals scored. Each animal has two PLM cells (PLML and PLMR).

C

Strain	% PLM cells showing surface ANV::GFP
P_{mec-7} vector, L1	10% (64)
P_{mec-7} vector, L2	10% (64)
P_{mec-7} vector, L3	5% (64)
P_{mec-7}*tat-1IR*, L1	50% (65)
P_{mec-7}*tat-1IR*, L2	57% (64)
P_{mec-7}*tat-1IR*, L3	60% (51)

D

Strain	% PLM cell missing
P_{mec-7} vector, L1	4% (50)
P_{mec-7} vector, L2	4% (67)
P_{mec-7} vector, L3	3% (66)
P_{mec-7}*tat-1IR*, L1	13% (55)
P_{mec-7}*tat-1IR*, L2	15% (62)
P_{mec-7}*tat-1IR*, L3	19% (62)
ced-1(e1735); P_{mec-7}*tat-1IR*, L1	7% (60)
ced-1(e1735); P_{mec-7}*tat-1IR*, L2	4% (61)
ced-1(e1735); P_{mec-7}*tat-1IR*, L3	3% (60)
psr-1(tm469); P_{mec-7}*tat-1IR*, L1	4% (61)
psr-1(tm469); P_{mec-7}*tat-1IR*, L2	5% (60)
psr-1(tm469); P_{mec-7}*tat-1IR*, L3	7% (61)

tat-1(tm1034) and *tat-3(tm1275)* animals are viable and superficially indistinguishable from each other. Both mutants display a low penetrance of lethality and dumpy (Dpy) phenotypes. *tat-1(tm1034)* animals also have increased numbers of spontaneous males.

When we stained exposed gonads of the *tat-1(tm1034)* and *tat-3(tm1275)* animals with annexin V, all germ cells in *tat-1(tm1034)* animals displayed strong PS staining on their surface (Fig. 1C). No germ cells from the *tat-3(tm1275)* animals were stained by annexin V (Fig. 1D). Germ cell staining for PS in *tat-1(tm1034)* animals was stronger and more widespread than that in *tat-1* RNAi animals (Fig. 1, B and D) and was not affected by loss of the *C. elegans* phospholipid scramblases (SOM text and fig. S2), some of which promotes PS externalization in apoptotic cells (*5*). Taken together, these results suggest that *tat-1* is essential for keeping PS from the outer leaflet of plasma membrane and provide in vivo evidence that a member of the aminophospholipid translocase family functions to restrict PS to the inner leaflet of the plasma membrane, possibly by promoting inward movement of PS from the outer leaflet.

A study using a fusion protein containing green fluorescent protein and annexin V (GFP::AnxV) as a PS sensor reached the opposite conclusion that *tat-1* promotes externalization of PS in *C. elegans* apoptotic cells (*8*). We think that the difference between the two studies could result from the relatively weak binding of GFP::AnxV in vivo to surface-exposed PS and a high-staining background (SOM text and fig. S3). The optimized ex vivo PS-staining protocol that we used generated strong and specific PS staining (fig. S3) (*5*), and we did not observe reduced PS staining of apoptotic germ cells in the *tat-1(tm1034)* mutant (SOM text and fig. S4), indicating that *tat-1* does not promote externalization of PS in apoptotic cells.

Because externalization of PS is a conserved event during apoptosis and has been proposed to serve as an engulfment signal to trigger phagocytosis of apoptotic cells (*5*, *9*, *10*), we examined whether loss of the *tat-1* activity affected apoptosis or removal of apoptotic cells in *C. elegans*. The *tat-1(tm1034)* mutation did not affect the numbers of embryonic cell corpses present in various embryonic stages in which most somatic cell deaths occur or the numbers of germ cell corpses in the germ line (fig. S5), suggesting that *tat-1* alone does not have a detectable role in apoptosis or removal of apoptotic cells. However, we observed that some cells were missing in the *tat-1(tm1034)* mutant and therefore used integrated transgenes carrying various GFP reporters that label specific cells or cell types to help identify the missing cells in the *tat-1* mutant. For example, the *bzIs8* transgene specifically labels six touch-receptor neurons (*11*). In *tat-1(tm1034); bzIs8* animals, all six touch cells were randomly lost in a certain percentage of animals (from 1% to 9% depending on the specific touch cells), and 19% of animals lost at least one touch-receptor neuron (Fig. 2, A and B). Touch-receptor neurons were rarely missing in *bzIs8* or *tat-3(tm1275); bzIs8* animals. A similar percentage of animals (24%) were missing at least one cell in *inIs179*; *tat-1(tm1034)* animals, in which 16 neurons were labeled by the $P_{ida\text{-}1}$*gfp* reporter (fig. S6, A and B) (*12*). Again, all neurons labeled by *inIs179* were randomly lost, and such cell loss was not seen in *inIs179* or *inIs179; tat-3(tm1275)* animals. The missing-cell phenotype of the *tat-1(tm1034)* mutant was not restricted to neurons; hypodermal, epithelial, and muscle cells were randomly lost as well. For example, wild-type animals contain an average of 80 body-wall muscle cells (labeled by the *ccIs4251* transgene) with a range from 71 to 90 muscle cells in individual animals (Fig. 2, C and D) (*13*). In *tat-1(tm1034)* animals, the average number of muscle cells was reduced to 77 ($P < 0.0001$, unpaired t test), ranging from 65 to 90 muscle cells, with 23% of animals containing less than 76 muscle cells and 15% of animals having more than 80 muscle cells. In comparison, only 3 to 6% of wild-type or *tat-3(tm1275)* animals have less than 76 muscle cells, and 43 to 47% of them have more than 80 muscle cells. Thus, loss of the *tat-1* activity but not loss of the *tat-3* activity causes indiscriminate cell loss in various cell types.

We then examined whether normal somatic cells also expose PS in the *tat-1(tm1034)* mutant. The ex vivo germ-cell PS-staining protocol cannot be applied to stain somatic cells, which are enclosed by a hard, impermeable eggshell. Expression of a secreted annexin V–GFP fusion similar to the one used by Zullig *et al.* (*8*) in the *tat-1(tm1034)* mutant did not reveal obvious surface PS exposure in normal somatic cells, possibly because of competition for binding to the annexin V–GFP fusion and high background staining. We therefore generated cell type–specific knockdown of the *tat-1* gene by expressing a *tat-1* inverted-repeat (IR) RNAi construct in six touch cells under the control of the *C. elegans mec-7* promoter ($P_{mec\text{-}7}$*tat-1IR*). This construct generates double-stranded RNA (dsRNA) that reduces gene expression in vivo (*14*). A high percentage of the posterior lateral microtubule (PLM) touch cells (50 to 60%) in transgenic animals carrying $P_{mec\text{-}7}$*tat-1IR* and expressing a secreted annexin V–GFP fusion under the control of heat-shock promoters (P_{hsp}ANV::GFP) displayed ANV::GFP on their surface (Fig. 3, B and C). In contrast, transgenic animals carrying a control vector and P_{hsp}ANV::GFP had a low percentage of PLM cells (5 to 10%) labeled by ANV::GFP, which may be nonspecific staining (Fig. 3, A and C). Furthermore, in transgenic animals carrying $P_{mec\text{-}7}$*tat-1IR*, 13 to 19% of the PLM neurons were missing, whereas in transgenic animals carrying the control vector few PLM neurons (3 to 4%) were lost (Fig. 3D). Together, these results demonstrate that reduction of *tat-1* activity may cause inappropriate PS exposure on the surface of somatic cells and the random loss of these cells.

We investigated the cause of random cell loss in the *tat-1(tm1034)* mutant. PS or oxidized PS exposed on the surface of apoptotic cells can act as a signal to trigger phagocytic removal of apoptotic cells (*5*, *9*, *15*, *16*). A loss-of-function mutation (*tm469*) in the *C. elegans psr-1* gene, which encodes a PS-binding phagocyte receptor (*5*, *17*), rescued the missing cell phenotype in the *tat-1* mutant and the $P_{mec\text{-}7}$*tat-1IR* animals (Figs. 2, B and D and 3D, and fig. S6B). *psr-1* has a minor role in *C. elegans* in removing apoptotic cells (*17*), which likely contain multiple engulfment signals, but appears to have a major role in the *tat-1* mutant to mediate removal of normal cells with surface-exposed PS. Similarly, a loss-of-function mutation (*e1735*) in the *ced-1* gene, which is important for recognition and engulfment of apoptotic cells (*18*), or a loss-of-function mutation (*n2433*) in *ced-3*, which encodes the key cell-killing caspase in *C. elegans* and cooperates with the phagocytosis process to kill cells (*19*–*21*), suppressed the missing cell phenotype of the *tat-1* mutant (Fig. 2, B and D, and fig. S6B). Thus, cells in the *tat-1* mutant are lost through a phagocytic mechanism that is used to remove apoptotic cells.

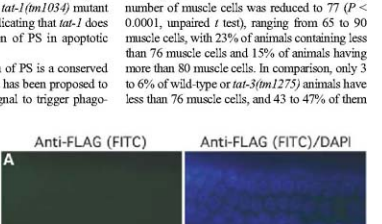

Fig. 4. Localization of TAT-1 to plasma membrane of *C. elegans* germ cells. Gonads from a *tat-1(tm1034); bzIs8* animal (**A**) and a *tat-1 (tm1034); smIs142; bzIs8* animal (**B**) were dissected out and stained with M2 monoclonal antibody (anti-FLAG) (*4*). *smIs142* is an integrated transgene carrying $P_{tat\text{-}1}$*tat-1::flag*. Images of *C. elegans* gonads with fluorescein isothiocyanate (FITC) staining (anti-FLAG) and FITC/4′,6′-diamidino-2-phenylindole (DAPI) staining are shown. The mosaic pattern of FITC staining in (B) may be due to partial germline silencing of the *smIs142* transgene (*25*). Scale bars indicate 6.5 μm.

We examined the cellular localization of TAT-1 by expressing a TAT-1 fusion protein tagged at its carboxyl terminus with a FLAG epitope under the control of the *tat-1* gene promoter ($P_{tat\text{-}1}$*tat-1::flag*). Several extrachromosomal transgene arrays and an integrated transgene (*smIs142*) carrying $P_{tat\text{-}1}$*tat-1::flag* were generated and all fully rescued the missing cell phenotype of the *tat-1(tm1034)* mutant (table S2). *smIs142* also partially rescued the germ cell PS exposure defect of the *tat-1(tm1034)* mutant (fig. S7). Immunostaining of gonads from the *smIs142* animals using a monoclonal antibody (M2) to the FLAG epitope revealed that TAT-1 localizes predominantly on the plasma membrane (Fig. 4).

Class IV P-type ATPases have been suggested to promote translocation of aminophospholipids [PS and phosphatidylethanolamine (PE)] from the outer leaflet to the inner leaflet of plasma membrane and thus may have a role in maintaining asymmetrical distribution of PS and PE on the lipid bilayer (*3*, *22*, *23*). However, in multicellular organisms, multiple members of this ATPase family exist (at least 14 were identified in mammals), which prevents genetic analysis of their in vivo functions (*3*, *22*, *24*). Our findings thus provide important in vivo evidence that a member of the aminophospholipid translocase family is involved in maintaining PS asymmetry on plasma membrane and that disruption of such PS asymmetry can result in indiscriminate removal of affected cells by neighboring phagocytes.

References and Notes

1. M. E. Auland, B. D. Roufogalis, P. F. Devaux, A. Zachowski, *Proc. Natl. Acad. Sci. U.S.A.* **91**, 10938 (1994).
2. J. K. Paterson *et al.*, *Biochemistry* **45**, 5367 (2006).
3. D. L. Daleke, *J. Lipid Res.* **44**, 233 (2003).
4. Materials and methods are available on *Science* Online.
5. X. Wang *et al.*, *Nat. Cell Biol.* **9**, 541 (2007).
6. Z. Darzynkiewicz *et al.*, *Cytometry* **13**, 795 (1992).
7. R. A. Harrison, S. E. Vickers, *J. Reprod. Fertil.* **88**, 343 (1990).
8. S. Zulfig *et al.*, *Curr. Biol.* **17**, 994 (2007).
9. V. A. Fadok *et al.*, *J. Immunol.* **149**, 4029 (1992).
10. V. A. Fadok, D. Xue, P. Henson, *Cell Death Differ.* **8**, 582 (2001).
11. D. C. Royal *et al.*, *J. Biol. Chem.* **280**, 41976 (2005).
12. T. R. Zahn, M. A. Macmorris, W. Dong, R. Day, J. C. Hutton, *J. Comp. Neurol.* **429**, 127 (2001).
13. L. Timmons, D. L. Court, A. Fire, *Gene* **263**, 103 (2001).
14. N. Tavernarakis, S. L. Wang, M. Dorovkov, A. Ryazanov, M. Driscoll, *Nat. Genet.* **24**, 180 (2000).
15. M. E. Greenberg *et al.*, *J. Exp. Med.* **203**, 2613 (2006).
16. H. Bayir *et al.*, *Biochim. Biophys. Acta* **1757**, 648 (2006).
17. X. Wang *et al.*, *Science* **302**, 1563 (2003).
18. Z. Zhou, E. Hartwieg, H. R. Horvitz, *Cell* **104**, 43 (2001).
19. J. Yuan, S. Shaham, S. Ledoux, H. M. Ellis, H. R. Horvitz, *Cell* **75**, 641 (1993).
20. P. W. Reddien, S. Cameron, H. R. Horvitz, *Nature* **412**, 198 (2001).
21. D. J. Hoeppner, M. O. Hengartner, R. Schnabel, *Nature* **412**, 202 (2001).
22. T. Pomorski, A. K. Menon, *Cell. Mol. Life Sci.* **63**, 2908 (2006).
23. J. Ding *et al.*, *J. Biol. Chem.* **275**, 23378 (2000).
24. K. Balasubramanian, A. J. Schroit, *Annu. Rev. Physiol.* **65**, 701 (2003).
25. W. G. Kelly, S. Xu, M. K. Montgomery, A. Fire, *Genetics* **146**, 227 (1997).

26. We thank Y. Shi for help with constructs; A. Fire for the *ccfs4251* strain, J. Hutton for the *ins179* strain, M. Hengartner for the *opls117* strain, M. Driscoll for the *bzIs8* strain and the $P_{mec\text{-}4}$mCherry construct, and X. Xie and T. Blumenthal for comments on the manuscript. This work was supported by the Burroughs Wellcome Fund Career Award (D.X.), a grant from MEXT of Japan (S.M.), NIH grant R01 GM59083 (D.X.), and Human Frontier Science Program grant RGP0016/2005-C (D.X.).

Supporting Online Material

www.sciencemag.org/cgi/content/full/320/5875/528/DC1
Materials and Methods
SOM Text
Figs. S1 to S7
Tables S1 and S2
References and Notes

29 January 2008; accepted 11 March 2008
10.1126/science.1155847

Vaccinia Virus Uses Macropinocytosis and Apoptotic Mimicry to Enter Host Cells

Jason Mercer and Ari Helenius*

Viruses employ many different strategies to enter host cells. Vaccinia virus, a prototype poxvirus, enters cells in a pH-dependent fashion. Live cell imaging showed that fluorescent virus particles associated with and moved along filopodia to the cell body, where they were internalized after inducing the extrusion of large transient membrane blebs. p21-activated kinase 1 (PAK1) was activated by the virus, and the endocytic process had the general characteristics of macropinocytosis. The induction of blebs, the endocytic event, and infection were all critically dependent on the presence of exposed phosphatidylserine in the viral membrane, which suggests that vaccinia virus uses apoptotic mimicry to enter cells.

Poxviruses are enveloped DNA viruses that differ from other animal viruses in their large size and complexity (*1*). For humans, the most dangerous is variola virus, the causative agent of smallpox and one of most devastating pathogens in history. The development of new antiviral strategies against poxviruses will require detailed information about their replication cycle (*2*).

During replication, two infectious forms of vaccinia are produced: intracellular mature virus (MV) and extracellular enveloped virus (EV). The binding of MVs to cells involves cell-surface glycosaminoglycans (*3*), and MVs have been observed binding to actin-containing fingerlike protrusions (*4*). The viral envelope can fuse directly with the plasma membrane (*5*), but productive entry occurs mainly by low pH–dependent endocytosis into large uncoated vacuoles (*5*).

To follow the entry of individual virions, we generated MVs with an enhanced yellow fluorescent protein (EYFP)–tagged core protein [EYFP-CORE-MVs (*6*)]. When added to cells expressing enhanced green fluorescent protein (EGFP)–actin or enhanced cyan fluorescent protein–actin, virions that bound to filopodia moved toward the cell body (Fig. 1A and movies S1 to S3). As seen with other viruses (*7*), the movement was uninterrupted, with a rate approximating that of actin retrograde flow (1.05 ± 0.38 μm/min, fig. S1).

When MVs reached the cell body, a dramatic change occurred in the plasma membrane: A large, roughly spherical bleb (diameter 2 ± 0.57 μm; n = 42 blebs) extruded at the site of contact with the virus, followed by the formation of further blebs along the cell body. Each bleb remained extended for 10 ± 2 s (n = 42) before actin accumulated on the membrane, and the bleb retracted within 18 ± 3 s (n = 42) (Fig. 1B, movies S4 to S6, and figs. S2 and S3). Bleb retraction and cortical actin reassembly coincided with virus entry. Blebbing peaked 30 min after virus addition (Fig. 1C). The fraction of blebbing cells increased with the multiplicity of infection (MOI), while the number of blebs per blebbing cell remained in the range of 75 to 125 (Fig. 1, D and E, and fig. S4). Thus, a single incoming MV induced a generalized state in the cell that promoted bleb formation along the entire cell body.

To test whether blebbing was needed for infection, we used blebbistatin, an inhibitor of myosin II–dependent blebbing (*8*). Infection was quantified with EGFP-expressing MVs (EGFP-EXPRESS-MVs) and fluorescence-activated cell sorting (FACS) (fig. S5) (*6*). Blebbistatin prevented the formation of MV-induced blebs (fig. S6) and inhibited infection by 65% (Fig. 1F), which suggests that bleb formation was involved in productive entry.

In addition to actin, blebs contained Rac1, RhoA, ezrin, and cortactin (Fig. 1G), which are important for plasma membrane blebbing under other conditions (*9*) and for MV entry (*4*). MV-

ETH Zurich, Institute of Biochemistry, Schafmattstrasse 18, ETH Hönggerberg HPM E6.3 Zurich, Switzerland.

*To whom correspondence should be addressed. E-mail: ari.helenius@bc.biol.ethz.ch

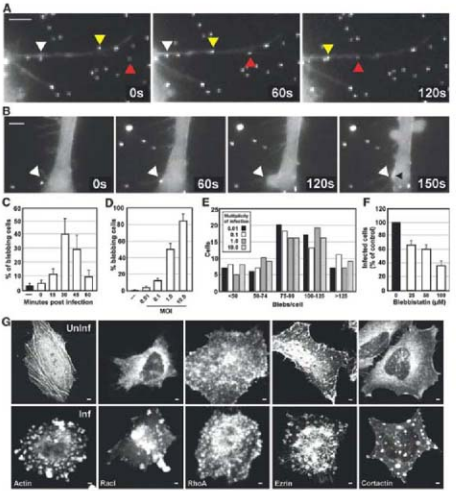

Fig. 1. Virion movement and membrane perturbation during MV entry. **(A)** EYFP-CORE-MVs were added to cells expressing GFP-actin. Arrowheads highlight virions. Scale bars, 2 μm (movies S1 to S3). **(B)** Imaging was performed as in **(A)**. The virion of interest is indicated by the white arrowheads. The actin patch at the site of bleb collapse is indicated by a black arrowhead. Scale bars, 2 μm. (movies S4 to S6). **(C)** Infected cells were fixed at the indicated times and scored for blebbing. Data are means of triplicate experiments ± SD. **(D)** Cells infected at varying MOIs (0.01 to 10) were fixed 30 min after infection and blebbing cells were quantified (for images, see fig. S4). Data are means of triplicate experiments ± SD. **(E)** Blebbing cells from (D) were analyzed for the number of blebs per cell. Results of triplicate experiments are shown. **(F)** Confluent blebbistatin-treated cells were infected with EGFP-EXPRESS-MVs. Infection was determined by fluorescence-activated cell sorting (FACS) (*6*). Data are means of triplicate experiments ± SD. **(G)** Fluorescently tagged proteins were visualized in uninfected (uninf) and infected (inf) cells. Images are displayed as a maximum projected *z* stack of 10 confocal slices. Scale bars, 2 μm.

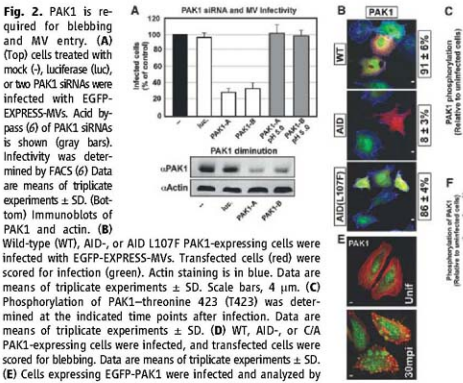

Fig. 2. PAK1 is required for blebbing and MV entry. **(A)** (Top) cells treated with mock (-), luciferase (luc), or two PAK1 siRNAs were infected with EGFP-EXPRESS-MVs. Acid bypass (*6*) of PAK1 siRNAs is shown (gray bars). Infectivity was determined by FACS (*6*) Data are means of triplicate experiments ± SD. (Bottom) Immunoblots of PAK1 and actin. **(B)** Wild-type (WT), AID-, or AID L107F PAK1-expressing cells were infected with EGFP-EXPRESS-MVs. Transfected cells (red) were scored for infection (green). Actin staining is in blue. Data are means of triplicate experiments ± SD. Scale bars, 4 μm. **(C)** Phosphorylation of PAK1–threonine 423 (T423) was determined at the indicated time points after infection. Data are means of triplicate experiments ± SD. **(D)** WT, AID-, or C/A PAK1-expressing cells were infected, and transfected cells were scored for blebbing. Data are means of triplicate experiments ± SD. **(E)** Cells expressing EGFP-PAK1 were infected and analyzed by confocal microscopy. Images are displayed as a maximum projected *z* stack of 10 confocal slices (*6*). Actin staining is in red. Scale bars, 4 μm. **(F)** Pretreated cells were infected with EGFP-EXPRESS-MVs. Lysates were analyzed for PAK1 phosphorylation. Data are means of triplicate experiments ± SD. Treatments were as follows: untreated (–), staurosporin (STAU), genistein (GENI), wortmannin (WORT), cytochalasin D (CYTO), latrunculin A (LATR), jaspakinolide (JASP), EIPA, and blebbistatin (BLEB). **(G)** Cells expressing WT or C/A PAK1 and pretreated with STAU, GENI, WORT, or EIPA were infected with EGFP-EXPRESS-MVs. Transfected cells were scored for infection. Data are means of triplicate experiments ± SD.

induced blebbing resembled that observed during cell motility, cytokinesis, and apoptosis (*9*–*11*).

Our investigations into the cellular factors required for MV blebbing and entry first focused on p21-activated kinase 1 (PAK1), an essential factor for MV infection. PAK1 is a serine-threonine kinase with a central role in cell motility (*12*). To validate the requirement for PAK1 in infection, we used two small interfering RNAs (siRNAs), which gave 82 and 76% knockdown of PAK1 protein (Fig. 2A, bottom). Infection was reduced by 74 and 68%, respectively (Fig. 2A, top). The PAK1 autoinhibitory domain (AID) inhibited infection by 83%, whereas an inactive AID (AID L107F) caused only a 5% reduction in infection (Fig. 2B). When MVs were added to cells, phosphorylation of threonine 423 of PAK1, which is essential for macropinocytosis (*13*), was detected (Fig. 2C).

Acid-mediated bypass (*6*) of PAK1 siRNA demonstrated that PAK1 was required for prefusion events (Fig. 2A, gray bars). PAK1 was also needed for blebbing: PAK1-AID reduced blebbing by 94%, whereas constitutive active (C/A T423E) PAK1 increased blebbing by 53% (Fig. 2D). Additionally, PAK1 localized into membrane blebs during infection (Fig. 2E).

Next, several perturbants were tested for effects on blebbing and infection, including dominant-negative (D/N) and C/A Rac1, C/A Arf6, and D/N dynamin-2, as well as inhibitors of RhoA, dynamin-2, PKC, serine, threonine, tyrosine- and PI 3-kinases (PI3Ks); Na^+/H^+ exchangers and macropinocytosis; endosomal fusion; actin dynamics; and blebbing.

Many perturbants inhibited both blebbing and infection, confirming that the two processes are linked. Both were dependent on tyrosine, serine-threonine, and PI3Ks; Na^+/H^+ exchangers; actin; Rac1; and PAK1 (Figs. 2 and 3, figs. S6 to S8, and table S1). After acid bypass, the inhibitors failed to block infection, indicating that each affected pre-fusion steps (Fig. 3C, pH 5.0). Bypass of monensin and bafilomycin A1 has been demonstrated (*5*). C/A Arf6 inhibited infection by 78% (Fig. 3D), whereas D/N dynamin 2 and dynasore had no impact (Fig. 3E and fig. S7).

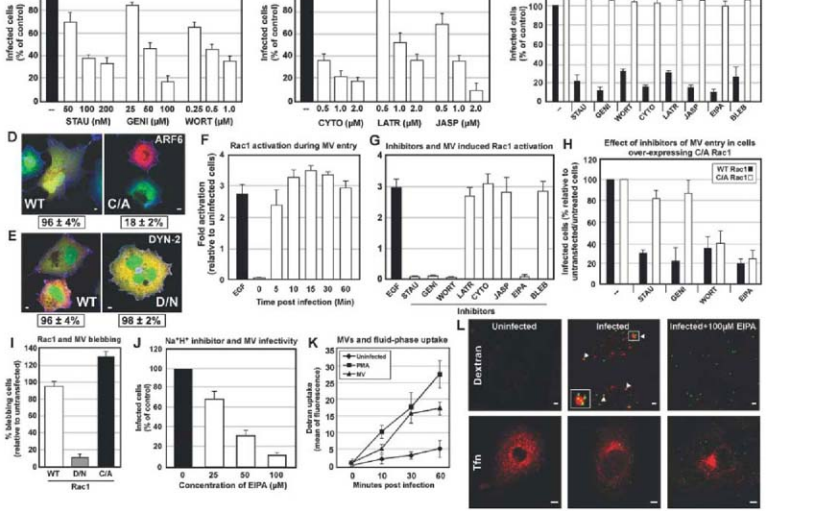

Fig. 3. MVs use macropinocytosis to enter cells. (**A** and **B**) The effect of kinase inhibitors and actin effectors on infectivity was assayed with FACS (*6*). Data are means of triplicate experiments ± SD. (**C**) Acid-mediated bypass was performed on inhibitor-treated infected cells. Infection was scored by FACS (*27*). Data are means of triplicate experiments ± SD. Abbreviations are as in Fig. 2F. (**D** and **E**) Cells expressing WT or mutant (C/A or D/N) Arf6 or Dyn 2 were infected with EGFP-EXPRESS-MVs. Cells were analyzed as in Fig. 2B (*28*). Data are means of triplicate experiments ± SD. Scale bars, 4 μm. (**F**) Activation of Rac1 was assessed at the indicated times [Cytoskeleton, Denver, CO (*6*)]. Data are means of triplicate experiments ± SD. (**G**) Experiments were performed as in Fig. 2F and analyzed as above. Inhibitors are abbreviated as in Fig. 2F. (**H**) Experiments were performed as in Fig. 2G. Data are means of triplicate experiments ± SD. (**I**) WT, D/N-, or C/A Rac1–expressing cells were infected with MVs. Transfected cells were scored for blebbing. Data are means of triplicate experiments ± SD. (**J**) Cells pretreated with EIPA were infected with EGFP-EXPRESS-MVs and analyzed by FACS (*6*). Data are means of triplicate experiments ± SD. (**K**) MV-infected cells were pulsed with 488-dextran 10 min before being harvested. Cells were analyzed by FACS (*6*) Untreated (negative control) and PMA (positive control) are shown. Data are means of triplicate experiments ± SD. (**L**) EYFP-CORE-MVs were internalized in the presence of 70-kD 568-dextran or 568-transferrin (Tfn). Cells were visualized for virions (green) and dextran or Tfn (red). The effect of EIPA treatment was assessed in parallel. Scale bars, 4 μm.

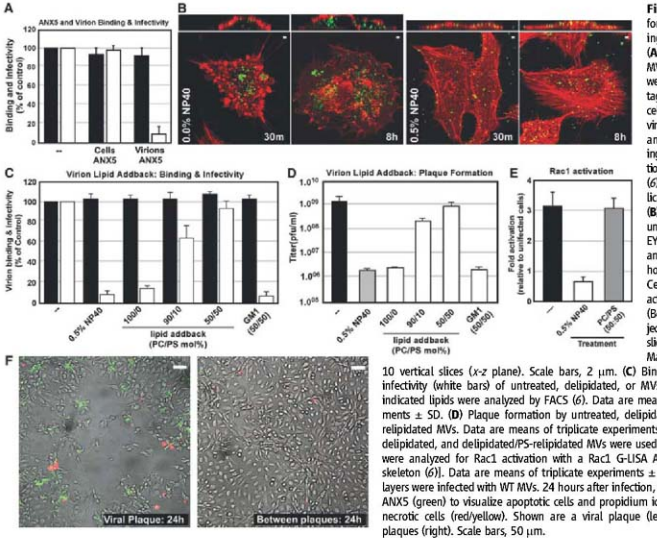

Fig. 4. PS is required for MV-induced signaling and internalization. **(A)** Cells or EYFP-CORE-MVs/EGFP-EXPRESS-MVs were pretreated with untagged ANX5 (*6*). Treated cells (cells ANX5) and virions (virions-ANX5) were analyzed for viron binding (black bars) and infection (white bars) by FACS (*6*). Data are means of triplicate experiments ± SD. **(B)** Cells were infected with untreated or delipidated EYFP-CORE-MVs (green) and fixed 30 min or 8 hours after virus addition. Cells were stained for actin (red), and visualized. (Bottom) Maximum *z* projection of 10 horizontal slices (*x*-*y* plane). (Top) Maximum *z* projection of 10 vertical slices (*x*-*z* plane). Scale bars, 2 μm. **(C)** Binding (black bars) and infectivity (white bars) of untreated, delipidated, or MVs relipidated with the indicated lipids were analyzed by FACS (*6*). Data are means of triplicate experiments ± SD. **(D)** Plaque formation by untreated, delipidated, and delipidated/relipidated MVs. Data are means of triplicate experiments ± SD. **(E)** Untreated, delipidated, and delipidated/PS-relipidated MVs were used to infect cells. Lysates were analyzed for Rac1 activation with a Rac1 G-LISA Activation Assay [Cytoskeleton (*6*)]. Data are means of triplicate experiments ± SD. **(F)** BSC40 monolayers were infected with WT MVs. 24 hours after infection, cells were stained with ANX5 (green) to visualize apoptotic cells and propidium iodide (red) to visualize necrotic cells (red/yellow). Shown are a viral plaque (left) and cells between plaques (right). Scale bars, 50 μm.

Rac1, a regulatory guanosine triphophatase of PAK1, was activated during MV entry (Fig. 3F). Staurosporin, genistein, wortmannin, and 5-*N*-ethyl-*N*-isopropyl-amiloride (EIPA) prevented activation of PAK1 and Rac1, whereas actin effectors and blebbistatin did not (Figs. 2F and 3G). C/A Rac1 and PAK1 restored infection in the presence of staurosporin and genistein but not wortmannin or EIPA (Figs. 2G and 3H). These results are consistent with the need for tyrosine and possibly serine–/threonine kinase, PI3K and Na^+/H^+ exchange upstream of PAK1 and Rac1, and downstream PI3K and Na^+/H^+ exchange activity. Additionally, D/N Rac1 inhibited blebbing 84%, and C/A Rac1 increased blebbing 30% (Fig. 3I). Although activated during infection (fig. S8A), RhoA inhibition did not prevent blebbing (fig. S8B) but accelerated infection as previously demonstrated (fig. S8, C and D) (*4*, *14*).

With this perturbation pattern, it was likely that MVs were using macropinocytosis (table S1 and Fig. 3) (*15*, *16*). Sensitivity to inhibitors of Na^+/H^+ exchangers is a characteristic of this pathway (*17*). With 85% inhibition of infectivity, EIPA was the most efficient inhibitor tested (Fig. 3J).

Consistent with macropinocytosis, internalization of 488-dextran was elevated fivefold within 30 min of MV addition (Fig. 3K). Microscopy showed that MVs co-internalized with a fluid-phase (568-dextran), but not a clathrin-mediated (568-transferrin), marker (Fig. 3L).

MVs may use macropinocytosis because of their large size. With few exceptions (*18*), pathogens the size of vaccinia are not internalized by clathrin- or caveolin/raft-mediated endocytosis. However, MVs are comparable in size to apoptotic bodies that are macropinocytosed by professional phagocytes and other cell types (*19*, *20*). The uptake of apoptotic debris is triggered by surface-exposed phosphatidylserine (PS) (*19*).

The MV membrane has been shown to be enriched in PS (36%) (*21*, *22*), and PS is required for infectivity (*23*). When exposed to 647-ANX5, a PS-binding protein, EYFP-CORE-MVs are stained, indicating that PS is exposed on the MV surface (fig. S9). When MV PS was masked with ANX5, infectivity (white bars) was inhibited by 90% without affecting binding (black bars) (Fig. 4A, virions ANX 5). Binding and infectivity were not affected when cells were pretreated with ANX5 (Fig. 4A, cells ANX 5).

To assess the role of viral PS, we treated MVs with Nonidet-P40 (NP-40), which causes a total loss of viral lipid and a dramatic drop in infectivity at a concentration of 0.5% or higher (fig. S10) (*21*, *24*). Extracted virions could bind cells, but they did not induce blebbing or entry (Fig. 4B, 30 min). After 8 hours, extracted MVs were still at the cell surface with no evidence of viral cytopathic effects, MV entry, or replication (Fig. 4B, 8 hours).

Using established methods (*21*), we restored phosphatidylcholine (PC) and varying amounts of PS (0, 10, or 50 mol %) to delipidated viruses. Restoration of PS was confirmed by ANX5 binding (fig. S9). Relipidated MVs bound cells normally (black bars), but only PS-reconstituted viruses exhibited restored infectivity and plaque formation (Fig. 4C, white bars, and Fig. 4D) (*21*). Liposomes containing another negatively charged lipid, ganglioside GM1, did not restore infectivity.

Additionally, delipidated MVs were highly attenuated for Rac1 activation, whereas PS-relipidated MVs (50 mol %) restored Rac1 activation to control levels (Fig. 4E). Thus, viral PS might be analogous to cellular PS in the elimination of apoptotic bodies.

Finally, we analyzed whether vaccinia-infected cells underwent apoptosis or necrosis. Cells at the edge of viral plaques displayed exposed PS (green), a hallmark of apoptosis (*27*), whereas few cells were necrotic (red) (Fig. 4F, left), suggesting that late-stage vaccinia-infected cells undergo apoptosis. Cells between plaques were neither apoptotic nor necrotic (Fig. 4F,

right). MV spread is therefore likely to be connected with apoptosis and a preprogrammed macropinocytic response of neighboring cells to apoptotic bodies.

Vaccinia MVs use macropinocytosis and apoptotic mimicry to enter host cells. There are several advantages of using this entry strategy. First, it permits endocytic internalization of particles too big for other viral endocytic mechanisms. Second, it allows the virus to enter many different cell types, because PS-mediated clearance of apoptotic material is common to most cells (*19*, *26*). Finally, by mimicking an apoptotic body, MVs may avoid immune detection as they spread to surrounding cells, because macropinocytosis of apoptotic debris suppresses the activation of innate immune responses (*26*). The lack of macrophage infiltration and T cell maturation during murine lung infection by vaccinia (*27*) may be explained by this "silent" mechanism of cell-to-cell spread.

References and Notes

1. B. Moss, D. M. Knipe, P. M. Howley, *Fields Virology* (Lippincott-Raven, Philadelphia, PA, 2007), vol. 5.
2. S. C. Harrison *et al.*, *Proc. Natl. Acad. Sci. U.S.A.* **101**, 11178 (2004).
3. G. C. Carter, M. Law, M. Hollinshead, G. L. Smith, *J. Gen. Virol.* **86**, 1279 (2005).
4. J. K. Locker *et al.*, *Mol. Biol. Cell* **11**, 2497 (2000).
5. A. C. Townsley, A. S. Weisberg, T. R. Wagenaar, B. Moss, *J. Virol.* **80**, 8899 (2006).
6. Materials and methods are available as supporting material on *Science* Online.
7. M. J. Lehmann, N. M. Sherer, C. B. Marks, M. Pypaert, W. Mothes, *J. Cell Biol.* **170**, 317 (2005).
8. J. Limouze, A. F. Straight, T. Mitchison, J. R. Sellers, *J. Muscle Res. Cell Motil.* **25**, 337 (2004).
9. G. T. Charras, C. K. Hu, M. Coughlin, T. J. Mitchison, *J. Cell Biol.* **175**, 477 (2006).
10. D. J. Fishkind, L. G. Cao, Y. L. Wang, *J. Cell Biol.* **114**, 967 (1991).
11. J. C. Mills, N. L. Stone, J. Erhardt, R. N. Pittman, *J. Cell Biol.* **140**, 627 (1998).
12. M. C. Parrini, M. Matsuda, J. de Gunzburg, *Biochem. Soc. Trans.* **33**, 646 (2005).
13. S. Dharmawardhane *et al.*, *Mol. Biol. Cell* **11**, 3341 (2000).
14. F. Valderrama, J. V. Cordeiro, S. Schleich, F. Frischknecht, M. Way, *Science* **311**, 377 (2006).
15. S. Mayor, R. E. Pagano, *Nat. Rev. Mol. Cell Biol.* **8**, 603 (2007).
16. S. B. Sieczkarski, G. R. Whittaker, *J. Gen. Virol.* **83**, 1535 (2002).
17. M. A. West, M. S. Bretscher, C. Watts, *J. Cell Biol.* **109**, 2731 (1989).
18. E. Veiga, P. Cossart, *Nat. Cell Biol.* **7**, 894 (2005).
19. P. M. Henson, D. L. Bratton, V. A. Fadok, *Curr. Biol.* **11**, R795 (2001).
20. N. Platt, R. P. da Silva, S. Gordon, *Trends Cell Biol.* **8**, 365 (1998).
21. Y. Ichihashi, M. Oie, *Virology* **130**, 306 (1983).
22. H. T. Zwartouw, *J. Gen. Microbiol.* **34**, 115 (1964).
23. M. Oie, *Virology* **142**, 299 (1985).
24. Y. Ichihashi, M. Oie, T. Tsuruhara, *J. Virol.* **50**, 929 (1984).
25. S. J. Martin *et al.*, *J. Exp. Med.* **182**, 1545 (1995).
26. M. L. Albert, *Nat. Rev. Immunol.* **4**, 223 (2004).
27. D. Hayasaka, F. A. Ennis, M. Terajima, *Virol. J.* **4**, 22 (2007).
28. We thank P. Traktman for providing viruses; H. Ewers for the production of liposomes; R. Sacher, B. Snijder, and L. Pelkmans for assistance with siRNA screening; and the members of the Helenius lab for helpful discussion. Funding was obtained from ETH Zurich and the Roche Foundation.

Supporting Online Material

www.sciencemag.org/cgi/content/full/320/5875/531/DC1
Materials and Methods
Figs. S1 to S10
Table S1
References
Movies S1 to S6

11 January 2008; accepted 29 February 2008
10.1126/science.1155164

Encoding Gender and Individual Information in the Mouse Vomeronasal Organ

Jie He,[1] Limei Ma,[1] SangSeong Kim,[1] Junichi Nakai,[2] C. Ron Yu[1]*

The mammalian vomeronasal organ detects complex chemical signals that convey information about gender, strain, and the social and reproductive status of an individual. How these signals are encoded is poorly understood. We developed transgenic mice expressing the calcium indicator G-CaMP2 and analyzed population responses of vomeronasal neurons to urine from individual animals. A substantial portion of cells was activated by either male or female urine, but only a small population of cells responded exclusively to gender-specific cues shared across strains and individuals. Female cues activated more cells and were subject to more complex hormonal regulations than male cues. In contrast to gender, strain and individual information was encoded by the combinatorial activation of neurons such that urine from different individuals activated distinctive cell populations.

Pheromones are a group of chemicals critical for social communication in many animal species (*1*, *2*). Information on sex, strain, social rank, reproductive status, and terrestrial ownership is represented in the complex pheromone components in urine and bodily secretions. In mice, detection of such complex chemical signals by the vomeronasal organ (VNO) and the olfactory epithelium plays an important role in triggering endocrine changes and eliciting innate territorial aggression and mating behaviors (*3*–*5*).

The rodent VNO expresses more than 250 receptors that detect pheromones and transmit the signals to the brain (*6*–*11*). It is not well understood how these neurons encode information about gender and individuals. Urine contains hundreds or even thousands of substances, only a handful of which have been identified as putative pheromones (*12*–*16*). The complexity of natural pheromone signals poses a challenge to our understanding of what information is transmitted to the vomeronasal neurons (*17*, *18*).

Each vomeronasal neuron expresses only one of the ~250 estimated pheromone receptor genes (*6*–*9*, *19*, *20*), and the receptor's activation elevates intracellular calcium (*21*). To visualize pheromone-induced activity in a large population of neurons, we generated tetO-G-CaMP2 transgenic mouse lines (*22*–*24*). When crossed to animals carrying the OMP-IRES-tTA allele (*25*), G-CaMP2 expression was restricted to the neurons in the olfactory system (Fig. 1, A and B, and Movie S1). Electrophysiological properties of the G-CaMP2–expressing VNO neurons, as well as their response to pheromones, were indistinguishable from those of the controls (fig. S1). The projection patterns of the sensory neurons and the innate mating and aggressive behaviors of the G-CaMP2 mice were also indistinguishable from those of wild-type and littermate control animals (figs. S2 to S5).

In VNO slices prepared from 2- to 6-month-old male or female animals, application of diluted urine elicited an increase in fluorescence in ~30 to 40% of G-CaMP2–positive neurons, some of which showed gender-specific responses (Fig. 1C and Movies S2 and S3). We did not observe significant differences between slices from male and female animals in detecting the gender-specific cues. Prolonged applications of urine elicited prolonged calcium increases (Fig. 1D). This nonadaptive nature of the responses was in agreement with electrophysiological recordings reported previously (*17*, *26*). In addition, the responses were dose dependent and were blocked by 2-APB and U71344, inhibitors of signaling pathways downstream of pheromone receptor activation (*21*, *27*) (Fig. 1, C and D, and fig. S7). Thus, the expression of G-CaMP2 provided us an easy and sensitive method to examine population responses of VNO neurons to multiple urine samples.

Initial analyses of VNO neuron response to male and female urine pooled from multiple individuals of the C57BL/6 strain showed that ~15% of G-CAMP2–positive cells responded to both male and female urine. About 8% and 12% of the cells

[1]Stowers Institute for Medical Research, 1000 East 50th Street, Kansas City, MO 64110, USA. [2]Laboratory for Memory and Learning, RIKEN Brain Science Institute, 2-1 Hirosawa, Wako-shi, Saitama, 351-0198, Japan.

*To whom correspondence should be addressed: cry@stowers-institute.org

responded specifically to pooled male or female urine, respectively (Fig. 1C), suggesting that urine contained cues that were recognized by the VNO neurons to discriminate gender. To determine whether the gender-specific cues were shared among different individuals, we used individual urine from three strains (CBA, C57BL/6, and CD-1) to stimulate the same VNO slices. The activation patterns of the VNO were analyzed both visually (Fig. 1E) and using heat map plots (fig. S6 and Fig. 2A). In ~2100 G-CaMP2–positive cells (a total of eight slices from six animals), 5.0% (n = 106) were activated by one or more male urine samples but not by female urine, whereas 9.5% (n = 200) were activated by at least one female sample. However, most of these cells responded only to a subset of the sex-specific samples, suggesting that they could not contribute unequivocally to gender discrimination. Only a very small population of cells responded exclusively to urine samples from all individuals of the same sex but not the other (Fig. 2A). Cells that responded to all male samples, the male urine–specific cells (MUSCs), constituted less than 1% of the G-CaMP2–expressing neurons (n = 20, 0.95%). The female urine–specific cells (FUSCs), which responded exclusively to all the female samples, constituted 2.6% (n = 54) of the cells. We did not observe obvious differences in the percentage of MUSCs and FUSCs in male or female VNO slices (table S1). This was consistent with the previous

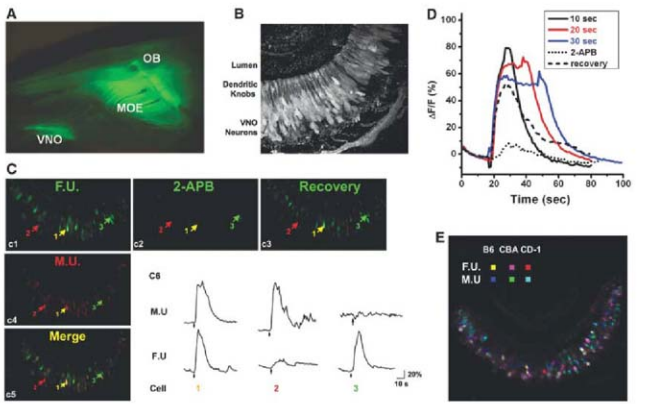

Fig. 1. Detection of urine-elicited responses in the VNO of G-CaMP2–expressing mice. **(A)** Expression of G-CaMP2 in the neurons of the main olfactory epithelium (MOE), the vomeronasal organ (VNO), and their axonal projections to the olfactory bulb (OB). **(B)** Two-photon image of a VNO slice used in an imaging experiment. **(C)** VNO responses to pooled C57BL/6 female urine (green) or male urine (red). The VNO slice (from a 4-month-old male) was stimulated with female urine (F.U.) under control (c1), treatment with 50 μM 2-APB (c2), and recovery (c3) conditions and male urine (c4, M.U.). Merge shows cells that respond to both male and female urine (c5). C6 shows the response traces of the three cells indicated in c1 to c5. **(D)** Fluorescence changes for a neuron responding to female urine applied for 10 (black), 20 (red), and 30 (blue) seconds, 10 s application following 2-APB treatment (black dot), and recovery (black dash), respectively. **(E)** The patterns of activation of a VNO slice by six different urine samples from different sex and strain animals are color-coded and shown in a merged picture.

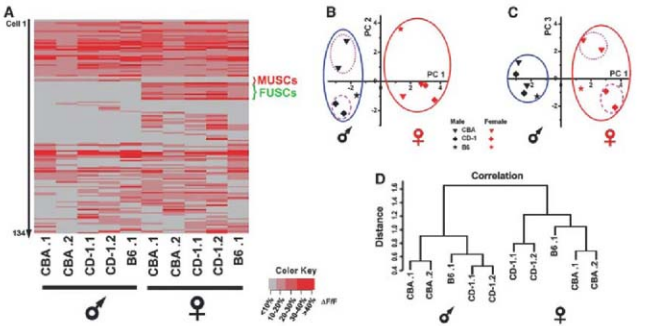

Fig. 2. VNO responses to individual male and female mouse urine. **(A)** Heat map of 134 VNO neurons from a single slice (from a 3-month-old male) that responded to male and female urine from C57BL/6 (B6), CBA, and CD-1 strains. **(B** and **C)** Principal components analysis of the data shown in two-dimensional plots for PC1 and PC2 in (B), and PC1 and PC3 in (C). Urine from males and females is labeled with black and red, respectively. **(D)** Hierarchical cluster analysis of responses shown in (A) is plotted as a dendrogram based on distance obtained from Pearson correlations between responses to different urine applications.

studies of pheromone receptor genes, which showed little sexual dimorphism in their expression patterns (*6*–*9*). The MUSCs and FUSCs were found in both G_o and G_{i2} layers in the VNO (table S2).

We applied cluster and principal components analysis (PCA) to identify the major variables that contributed to the differences in urine signals. Cluster analysis of the 134 responsive cells in Fig. 2 showed that the patterns of activation were grouped according to gender (Fig. 2D). Within each group, the samples were further grouped by strain. In PCA, the first principal component (PC1,

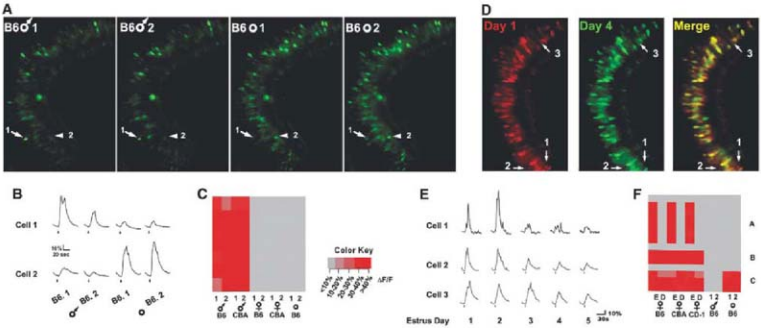

Fig. 3. Hormone regulation of sex pheromones. **(A)** Responses to urine from two C57BL/6 males and castrated males in a VNO slice from a 2-month-old female. Two cells with differential responses are indicated. **(B)** Response traces of the cells indicated in (A). **(C)** A heat map showing all identified MUSCs, none of which responded to castrate urine. **(D)** Responses to female urine collected from a C57BL/6 mouse after injection of pregnant mare serum gonadotrophin in a VNO slice (from a 3-month-old male). Responses to urine collected on day 1 and day 4 are shown. Three cells with differential responses are indicated. **(E)** Response traces of the cells marked in (A). **(F)** A heat map showing the identified FUSCs (19 cells from two slices from a 3-month-old male and a 2-month-old female). Group A cells were activated by estrous urine from all three strains. Group B was activated by both estrous and diestrus urine, but not castrate urine. Group C responded to estrus, diestrus, and castrate urine. ♂, ♀, and ○ represent male, female, and castrate animals, respectively; E, day 1 (estrus); D, day 4 (diestrus).

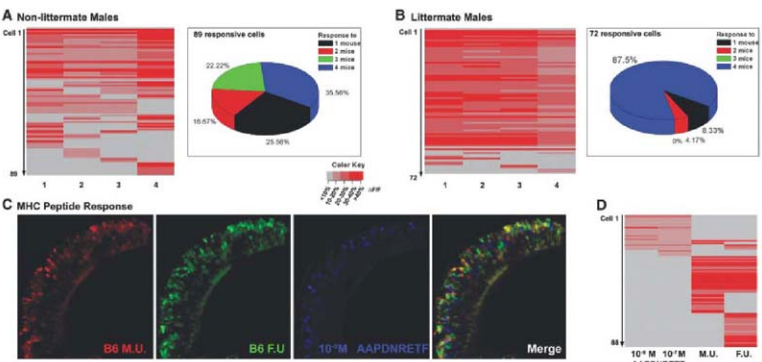

Fig. 4. Response of VNO neurons to different individuals and to MHC peptide. **(A** and **B)** Heat maps and pie charts of responses to urine from non-littermates (A) and littermates (B). The pie charts show percentages of cells activated by different numbers of urine samples. **(C)** Response patterns of a VNO slice to urine from a C57BL/6 male, a C57BL/6 female, and 10^{-9} M AAPDNRETF peptide, identified in the C57BL/6 strain. **(D)** A heat map for the responses summarizing the responses. The slice was from a 2-month-old female.

~35% of variance) separated the urine by gender. Interestingly, strains of the males were separated by the second principal component (PC2, 18% of variance) (Fig. 2B), whereas strains of the females were separated by PC3 (13%) (Fig. 2C). Analyses of multiple slices from both male and female animals produced similar results.

Each principal component is a linear summation of contribution by different cells in the group. Although MUSCs and FUSCs only represented <10% of all responding cells, they had the highest coefficient values and contributed a weighted average of >30% to PC1 (fig. S8). Further analyses by removing the MUSCs and FUSCs from the PCA pool showed that this "virtual knockout" compromised gender discrimination. Without MUSCs and FUSCs, urine samples were no longer segregated according to gender (fig. S9B). Removing equal numbers of cells that were activated only by subsets of sex-specific urine samples or removing equal numbers of random cells had little impact on segregation according to gender (fig. S9, C to F). Thus, despite their small numbers, the MUSCs and FUSCs appeared essential for gender discrimination.

The MUSCs and FUSCs must recognize gender-specific cues emitted by individual mice. Altering the sexual characteristics of an animal should affect the expression of such cues. We thus analyzed the patterns of activation by urine from castrated C57BL/6 males. Castrate urine activated more cells than male urine (Fig. 3, A and B, and fig. S10), but it no longer activated the MUSCs (Fig. 3C). Concurrent with the loss of response from MUSCs, a number of cells that did not respond to any male urine were activated, some of which were FUSCs (Fig. 3F and fig. S10).

In contrast to MUSCs, female-specific cells recognized cues that were regulated by more complex hormonal states, such as estrus cycles. We induced ovulation and collected urine daily from the same female mice throughout their estrus cycles. Urine from different time points during the estrus cycle elicited distinct patterns of activation (Fig. 3, D to F). Estrus urine activated more cells (fig. S11), and some of the additional cues were shared across individuals of different strains. These cues thus activated additional FUSCs (Fig. 3F and fig. S10).

In addition to gender, urine also provides information that identifies individuals. Indeed, our experiments showed that no two urine samples elicited identical patterns of activation. The activation patterns in the VNO distinguished not only gender but also the strains of the animals (Fig. 2D). Furthermore, littermates from the same strain were distinguishable, and such distinction was significantly larger than variations among repeated applications of the same sample (fig. S12).

How are individuals distinguished? The principal components PC2 and PC3 were composed of a large population of cells. More than 50% of responding cells showed activation by multiple samples, suggesting that individual information could be encoded by the combinatorial activation of the neurons (Fig. 2A). A combinatorial code predicts that urine from similar animals activates more common cells and fewer unique cells and vice versa. We examined the responses to urine samples from littermate and non-littermate C57BL/6 males. For non-littermates, ~36% of the responsive cells were shared by all four male urine samples (Fig. 4A), whereas for littermate urine, this number increased to ~87.5% (Fig. 4B). Concurrent with the increase in shared cells, the number of cells responding to single urine samples decreased from 25% to ~8.3% (Fig. 4, A and B). These observations were consistent with the prediction of a combinatorial code for individual identities.

If individuals are identified by the combinatorial activation of VNO neurons, are there cells providing unique identifications for the strains? Recent evidence suggests that the MHC class I peptides may serve as strain-specific signals by directly activating the VNO neurons (*16*). Because each peptide is unique to a specific strain, one expects to find strain-specific cells that are activated by urine samples from different individuals of the same strain. Analyses of the activation patterns in our experiments, however, did not provide evidence for such strain-specific cells, even when the analyses were expanded to ~12,000 neurons (also see Fig. 2). We further compared responses elicited by strain-specific MHC class I peptides to those by urine of the same strain. Figure 4, C and D, shows one such experiment with AAPDNRETF, a MHC class I peptide identified in the C57BL/6 strain, and urine from male and female C57BL/6 mice. The peptides indeed elicited responses from a subset of VNO neurons, but the cells activated by urine and by the peptides did not overlap.

Our experiments demonstrate that the mouse VNO encodes information of gender and individual in urine pheromones with two distinct strategies. Gender is encoded by a small percentage of dedicated neurons, the MUSCs and FUSCs. Because the VNO expresses ~250 pheromone receptors, the MUSCs correspond to ~2 to 3 receptors. This result, together with the finding of a single male-specific peptide in the mouse exocrine gland (*28*), suggests that a small number of testosterone-dependent cues is required for male identification. FUSCs represent a larger percentage of cells (~3%). The number difference in gender-specific cells may reflect the more complex physiology and hormonal regulation in female animals.

Individual information, on the other hand, is encoded by the combinatorial activation of VNO neurons rather than dedicated cells that respond specifically to class I MHC peptides. Fragments of the MHC complexes were found in considerable amounts in urine (*29*), but it has never been demonstrated that MHC class I peptides exist in detectable free form in urine (*29*). It remains possible that the skin or body glands may contain these peptides as natural ligands instead. Pheromone signals in urine that identify strains may result from the expression of a set of pheromones or the carriers of pheromones, such as the major urinary proteins that are known to be genetically determined (*30*, *31*). Using a combinatorial code to represent individuals and strains is likely to be advantageous because 100 to 200 receptors can provide a virtually unlimited coding space. In contrast, information about gender and certain hormone-regulated states is perhaps better served by dedicated cells, because the information is largely shared by animals of different strains as a result of common physiology.

References and Notes

1. M. C. Birch, *Pheromones* (American Elsevier, New York, 1974).
2. T. D. Wyatt, *Pheromones and Animal Behaviour* (Cambridge Univ. Press, New York, 2003).
3. P. A. Brennan, K. M. Kendrick, *Philos. Trans. R. Soc. London* **361**, 2061 (2006).
4. M. Halpern, A. Martínez-Marcos, *Prog. Neurobiol.* **70**, 245 (2003).
5. E. B. Keverne, *Science* **286**, 716 (1999).
6. C. Dulac, R. Axel, *Cell* **83**, 195 (1995).
7. G. Herrada, C. Dulac, *Cell* **90**, 763 (1997).
8. H. Matsunami, L. B. Buck, *Cell* **90**, 775 (1997).
9. N. J. Ryba, R. Tirindelli, *Neuron* **19**, 371 (1997).
10. L. Belluscio, G. Koentges, R. Axel, C. Dulac, *Cell* **97**, 209 (1999).
11. I. Rodriguez, P. Feinstein, P. Mombaerts, *Cell* **97**, 199 (1999).
12. J. G. Vandenbergh, J. S. Finlayson, W. J. Dobrogosz, S. S. Dills, T. A. Kost, *Biol. Reprod.* **15**, 260 (1976).
13. M. Novotny, F. J. Schwende, D. Wiesler, J. W. Jorgenson, M. Carmack, *Experientia* **40**, 217 (1984).
14. M. Novotny, S. Harvey, B. Jemiolo, J. Alberts, *Proc. Natl. Acad. Sci. U.S.A.* **82**, 2059 (1985).
15. B. Jemiolo, S. Harvey, M. Novotny, *Proc. Natl. Acad. Sci. U.S.A.* **83**, 4576 (1986).
16. T. Leinders-Zufall *et al.*, *Science* **306**, 1033 (2004).
17. T. E. Holy, C. Dulac, M. Meister, *Science* **289**, 1569 (2000).
18. M. Luo, L. C. Katz, *Curr. Opin. Neurobiol.* **14**, 428 (2004).
19. H. Yang, P. Shi, Y. P. Zhang, J. Zhang, *Genomics* **86**, 306 (2005).
20. W. E. Grus, P. Shi, Y. P. Zhang, J. Zhang, *Proc. Natl. Acad. Sci. U.S.A.* **102**, 5767 (2005).
21. T. Leinders-Zufall *et al.*, *Nature* **405**, 792 (2000).
22. M. Gossen, H. Bujard, *Proc. Natl. Acad. Sci. U.S.A.* **89**, 5547 (1992).
23. G. Ji *et al.*, *J. Biol. Chem.* **279**, 21461 (2004).
24. J. Nakai, M. Ohkura, K. Imoto, *Nat. Biotechnol.* **19**, 137 (2001).
25. C. R. Yu *et al.*, *Neuron* **42**, 553 (2004).
26. B. G. Leypold *et al.*, *Proc. Natl. Acad. Sci. U.S.A.* **99**, 6376 (2002).
27. P. Lucas, K. Ukhanov, T. Leinders-Zufall, F. Zufall, *Neuron* **40**, 551 (2003).
28. H. Kimoto, S. Haga, K. Sato, K. Touhara, *Nature* **437**, 898 (2005).
29. P. B. Singh, R. E. Brown, B. Roser, *Nature* **327**, 161 (1987).
30. R. J. Beynon, J. L. Hurst, *Biochem. Soc. Trans.* **31**, 142 (2003).
31. J. L. Hurst *et al.*, *Nature* **414**, 631 (2001).

32. Supported by funding from Stowers Institute and NIH (NIDCD 008003) to C.R.Y. We thank Q. Qiu, W. Wiegraebe, E. Gillespie, P. Zelalem, G. Hattem, D. Zhu, M. Durnin, M. Elmore, S. Klinefelter, K. Cavanaugh, and the Lab Animal Services Facility, the Histology Core, Imaging Center, and Proteomics Center at Stowers Institute for technical assistance. We also thank M. Gibson, R. Krumlauf, H. Y. Mak, and K. Si for thoughtful discussions and critical reading of the manuscript.

Supporting Online Material

www.sciencemag.org/cgi/content/full/320/5875/535/DC1
Materials and Methods
Figs. S1 to S12
Tables S1 and S2
References
Movies S1 to S3

21 December 2007; accepted 20 March 2008
10.1126/science.1154476

Rare Structural Variants Disrupt Multiple Genes in Neurodevelopmental Pathways in Schizophrenia

Tom Walsh,[1*] Jon M. McClellan,[2*†] Shane E. McCarthy,[3*] Anjené M. Addington,[4*] Sarah B. Pierce,[4] Greg M. Cooper,[‡] Alex S. Nord,[5] Mary Kusenda,[5,6] Dheeraj Malhotra,[3] Abhishek Bhandari,[3] Sunday M. Stray,[1] Caitlin F. Rippey,[5] Patricia Roccanova,[3] Vlad Makarov,[3] B. Lakshmi,[3] Robert L. Findling,[7] Linmarie Sikich,[8] Thomas Stromberg,[4] Barry Merriman,[9] Nitin Gogtay,[4] Philip Butler,[4] Kristen Eckstrand,[4] Laila Noory,[4] Peter Gochman,[4] Robert Long,[4] Zugen Chen,[9] Sean Davis,[10] Carl Baker,[5] Evan E. Eichler,[5] Paul S. Meltzer,[10] Stanley F. Nelson,[9] Andrew B. Singleton,[11] Ming K. Lee,[1] Judith L. Rapoport,[4] Mary-Claire King,[1,5] Jonathan Sebat[3]

Schizophrenia is a devastating neurodevelopmental disorder whose genetic influences remain elusive. We hypothesize that individually rare structural variants contribute to the illness. Microdeletions and microduplications >100 kilobases were identified by microarray comparative genomic hybridization of genomic DNA from 150 individuals with schizophrenia and 268 ancestry-matched controls. All variants were validated by high-resolution platforms. Novel deletions and duplications of genes were present in 5% of controls versus 15% of cases and 20% of young-onset cases, both highly significant differences. The association was independently replicated in patients with childhood-onset schizophrenia as compared with their parents. Mutations in cases disrupted genes disproportionately from signaling networks controlling neurodevelopment, including neuregulin and glutamate pathways. These results suggest that multiple, individually rare mutations altering genes in neurodevelopmental pathways contribute to schizophrenia.

Schizophrenia is a debilitating neuropsychiatric illness with severe individual, family, and societal burdens. The illness typically arises in late adolescence or early adulthood, with prevalence ~1% worldwide. The phenotype is heterogeneous and complex, with multiple genes and environmental exposures likely involved. Family, twin, and adoption studies all support a strong genetic influence, although patterns of inheritance are variable and not consistent with a single monogenic Mendelian trait (*1*).

The present working hypothesis for genetic influences on schizophrenia is the "common disease–common allele" model (*2*), in which the illness is caused by combinations of common alleles, each contributing a modest effect. We propose an alternative model: that some mutations predisposing to schizophrenia are highly penetrant, individually rare, and of recent origin, even specific to single cases or families (*3*).

Genomic microduplications and microdeletions, also known as structural variants or copy-number variants (CNVs), underlie many serious illnesses, including neurological and neurodevelopmental syndromes (*4*). Previously, we found a significantly increased frequency of de novo deletions and duplications in children with autism spectrum disorders (*5*), suggesting that rare structural variants collectively account for a larger proportion of these disorders than previously recognized. Direct methods for detection of microdeletions and microduplications can be used for gene discovery in other psychiatric disorders as well.

The hypothesis that chromosomal mutations may cause schizophrenia is not new. Karyotypic abnormalities have been detected in affected individuals or families (*6*), including events that led to the discovery of potential disease-causing mutations in *DISC1* (*7*), *PDE4B* (*7*), and *NPAS3* (*8*). Deletions at 22q11.2 are also associated with schizophrenia (*9*). However, the ability to detect structural mutations associated with schizophrenia was historically limited to large events identifiable by karyotype. The development of microarray-based methods now enables the detection of much smaller events. These methods have revealed structural mutations involving genes in neurodevelopmental pathways in individuals with schizophrenia, including a deletion disrupting *NRXN1* in affected siblings (*10*), a de novo duplication involving *APBA2* in one patient (*10*), and deletions containing *CNTNAP2* in two unrelated patients (*11*).

If severe mutations leading to schizophrenia are individually rare, then each individual mutation will be responsible for the disorder's occurrence in only one or a few patients. The overall involvement of rare mutations in the illness can be tested statistically by comparing the collective frequency of rare variants in cases with their collective frequency among controls. We examine whether rare structural mutations throughout the genome are more frequent among persons with schizophrenia than among unaffected individuals. We then examine whether genes disrupted by structural mutations in cases are more likely than genes disrupted in controls to encode proteins critical to brain development.

Genome-wide scans for structural variants greater than 100 kb were carried out on genomic DNA of 418 individuals, including 150 persons with schizophrenia or schizoaffective disorder meeting DSM-IV criteria and 268 healthy individuals (controls) aged 35 years or older who were free of signs of neurological or psychiatric illness. Detailed clinical information regarding the cases is provided in the supporting online material [(*12*) and table S1]. Distributions of racial ancestries were the same in cases and controls. Representational oligonucleotide microarray analysis 85K probe microarrays were used for event discovery. Illumina 550K microarrays and NimbleGen 2.1M feature HD2 microarrays were used to validate events and refine genomic breakpoints (*12*). Stringent quality-control criteria were applied to microarray data to obtain reliable measures of intensity, to exclude false positives, and to ensure that ascertainment of structural variants was consistent between cases and controls (*12*). First, frequencies in cases versus controls were compared for the 115 common variants (i.e., with frequency >1%) that passed our quality-control criteria and were verified by an independent method. Frequencies of these common variants did not differ between cases and controls (fig. S1). Second, detection sensitivity of rare variants was measured by simulating structural variants of various sizes at many different genomic locales and screening for them in blind tests. Detection sensitivity varied by event size and locale but was the same in cases and controls (fig. S2). Variants that were ultimately included in this study passed all these quality-control tests [see also (*12*)] and met our criteria for rare variants, defined as those not previously described on the Database of Genomic Variants, version 3, 29 November 2007 update (*13*). In the 418 cases and controls, we identified and validated 53 previously unreported microdeletions and microduplications, of sizes ranging from 100 kb to 15 MB.

Individuals with schizophrenia were more than three times as likely as controls to harbor rare structural variants that deleted or duplicated one or more genes (Table 1, $P = 0.0008$). Cases with onset of psychotic symptoms at age 18 years or younger were more than four times as likely as controls to harbor such variants (Table 1, $P = 0.0001$). In contrast, there was no significant difference in the proportions

[1]Department of Medicine, University of Washington, Seattle, WA 98195, USA. [2]Department of Psychiatry, University of Washington, Seattle, WA 98195, USA. [3]Cold Spring Harbor Laboratory, Cold Spring Harbor, NY 11724, USA. [4]Child Psychiatry Branch, National Institute of Mental Health, National Institutes of Health (NIH), Bethesda, MD 20892, USA. [5]Department of Genome Sciences, University of Washington, Seattle, WA 98195, USA. [6]Graduate Program in Genetics, State University of New York, Stony Brook, NY 11794, USA. [7]Department of Psychiatry, Case Medical Center, Cleveland, OH 44106, USA. [8]Department of Psychiatry, University of North Carolina, Chapel Hill, NC 27599, USA. [9]Department of Human Genetics, University of California, Los Angeles, CA 90095, USA. [10]Cancer Genetics Branch, National Cancer Institute, NIH, Bethesda, MD 20892, USA. [11]Neurogenetics Laboratory, National Institute on Aging, NIH, Bethesda, MD 20892, USA.

*These authors contributed equally to this work.
†To whom correspondence should be addressed. E-mail: drjack@u.washington.edu

of cases versus controls carrying rare mutations that did not alter any genes (table S2).

We tested the same hypothesis in an independent series of cases and controls, using a rigorously characterized cohort of youth with childhood-onset schizophrenia (COS). COS is a rare and typically more severe form of the illness (*14*). Of the 92 patients in this cohort, 9 patients known to harbor major chromosomal abnormalities (*15*–*17*) were excluded from this analysis, leaving 83 individuals. Given the heterogeneous ancestries of the COS patients, we evaluated the nontransmitted chromosomes of available parents ($n = 154$) as controls. Parental relationships were validated by genotyping multiple polymorphic markers. Because each parent contributed one haploid nontransmitted genome to analysis, the effective diploid sample size of our control group was 154/2 or 77. Genome-wide scans for structural variants >100 kb and ≥20 single-nucleotide polymorphisms (SNPs) were carried out on genomic DNA from COS cases and their parents by Affymetrix 500K SNP arrays (Nsp I and Sty I chips). All events were validated by Agilent 185K or 244K array comparative genomic hybridization and by custom bacterial artificial chromosome arrays targeting genomic regions of segmental duplications (*18*). Rare variants were defined by the same criteria as for those in the original series. Insofar as possible, genotypes from parents were used to determine whether variants were de novo or inherited.

In the COS cases, we identified and validated 27 previously unreported deletions and duplications in 23 individuals. A 2.5-MB deletion on chromosome 2q31.2-q31.3 and a 183-kb duplication on Yq11.221 were not inherited from confirmed parents and were therefore presumptively de novo; other events were either inherited or of unknown origin. A 115-kb deletion on chromosome 2p16.3 disrupting *NRXN1* was found in identical twins concordant for COS. Deletions in *NRXN1* have been reported in other patients with schizophrenia (*10*), mental retardation (*19*), and autism (*20*). In addition, two COS cases harbored the recurrent microduplication of 500-kb on chromosome 16p11.2 that was recently associated with autism and also was detected in two individuals with bipolar disorder (*21*, *22*). As found with the 16p11.2 duplication in autism (*21*, *22*), some duplications and deletions in COS patients were inherited from unaffected parents.

Among the 83 individuals with COS, 23 (28%) harbored one or more rare structural variants that deleted or duplicated genes; 4 individuals carried more than one such event (table S3). Among the 77 controls constructed from nontransmitted chromosomes of the COS cases' parents, 10 (13%) carried such variants. As for the original series, individuals with schizophrenia were significantly more likely than controls to harbor rare structural variants that altered genes (Table 1, $P = 0.03$). The proportion of controls harboring a rare deletion or duplication was higher in the COS series than in the original series. Schizophrenia of very young onset is associated with more severe family history as compared with schizophrenia of older onset (*14*), so parents of COS cases are likely to harbor more genomic lesions related to mental illness as compared with parents of persons from the general population. The use of nontransmitted parental chromosomes as controls is therefore likely to be very conservative. Deletions and duplications in COS cases and their parents were screened with different platforms from those used in the original series of cases and controls, but within each series, screening was the same for cases and controls. Definitions and sizes of CNVs are not yet identical across platforms (*13*).

Structural mutations that disrupt genes (rather than deleting or duplicating entire genes) may be especially likely to have biological consequences. Gene disruptions include premature truncation, internal deletion, gene fusion, or disruption of regulatory or promoter elements (*23*). Therefore, in our original series, we determined the breakpoints of genomic deletions and duplications in cases and controls by high-density microarray analysis and genomic sequencing (*12*). Genes disrupted by the breakpoints of each event were identified (Table 2). Individuals with schizophrenia were significantly more likely than controls to harbor rare structural variants that directly disrupted one or more genes (Table 1).

Virtually every rare structural mutation detected in our original series was different. Some deletions and duplications were multiple megabases in size; other variants altered only one or a few genes. Some events in unrelated patients altered the same genes, but with subtly different genomic breakpoints. For example, similar structural variants on chromosome 18p11 disrupted genes *LAMA1* and *PTPRM* in a case in the original series (Table 2) and in a case with COS (table S3).

Next, we assessed whether the functions of the genes disrupted in cases or controls might be related to schizophrenia. From our original series, for which disrupted genes were fully identified, we compared genes disrupted in cases versus those disrupted in controls using PANTHER (*24*) and Ingenuity Pathways Analysis (IPA) (*25*) classification systems. These programs enable one to determine whether an experimentally derived set of genes is overrepresented, as compared with all known genes (*26*), in one or more functionally defined pathways. The analyses are undirected: that is, no a priori selection is imposed on the pathways to be queried.

Genes disrupted by structural variants in our series of cases were significantly overrepresented in pathways important for brain development, including neuregulin signaling, extracellular signal–regulated kinase/mitogen-activated protein kinase (ERK/MAPK) signaling, synaptic long-term potentiation, axonal guidance signaling, integrin signaling, and glutamate receptor signaling (Table 3). Of the 24 genes disrupted by microdeletions or microduplications in cases, 11 genes—*ERBB4*, *MAGI2*, *DLG2*, *PRKCD*, *PRKAG2*, *PTK2*, *CAV1*, *GRM7*, *SLC1A3*, *PTPRM*, and *LAMA1*—were components of one or more of these pathways. Genes disrupted in controls were not overrepresented in any pathway. It is therefore important that this association was found only for cases and not for controls, that this association was not the result of the larger number of genes disrupted by case events [(*12*) and

Table 1. Individuals with schizophrenia and controls with novel structural variants (SVs) of size >100 kb. Obs, observations; OR, odds ratio; CI, confidence interval.

Subjects	*n*	Obs	Proportion with SV	*P*†	OR	95% CI	Obs	Proportion with SV	*P*†	OR	95% CI
		SVs that duplicate or delete genes					*SVs that disrupt genes*				
Cases	150	22	0.15	0.0008	3.37	1.64, 6.91	16	0.11	0.012	2.79	1.26, 6.18
Cases, onset <18 years	76	15	0.20	0.0001	4.82	2.18, 9.90	10	0.13	0.007	3.54	1.44, 8.69
Controls	268	13	0.05				11	0.04			
COS cases	83	23	0.28	0.03	2.57	1.13, 5.83					
COS controls*	77	10	0.13								

*COS controls: nontransmitted chromosomes from parents of COS cases. †Two-tailed Fisher Exact Tests for comparisons of numbers of cases versus numbers of controls with event.

table S4], and that the signaling pathways implicated were specifically involved with brain development.

Mutations in two genes, *ERBB4* and *SLC1A3*, are predicted to have particularly deleterious effects on function. For each of these genes, we experimentally characterized mutant transcripts in the affected individuals. The *ERBB4* gene, which encodes a type I transmembrane tyrosine kinase receptor for neuregulins, is disrupted by a 399-kb deletion in one case (Fig. 1A). Using 3′ rapid amplification of cDNA ends, we determined that the mutant allele produces an alternate transcript in which exons 1 to 19 are spliced to 198 base pairs (bp) of the intergenic sequence located downstream of *ERBB4* and the deleted genomic region (Fig. 1B). The alternate transcript is predicted to encode amino acids 1 to 767 of ERBB4 followed by a novel extension of 15 amino acids, which would result in a protein lacking most of the intracellular kinase domain (Fig. 1C). The predicted mutant protein is likely to function similarly to an engineered dominant-negative ERBB4 (DN-ErbB4) (Fig. 1D), which causes defects in neuronal migration (*27*) and synaptic neurotransmission (*28*, *29*).

SLC1A3, a glutamate transporter widely expressed in glial cells, regulates neurotransmitter concentrations at excitatory glutaminergic synapses (*30*). Elevated levels of *SLC1A3* message have been described in postmortem thalamus tissue of individuals with schizophrenia (*31*). The 503-kb deletion in another case disrupts both *SLC1A3* and *SKP2* and leads to a chimeric transcript expressed in patient lymphoblasts (Fig. 1E). The predicted fusion protein is likely to differ in expression and function from that of wild-type SLC1A3.

These genes and nine other genes disrupted by structural variants in cases contribute to cellular signaling networks critical to neuronal cell growth, migration, proliferation, differentiation, apoptosis, and synapse formation (*32*). ERBB4 is a receptor for neuregulin (NRG1) and interacts with MAGI2 at neuronal synapses (*33*) and with DLG2 (*34*). The NRG1-ERBB4 complex helps regulate neuronal migration and differentiation, neurotransmitter receptor expression, glial proliferation, and synaptic plasticity (*35*) and is critical to the development of glutamate networks (*28*, *29*). GRM7 [a G protein–coupled metabotropic glutamate receptor (*36*)] and SLC1A3 [a glutamate transporter (*30*)] are also involved with glutamate signaling. Glutamate is the primary excitatory neurotransmitter (*37*) in the human brain. Glutamate pathways coregulate intracellular signaling cascades, including ERK/MAPK (*38*), nitric oxide (*39*), and integrin (*40*) signaling pathways: all of which play key roles in the orchestration of neurogenesis and

Table 2. Novel SVs in genomic DNA that delete (del) or duplicate (dup) genes in schizophrenia cases and controls. Chr, chromosome; hg18, human genome assembly 18 (March 2006). Dashes indicate that no gene was disrupted by SV breakpoints.

Chr	Start (hg18)	End (hg18)	Size (bp)	Type	Duplicated or deleted genes	Genes disrupted by SV breakpoints	Age onset (years)
			Cases (n = 150)				
1	144,943,150	146,292,286	1,349,136	del	11	*NBPF10*	25*
1	232,464,245	232,673,340	209,095	dup	3	*SLC35F3, TARBP1*	24
2	48,648,754	49,319,683	670,929	dup	3	*STON1-GTF2A1L*	25*
2	211,792,494	212,191,651	399,157	del	1	*ERBB4*	13
3	7,177,597	7,314,117	136,520	del	1	*GRM7*	17
3	53,056,517	53,191,698	135,181	dup	2	*PRKCD*	22
3	197,224,662	198,573,215	1,348,553	del	20	-	18
5	36,190,704	36,693,387	502,683	del	4	*SKP2, SLC1A3*	13
7	77,358,702	77,857,149	498,447	dup	2	*MAGI2, PHTF2*	18
7	100,298,156	115,966,446	15,668,290	dup	82	*SLC12A9, CAV1*	18
7	151,069,763	151,531,755	461,992	dup	4	*PRKAG2, MLL3*	15
8	142,025,432	142,393,948	368,516	dup	3	*PTK2*	12
9	2,013,316	3,118,374	1,105,058	dup	4	*SMARCA2*	>18
9	3,104,250	3,544,339	440,089	del	1	-	11
9	25,325,531	25,852,420	526,889	dup	1	-	13
11	33,260,889	33,540,102	279,213	dup	2	*HIPK3, C11orf41*	22
11	83,680,969	83,943,977	263,008	del	1	*DLG2*	25
14	53,485,363	53,768,132	282,769	dup	1	-	18
18	7,070,926	7,565,943	495,017	dup	2	*LAMA1, PTPRM*	16
19	59,045,962	59,363,706	317,744	dup	13	*TMC4*	16
22	32,048,581	32,715,286	666,705	dup	1	*LARGE*	13
Y	1	57,772,954	57,772,954	dup	entire Y	-	18
Y	57,571,543	57,723,933	152,391	dup	1	-	19
			Controls (n = 268)				
1	99,984,742	100,204,503	219,761	del	2	*FRRS1*	
2	8,171,653	8,581,679	410,026	del	1	-	
3	79,667,848	81,408,551	1,740,703	del	1	*ROBO1*	
6	95,730,630	96,143,673	413,043	del	1	*MANEA*	
7	84,336,008	84,699,929	363,921	del	1	-	
7	111,033,890	112,334,786	1,300,896	dup	6	*FLJ31818*	
7	127,083,558	127,422,401	338,843	del	1	*SND1*	
8	8,144,616	11,755,764	3,611,148	del	20	*CTSB*	
9	12,641,413	13,216,945	575,532	dup	3	*MPDZ*	
12	24,583,650	25,248,947	665,297	dup	7	*SOX5, LYRM5*	
12	29,793,043	29,990,037	196,994	del	1	*TMTC1*	
16	69,395,935	69,748,827	352,892	del	2	*HYDIN*	
22	30,898,828	31,191,488	292,660	dup	5	*BPIL2*	

*Same individual.

Table 3. Pathways and processes overrepresented by genes disrupted in schizophrenia cases. No pathways were overrepresented by genes disrupted in controls.

Pathway or process	*P* value
Signal transduction*	0.012
Neuronal activities*	0.049
Nitric oxide signaling†	0.0002
Synaptic long-term potentiation†	0.0005
Glutamate receptor signaling†	0.003
ERK/MAPK signaling†	0.004
Phosphatase and tensin homolog signaling†	0.007
Neuregulin signaling†	0.008
Insulin-like growth factor 1 signaling†	0.008
Axonal guidance signaling†	0.015
Synaptic long-term depression†	0.017
G protein–coupled receptor signaling†	0.034
Integrin signaling†	0.036
Ephrin receptor signaling†	0.042
Sonic hedgehog signaling†	0.044

*Undirected PANTHER analysis (*17*). †Undirected IPA (*18*).

neural circuitry (*41*–*43*). Aberrations of NRG1-ERBB4 pathways and of glutamate neurocircuitry have been implicated previously in schizophrenia. *NRG1* is among the best-supported susceptibility genes in association studies of schizophrenia (*1*). Variants of *ERBB4* and interactions among genes in the NRG1-ERBB signaling pathway have also been associated with the illness (*44*–*46*).

In two independent cohorts, we found structural variants altering genes to be more common among individuals with schizophrenia than among controls. Our design does not prove the involvement with the illness of any specific variant or even the involvement of any specific gene. Rather, these results suggest that schizophrenia can be caused by rare mutations that disrupt genes in pathways of neuronal development and regulation. This model suggests a new approach to gene discovery for schizophrenia and likely for other psychiatric disorders. Neurodevelopmental pathways involve hundreds of genes. A severe mutation in any one of these genes may lead to a psychopathological phenotype. Furthermore, independent mutations in the same gene or genomic region, such as 16p11.2 or *NRXN1*, may lead to expression of different neurodevelopmental phenotypes, ranging from schizophrenia to autism to mental retardation (*10*, *19*–*21*) or to no clinical manifestation at all. Variable expression may arise by different genetic or epigenetic "second hits" or simply by chance.

Gene discovery efforts should focus on methods that allow detection of structural mutations genome-wide in affected individuals. Any gene harboring a deleterious structural mutation becomes a candidate gene to be screened by other methods for additional, presumably smaller, deleterious mutations in unrelated individuals. This second analytic step would entail complete analysis of variation of a limited number of candidate genes in a very large number of cases and controls. The underlying hypothesis is that a gene harboring one mutation for an illness is likely to harbor more than one mutation. Although each mutation may be individually rare, the total number of disease-causing variants in a gene relevant to the disorder may collectively explain a substantial number of cases. The long-term goals are to identify all genes with mutations leading to the illness and to develop treatment and prevention strategies tailored toward the remediation of the altered pathways.

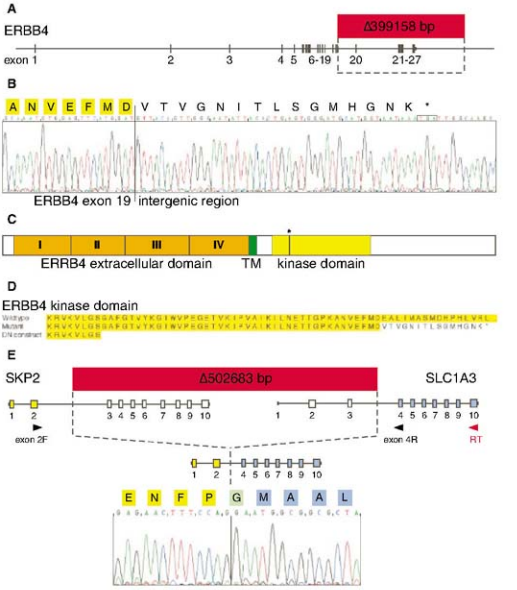

Fig. 1. Structural mutations in genomic DNA from schizophrenia patients leading to expression of truncated *ERBB4* and to expression of an in-frame fusion of *SKP2* and *SLC1A3*. **(A)** Genomic structure of the 399-kb deletion in *ERBB4* in a schizophrenia case. **(B)** cDNA sequence of the mutant *ERBB4* transcript detected in the patient's lymphoblasts, in which the sequence from exon 19 is spliced to the downstream intergenic sequence, with encoded amino acids indicated above (*47*). **(C)** Domain structure of the ERBB4 protein with the site of mutation indicated (*). TM, transmembrane domain. **(D)** Amino acid sequence of the wild-type ERBB4 kinase domain as compared with that of mutant ERBB4 and of an engineered dominant-negative ERBB4 construct (DN construct) that disrupts signaling (*27*). The predicted mutant protein has a truncated kinase domain and a novel 15 amino acid extension followed by a stop. Kinase domain amino acids are highlighted in yellow. **(E)** Chimeric *SKP2-SLC1A3* gene formed by a 503-kb deletion in a schizophrenia case. The indicated fusion transcript, including exons 1 and 2 of *SKP2* (yellow) and exons 4 to 10 of *SLC1A3* (blue), was detected in the patient's lymphoblasts. The cDNA sequence and encoded amino acids surrounding the point of fusion are shown. Arrows indicate locations of primers used to amplify the fusion region by reverse transcription polymerase chain reaction.

References and Notes

1. P. J. Harrison, D. R. Weinberger, *Mol. Psychiatry* **10**, 40 (2005).
2. K. E. Lohmueller, C. L. Pearce, M. Pike, E. S. Lander, J. N. Hirschhorn, *Nat. Genet.* **33**, 177 (2003).

3. J. M. McClellan, E. Susser, M.-C. King, *Br. J. Psychiatry* **190**, 194 (2007).
4. J. A. Lee, J. R. Lupski, *Neuron* **52**, 103 (2006).
5. J. Sebat *et al.*, *Science* **316**, 445 (2007).
6. D. J. MacIntyre, D. H. R. Blackwood, D. J. Porteous, B. S. Pickard, W. J. Muir, *Mol. Psychiatry* **8**, 275 (2003).
7. J. E. Chubb, H. J. Bradshaw, D. C. Soares, D. J. Porteous, J. K. Millar, *Mol. Psychiatry* **13**, 36 (2008).
8. D. Kamnasaran, W. J. Muir, M. A. Ferguson-Smith, D. W. Cox, *J. Med. Genet.* **40**, 325 (2003).
9. H. Liu *et al.*, *Proc. Natl. Acad. Sci. U.S.A.* **99**, 16859 (2002).
10. G. Kirov *et al.*, *Hum. Mol. Genet.* **17**, 458 (2008).
11. J. L. Friedman *et al.*, *Mol. Psychiatry* **13**, 261 (2008).
12. Materials and methods are available as supporting material on *Science* Online.
13. A. J. Iafrate *et al.*, *Nat. Genet.* **36**, 949 (2004).
14. J. L. Rapoport, G. Inoff-Germain, *Curr. Psychiatry Rep.* **2**, 410 (2000).
15. A. Sporn *et al.*, *Mol. Psychiatry* **9**, 225 (2004).
16. J. R. Idol, A. M. Addington, R. T. Long, J. L. Rapoport, E. D. Green, *J. Autism Dev. Disord.* **38**, 668 (2008).
17. J. L. Seal *et al.*, *J. Med. Genet.* **43**, 887 (2006).
18. A. J. Sharp *et al.*, *Am. J. Hum. Genet.* **77**, 78 (2005).
19. J. M. Friedman *et al.*, *Am. J. Hum. Genet.* **79**, 500 (2006).
20. The Autism Genome Project Consortium, *Nat. Genet.* **39**, 319 (2007).
21. R. A. Kumar *et al.*, *Hum. Mol. Genet.* **17**, 628 (2007).
22. L. A. Weiss *et al.*, *N. Engl. J. Med.* **358**, 667 (2008).
23. J. R. Lupski, P. Stankiewicz, *PLoS Genet.* **1**, e49 (2005).
24. H. Mi, N. Guo, A. Kejariwal, P. D. Thomas, *Nucleic Acids Res.* **35**, D247 (2007).
25. Ingenuity Systems, www.ingenuity.com.
26. National Center for Biotechnology Information, National Library of Medicine, Bethesda, MD, www.ncbi.nlm.nih.gov.
27. C. Rio, H. L. Rieff, P. Qi, T. S. Khurana, G. Corfas, *Neuron* **19**, 39 (1997).
28. R. S. Woo *et al.*, *Neuron* **54**, 599 (2007).
29. B. Li, R. S. Woo, L. Mei, R. Malinow, *Neuron* **54**, 583 (2007).
30. P. M. Beart, R. D. O'Shea, *Br. J. Pharmacol.* **150**, 5 (2007).
31. R. E. Smith, V. Haroutunian, K. L. Davis, J. H. Meador-Woodruff, *Am. J. Psychiatry* **158**, 1393 (2001).
32. K. M. Giehl, *Prog. Exp. Tumor Res.* **39**, 1 (2007).
33. J. D. Buxbaum *et al.*, *Mol. Psychiatry* **13**, 162 (2008).
34. R. A. Garcia, K. Vasudevan, A. Buonanno, *Proc. Natl. Acad. Sci. U.S.A.* **97**, 3596 (2000).
35. R. M. Esper, N. S. Pankonin, J. A. Loeb, *Brain Res. Rev.* **51**, 161 (2006).
36. A. Malkoff, C. Pilling, K. Harrington, P. Emson, *Brain Res. Mol. Brain Res.* **40**, 165 (1996).
37. M. Nedergaard, T. Takano, A. J. Hansen, *Nat. Rev. Neurosci.* **3**, 748 (2002).
38. J. Q. Wang, E. E. Fibuch, L. Mao, *J. Neurochem.* **100**, 1 (2007).
39. S. Sammut, D. J. Park, A. R. West, *J. Neurochem.* **103**, 1145 (2007).
40. J. A. Bernard-Triffo *et al.*, *J. Neurochem.* **93**, 834 (2005).
41. J. B. Manent, A. Represa, *Neuroscientist* **13**, 268 (2007).
42. J. I. Heng, G. Moonen, L. Nguyen, *Eur. J. Neurosci.* **26**, 537 (2007).
43. C. A. Ghiani *et al.*, *Neurochem. Res.* **32**, 363 (2007).
44. N. Norton *et al.*, *Am. J. Med. Genet. B Neuropsychiatr. Genet.* **141**, 96 (2006).
45. A. J. Law, J. E. Kleinman, D. R. Weinberger, C. S. Weickert, *Hum. Mol. Genet.* **16**, 129 (2007).
46. I. Benzel *et al.*, *Behav. Brain Funct.* **3**, 31 (2007).
47. Single-letter abbreviations for the amino acid residues are as follows: A, Ala; C, Cys; D, Asp; E, Glu; F, Phe; G, Gly; H, His; I, Ile; K, Lys; L, Leu; M, Met; N, Asn; P, Pro; Q, Gln; R, Arg; S, Ser; T, Thr; V, Val; W, Trp; and Y, Tyr.
48. We thank M. Wigler, E. Susser, and J. Watson for helpful discussion. This work was supported by The Forrest C. and Frances H. Lattner Foundation; a NARSAD Young Investigator Award; The NARSAD Constance and Steven Lieber Distinguished Investigator Award; The Simons Foundation; a gift of Ted and Vada Stanley; The Stanley Medical Research Foundation; the Howard Hughes Medical Institute; NIH grants HD043569, MH061464, MH061528, MH061355, NS052108, RR025014, and RR000046; NIH intramural research programs of the National Institute on Aging and the National Institute of Mental Health; and the Mental Health Division, Washington State Department of Social and Health Services.

Supporting Online Material

www.sciencemag.org/cgi/content/full/1155174/DC1
Materials and Methods
Figs. S1 to S3
Tables S1 to S4
References

2 January 2008; accepted 14 March 2008
Published online 27 March 2008;
10.1126/science.1155174
Include this information when citing this paper.

Metabolic Diversification—Independent Assembly of Operon-Like Gene Clusters in Different Plants

Ben Field and Anne E. Osbourn*

Operons are clusters of unrelated genes with related functions that are a feature of prokaryotic genomes. Here, we report on an operon-like gene cluster in the plant *Arabidopsis thaliana* that is required for triterpene synthesis (the thalianol pathway). The clustered genes are coexpressed, as in bacterial operons. However, despite the resemblance to a bacterial operon, this gene cluster has been assembled from plant genes by gene duplication, neofunctionalization, and genome reorganization, rather than by horizontal gene transfer from bacteria. Furthermore, recent assembly of operon-like gene clusters for triterpene synthesis has occurred independently in divergent plant lineages (*Arabidopsis* and oat). Thus, selection pressure may act during the formation of certain plant metabolic pathways to drive gene clustering.

Triterpenes protect plants against pests and diseases and are also important drugs and anticancer agents (*1*–*4*). Like sterols, these compounds are synthesized from the isoprenoid pathway by cyclization of 2,3-oxidosqualene (*1*, *3*). The *Arabidopsis* genome contains 13 predicted oxidosqualene cyclase (OSC) genes (*3*, *5*). Of these, one encodes cycloartenol synthase (CAS), which is required for sterol biosynthesis, and another encodes lanosterol synthase (LAS), which is conserved across the eudicots and whose function in plants is unknown (Fig. 1A). The 11 remaining OSCs fall into two major clades (I and II) (Fig. 1A). These OSCs produce various triterpenes when expressed in yeast. However, their function in *Arabidopsis* is unknown. The OSCs in clade I have close homologs in other eudicots; those in clade II appear to be restricted to the Brassicaceae family and show homology to a single OSC from *Brassica napus*.

Oat (*Avena* spp.), a monocot that diverged from the eudicots ~180 million years ago, produces defense-related triterpenes known as avenacins. The first committed step in avenacin synthesis is catalyzed by the OSC β-amyrin synthase (encoded by *Sad1*) (*6*). *Sad1* is hypothesized to have arisen from a duplicated monocot CAS-like gene after the separation of wheat and oat ~25 million years ago (*6*, *7*). The second step in avenacin biosynthesis is mediated by SAD2, a member of the newly described monocot-specific CYP51H subfamily of cytochrome P450 enzymes (CYP450s) (*8*). *Sad1* and *Sad2* are embedded in a gene cluster that includes genes required for acylation, glucosylation, and other steps in the pathway (*2*, *7*). The avenacin biosynthesis genes are tightly regulated and expressed only in the root epidermis, the site of accumulation of the pathway end product (*6*, *8*). The avenacin gene cluster lies within a region of the oat genome lacking synteny with rice and other cereals (*7*).

We examined the genomic regions around each of the 13 *Arabidopsis* OSC genes in the *Arabidopsis* genome to establish whether genes for triterpene synthesis might be clustered (*9*). Four OSC genes are flanked by genes predicted to encode other classes of enzymes implicated in secondary metabolism. These four OSCs all belong to clade II, which appears to have undergone accelerated evolution compared with other *Arabidopsis* OSCs (Fig. 1A). We focused on a region containing four contiguous genes predicted to encode an OSC (*At5g48010*), two CYP450s (*At5g48000* and *At5g47990*), and a BAHD family acyltransferase (ACT) (*At5g47980*) (Fig. 1B). The expression of all four genes is highly correlated (Fig. 1C) and occurs primarily in the root epidermis (fig. S1), which suggests that the genes are functionally related (*10*).

The OSC gene within this region, *At5g48010*, converts 2,3-oxidosqualene to the triterpene thalianol when expressed in yeast (*11*). However, thalianol has not been reported in plants. We detected low levels of thalianol in roots but not leaves of wild-type *Arabidopsis* (Fig. 2, C and D), consistent with the expression of *At5g48010*. Thalianol was not detectable in root extracts of a null insertion mutant of *At5g48010* (*thas1-1*) (Fig. 2E), which indicated that the *At5g48010* gene product [hereafter, named thalianol synthase (THAS)] is required for synthesis of thalianol in *Arabidopsis*

Department of Metabolic Biology, John Innes Centre, Colney Lane, Norwich NR4 7UH, UK.
*To whom correspondence should be addressed. E-mail: anne.osbourn@bbsrc.ac.uk

roots. Overexpression of THAS in *Arabidopsis* resulted in thalianol accumulation in leaves (Fig. 2F) and in dwarfing (Fig. 3A). Mutations in the gibberellin, brassinosteroid, and primary sterol pathways can result in dwarfing (*12*–*14*). However, the dwarf phenotype of the THAS-overexpressing lines was not rescued by application of gibberellin or brassinosteroid, and the sterol content of these plants was not significantly altered ($P > 0.05$, Student's t test, $n = 3$), which suggests that thalianol may be detrimental to plant growth.

Gas chromatography–mass spectrometry (GC-MS) analysis of wild-type root extracts revealed additional peaks that were absent in *THAS* mutants [(Fig. 4A); wild type and *thas1-1*]. Because these peaks were dependent on *THAS*, this suggested that thalianol (peak 1) is converted to unknown downstream products in wild-type *Arabidopsis* plants (peaks 2a, 2b, 2c, 3a, and 3b). Therefore, the coexpressed genes adjacent to *At5g48010* (*THAS*) were examined to determine

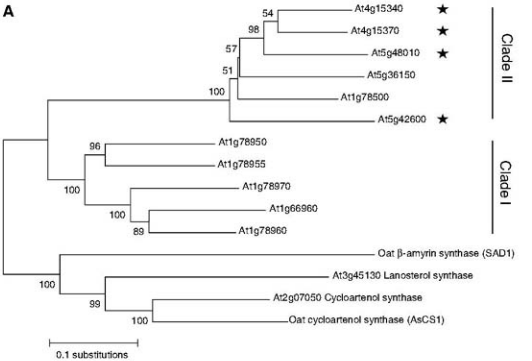

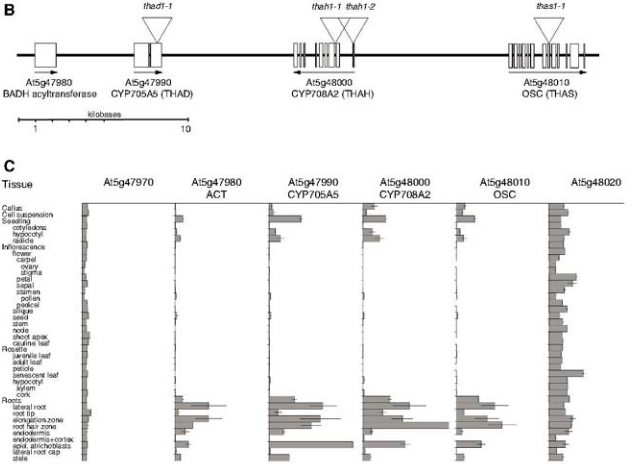

Fig. 1. **(A)** Neighbor-joining tree of *Arabidopsis* and oat OSC enzymes (percent bootstrap support indicated). *Arabidopsis* OSCs are indicated with *Arabidopsis* Genome Initiative gene codes. Those genes residing in candidate metabolic gene clusters are starred. Oat OSC National Center for Biotechnology Information accession numbers: SAD1 (CAC84558), AsCS1 (CAC84559). **(B)** Map of the triterpene gene cluster on *Arabidopsis* chromosome 5. T-DNA insertion mutants are indicated. **(C)** Microarray expression profiles of the genes in Fig. 1B and the two immediately flanking genes *At5g47970* and *At5g48020* (neither of which are implicated in secondary metabolism). Absolute expression values are shown with identical scales (± SE, $n \geq 3$). Data were retrieved from Genevestigator (*26*). The genes in Fig. 1B were highly coexpressed across 392 microarray experiments [average correlation coefficient (r) = 0.86]. The flanking genes were not coexpressed with genes in the cluster region or with one another ($r < 0.15$). Coexpression analysis was performed at the BioArray Resource (*27*) with data from NASCArrays (http://arabidopsis.info/).

whether they function in thalianol modification. We analyzed transferred DNA (T-DNA) insertion mutants in *At5g48000*, which is immediately adjacent to *THAS*. *At5g48000* is predicted to encode a CYP450 (CYP708A2) belonging to the functionally uncharacterized CYP708 family, a CYP450 family specific to the Brassicaceae (*15*). Root extracts of mutants affected at *At5g48000* (*thah1-1* and *thah1-2*) showed increased thalianol levels compared with the wild type (Fig. 4A and fig. S3, A and B), which suggests that the CYP450 encoded by *At5g48000* is required for conversion of thalianol to a downstream product. Furthermore, we observed that peaks 2a to 3b were absent in root extracts of *thah1-1* (Fig. 4A) and, so, may correspond to downstream pathway intermediates.

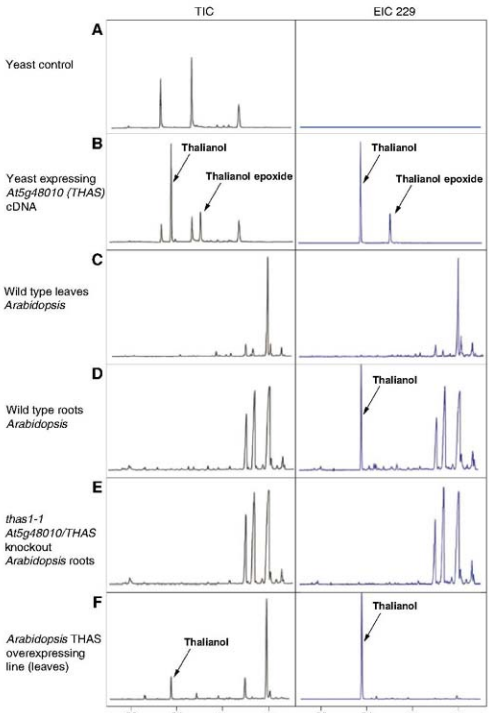

Fig. 2. Extracts from yeast and *Arabidopsis* were analyzed for triterpene content by GC-MS: TIC, total ion chromatograms; EIC 229, extracted ion chromatograms at a mass-charge ratio (*m/z*) of 229. Data are representative of at least two separate experiments, each with triplicate samples. **(A)** Yeast empty-vector control; **(B)** yeast expressing the *At5g48010* cDNA; **(C** and **D)** from wild-type *Arabidopsis*; **(E)** from an *At5g48010* (*thas1-1*) knockout line, **(F)** from an *Arabidopsis* line overexpressing *THAS*. The ion fragmentation pattern of thalianol was as reported (fig. S2) (*11*). Thalianol epoxide, a product of bis-oxidosqualene cyclization, was detected in yeast only. The chromatograms are scaled to the highest peak. Unlabeled peaks are sterols.

The second CYP450 in this region (*At5g47990*) (Fig. 1B) belongs to the CYP705 family, another functionally uncharacterized Brassicaceae-specific CYP450 family (*16*). The CYP705 and CYP708 families belong to the CYP71 and CYP85 clans respectively, which demonstrates that *At5g47990* is not a tandem duplicate of *At5g48000*. Null insertion mutants and RNA interference (RNAi) knockdown lines for *At5g47990* had enhanced levels of peaks 2a and 2b relative to wild-type plants (Fig. 4A and fig. S3, C and D). Peaks 2a, 2b, and 2c, with similar ion fragmentation patterns, were identified as thalian-diol [(3*S*,13*S*,14*R*)-malabarica-8,17,21-trien-3,?-diol] (fig. S4) and are likely to represent different thalian-diol isomers. Peaks 2a to 2c were not present in root extracts of *thas1-1*, which confirmed that production of thalian-diol depends on THAS (Fig. 4A). These peaks were also absent from root extracts of *thah1-1* (Fig. 4A), which implicated *At5g48000* in thalian-diol biosynthesis. Overexpression of THAH with THAS in *Arabidopsis* leaves resulted in conversion of thalianol to thalian-diol (fig. S6A), and overexpression of THAH in *thah1-1* restored the thalianol pathway (fig. S6B). On the basis of these data, we concluded that *At5g48000* encodes thalianol hydroxylase (hereafter, referred to as THAH). Plants that overaccumulate thalian-diol are dwarfed (fig. S6B), which suggests that thalian-diol, like thalianol, is detrimental to growth when produced in the above-ground parts of the plant.

The increased levels of thalian-diol in *thad1-1* suggested that *At5g47990* was required for conversion of thalian-diol to a further downstream product. We observed that peaks 3a and 3b, which are present in wild-type plants, are absent in *thas1-1*, *thah1-1*, and *thad1-1* (Fig. 4A). These two peaks were identified as isomers of desaturated thalian-diol [(3*S*,13*S*,14*R*)-malabarica-8,15,17,21-tetraen-3,?-diol] (fig. S5). Conversion of thalian-diol to desaturated thalian-diol involves introduction of a double bond at carbon 15 (Fig. 4). CYP450 enzymes can catalyze desaturation reactions of this kind [see ref. (*17*)]. On the basis of these data, we concluded that *At5g47990* encodes thalian-diol desaturase (hereafter, referred to as THAD).

These data show that *THAS*, *THAH*, and *THAD* are contiguous coexpressed genes encoding biosynthetic enzymes required for three consecutive steps in the synthesis and modification of thalianol (Fig. 4B). The fourth gene in the cluster (*At5g47980*) is predicted to encode a BAHD acyltransferase (ACT). As for THAS, THAH, and THAD, this enzyme also belongs to a Brassicaceae-specific enzyme subgroup. Because *At5g47980* has an expression pattern very similar to that of *THAS*, *THAH*, and *THAD* and is implicated in secondary metabolism, it is likely to be required for modification of desaturated thalian-diol. However, we have not detected acylated desaturated thalian-diol in *Arabidopsis* root extracts. This may be because this compound is further modified or sequestered or is present at very low levels.

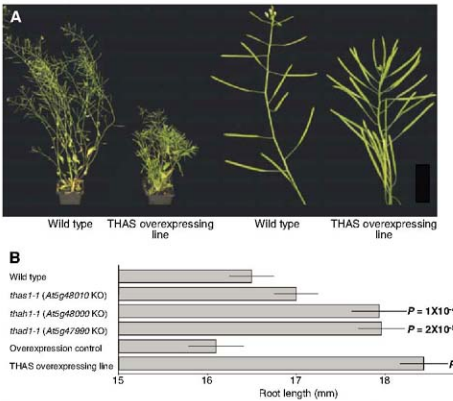

Fig. 3. **(A)** Plants overexpressing thalianol synthase (THAS) are dwarfed. **(B)** Roots from 7-day-old plants that accumulate thalianol (*thah1-1*) or thalian-diol (*thad1-1*) are significantly longer than those of the wild type or *thas1-1* (which lacks the entire pathway). Plants that overexpress THAS and, thus, have elevated levels of thalianol also have significantly longer roots than the control. Error bars are ± SE, n = 68 to 90 for three replicate experiments.

The avenacin gene cluster in oat (*Avena* spp.) confers broad-spectrum resistance to fungal pathogens (*2*). We tested whether the *Arabidopsis* thalianol gene cluster was also defense-related. We challenged the roots of mutant and wild-type plants with strains of fungal and bacterial plant pathogens (*Alternaria brassicicola*, *Botrytis cinerea*, and *Pseudomonas syringae* pv tomato DC3000) but saw no discernible differences in disease progression (fig. S7). However, examination of data from a recent survey of genome-wide polymorphisms in *Arabidopsis* (*18*) revealed that the thalianol pathway genes represent one of the most conserved regions of the genome. This is the hallmark of a recent selective sweep and implies that this gene cluster confers an important (and as yet unidentified) selective advantage.

Genes for most metabolic pathways are not clustered in plants. However, clustering facilitates the inheritance of beneficial combinations of genes (*7*, *19*, *20*); furthermore, disruption of metabolic gene clusters can lead to accumulation of deleterious intermediates (*21*). The observations that ectopic overaccumulation of thalianol (Fig. 2A) or thalian-diol (fig. S6B) lead to severe dwarfing in *Arabidopsis* are consistent with a need for tight coordinate regulation of the pathway. It is noteworthy that lines that accumulate elevated levels of either of these compounds have significantly longer roots than the wild type (Fig. 3B), which suggests distinct and organ-specific effects of thalianol and thalian-diol on plant growth. We

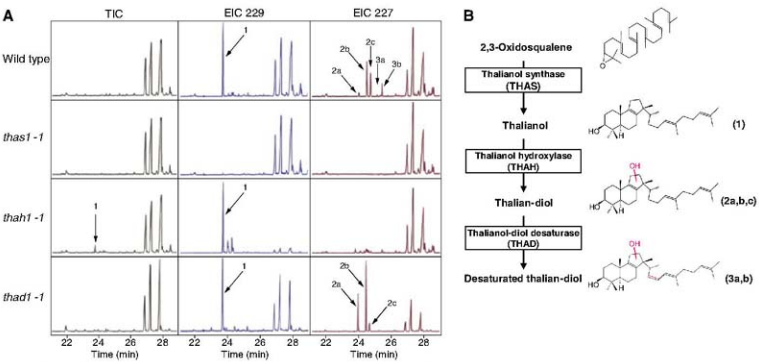

Fig. 4. **(A)** Detection of thalianol (1) and other pathway intermediates in root extracts from wild-type and T-DNA insertion lines. TIC, total ion chromatograms; EIC 227 and 229, extracted ion chromatograms at *m/z* of 227 and 229, respectively. **(B)** Scheme of the thalianol pathway showing the structures of 2,3-oxidosqualene, thalianol (1), thalian-diol (2a, 2b, and 2c), and desaturated thalian-diol (3a and 3b) (see figs. S2, S4, and S5, for respective ion fragmentation patterns). The hydroxyl group introduced to thalianol by THAH to give thalian-diol is drawn in red. GC-MS ionization data indicate that this hydroxyl group is located at one of the four available carbon positions in rings B or C. Peaks 2a to 2c are isomers of thalian-diol and are likely to differ in the position of the hydroxyl group. Because of the low levels of these compounds in *Arabidopsis* root extracts, we were unable to determine the precise position of the hydroxyl group in these isomers by nuclear magnetic resonance. The chromatograms are scaled to the highest peak. The peaks between 26 and 28 min (TIC/EIC) are plant sterols. The data are representative of at least two separate experiments, each with triplicate samples.

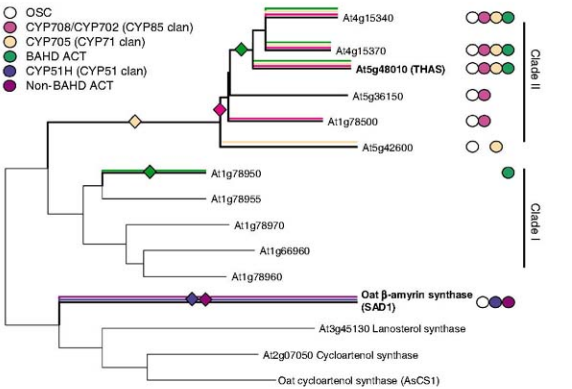

Fig. 5. Model of thalianol cluster evolution. The OSC tree is as in Fig. 1. Colored circles next to each OSC indicate the presence of adjacent genes encoding specific classes of other biosynthetic enzymes (see key). The colored diamonds indicate points at which common ancestors of genes for these other specific classes of enzyme are hypothesized to have become located in the vicinity of an ancestral OSC gene. The reconstruction minimizes the number of rearrangement and gene loss events required to reach the present-day chromosomal arrangement. The product of *At5g48010* (the OSC gene that lies within the functional gene cluster reported in this paper) is indicated in bold. The existence of other triterpene gene clusters is inferred by association of other clade II OSCs with genes for other enzymes implicated in secondary metabolism.

note that the four coexpressed genes within the thalianol gene cluster have marked histone H3 lysine 27 trimethylation, whereas the immediate flanking genes do not (*22*), which suggests that clustering may also facilitate coordinate regulation of the gene cluster at the chromatin level.

Although oats and *Arabidopsis* both contain gene clusters for triterpene synthesis (the avenacin and thalianol clusters, respectively), these two gene clusters are unlikely to share a common origin. This is supported by the fact that the oat *Sad1* and *Sad2* genes do not have orthologs in *Arabidopsis* and are monocot-specific (*6*–*8*). Furthermore, there is no evidence for horizontal transfer of either gene cluster from microbes or elsewhere. Phylogenetic analysis suggests that an ancestral gene cluster formed in *Arabidopsis* around the progenitor of the lineage-specific OSC clade II (Fig. 5). Sequential rearrangements, duplications, and gene loss presumably led to formation of the present-day thalianol cluster. Cluster formation may have been accompanied by the rapid expansion and functional diversification of the lineage-specific OSC clade II, along with the lineage-specific CYP702/708, CYP705, and ACT gene families. In addition, whereas THAS makes thalianol, the other OSCs in clade II produce different triterpene products when expressed in yeast (*3*, *5*). Some of these OSCs may be components of other functional triterpene gene clusters (Fig. 1A), as suggested by genome-wide coexpression of CYP450s (*23*).

An obvious assumption may be that gene clusters of the kind that we have observed were inherited from early evolutionary progenitor species. However, our data clearly indicate that the thalianol and avenacin gene clusters are the products of separate and recent evolutionary events. This finding suggests that eukaryotic genomes are capable of remarkable plasticity and can assemble operon-like gene clusters de novo, which raises intriguing questions about the molecular mechanisms and evolutionary pressures that have acted to cause these gene clustering arrangements to assemble and become fixed. Comparative genomics will now enable us to trace the origins of such gene clusters and so to gain insights into the mechanisms that drive their formation. A further intriguing question is concerned with why genes for some metabolic pathways are clustered, whereas others are not. Our identification of two triterpene gene clusters [for thalianol in *Arabidopsis* (this paper) and for avenacins in oat (*2*, *6*–*8*, *10*)] implies that triterpene pathways may be predisposed to gene clustering. There are two other examples of gene clusters for plant defense compounds (for rice diterpenes and maize benzoxazinoids) (*19*, *24*, *25*). As we learn more about why genes for some metabolic pathways are clustered and others are not, we may need to redefine our understanding of plant metabolism.

References and Notes

1. K. Hostettmann, A. Marston, *Saponins* (Cambridge Univ. Press, Cambridge, 1995).
2. K. Papadopoulou, R. E. Melton, M. Leggett, M. J. Daniels, A. E. Osbourn, *Proc. Natl. Acad. Sci. U.S.A.* **96**, 12923 (1999).
3. D. R. Phillips, J. M. Rasbery, B. Bartel, S. P. Matsuda, *Curr. Opin. Plant Biol.* **9**, 305 (2006).
4. K. T. Liby, M. M. Yore, M. B. Sporn, *Nat. Rev. Cancer* **7**, 357 (2007).
5. I. Abe, *Nat. Prod. Rep.* **24**, 1311 (2007).
6. K. Haralampidis *et al.*, *Proc. Natl. Acad. Sci. U.S.A.* **98**, 13431 (2001).
7. X. Qi *et al.*, *Proc. Natl. Acad. Sci. U.S.A.* **101**, 8233 (2004).
8. X. Qi *et al.*, *Proc. Natl. Acad. Sci. U.S.A.* **103**, 18848 (2006).
9. Materials and methods are available as supporting material on *Science* Online.
10. M. B. Eisen, P. T. Spellman, P. O. Brown, D. Botstein, *Proc. Natl. Acad. Sci. U.S.A.* **95**, 14863 (1998).
11. G. C. Fazio, R. Xu, S. P. Matsuda, *J. Am. Chem. Soc.* **126**, 5678 (2004).
12. M. Koornneef, J. H. Vanderveen, *Theor. Appl. Genet.* **58**, 257 (1980).
13. T. Yokota, *Trends Plant Sci.* **2**, 137 (1997).
14. S. D. Clouse, *Plant Cell* **14**, 1995 (2002).
15. B. Hamberger, J. Bohlmann, *Biochem. Soc. Trans.* **34**, 1209 (2006).
16. D. R. Nelson, M. A. Schuler, S. M. Paquette, D. Werck-Reichhart, S. Bak, *Plant Physiol.* **135**, 756 (2004).
17. A. E. Rettie, A. W. Rettenmeier, W. N. Howald, T. A. Baillie, *Science* **235**, 890 (1987).
18. J. O. Borevitz *et al.*, *Proc. Natl. Acad. Sci. U.S.A.* **104**, 12057 (2007).
19. A. Gierl, M. Frey, *Planta* **213**, 493 (2001).
20. S. Wong, K. H. Wolfe, *Nat. Genet.* **37**, 777 (2005).
21. P. Mylona *et al.*, *Plant Cell* **20**, 201 (2008).
22. X. Zhang *et al.*, *PLoS Biol.* **5**, e129 (2007).
23. J. Ehlting, N. J. Provart, D. Werck-Reichhart, *Biochem. Soc. Trans.* **34**, 1192 (2006).
24. R. Jonczyk *et al.*, *Plant Physiol.* **146**, 1053 (2008).
25. K. Shimura *et al.*, *J. Biol. Chem.* **282**, 34013 (2007).
26. P. Zimmermann, M. Hirsch-Hoffmann, L. Hennig, W. Gruissem, *Plant Physiol.* **136**, 2621 (2004).
27. K. Toufighi, S. M. Brady, R. Austin, E. Ly, N. J. Provart, *Plant J.* **43**, 153 (2005).

28. We thank D. Baulcombe, L. Dolan, R. Field, S. Kopriva, K. Papadopoulou, P. Shaw, A. Smith, D. Studholme, and T. Wang for comments; John Innes Center (JIC) Metabolite Services for metabolite analysis; L. Peña-Rodríguez and M. Rejzek for advice on chemistry; R. Melton and members of the Sainsbury laboratory for assistance with the pathogenicity work; and the Biotechnology and Biological Sciences Research Council (U.K.) for funding.

Supporting Online Material

www.sciencemag.org/cgi/content/full/1154990/DC1
Materials and Methods
Figs. S1 to S8
Table S1
References

8 January 2008; accepted 7 March 2008
Published online 20 March 2008;
10.1126/science.1154990
Include this information when citing this paper.

Mechanism of Self-Sterility in a Hermaphroditic Chordate

Yoshito Harada,[1]* Yuhei Takagaki,[1] Masahiko Sunagawa,[1] Takako Saito,[1] Lixy Yamada,[2] Hisaaki Taniguchi,[2] Eiichi Shoguchi,[3] Hitoshi Sawada[1]*

Hermaphroditic organisms avoid inbreeding by a system of self-incompatibility (SI). A primitive chordate (ascidian) *Ciona intestinalis* is an example of such an organism, but the molecular mechanism underlying its SI system is not known. Here, we show that the SI system is governed by two gene loci that act cooperatively. Each locus contains a tightly linked pair of polycystin 1–related receptor (*s-Themis*) and fibrinogen-like ligand (*v-Themis*) genes, the latter of which is located in the first intron of *s-Themis* but transcribed in the opposite direction. These genes may encode male- and female-side self-recognition molecules. The SI system of *C. intestinalis* has a similar framework to that of flowering plants but utilizing different molecules.

Self-incompatibility (SI) is a system found in many hermaphroditic organisms, including flowering plants, which prevents self-fertilization and promotes outcrossing (*1*). Fertilization strategies based on the recognition of self or nonself have been reported (*2*, *3*). Known SI systems include multiple proteins that are encoded within a specific gene locus termed the SI specificity–determining locus. The self-recognition, or allorecognition, process requires a male factor and a female factor, and both of these factors must cosegregate chromosomally to enable successful inheritance of the allospecific interaction. Tight genetic linkage of the male and female SI genes is a common key feature in the previously characterized plant SI systems (*4*).

The invertebrate chordate *Ciona intestinalis* has a highly evolved SI system. Interest in the ascidian SI system dates back to the works of Thomas Hunt Morgan (*5*–*8*). Quite a bit is known about the *Ciona* SI system: (i) A self/nonself-discrimination site resides on the egg's vitelline coat (VC), which is an acellular matrix surrounding the egg (*9*). The VC shows higher affinity to the nonself sperm than to the self sperm. Fertility of sperm is closely related to its capability to bind to the VC (*9*, *10*). This suggests that the male SI factor is expressed on the sperm surface. (ii) Acquisition of self-sterility takes place during oocyte maturation (*11*). (iii) The barrier against self-fertilization is abolished by treatment with mildly acidic seawater or by addition of proteases (*5*). When treating eggs with weak acid to allow self-fertilization (Fig. 1A), Morgan observed two types of cross-sterility, which is nonself sterility between gametes from different animals, within the obtained self-fertilized F_1 siblings (*6*, *7*): one-way cross-sterility and bidirectional cross-sterility. In the case of one-way cross-sterility, the eggs are fertilized by nonself-sperm, but no fertilization occurs in the opposite gamete combination. On the other hand, no fertilization is observed in both gamete combinations in bidirectional cross-sterility. Occurrence of one-way cross-sterility is unlikely to be due to a crossover between the male and female SI genes, which would soon disrupt the SI system during a few generations. Instead, Morgan introduced a "haploid sperm hypothesis" to explain this phenomenon, which proposes that SI specificity is determined by haploid expression in sperm but by diploid expression in eggs (Fig. 1B) (*6*–*8*). According to this hypothesis, a parent heterozygous at the SI locus (represented as A/a) produces two populations of sperm (A-sperm and a-sperm), either of which can fertilize two types of homozygous eggs (A/A and a/a). In contrast, sperm (A-sperm and a-sperm) from two types of homozygotes (A/A and a/a) are unable to fertilize heterozygous eggs (A/a), because heterozygote eggs have (in the VC) both types of female SI gene products.

We repeated Morgan's self-fertilization experiment (Fig. 1A) (*12*) and obtained several batches of F_1 populations, among which were two batches (H and G) that we analyzed in detail and obtained noncontradictory results (figs. S1 and S2). Batch H contained 23 self-fertilized siblings from a single parent. We examined the pairwise sterility or fertility of gametes from these 23 animals and one nonsibling animal as a control in all the 576 (= 24 × 24) combinations (fig. S1A). According to the pattern of cross-sterility, 23 selfed F_1 siblings were clustered into six distinct groups (fig. S1B). Gametes were bidirectionally sterile within each group, but reciprocal fertility and one-way sterility were observed between different groups. This grouping agreed well with that predicted from an expanded version of the above-mentioned genetic scheme based on the "haploid sperm hypothesis" to two SI loci (designated as locus A and B) system (Fig. 1C, also see fig. S1B).

We then undertook the positional cloning of these two loci by searching for genetic markers that show a similar segregation pattern as that predicted from the above genetic scheme. Genetic mapping using the H batch revealed that loci A and B reside in chromosomes 2q and 7q, respectively (tables S1 and S2). Fine mapping was followed utilizing the G and H batches, and the candidate regions of loci A and B were finally restricted to as narrow as 170 kilobase pairs and 1 megabase pair long, respectively (fig. S3). Locus A appeared to contain only about 20 transcription units (table S3). No overall synteny between these two loci was observed with two exceptions.

Synteny was observed for a homolog of the mammalian *PKD1* (*polycystin-1*) gene, a causative gene for autosomal dominant polycystic kidney disease (ADPKD), which was found in both loci (Fig. 2A and figs. S4 and S5). We designated these two PKD1 homologs as *s* (sperm)-*Themis-A* (in locus A) and *-B* (in locus B), respectively. (Themis is a Greek goddess who is the embodiment of divine order, law, and custom and prohibits incest.) PKD1 is a transmembrane receptor and interacts with PKD2 (polycystin-2), which is a product of another causative gene for ADPKD and structurally related to PKD1, to act as a calcium-permeable cation channel complex (*13*, *14*). It is thought that in this complex PKD1 plays a role to modulate the ion conductance of the PKD2 channel (*15*). PKD1 family members of other organisms are known to play key roles in fertilization. For example, in sea urchin sperm, the acrosome reaction requires activation of two PKD1 orthologs (REJ1 and REJ3, receptor for egg jelly) (*16*, *17*). REJ3 is shown to bind physically to the sea urchin PKD2 ortholog (suPC2) in the plasma membrane over the acrosomal vesicle (*18*). Also, in flies, there may be involvement of PKD1 members in the gamete interaction process because disruption of the *PKD2* gene results in male sterility without affecting spermatogenesis (*19*). PKD1 family members usually contain 11 transmembrane domains, and s-Themis-B also contains these putative 11 domains. In contrast, s-Themis-A is a diverse member and contains five transmembrane domains. Both versions of s-Themis are polymorphic in the N-terminal hypervariable regions (fig. S6, A and B; see supporting online text). For example, only 29% of amino acids (42% of nucleotides) were identical between two alleles of s-Themis-B shown in fig. S6B, whereas it is reported that genome sequences derived from two homologous chromosomes in *C. intestinalis* show more than 99% identity to each other in coding regions at the nucleotide level (*20*). A and B s-Themis are relatively conserved in the C-terminal side of the REJ module and contain a signal peptide, an N-terminal hypervariable region, an REJ module, and a heterotrimeric GTP–binding protein (G protein)–coupled receptor proteolytic site (GPS) domain in the extracellular region and a lipoxygenase homology domain in the cytoplasmic region (Fig. 2A and figs. S4 and S5). Transcripts of *s-Themis-A* and *-B* were found in a testis cDNA library (*21*) (also see table S3), which suggested that these gene products are on spermatozoa.

[1]Sugashima Marine Biological Laboratory, Graduate School of Science, Nagoya University, Sugashima, Toba 517-0004, Japan. [2]Division of Disease Proteomics, Institute for Enzyme Research, the University of Tokushima, 3-15-18 Kuramoto-cho, Tokushima 770-8503, Japan. [3]Department of Zoology, Graduate School of Science, Kyoto University, Oiwake-cho Kitashirakawa Sakye-ku, Kyoto 606-8502, Japan.

*To whom correspondence should be addressed. E-mail: yharada@bio.nagoya-u.ac.jp (Y.H.); hsawada@bio.nagoya-u.ac.jp (H.S.)

The other gene shared by both loci was a fibrinogen-like gene (Fig. 2A and figs. S4 and S5). In parallel with this genetic study, we are currently identifying VC components in this species by mass spectrometry–based proteomic analysis. Among about 20 proteins encoded in the candidate region for locus A, the fibrinogen-like molecule turned out to be the only one included in the identified VC components (table S3; figs. S6C and S7). Similarly, another fibrinogen-like protein encoded in the candidate region for locus B was also found in the VC (figs. S6D and S7). We thus designated these genes as *v* (vitelline coat)-*Themis*-*A* and -*B*. Both v-Themis proteins were relatively small, consisting of a single fibrinogen-α/β/γ-chain C-terminal globular domain, but extremely polymorphic (fig. S6, C and D; see supporting online text). This domain is known to be responsible for the self/nonself (pathogen)–discrimination in the innate immunity system of a horseshoe crab (*22*). The *v-Themis* genes locate within the long first intron of respective *s-Themis* genes, which are transcribed in the opposite direction (Fig. 2B and figs. S4 and S5). The hypervariable regions of *s-Themis* and *v-Themis* were adjoining in both loci.

Taking these findings together, we propose that SI is controlled by two loci in *C. intestinalis*, each of which contains a male determinant *s-Themis*, and a female determinant *v-Themis* (Fig. 2C). *s-Themis* and *v-Themis* may have many different alleles, and these genes comprise a single haplotype because of their extreme genetic proximity. We propose that s-Themis factors act as receptors that can specifically interact with the corresponding v-Themis encoded in the same haplotype. It is possible that when these two s-Themis receptors recognize respective autologous v-Themis ligands as self on the VC, a sperm regards the egg as self (deduction from the genetic scheme shown in Fig. 1C) and actively weakens its binding ability to the VC in order to detach. Previous cytological observations show that self sperm can bind well to the autologous VC initially, but it will detach within a few minutes (*9*, *10*). We speculate that such duration reflects the time consumed by sperm to execute a series of self-recognition reactions. *Ciona savignyi*, a close relative of *C. intestinalis*, is reported to be a self-fertile species; however, self/nonself-discrimination still takes place in this species, resulting in a longer time requirement for self-fertilization than for cross-fertilization (*23*). The PKD1 signal is known to induce the elevation of cytoplasmic [Ca^{2+}] via the PKD2 channel (*24*). It is possible that the elevation of [Ca^{2+}] in the sperm cytoplasm may be involved in these processes.

Histocompatibility in the colonial ascidian, *Botryllus schlosseri*, is controlled by a single highly polymorphic locus, *Fu/HC*. Candidates for *Fu/HC* genes (*cFu/HC*, *fester*) have been recently discovered (*25*, *26*). *cFu/HC* encodes an immunoglobulin superfamily member containing epidermal growth factor (EGF)–like repeats, whereas *fester* is a Sushi domain–containing gene. Sushi domains are also found in sp56, a mouse sperm protein thought to be involved in binding sperm to the egg zona pellucida (*27*). Allorecognition involved in the *Botryllus* histocompatibility may be more complicated than that in the *Ciona* SI system because the former includes an acquired immunity–like mechanism mediated by individual specific splice variants of *fester* (*26*). In another solitary ascidian *Halocynthia roretzi*, we previously reported a 70-kD VC protein, HrVC70, consisting of 12 EGF-like repeats, as a candidate for the female SI factor (*28*). Possible involvement of homologs of *s-Themis*–*v-Themis* in the SI system of *H. roretzi* remains to be determined.

In flowering plants, such as Brassicaceae, pollen expresses S-locus cysteine-rich protein (SCR), a ligand for an S-locus receptor kinase (SRK) that is expressed in stigma, and both multiallelic genes are located in an *S-locus*,

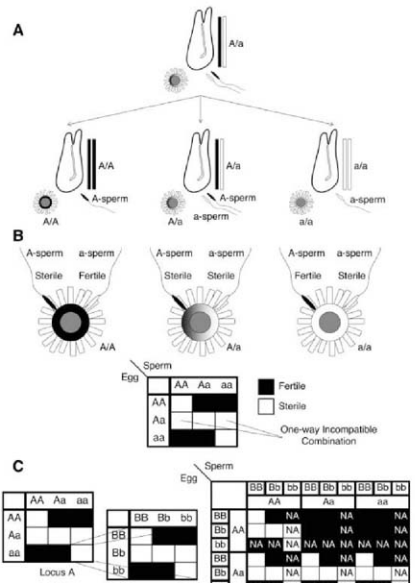

Fig. 1. Genetic studies on the SI system in *C. intestinalis*. **(A)** Schematic diagram of the breeding of selfed F_1 siblings. The double lines beside the animals represent the diploid hypothetical SI gene. Artificial self-fertilization of an animal, which is heterozygous in the gene concerned, produces three types of F_1 siblings (two types of homozygotes and one heterozygote). **(B)** The "haploid sperm hypothesis" originally proposed by Morgan. A predicted fertility or sterility for each combination of genotypes is shown in a (3 × 3) panel (bottom). **(C)** Summary of the pairwise fertility or sterility between the selfed F_1 siblings (batch H) (see fig. S1 for details). The results summarized on the right show a nested pattern of the (3 × 3) units shown in (B), left. This indicates that there are two SI loci in *Ciona* system (shown as A and B), both of which function in the manner shown in (B). It should be noted that a self-recognition signal in either locus A or B is not sufficient to block fertilization, but both signals are necessary for the establishment of sterility. Two alleles in locus A (B) were indicated as A (B) and a (b). The bb homozygotes were absent in the 23 siblings investigated (because of possible impairment in development or growth) and are indicated as NA (not available).

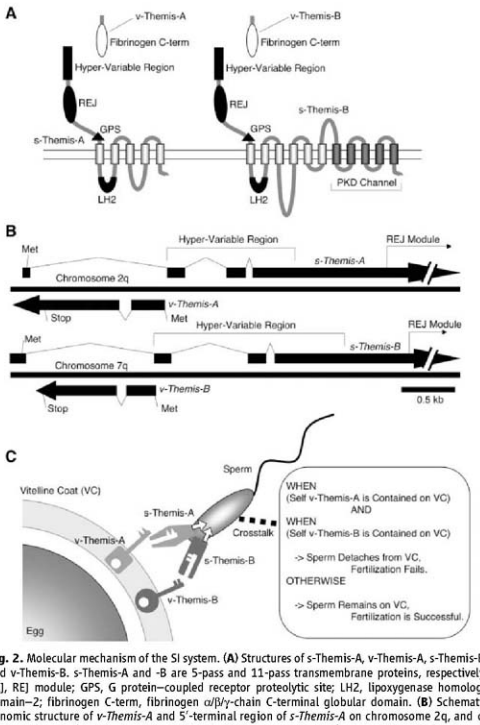

Fig. 2. Molecular mechanism of the SI system. **(A)** Structures of s-Themis-A, v-Themis-A, s-Themis-B, and v-Themis-B. *s-Themis-A* and *-B* are 5-pass and 11-pass transmembrane proteins, respectively. RE], RE] module; GPS, G protein–coupled receptor proteolytic site; LH2, lipoxygenase homology domain–2; fibrinogen C-term, fibrinogen α/β/γ-chain C-terminal globular domain. **(B)** Schematic genomic structure of *v-Themis-A* and 5′-terminal region of *s-Themis-A* on chromosome 2q, and of *v-Themis-B* and 5′-terminal region of *s-Themis-B* on chromosome 7q (see figs. S4 and S5). *v-Themis* locates within the first intron of the respective *s-Themis*. Met, predicted translation initiation site; Stop, translation termination site. **(C)** A model of s-Themis/v-Themis–mediated SI system. We propose that when both s-Themis-A and -B ("key holes") on the sperm surface recognize respective v-Themis ("keys") on the VC as self, sperm detaches. Otherwise, sperm remains on the VC and then penetrates through the VC to fertilize the egg.

which is inherited as one segregating unit (*1*). It is known that a specific interaction between SCR and SRK in the same haplotype triggers SRK activation, which inhibits pollen tube elongation in stigma and prevents self-fertilization (*1*). Taking these systems into account, we note that a framework of an animal SI system observed in *C. intestinalis* is strikingly similar to those of flowering plants, although they utilize different molecules in their self-recognition strategies.

References and Notes

1. S. Takayama, A. Isogai, *Annu. Rev. Plant Biol.* **56**, 467 (2005).
2. L. A. Casselton, *Heredity* **88**, 142 (2002).
3. T. Boehm, *Cell* **125**, 845 (2006).
4. M. K. Uyenoyama, *New Phytol.* **165**, 63 (2005).
5. T. H. Morgan, *J. Exp. Zool.* **80**, 19 (1939).
6. T. H. Morgan, *J. Exp. Zool.* **90**, 199 (1942).
7. T. H. Morgan, *J. Exp. Zool.* **95**, 37 (1944).
8. N. Murabe, M. Hoshi, *Zoolog. Sci.* **19**, 527 (2002).
9. F. Rosati, R. De Santis, *Exp. Cell Res.* **112**, 111 (1978).
10. K. Kawamura, H. Fujita, M. Nakauchi, *Dev. Growth Differ.* **29**, 627 (1987).
11. R. De Santis, M. R. Pinto, *Mol. Reprod. Dev.* **29**, 47 (1991).
12. Materials and methods are available as supporting material on *Science* Online.
13. A. L. Kierszenbaum, *Mol. Reprod. Dev.* **67**, 385 (2004).
14. P. Delmas, *Cell* **118**, 145 (2004).
15. K. Hanaoka *et al.*, *Nature* **408**, 990 (2000).
16. G. W. Moy *et al.*, *J. Cell Biol.* **133**, 809 (1996).
17. K. J. Mengerink, G. W. Moy, V. D. Vacquier, *J. Biol. Chem.* **277**, 943 (2002).
18. A. T. Neill, G. W. Moy, V. D. Vacquier, *Mol. Reprod. Dev.* **67**, 472 (2004).
19. Z. Gao, D. M. Ruden, X. Lu, *Curr. Biol.* **13**, 2175 (2003).
20. J. H. Kim, M. S. Waterman, L. M. Li, *Genome Res.* **17**, 1101 (2007).
21. K. Inaba *et al.*, *Mol. Reprod. Dev.* **62**, 431 (2002).
22. S. Gokudan *et al.*, *Proc. Natl. Acad. Sci. U.S.A.* **96**, 10086 (1999).
23. D. Jiang, W. C. Smith, *Biol. Bull.* **209**, 107 (2005).
24. A. Giamarchi *et al.*, *EMBO Rep.* **7**, 787 (2006).
25. A. W. De Tomaso *et al.*, *Nature* **438**, 454 (2005).
26. S. V. Nyholm *et al.*, *Immunity* **25**, 163 (2006).
27. L. H. Bookbinder, A. Cheng, J. D. Bleil, *Science* **269**, 86 (1995).
28. H. Sawada *et al.*, *Proc. Natl. Acad. Sci. U.S.A.* **101**, 15615 (2004).
29. We thank N. Murabe, Y. Sasakura, K. Hirayama, K. Tsuzuki, H. Takahashi, N. Satoh, and past and present members of our laboratory, especially K. Kobayashi. We also thank C. C. Lambert and G. Lambert for reading the manuscript. This study was supported by a Grant-in-Aid for Young Scientists (type B) from the Ministry of Education, Culture, Sports, Science, and Technology (MEXT) to Y.H. (18770198); research fellowship of the Japan Society for the Promotion of Science (JSPS) for young scientists to L.Y.; Grants-in-Aid for the 21st Century Center-of-Excellence Program "Disease Proteomics" and the Knowledge Cluster Initiative by MEXT to H.T.; Grants-in-Aid for Exploratory Research (16659021, 19659018) from MEXT to H.S. Sequence information has been deposited at the DNA Data Bank of Japan with the accession numbers AB364513 [*s-Themis-A* (JGI)], AB364514 [*s-Themis-B* (JGI)], AB364515 [*v-Themis-A* (JGI)], AB364516 [*v-Themis-B* (JGI)], AB372099 [*s-Themis-A* (H2)], AB372101 [*s-Themis-B* (H2)], AB372098 [*v-Themis-A* (H2)], and AB372100 [*v-Themis-B* (H2)].

Supporting Online Material

www.sciencemag.org/cgi/content/full/1152488/DC1
Materials and Methods
SOM Text
Figs. S1 to S7
Tables S1 to S3
References

1 November 2007; accepted 10 March 2008
Published online 20 March 2008;
10.1126/science.1152488
Include this information when citing this paper.

Dynamic Light-Scattering System

The DynaPro is an automated, noninvasive, dynamic light-scattering system for biomolecular characterization. The DynaPro Titan Plate Reader incorporates patented technology to deliver superior light-scattering performance as well as integrated data collection and analysis software designed for stable and accurate protein batch analysis. The reader can perform fast and accurate sample analysis in a wide range of applications, including researching antibody formulations in a variety of solution conditions, screening proteins prior to crystallization trials, and bioprocessing and quality control of viral particles in vaccines. Because the DynaPro does not suck samples from the well plate into the sample cell where measurements are taken, it does not perturb the sample. Devices that rely on this sucking process can damage the sample, leading to inaccurate measurements, longer sample times, and potential sample contamination. The DynaPro's noninvasive technology measures the sample automatically in industry-standard microplates. Once the data have been collected, the protein samples can be retrieved and the plates discarded, with no cleaning required.

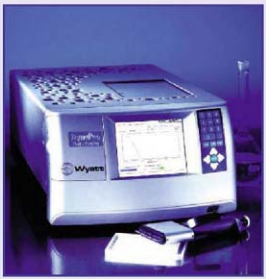

Wyatt Technology
For information + 44 1477 539539
www.wyatt.com

Laser Scanning Microscopy Software

The ZEN 2007 is an integrated suite of digital imaging software that reduces the complexity of the interface without diminishing the range and scope of the functions. ZEN does this by switching between Basic and Professional mode in response to user input, allowing users to focus their full attention on the specimen. The ZEN user interface is clearly structured and flexible, allowing it to be individually tailored to each experiment and user. It is organized into three zones that follow the typical workflow of experiments. Image acquisition and microscope control tools are on the left. The central worktable for image viewing takes up the majority of the screen, and file management tools sit on the right. The left toolbar automatically adapts to each user's personal requirements and can be decoupled and freely positioned on the screen if required. ZEN's center pane is optimized for displaying and interacting with the acquired image data. The tools are clearly arranged under the image and activate and deactivate as necessary. In Expose mode, images from up to three image containers can be opened simultaneously to allow comparison.

Zeiss
For information +44 (0) 845 226 3036
www.zeiss.co.uk

Optical Filters

New Edge Filters feature both Long Pass and Short Pass optical filters. The Short Pass filters every 50 nm from 450 nm to 1,000 nm. The Long Pass filters every 50 nm from 500 nm to 1,500 nm. The filters are ring-mounted and scribed and sealed for moisture protection. They can be used in combination for custom filtering. They also provide fine-tuned cut-on and cut-off wavelengths by changing the angle of incidence.

Optometrics
For information 978-772-1700
www.optometrics.com

Versatile Dry Baths

The EchoTherm SC20XT and SC25XT models are shaking, heating, and chilling dry baths. The SC20XT is a simple digital unit, while the SC25XT is fully programmable, with a five-program memory. Both have a temperature range from -20°C to 100°C and incorporate a variable speed orbital shaker for mixing and controlling the temperature of samples simultaneously. Both units accommodate accessory sample blocks for 0.2-ml, 0.5-ml, 1.5-ml, 15-ml, and 50-ml centrifuge tubes. Also available are blocks for 2-ml vials, 20-ml scintillation vials, polymerase chain reaction tubes and plates, 96-well and 384-well assay plates of all shapes, deep-well assay plates, and various sizes of test tubes. The units are Peltier-driven, with control to 1°C and shaking range from 200 rpm to 1,000 rpm. These instruments can be used to run temperature/time profiles, unattended restriction digestions and ligations, and automatic enzyme reactions and deactivations; for storing DNA libraries at the workstation; and more.

Torrey Pines Scientific
For information 760-471-9100
www.torreypinesscientific.com

Tyrosine Kinases with BioForm Technology

The coupling of Millipore Tyrosine Kinases with BioForm technology provides a more biologically relevant environment for cell signaling research and discovery efforts. Conventional analysis of membrane protein signaling involves studying a single protein interacting with a single partner. Such analysis loses rich, two-dimensional information afforded by organization of proteins on the membrane surface. BioForm Technology enables the unique assembly of histidine-tagged proteins in an environment that mimics the one created by a cell membrane. This template restores the organizing features of the membrane without the difficulties of membrane preparation and reconstruction procedures. The technology is adaptable to high-throughput assay format and is applicable to many signaling systems. These Tyrosine Kinases can be used in many stages of drug discovery research, including early stage drug screening, signal transduction, and regulation of enzymatic activity.

Millipore
For information 800-548-7853
www.millipore.com

Electronically submit your new product description or product literature information! Go to **www.sciencemag.org/products/newproducts.dtl** for more information.

Newly offered instrumentation, apparatus, and laboratory materials of interest to researchers in all disciplines in academic, industrial, and governmental organizations are featured in this space. Emphasis is given to purpose, chief characteristics, and availability of products and materials. Endorsement by *Science* or AAAS of any products or materials mentioned is not implied. Additional information may be obtained from the manufacturer or supplier.